

Model Quality of Interaction Phenomena between RC Frame and Masonry Infills under Horizontal Cyclic Loading

A dissertation by

Muhammad Hisham AL Hanoun

Submitted in partial fulfillment of the
requirements for the degree of

Dr.-Ing.

Supervisors

Prof. Dr.-Ing. habil. C. Könke

Dr.-Ing. J. Schwarz

June 26, 2019

Reviewer:

1.	Prof. Dr.-Ing. habil. Carsten Könke
2.	Dr.-Ing. Jochen Schwarz
3.	Assist. Prof. Dr. Davorin Penava
4.	Prof. Dr.-Ing. Ekkehard Fehling

Day of Disputation:

October 23, 202

ABSTRACT

Past and current damaging earthquakes have repeatedly shown that unreinforced masonry (URM) infill walls on one hand contribute to the global behavior and stiffness of the structure and on the other hand dominate the damage pattern of Reinforced Concrete (RC) frame structures with URM infill walls. During an earthquake structures are subjected to a three dimensional acceleration field. Thus the URM infill walls undergo simultaneous in- and out-of-plane loading. Therefore, convenient modeling of URM infill walls and their impact on RC frames is fundamental to assess the seismic response of RC frames with URM infill walls.

Since the mid-1950s, a number of distinct approaches in the field of analysis of infilled frames lead to different numerical macromodels. The equivalent strut model is the most common one. A main disadvantage of the strut models is the disability to represent the out-of-plane response of an infill masonry panel. Accordingly, in 2007, 3D strut and tie model was suggested which directly couple the in- (IP) and out-of-plane (OoP) forces in the URM infill wall. Subsequently, utilizing diagonal beam-column members with fiber element cross sections a set of new models have been proposed. The proposed models consider both the IP and OoP response of the infill wall, as well as the interaction between IP and OoP capacities.

In this research, a comprehensive literature review of the available numerical macromodels for predicting IP and especially OoP response will be presented. The beam column type macromodel for URM infill walls will be elaborated and then, given the problems associated with the beam-column element model, a new calibration procedure will be proposed. Experimental results from a 1:2.5 scaled and 1:1 scale laboratory test are utilized for the assessment and validation of the existing and proposed adapted models. Finally, the newly proposed infill model is implemented in a set of RC frame structures with URM infill walls. The considered RC buildings with different number of stories and material properties are subjected to a set of time histories from earthquake records. Then, a numerical damage assessment/evaluation of the representative frame structures under the consideration of OoP failure pattern is achieved in accordance to the damage description of the EMS-98.

BLANK PAGE

ACKNOWLEDGEMENTS

First and foremost, my special heartily thanks to my doctoral fathers Dr.-Ing Jochen Schwarz and Prof. Dr.-Ing. Carsten Könke who encouraged and directed me during my research. Their motivation, enthusiasm, and immense knowledge brought this work towards a completion. I am also deeply thankful to Dr.-Ing. Lars Abrahamczyk for the extraordinarily productive discussion throughout my study and the insightful, valuable comments on the early versions of the thesis. I am also so thankful to my fellow students in GRK1462. Their names cannot be disclosed, but I very much appreciate their help and transparency during the work in the research training group GRK1462 which is funded by the German Research Foundation (DFG). Their financial support to my research is highly appreciated.

Last but not the least; I am as well thankful to my family in Syria who encouraged me throughout the time of my research. Although the horrible war in our homeland, they have always been supportive to pursue my study here in Germany.

June 26, 2019

Muhammad Hisham AL Hanoun

BLANK PAGE

TABLE OF CONTENTS

Table of Contents

Abstract	i
Acknowledgements	iii
Table of Contents	v
List of Figures	ix
List of Tables	xi
Statement of Original Authorship	xiii
Chapter 1: Introduction.....	1
1.1 Motivation	1
1.2 Objectives of the Study	3
1.3 Methodology and Research Approach	4
1.4 Thesis Outlines.....	5
Chapter 2: Review of the Primary and Secondary Macromodels.....	9
2.1 Introduction	9
2.2 Primary Element Macromodels	10
2.3 Secondary Element In-Plane Macromodels.....	12
2.4 Secondary Element Out-of-Plane Macromodels.....	16
2.5 Quality Ranking with Respect to the Covered Interaction Phenomena.....	21
Chapter 3: Experience Based Validation of the Model Input Parameters ...	25
3.1 General	25
3.2 Secondary Element Empirical Strength Models	26
3.3 Experimental Samples.....	28
3.3.1 Recorded input/output Parameters	28
3.3.2 Analytical/Experimental Results.....	29
3.4 Types of Primary and Secondary Elements due to Material Variability	31
3.5 Classification Scheme for Primary and Secondary Elements	35
3.6 Summary.....	37
Chapter 4: Primary Macromodel Assessment	39
4.1 Experimental Review (Multi-Story RC Systems).....	39
4.2 Reference Object Description	41
4.3 Implemented Numerical Modeling Approaches	43
4.3.1 Primary Element Models	43
4.3.2 Secondary Element Models	44
4.4 Dynamic Analysis and Simulation Results.....	45
4.5 Quality assessment of the Primary Macromodels	46

Chapter 5: Macromodel for URM Infill Walls.....	51
5.1 Introduction	51
5.2 Primary Elements Model.....	52
5.3 In-Plane Secondary Element Model.....	52
5.4 Developed In & Out-of-Plane Secondary Element Model	54
5.4.1 Proposed Development.....	55
5.4.2 Damage Definition.....	59
5.4.3 Element Removal Algorithm for Secondary Element.....	61
5.4.4 Macromodel Implementation.....	62
5.4.5 In-Plane Calibration	63
5.4.6 Out-of-Plane Calibration	64
5.4.7 In-Plane and Out-of-Plane Interaction	67
5.5 Model Verification.....	68
5.5.1 Considered Models	68
5.5.2 Numerical Models and Verification of the Results	69
5.6 Model Validation	72
5.6.1 Comparative Study Utilizing Reference Object ELSA	72
5.6.2 Discussion of the Results.....	73
5.6.3 Interaction Quality	74
5.6.4 Reference Object FRAMA	76
5.6.5 Considered Models and Discussion of the Results	79
5.7 Summary	86
Chapter 6: Application to 3D Multi-Story Structures	89
6.1 Introduction	89
6.2 Seismic Action for Horizontal Cyclic Excitation	90
6.2.1 Representative Time Histories for the Site Categories of German Code	90
6.2.2 Representative Time Histories as per the European Database.....	90
6.3 Definition of Assessment Criteria.....	91
6.4 Case Study 1	92
6.4.1 Model Description.....	92
6.4.2 Fundamental Natural Periods.....	93
6.4.3 Interstory Drifts.....	94
6.4.4 Damage Prognosis.....	98
6.4.5 Interstory Drifts as a Function of the Scaled Seismic Records	102
6.5 Case Study 2.....	105
6.5.1 Model Description.....	105
6.5.2 Fundamental Natural Period	107
6.5.3 Incremental Dynamic Curves	107
6.5.4 Average Interstory Drifts.....	108
6.5.5 Damage Prognosis.....	110
6.6 Developed Model Quality Ranking	116
6.7 Summary	119
Chapter 7: Conclusions and Outlook.....	123
7.1 Conclusions	123
7.2 Outlook.....	126

Bibliography	127
Appendices	137
List of Figures.....	139
List of Tables	142
Appendix A: Database Samples	143
Appendix B: Reference Objects Structural Details	151
Appendix C: Primary Element Macromodels Assessment	155
Appendix D: Verification of the Results	165
Appendix E: Secondary Elements Macromodels Assessment	171
Appendix F: Application to 3D Multi-Story Structures	223

BLANK PAGE

LIST OF FIGURES

Figure 1.1 Observed failure patterns according to Schwarz et al. (2000).....	2
Figure 2.1 Models of RC frame elements	11
Figure 2.2 Single equivalent strut model (Polyakov, 1957).....	12
Figure 2.3 Multi equivalent strut model (Chrysostom, 1991).....	13
Figure 2.4 Two diagonal strut and shear link model (Crisafulli, 1997)	13
Figure 2.5 Multi diagonal strut model aligned unparallelled (El-Dakhakhni et al., 2003)	14
Figure 2.6 Nonlinear concentrator model (Puglisi et al., 2009)	14
Figure 2.7 Shear link model (Rodrigues et al., 2010)	15
Figure 2.8 Dual compression strut model (Burton & Deierlein, 2013).....	15
Figure 2.9 Discretized model proposed by: a) Calìo et al. (2012), b) Nemati (2015)	16
Figure 2.10 Eight diagonal nonlinear compression strut with linear tension link model (Hashemi & Mosalam, 2007).....	17
Figure 2.11 Diagonal beam-column element model (Kadysiewski & Mosalam, 2008)	17
Figure 2.12 Fiber section discretization	18
Figure 2.13 Shear link element as a 3D model (Furtado et al., 2015)	19
Figure 2.14 Eight strut model (Di Trapani et al., 2017).....	20
Figure 2.15 One diagonal strut model with in-plane and out-of-plane springs.....	20
Figure 2.16 Two diagonal fiber elements model (Oliaee & Magenes, 2017).....	21
Figure 2.17 Five lumped nonlinear elements model (Mazza, 2018)	21
Figure 3.1 Database including all tests collected from literature.....	28
Figure 3.2 Experimental/analytical peak strength.....	30
Figure 3.3 The calculated coefficient β	31
Figure 3.4 Experimental damage of specimen 4 according to Mehrabi et al. (1996)	32
Figure 3.5 Experimental damage of specimen (S) according to Kakaletsis (2007).....	33
Figure 3.6 The database classified samples.....	37
Figure 4.1 Experimental specimen according to Negro et al. (1996): a) plane and experimental layouts, b) elevation view and c) used time history	42
Figure 4.2 Plastic hinge definition: a) Moment–plastic rotation relationship in a typical MPH, b) A typical 3D interaction yield surface for the axial-force/biaxial-moment interaction in a PMM plastic hinge	43
Figure 4.3 Uniaxial stress–strain relationships: a) steel, b) concrete	44
Figure 4.4 Pivot model used as a representative of URM wall.....	45
Figure 4.5 Bare frame top storey displacement: numerical vs. experimental	47
Figure 4.6 Infilled frames top storey displacement: numerical vs. experimental.....	48
Figure 4.7 Correlation between experimental and numerical displacement time-histories	50
Figure 5.1 Equivalent strut model with concrete material.....	52
Figure 5.2 Experimental/numerical envelope curve: a) specimen S1C-2, b) specimen unit2.....	54
Figure 5.3 Proposed URM infill wall model	56
Figure 5.4 End forces and displacements in a generic beam-column element.....	59
Figure 5.5 Material limit states (schematic view)	60
Figure 5.6 Schematic damage scenarios of infill walls on RC frame structures according to Abrahamczyk et al. (2010).	60
Figure 5.7 Element removal algorithm according to Mosalam et al. (2015)	62
Figure 5.8 Macromodel implementation flowchart.....	63
Figure 5.9 Experimental specimen S1C-2 according to Cavaleri et al. (2014):	64
Figure 5.10 Experimental/numerical hysteretic loops (Cavaleri et al., 2014).....	64
Figure 5.11 Experimental model according to Cavaleri et al. (2004) of specimen.....	66
Figure 5.12 Comparison of the Experimental and Numerical OoP response	66
Figure 5.13 Experimental/numerical cyclic IP response	68
Figure 5.14 Experimental/Numerical monotonic OoP response.....	68
Figure 5.15 Comparison of numerical capacity curves between the proposed and.....	70
Figure 5.16 Experimental/numerical OoP response of specimen 2b.....	71
Figure 5.17 Experimental/numerical OoP response of specimen 4b:.....	71
Figure 5.18 Experimental/numerical OoP response of: a) specimen inf_04 without IP damage, b) specimen TA3 after 1% pre in-plane drift ratio	72
Figure 5.19 Numerical OoP response by using the.....	72

Figure 5.20 Experimental/numerical top displacement: a) M#1, (b) M#4.....	75
Figure 5.21 Experimental/numerical top displacement: a) M#5_org, b) M#5_dev	75
Figure 5.22 Damage distribution: a) Observed experimental, b) predicted numerical	76
Figure 5.23 Normalized shear force applied to column	77
Figure 5.24 Elevation and plan view of the experimental infilled structure (<i>Sigmund et al., 2014</i>)	78
Figure 5.25 Used incremental time history in the experimental simulation	78
Figure 5.26 Experimental/numerical top displacement by using M#5_dev proposed macromodel at different intensity level: a) 0.1g, b) 0.4g, c) 0.8g, and d) 1.2g.....	80
Figure 5.27 Experimental/numerical (M#5_dev) maximum interstorey drift:.....	81
Figure 5.28 Top story correlation	81
Figure 5.29 Individual and cumulative Error E-RMS results acc. to <i>Furtado et al. (2018)</i> and by using the proposed developed macromodel.....	83
Figure 5.30 Normalized IP_OoP deformation path inside the failure curve (Story 1)	84
Figure 5.31 Damage prognoses: a) observed experimental, predicted, b) predicted numerical	85
Figure 6.1 DIN4149 code spectra representative ground motion used in.....	90
Figure 6.2 European code spectra representative ground motion used in.....	91
Figure 6.3 Conceptual numerical abstraction and results evaluation	91
Figure 6.4 Case study 1 structure: a) plane layout, b) elevation view	92
Figure 6.5 Three story models maximum interstorey drift acc. to the considered ground motions at 0.3g PGA: a) bare, b) full infilled and c) soft story	95
Figure 6.6 Five story models maximum interstorey drift acc. to the considered ground motions at 0.3g PGA: a) bare, b) full infilled and c) soft story	96
Figure 6.7 Seven story models maximum interstorey drift acc. to the considered ground motions at 0.3g PGA: a) bare, b) full infilled and c) soft story	96
Figure 6.8 Three story models maximum interstorey drift acc. to the considered ground motions at 0.5g PGA: a) bare, b) full infilled and c) soft story	97
Figure 6.9 Five story models maximum interstorey drift acc. to the considered ground motions at 0.5g PGA: a) bare, b) full infilled and c) soft story	97
Figure 6.10 Seven story models maximum interstorey drift acc. to the considered ground motions at 0.5g PGA: a) bare, b) full infilled and c) soft story	98
Figure 6.11 Seven ground motions average maximum interstorey drift	103
Figure 6.12 Structural layouts of the case study 2 building.....	106
Figure 6.13 Maximum interstorey drift due to incremental dynamic analysis: a) Strong RC frame models, b) Weak RC frame models	109
Figure 6.14 Average interstorey drift.....	111
Figure 6.15 Average interstorey drift as a function of PGA.....	111

LIST OF TABLES

Table 2.1 Quality calculation of the 2D models	22
Table 2.2 Quality ranking of the 2D models	23
Table 2.3 Quality calculation of the 3D models	23
Table 2.4 Quality ranking of the 3D models	24
Table 3.1 URM infill wall maximum strength proposals for empirical models.....	27
Table 3.2 The parameter K_{11} & K_{22}	27
Table 3.3 Recorded input parameters.....	29
Table 3.4 Calculated error and coefficient of variation.....	29
Table 3.5 Parameter β	30
Table 3.6 URM class according to <i>Mehrabi et al. (1996)</i>	32
Table 3.7 URM class according to <i>Kakaletsis (2007)</i>	32
Table 3.8 URM class according to <i>Šipoš et al. (2018)</i>	34
Table 3.9 Typical damage of the RC frame with URM infills for the defined frame and wall classes according to <i>Tempestti et al. (2017)</i>	34
Table 3.10 Classification scheme	36
Table 3.11 RC frame classification parameters	36
Table 4.1 Correlation between experimental & numerical displacement time histories.....	50
Table 5.1 Geometric and Material Properties of the Infill Walls	53
Table 5.2 Material Properties of Diagonal Struts.....	54
Table 5.3 Definition and description of Local Damage Grades (LDG) according to <i>Schwarz et al. (2006, 2015)</i>	61
Table 5.4 Material Properties of Diagonal Struts for Infills	64
Table 5.5 Geometric and Material Properties of the Infill Wall	66
Table 5.6 Material Properties of Diagonal Struts for Infills	66
Table 5.7 Experimental/numerical comparison of the Eigen frequency for infill walls	66
Table 5.8 Material properties of diagonal struts for infills	67
Table 5.9 Frequency and modified geometry of the diagonal strut.....	68
Table 5.10 Natural periods of the infilled structure	73
Table 5.11 Weight of model per element [kN].....	77
Table 5.12 Reduced diagonal strut width [mm].....	79
Table 5.13 Cumulative Error E_{-RMS} , individual error and error for each storey.....	83
Table 6.1 RC frame material properties	92
Table 6.2 URM masonry infills material properties and thickness	93
Table 6.3 Natural periods for the studied numerical models	93
Table 6.4 Damage prognosis for (EQ.6/C-S) seismic actions at 0.1g PGA.....	100
Table 6.5 Damage prognosis for (EQ.6/C-S) seismic actions at 0.3g PGA.....	101
Table 6.6 Damage prognosis for (EQ.6/C-S) seismic actions at 0.5g PGA.....	102
Table 6.7 Global damage of the 3 story model.....	104
Table 6.8 Global damage of the 5 story model.....	104
Table 6.9 Global damage of the 7 story model.....	105
Table 6.10 RC frame material properties	106
Table 6.11 RC columns shear capacity	106
Table 6.12 URM masonry infills material properties.....	107
Table 6.13 Natural periods for the studied numerical models	107
Table 6.14 Damage prognosis for (EQ.6) seismic actions for strong RC frame models	113
Table 6.15 Damage prognosis for (EQ.6) seismic actions for weak RC frame models.....	114
Table 6.16 Global damage of the strong RC models	115
Table 6.17 Global damage of the weak RC models	116
Table 6.18 Assigned ranking values	117
Table 6.19 Final ranking	118

BLANK PAGE

STATEMENT OF ORIGINAL AUTHORSHIP

The work contained in this thesis has not been previously submitted to meet requirements for an award at this or any other higher education institution. To the best of my knowledge and belief, the thesis contains no material previously published or written by another person except where due reference is made.

BLANK PAGE

Chapter 1: Introduction

1.1 Motivation

Reinforced concrete (RC) frame buildings with unreinforced masonry (URM) infill walls are widely used throughout the world. Typically, URM infill walls are considered as interior and exterior walls for architecture partitions targets. *Paulay et al. (1992)* report that URM walls may have positive or negative effects on the structure's overall response. The positive influence is due to the fact that the URM walls add, at least during the initial stages of an earthquake, lateral force resisting capacity and increase damping of the structure (*Penava et al., 2018*). However, the presence of infill masonry walls develops new failure modes such as short columns, soft stories and torsional failure. Usually, these failure modes are not taken into consideration during structure design. *Bashandy et al. (1995)* concluded that masonry infilled RC frame provides a base shear of up to 100% more than bare frame. Therefore, *Crisafull et al. (1997)* recommended to take the contribution of the infill walls into consideration, especially they already exist and offer a more realistic view in seismic assessment of existing vulnerable buildings.

The surveys on damaged and collapsed reinforced concrete RC buildings in recent earthquakes indicated that the poor performance is associated with the influence of URM infill walls (*Kadysiewski et al., 2009*). In case of an earthquake a typical unreinforced masonry infill wall is subjected to a three dimensional acceleration field and undergoes simultaneous in-plane (IP) and out-of-plane loading (OoP) (*Penava et al., 2017*). Depending on the direction of seismic action, the observed damage mechanisms on URM may be classified as IP or OoP. In-plane damage is caused mainly by inter-story drift. The typical in-plane damage mechanisms can be classified as cracking due to separation from the structural frame, cracking due to horizontal bed joint sliding, cracking due to tension across the diagonals of the panel, and cracking due to crushing of panel corners.

Out-of-plane overturning collapse is the most dominated mechanism in perpendicular wall direction. The OoP overturning effects are in fact increased by the shear

cracking damage due to the horizontal in-plane components of seismic action and the interstory drift in the OoP direction, which causes the separation from the upper beam.

For low to mid-rise URM infilled RC frames, ground story infill walls are expected to be damaged first since they are subjected to highest IP demands. However, under the effect of bidirectional loading, where the two components of a ground motion are equally significant, infill walls of the upper stories may fail under the combination of IP and OoP effects. The magnitude of IP demands reduces at the upper stories, while that of OoP forces increases due to the increase of accelerations, subjecting the upper story infill walls to failure under the effects of IP and OoP interaction. Figure 1.1 shows different types of infill wall failures caused by the 1999 Düzce, Turkey earthquake (*Schwarz et al., 2000*).

After L'Aquila earthquake in 2009 (*Braga et al., 2009*) a conducted damage survey showed that the greatest damage is located on the lower stories (up to the second story in taller buildings). On the contrary, collapse due to out-of-plane mechanisms is expected on the upper stories of buildings (due to higher expected accelerations). Therefore, the collapse due to out-of-plane mechanisms has to be ascribed to the early presence of heavy in-plane induced cracking. In fact, in-plane actions can cause disconnection of the infill panels from structural elements, reducing their seismic capacity.

Since the mid-1950s, a number of distinct approaches in the field of analysis of infilled frames lead to different numerical macromodels. The equivalent strut model is the most common one. A main disadvantage of the strut models is the disability to represent the out-of-plane response of an infill masonry panel.



a) Collapse of the bottom floor



b) Moderate damage of the URM infill walls



c) Moderate in-plane damage

Figure 1.1 Observed failure patterns according to *Schwarz et al. (2000)*

1.2 Objectives of the Study

This study focuses on cyclic response of reinforced concrete structures with unreinforced masonry infill walls using macromodeling methodology. In order to evaluate the behaviour under lateral load of RC frame structures with URM infill walls, it is necessary to define an appropriate numerical model which is capable to describe the global and local structural response, i.e. to simulate precisely the interaction phenomena between the RC frame and URM infill panel and on the other hand the macromodel has to be able to describe the 3D behaviour of the URM infill wall regarding the in-plane and out-of-plane response and the interaction between both of them.

Several macromodels are proposed in literature for both RC frame members and URM infill walls. In this study, the global models, i.e. models with lumped plasticity concept, are used to represent the response of RC elements, whereas, the equivalent strut model with different configuration will be considered as representative models for the URM infill panel. The subject matter of this study is to perform an in depth assessment of the existing macromodels. Furthermore, quality assessment of the forecasting available model in structural engineering is often achieved based on the gained phenomenological experience of an engineer. Alternatively in this research the model quality will be evaluated by comparing the experimental and numerical results. Subsequently, the main objectives of this study can be summarized as follow:

1. Literature review on the available macromodels of RC frame elements and URM infill walls;
2. Creation of a homogenous extensive database of experimental tests on RC frames infilled without opening. The experimental responses of the infills under lateral loads are obtained and the main related URM maximum strength empirical models existing in literature are investigated and compared with the experimental results. A simple equation for predicting the maximum capacity of the URM infill walls is proposed to be further used in the calibration of the numerical models;
3. Giving the problematic response of the beam-column elements macromodel, conceptual calibration procedures will be proposed to improve the numerical behaviour of that model (in- and out-of-plane response);

4. Detailed evaluation/assessment of the utilized macromodels of RC frame structures with URM infill walls will be performed, to this purpose, experimental results from a 1:2.5 scaled and 1:1 scale laboratory test are utilized for the assessment;
5. Study of a set of RC frame structures with URM infill walls with different number of stories which will be subjected to a set of time histories earthquake records utilizing the improved 3D macromodel. Thus, an analytical vulnerability assessment of representative frame structures under the consideration of out-of-plane failure can be achieved in correspondence to the damage description of the EMS-98.
6. Finally, to assess the proposed model quality, a comprehensive discussion about the model enhanced performance is taken depending on the achieved results in chapter 5.

1.3 Methodology and Research Approach

1. This research takes a step forward in the practical macromodeling and analysis of URM infill walls. A new single-strut macroelement model is presented in this study to simulate the IP and OoP behaviour of masonry infill walls.
2. The developed single strut macroelement is represented by fiber-section beam-column elements and are able to capture the IP, OoP response of the URM infill panel as well as the interaction between the IP and OoP actions. A simple calibration method is presented, and the model is sufficiently simple and efficient that it can be used for the static or dynamic analysis of an entire structural system. The model has been validated with experimental data available in the literature.
3. Procedures are proposed for calculating the strength properties of the cross-section fibers used in the beam-column element that comprises the infill panel model. The presented calculation steps, based on the database results, ensure that the target IP axial strength and OoP bending strength for the infill panel model will be satisfied.
4. For the OoP calibration, a full-scale experimental specimen was used to propose a procedure for calculating the OoP frequency f_{OoP_FEM} utilizing elastic shell elements and then tuning the macromodel OoP inertia I_{OoP_macro}

to match the shell model frequency. The use of these procedures confirm that the global responses of the URM infill panels will be closely approximated, relative to a case in which the panels are modeled in detail such as using finite elements.

5. Finally, two case studies, using the proposed infill model as part of a larger RC moment frame building model, are presented. The investigated structures, with different number of stories and provided with different infills layout (weak, medium and strong), are subjected to a set of time histories. Thus, an analytical vulnerability assessment of representative frame structures under the consideration of out-of-plane failure can be achieved in correspondence to the damage description of the EMS-98 (*Grünthal et al., 1998*).

1.4 Thesis Outlines

Chapter 2 contains a comprehensive literature review on the available macromodels for URM infill panels. The existing models are categorized into two groups: the first one includes the “conventional” 2D macromodels which have the capability to represent the IP behaviour of the masonry infill walls; the second group the up-to-date 3D models. These models have the feature of simulating both IP-OoP response of the infill walls and the interaction between both components. The conducted experimental studies on the multi-story infilled structures are presented and finally a summary about the expected damage is drawn.

Chapter 3 introduces the collection of 51 experimental samples which were carried out on simplified RC frame with URM infill walls without opening, i.e. 1 story – 1 bay. Most of the considered samples were tested in the IP direction and in few of them the test was conducted to evaluate the OoP response and the interaction between IP and OoP. The samples are systemized in database and then are used to evaluate the most widely considered empirical models to calculate the IP shear strength of the URM infill panels. Further, the OoP test in the database is used to calibrate the URM macromodel developed in this research. Finally, for a classification target of the available samples in the database a review on the experimental and numerical studies available in the literature is achieved. Then the most applicable and up to date methodology is considered as a classification scheme in this study.

Chapter 4 main focus is to present a review about the available modeling techniques of RC frame elements; subsequently the concept of concentrated plasticity is adopted considering two different types of lumped nonlinear hinges. Namely, the element with rigid plastic hinges and fiber section hinges. To evaluate the used macromodels for RC frame the experimental results of four story RC structure (*Negro et al., 1996*), without and with infill walls, are utilized. Accordingly, 3D macromodels of the experiment with different phases, namely, bare, full infill and open ground story, are constructed and nonlinear dynamic analysis is performed. The comparison of the experimental and numerical results illustrates clearly the superiority of the fiber hinge concept to be used as simplified macromodel of RC frame elements.

Chapter 5 adopted the concept of plastic hinge with fiber section to be used for modeling RC frame elements due to the evaluation results of chapter 4.

According to the detailed state of the art of the URM infill walls macromodels in chapter 2 an improved infill wall model, consisting of a diagonal beam-column element, with a cross section composed of nonlinear fiber elements is presented in chapter 5. The infill wall panel stiffness, strength, and limit state deformation are based on values provided by other means, such as FEMA 356 and EMS-98.

The derivations of the properties of the model are outlined in detail, such that the dynamic properties of the infill model match those calculated using a two-way bending slab shell element pinned at the frame elements at all edges. The behaviour of a simple one-panel model is then demonstrated, using the available sample results in the already collected database.

Then, one is chosen and the newly developed URM infill wall macromodel is validated against experimental results of 1:2.5, 1:1 scaled three story and four story RC structures with URM infill walls respectively. Further the model results are compared with the results of other URM macromodels which are considered in this study.

Chapter 6 utilizes the improved infill wall model in examples RC frame structures with URM infill panel's analysis. The model is incorporated into a set of overall models of a multi-story RC frame building with infill walls, and analysed for its response to a suite of seven ground motion time histories. For each analysis, the time histories are scaled to a common intensity of level acceleration.

A vulnerability analysis is carried out for a global response of the buildings. For this case the interstory drift ratio (IDR) is examined. Further, to check the local response quantities, the fiber strains of the RC frame element and URM infill panels are recorded and then the damage state for each analysed structure is determined according to EMS-98 (*Schwarz et al., 2006*)

Chapter 7 presents a summary of the thesis, conclusions, and discussions for further developments in infill wall and reinforced concrete models.

BLANK PAGE

Chapter 2: Review of the Primary and Secondary Macromodels

2.1 Introduction

Modeling the composite reinforced concrete (RC) frame with unreinforced masonry (URM) infill wall structural system is highly linked to the system's changing and complex behaviour. This in fact makes it troublesome to create such models being physically and computationally able to represent the real system. In the last few decades, the above mentioned phenomenon was the main concern of several researchers. Thus, many experimental and analytical studies are provided and different modeling technique able to simulate the system's behaviour proposed.

Generally, the offered modeling technique could be categorized as micro modeling (which is out of this research concern) and macromodeling which is discussed in detail in this research.

In case of URM in-plane (IP) response, macromodeling approach implements a global structural member composed most often of equivalent diagonal strut able to resist axial forces only. When the URM out-of-plane (OoP) behaviour need to be considered then the equivalent element is a beam-column element resists in-plane axial forces and out of plane moments. Disadvantages of this method include the inability to produce different failure modes and need for comprehensive experimental data to determine the properties of equivalent element geometric and material properties.

2.2 Primary Element Macromodels

Up to date, numerous modeling strategies have been proposed to simulate the structural behaviour of reinforced concrete (RC) frame structures with unreinforced masonry (URM) infill walls. However, the complex nonlinear behavior of RC structures especially when it is subjected to random load reversals still lead to large discrepancies among these models. As a result of that, the need for more reliable and practical numerical tools to predict inelastic seismic response of RC structures is both critical and relevant. The level of sophistication in each model corresponds to the level or degree of discretization. To this extent, *Taucer et al. (1991)* roughly divided modeling strategies into three categories in accordance with the increasing level of refinement and complexity:

1. Lumped (global) models: Lumped models were firstly developed by centralizing all inelasticity of the elements into critical regions (such as column ends, beam-column joints as well as locations near mid-span) as it was widely observed in part of experimental studies and field observations. Additionally, any kind of hysteretic law can be assigned to the lumped plasticity model to consider effectively the nonlinear cyclic behavior as well as stiffness deterioration due to cracking. In the definition of rules for loading, unloading and reloading, a large number of choices are possible, to include or to neglect phenomena such as the effect of shear, interaction between moment and axial load, biaxial bending and slippage of rebars (*Negro et al., 1994*).
2. Fiber models: In fact, these models are a subcategory of the global models. Inelastic behavior is either limited to the member end (lumped plasticity models), or distributed along the member (spread plasticity models). A better description of the element inelastic behavior should account for the spread of inelastic deformations into the member since nonlinearity may occur at any element section. The first distributed model was introduced by *Soleimani et al. (1979a)*. In this model, a zone of inelastic deformation spreads from the beam-column interface into the member as a function of loading history. The first element with distributed nonlinearity was formulated with the classical stiffness method, also called displacement method, using cubic Hermitian polynomials. The main shortcoming is that displacement-based element will

encounter numerical instability problems and obtain inaccurate results when elements are suffered from high level of nonlinearity (*Taucer et al., 1991; Spacone et al., 1996*). Therefore, recent efforts mainly focus on another method called force-based or flexibility-based model which strictly satisfies the equilibrium of internal forces along the element even when strain softening occurs. Similar to displacement-based elements, reinforced concrete elements can be subdivided into longitudinal fibers represented by uniaxial constitutive relationships of concrete and reinforcing steel (see Figures 2.1 a to d).

3. Finite element models, represents a detailed micromodeling solution in which material constitutive relationships are assigned to each element (*Penava et al., 2016*). It is obvious that this latter approach represents the most detailed way to represent the elements; it is computationally demanding, and it asks for the definition of numerous input parameters that, in turn, need to be calibrated.

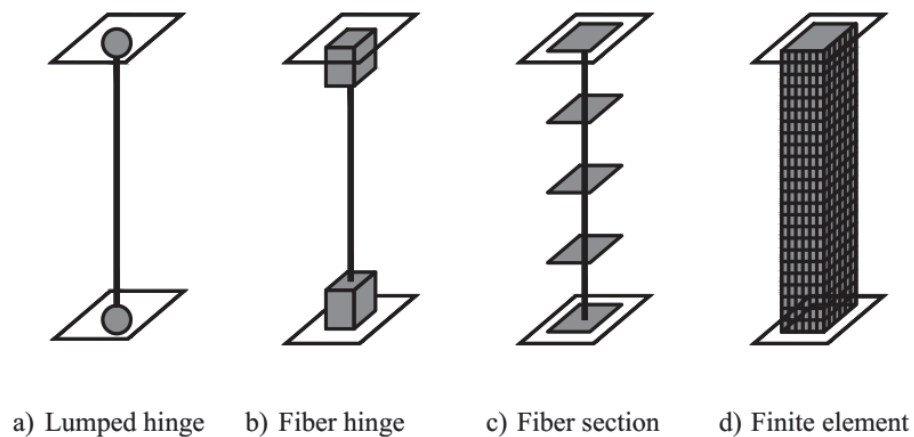


Figure 2.1 Models of RC frame elements

In the present study, elements of the global type, i.e., macromodeling approach, are used. There are many aspects for this choice:

1. Macromodel has more advantages for wide practical application due to its simplicity and short time of the analysis. Therefore, they are the most appropriate models to be used in parametric analyses.
2. Solid knowledge in the numerical analysis strategies is not required. Once a simplified procedure is provided, it may be used by professional engineers as a practical tool for design and evaluation of existing structures.

3. In the numerical analysis it is easily possible to check the effect of including or neglecting a mechanical phenomenon of the model such as strength or stiffness degradation, pinching and rebar yielding and slippage.

2.3 Secondary Element In-Plane Macromodels

The concept of equivalent diagonal strut was first proposed by *Polyakov (1957)* based on the investigation of a three story infilled structure (Figure 2.2). *Holmes (1961)*, who worked with brick masonry infilled steel frames, introduced the empirical equation to replace the panel with an equivalent diagonal strut, having cross section width w equal to one third of the diagonal length d . In the following years, more detailed equation proposed by several other researches, mainly basing the identification of the equivalent width on the ratio between the elastic characteristics of the infill and the surrounding frame (*e.g. Dawe & Seah (1989); Durrani & Luo (1994); Mainstone (1971, 1974); Saneinejad & Hobbs (1995); Stafford Smith (1966)*).

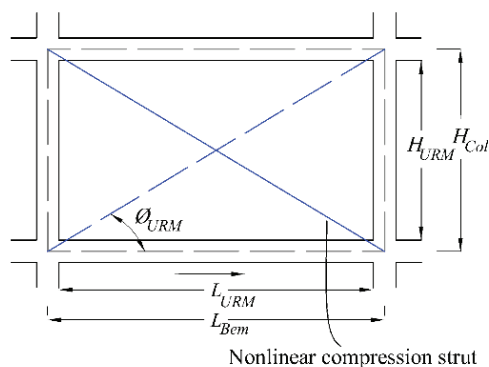


Figure 2.2 Single equivalent strut model (*Polyakov, 1957*)

After introducing several studies by using single diagonal strut models, many researchers proposed the use of multi strut models, to address the local shear failure of the primary RC frame elements (columns and beams) due to the transferred shear forces by URM masonry wall to the surrounding RC frame, proposed the use of a multi strut model. *Chrysostom (1991)* and *Chrysostom (2002)* assigned three compression only inclined struts in each diagonal direction whose behaviour was defined by strength envelope and equation of hysteresis loop. Off-diagonal struts which are responsible to provide the required interaction between URM masonry wall and surrounding frame were proposed to be fixed in critical locations along the

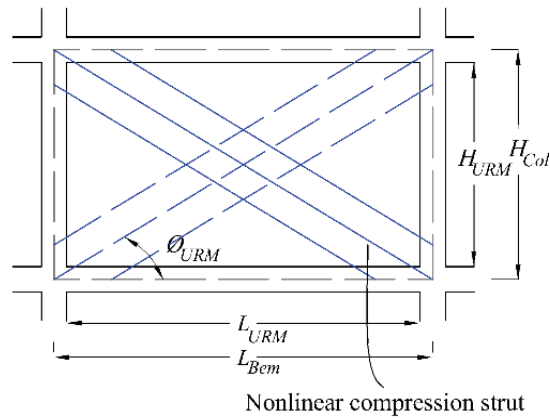


Figure 2.3 Multi equivalent strut model (*Chrysostom, 1991*)

frame members. Stiffness and strength degradation of masonry infills were considered in their model (Figure 2.3).

Crisafulli (1997), introduced a two diagonal strut element in combination with a shear spring element (Figure 2.4). In this model the elements are linked to the axial compressive and shear stress constitutive law for masonry, respectively. Thus the proposed macro element distinguished different independent failure types of URM infill walls for the first time; however the model definition requires about ten experimental material parameters, which is usually cumbersome.

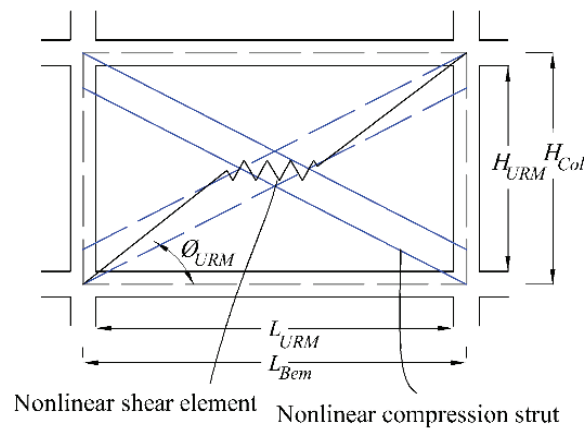


Figure 2.4 Two diagonal strut and shear link model (*Crisafulli, 1997*)

El-Dakhakhni et al. (2003) also modeled the URM masonry panel as six diagonal strut elements, three in each direction, one of them is concentric and the other two are unparallelled configured along the panel's diagonal length (Figure 2.5). Hence the URM infill wall transferred shear forces are increased in the beams and columns of the surrounding RC frame.

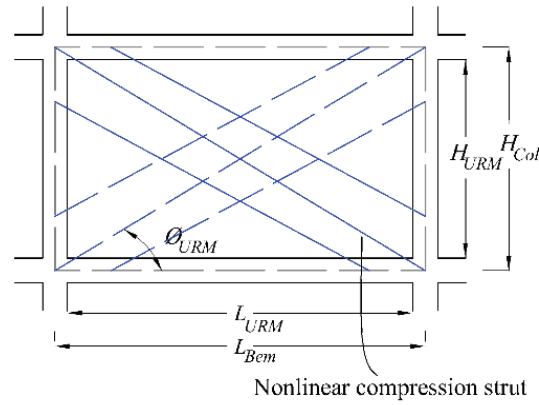


Figure 2.5 Multi diagonal strut model aligned unparallelled (*El-Dakhakhni et al., 2003*)

Since the URM masonry infill wall is a unique element and the strut modeling technique replace the URM by two independent bars, *Puglisi et al. (2009)* reported that in the traditional bi-diagonal masonry models, the behavior laws and hysteretic rules of each diagonal do not influence the other. Accordingly, a simple modification in diagonal strut system was proposed so that to consider coupling between two bars. A plastic concentrator was included at intersection of the bars to capture inelastic behaviour of the wall. It also links the two bars to account for the transfer of forces between them (Figure 2.6).

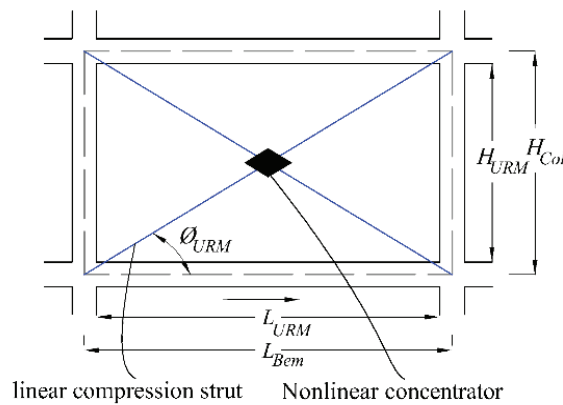


Figure 2.6 Nonlinear concentrator model (*Puglisi et al., 2009*)

Due to the same argument as *Puglisi et al. (2009)* presented in his work regarding the unity of masonry infill wall panel, *Rodrigues et al. (2010)* have introduced his bi-diagonal compression strut panel. URM infill panel was represented by a central axially nonlinear element linking between four support strut elements with elastic behaviour. Nonlinear hysteresis behavior of the central element was accounted for utilizing pinching material model which has the capability to produce loading,

unloading and reloading rules considering stiffness and strength degradation as well as pinching effect (Figure 2.7).

Burton & Deierlein (2013), proposed a dual compression only strut model as Figure 2.8 depicts. In this model, a diagonal strut is placed between the nodes representing the beam-column joints, and an off-diagonal strut is used to capture the column infill interaction. Based on the investigation by **Chrysostom (1991)** regarding the force and stiffness distribution between central and off diagonal strut, **Burton & Deierlein (2013)** suggested that 25% of the total strut strength is assigned to the off-diagonal strut and 75% to the central strut.

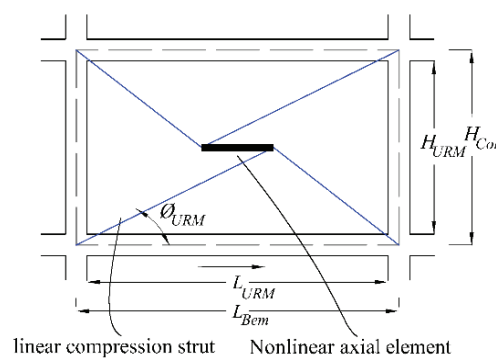


Figure 2.7 Shear link model (*Rodrigues et al., 2010*)

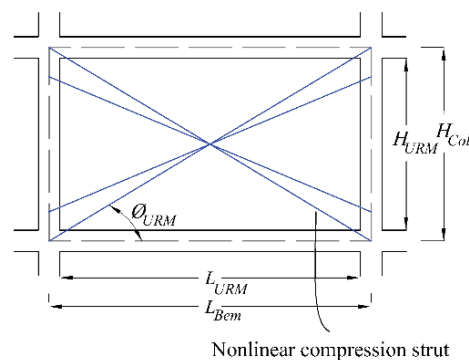


Figure 2.8 Dual compression strut model (*Burton & Deierlein, 2013*)

Since, the previously mentioned macromodels lack the ability to represent all failure type of the URM infill walls and to address correctly the presence of openings, recently a new discrete macromodel was introduced by **Caliò et al. (2012)** to assess the performance of masonry structures under lateral and vertical loadings (Figure 2.9 a). Subsequently, in purpose to more accurate represent the shear behaviour of the URM infill panel, the proposed model by **Caliò et al. (2012)** was more refined by **Nemati (2015)** as Figure 2.9 b depicts.

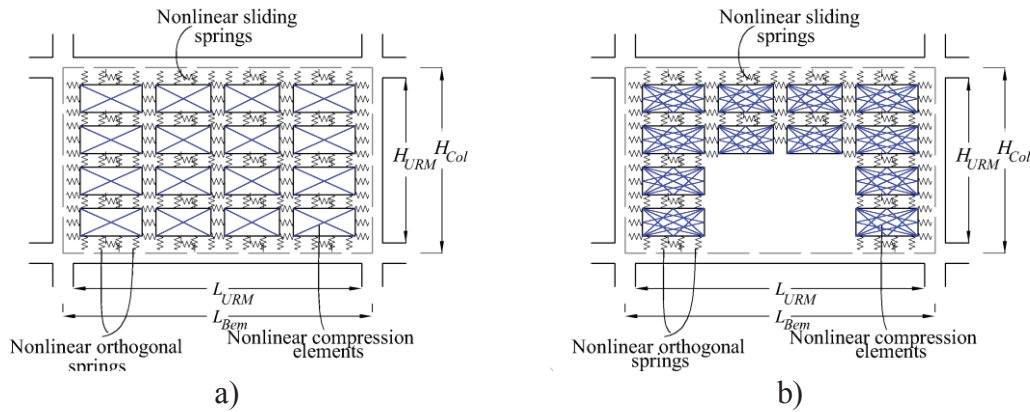


Figure 2.9 Discretized model proposed by: a) *Calio et al. (2012)*, b) *Nemati (2015)*

2.4 Secondary Element Out-of-Plane Macromodels

The aforementioned elaborated numerical models have two dimension configurations, so they are not capable to consider the out-of-plane response of the URM infill panel. *Hashemi & Mosalam (2007)* introduced a 3D strut-and-tie (SAT) macromodel. The model is composed of eight compressions-only struts assigned a particular stress-strain constitutive model. The struts are connected with a tension only link element at the centre of the URM panel. Arching effect was considered by shifting the mid span joint of each strut normally to the plane of the URM (Figure 2.10). The interaction between IP and OoP response was accounted by the concept of failure surface, which was derived on the basis of refined FE numerical model according to the results of pushover analysis at different level of applied constant out-of-plane force normal to the URM panel.

Kadysiewski & Mosalam (2008) in their further work proved that, the previously proposed numerical model shows some problematical behaviour due to specific loading cases. As example, the IP-OoP loading path may not fulfill the defined interaction relation. Additional problem is numerical instability due to high IP displacement and OoP loads. Consequently, they proposed a new model which considers the IP and OoP behavior and the interaction between them in both directions. In the model, each infill wall is represented by a single diagonal element, composed of two force-based beam-column elements represented as “Beam-Column element with Fiber Hinges” available in OpenSees (*McKenna et al., 2000*) and connected at a midpoint node withan assigned lumped mass for the consideration of the response of the infill wall in the OoP direction (Figure 2.11).

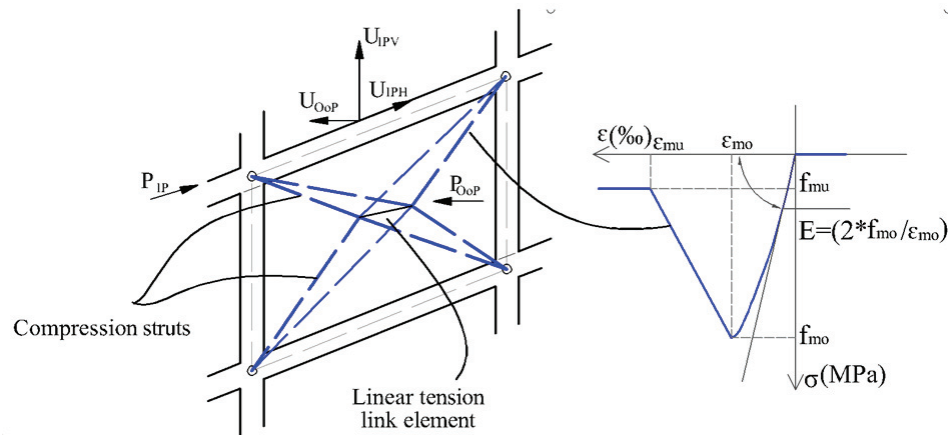


Figure 2.10 Eight diagonal nonlinear compression strut with linear tension link model (Hashemi & Mosalam, 2007)

The cross-section of the beam-column element is modeled by locating nonlinear fibers along a line in the OoP direction (Figure 2.12). In this way, the beam-column element acts as truss and flexural element in the IP and OoP directions, respectively. Equivalent element parameters identification can be summarized according to the following steps:

1. Determine the IP elastic parameters in terms of stiffness and strength;
2. Calculate OoP first natural frequency by using the URM estimated freq's, assuming it spans vertically, with simply supported ends;
3. Calculate OoP yielding bending moment and the corresponding OoP point force;
4. Generate axial force-bending moment interaction curve (P-M), by using the previously calculated IP strength and OoP yielding bending moment as "anchors" of the following expression (number of points on the interaction curve equal to the number of fibers);

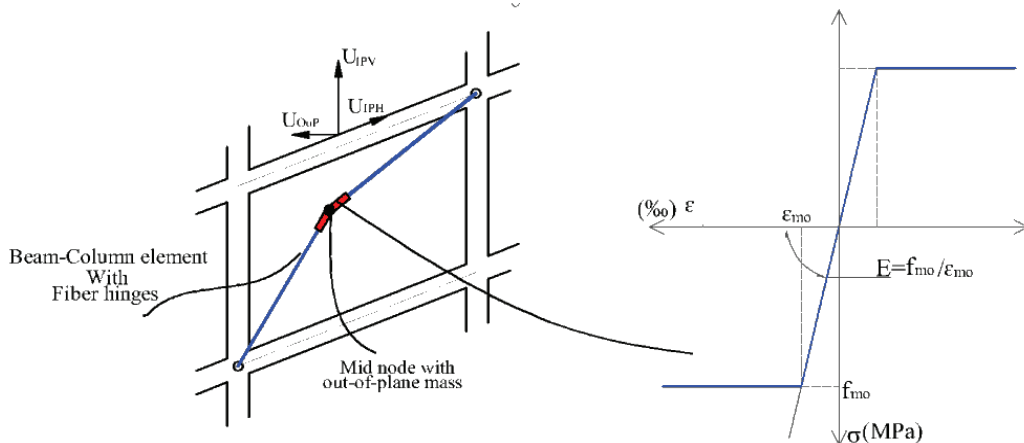


Figure 2.11 Diagonal beam-column element model (Kadysiewski & Mosalam, 2008)



Figure 2.12 Fiber section discretization

5. Once generated, the interaction surface, the weighted fiber properties are calculated in terms of (the characteristics of the i fibers are assigned in terms area A_i , distance from the y axis z_i , yielding strength f_{yi} and yielding strain e_{yi}), to match the failure surface following specified procedures, then elastic-perfectly plastic constitutive law is assigned for each fiber.

Mosalam & Günay (2009) In order to explicitly account for the failure of URM infill walls during an earthquake excitation under combined IP and OoP effects, the above described analytical infill wall macromodel is implemented in a previously developed progressive collapse algorithm. In that regard, the IP deformation is described by the relative horizontal displacement between the top and bottom nodes of the diagonal strut. On the other hand, the OoP displacement is determined at the midpoint node where the lumped OoP mass is attached.

Furtado et al. (2015) developed an equivalent bi-diagonal compression strut model to evaluate the behavior of masonry infill walls which were subjected to cyclic loads. As damage on panel in one direction affects its behavior in the other direction, the proposed model utilized the element removal algorithm, which was basically developed by **Kadysiewski & Mosalam (2009)** to consider in-plane and out-of-plane behavior (Figure 2.13).

Di Trapani et al. (2017) suggested the use of four pinned beam-column elements with distributed plasticity utilizing the concept of fiber section for each integration point along each element. The model assumes that the in-plane and the main out-of-plane responses are mainly provided by the diagonal elements and the horizontal and vertical elements are mainly responsible to represent the 2-way bending mechanism. The model was validated against several experimental specimens which were tested out of plane with and without previous in plane damage. Figure 2.14 illustrates a schematic view of the proposed model.

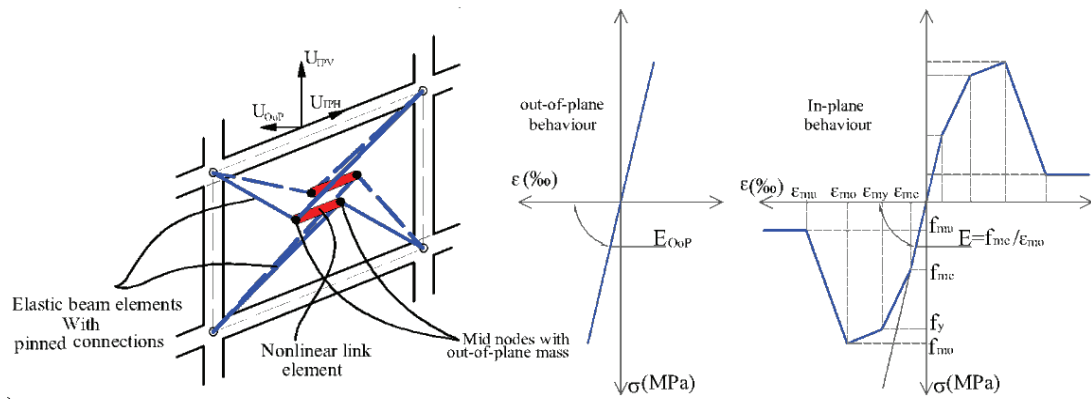


Figure 2.13 Shear link element as a 3D model (Furtado *et al.*, 2015)

Ricci *et al.* (2017) carried out a comprehensive literature review on the available tests that have been conducted on the OoP behaviour of the URM infill panel and the IP-OoP interaction. The collected experiments were then systemised in a database and empirical formulas derived for predicting the OoP capacity curve. Then, a macromodel was presented that considers the IP behaviour utilizing a zero length nonlinear spring linked with **Panagiotakos & Fardis (1996)** force-displacement relationship. On the other hand the OoP behaviour is represented through a second zero length element with the capacity curve deduced from the database (Figure 2.15). Finally the interaction is considered by a linear reduction of the IP and OoP capacity curves due to the achieved IP and OoP drift respectively.

To investigate the effect IP- OoP interaction in the case of RC frame infilled frames, **Longo *et al.* (2018)** recalibrated the model previously proposed by **Kadysiewski & Mosalam (2008)**. In his work, the IP and OoP strength are calculated according to EC6 (CEN 2006). To introduce the URM infill panel stiffness reduction after yielding, a softening part is added to the elastic-plastic material model which was presented in the original model. Then the model has been validated, utilizing the principle of pushover analysis, against the experimental results proposed by **Calvi *et al.* (2004)**.

Utilizing the experimental test data which were carried out by **Hak *et al.* (2014)**, a new URM infill model is calibrated and proposed by **Oliaee & Magenes (2017)**.

As Figure 2.16 shows, the model is composed of two diagonal fiber section elements. The left side elements are diagonal struts to represent the IP response while the right side elements are diagonal beams controlling the OoP behaviour.

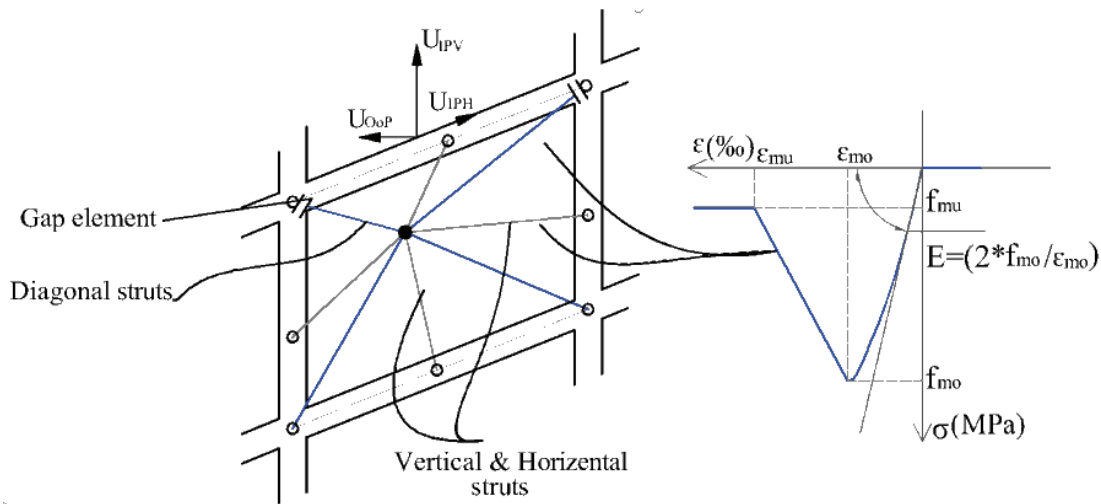


Figure 2.14 Eight strut model (Di Trapani et al., 2017)

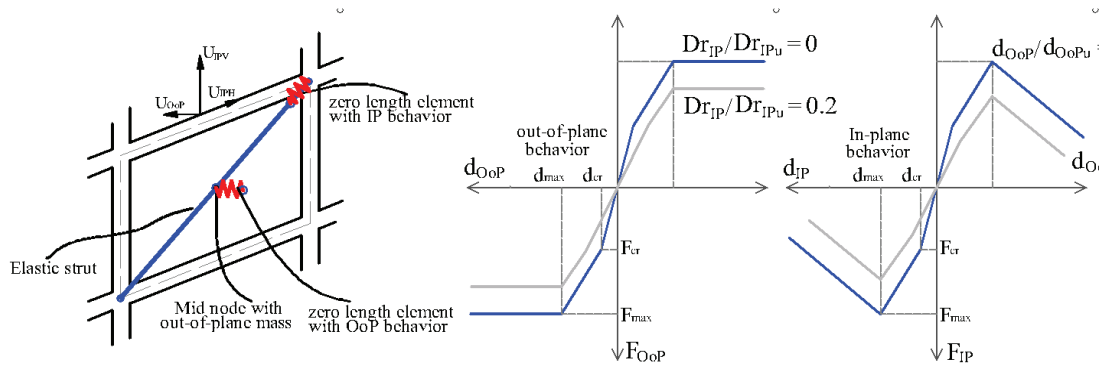


Figure 2.15 One diagonal strut model with in-plane and out-of-plane springs (Ricci et al., 2017)

A concrete constitutive law with zero tension branch is adopted to represent the URM panel behaviour. The IP-OoP interaction is introduced by modifying the peak strain (ϵ_{m0}) of the material model and by linearly decreasing the fiber element's thickness due to the IP interstory drift ratio.

Finally, a very recent macromodel is proposed by *Mazza (2018)*. As Figure 2.17 illustrates the model consists of five elements enhanced with the lumped plasticity approach. A tri-linear material law is assigned to the horizontal truss element to represent the IP response while the OoP behaviour is reproduced through the diagonal beam elements with bilinear material law. The model is calibrated by using the experimental results by *Hak et al. (2014)* and *Furtado et al. (2015)*.

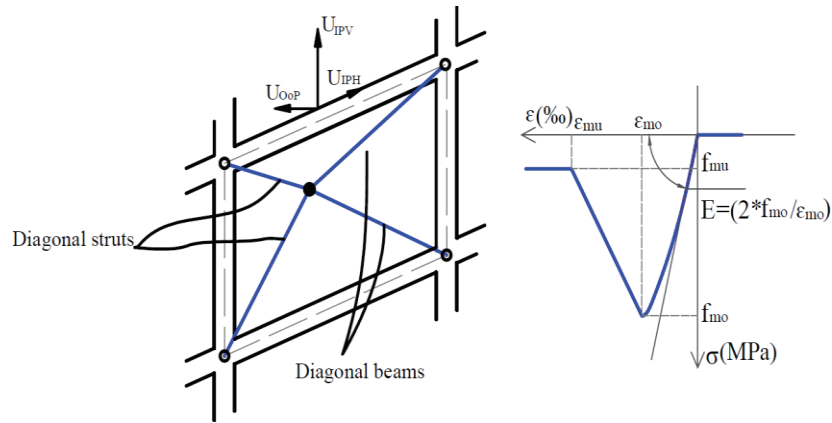


Figure 2.16 Two diagonal fiber elements model (Oliaee & Magenes, 2017)

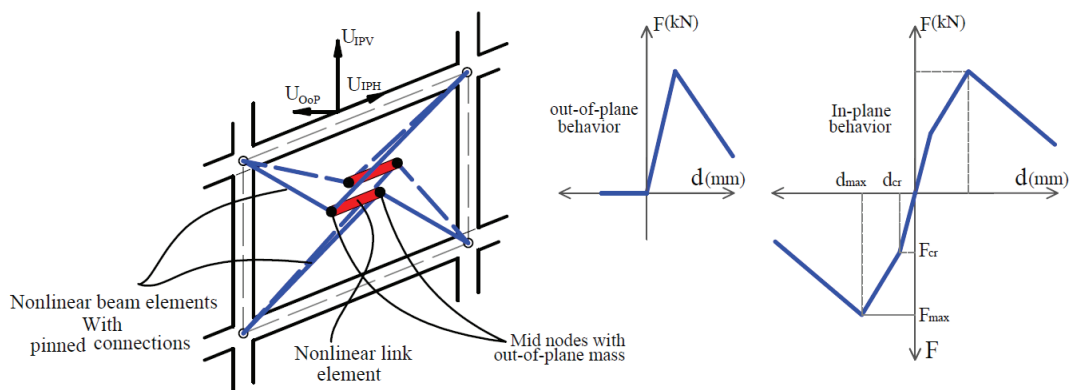


Figure 2.17 Five lumped nonlinear elements model (Mazza, 2018)

2.5 Quality Ranking with Respect to the Covered Interaction Phenomena

The evaluation of the above described models is done based on an introduced quality index. A quality index value between 1 and 4 is assigned to each model.

The higher the calculated quality index the better the model is. The assigned quality index value is based on the models ability to represent the response of the URM infill wall and it's interaction with the surrounding RC frame elements. Thus, the here considered key parameters and corresponding quantity values for the investigated 2D URM models are:

- Interactions between the URM infill and the of the surrounding frame elements. Force transfers to the joints ($Q_{int}=0$), whereas ($Q_{int}=1$ and 2) are assigned to the model in case the forces transfer to the joints, columns and beam, columns respectively.
- Number of elements required to compose the model. Thus 0 is given to the model in case the number of elements is equal or more than one and the forces transfer to the beam-column joints, whereas 1 is assigned to the model

in the opposite case (the number of elements are more than one in each direction and the forces transfer to the surrounding frame elements).

- In case the model is calibrated with the experimental data 1 is given and 0 if not.

The 3D models are ranked likewise the 2D models, but since different nonlinearity concept are adopted to represent the behaviour of the URM infill walls one more parameter, nonlinearity approach, is considered in case of 3D macromodels. A value of 0 is given to the model in case of fiber section with distributed plasticity and 1 in case of fiber section with lumped plasticity or lumped plastic hinges.

Table 2.1 and 2.2 show the assigned values for each 2D model and the quality ranking respectively.

Table 2.3 and 2.4 display the given values for each 3D model and the quality ranking respectively.

Table 2.1 Quality calculation of the 2D models

2D Model No.	Int. w/ RC frame	No. of elements	IP calibration	Q_{ind}
1	0	0	1	1
2	2	1	0	3
3	1	1	1	3
4	0	0	1	1
5	2	1	1	4
6	0	0	1	1
7	0	0	1	1
8	1	1	1	3
9	2	1	1	4

Table 2.2 Quality ranking of the 2D models

No.	2D Model	Required elements	Interaction with RC frame	Q_{ind}
1	<i>Polyakov (1960)</i>	2 diagonal linear compression struts	Joint	1
2	<i>Chrysostom (1991)</i>	6 diagonal nonlinear compression struts	Column, Beam and joint	3
3	<i>Crisafulli (1997)</i>	4 diagonal nonlinear compression struts and nonlinear shear link	Column and joint	3
4	<i>Decanini et al. (2004)</i>	2 diagonal nonlinear compression struts	Joint	1
5	<i>El-Dakhakhni et al. (2003)</i>	6 diagonal nonlinear unparallelled compression struts	Column, Beam and joint	4
6	<i>Puglisi et al. (2009)</i>	4 diagonal linear struts and plastic concentrator	Joint	1
7	<i>Rodrigues et al. (2010)</i>	4 diagonal linear struts and nonlinear shear link	Joint	1
8	<i>Burton & Deierlein (2013)</i>	4 diagonal nonlinear compression struts	Column and joint	3
9	<i>Caliò et al. (2012)</i>	2 diagonal struts; orthogonal and sliding springs (each element)	Column, Beam and joint	4

Table 2.3 Quality calculation of the 3D models

3D Model No.	Int. w/ RC frame	No. of elements	IP calibration	OoP calibration	Nonlinearity approach	Q_{ind}
11	0	1	0	0	1	2
12	0	0	1	0	1	2
13	0	0	0	1	0	1
14	0	0	1	1	0	2
15	0	1	0	1	1	3
16	0	0	1	0	1	2
17	0	0	1	1	1	3

Table 2.4 Quality ranking of the 3D models

No.	3D Model	Required elements	Interaction with RC frame	Q_{ind}
11	<i>Kadysiewski & Mosalam (2008)</i> M#5_org	1 diagonal linear strut with 2 nonlinear fiber section	Joint	2
12	<i>Furtado et al. (2015)</i> M#4	4 diagonal linear struts and nonlinear shear link	Joint	2
13	<i>Oliaee & Magenes (2016)</i>	4 diagonal nonlinear compression struts	Joint	1
14	<i>Di Trapani et al. (2017)</i>	4 diagonal nonlinear compression struts	Joint	2
15	<i>Ricci et al. (2017)</i>	1 diagonal linear strut with 2 nonlinear zero length element	Joint	3
16	<i>Longo et al. (2018)</i>	1 diagonal linear strut with 2 nonlinear fiber section	Joint	2
17	<i>Mazza (2018)</i>	4 diagonal nonlinear beams with 1 nonlinear axial link	Joint	3

Chapter 3: Experience Based Validation of the Model Input Parameters

3.1 General

Reinforced Concrete (RC) framed structures with unreinforced masonry walls (URM) are a very common structural system worldwide. In general the contribution of the URM infill panel in the structural system functionality is neglected, however many researchers proved experimentally the significant role of the URM infill walls in the global and local response of such a structural system. It confirms the observations after past and recent events. Therefore, a convenient numerical modeling scheme is considered as one of the main issues to reflect the effect of URM panels. Considerable numbers of equations have been presented in the literature to be used in the calibration of the URM numerical models. In this chapter, a database for RC frame and URM infill wall is collected and organized. In order to choose a convenient equation for the calibration of the URM infill panel numerical model, the main widely used relationships to predict the URM capacity are selected and evaluated against the available experimental results in the collected database. Finally, for a classification target of the available samples in the database the ratio of the shear and moment capacity of the RC frame column was used as an index to classify the RC frame as ductile (strong) and non-ductile (weak). Furthermore, since the stiffness of the infill controls the behaviour of the infill it is used to classify the infill as strong or weak.

3.2 Secondary Element Empirical Strength Models

The first model considered herein to define the envelope curve of the force-displacement relationship for the equivalent strut is the model proposed by *Bertoldi et al. (1993)*. Such a model is the only one among those considered herein that is able to account for and predict the failure mode that can be exhibited by the infill panel. It was proposed and validated on the basis of experimental results, mostly including tests on structural-masonry walls. The ultimate capacity depends on the predicted failure mode (depending on the infill mechanical properties, such as cracking shear strength obtained by diagonal compression tests, sliding strength of the bed joints derived from triplet tests, compressive strength of masonry, and vertical stress acting on the infill).

Model by *Panagiotakos & Fardis (1996)* was calibrated on the basis of eight tests on infilled RC frames with hollow masonry bricks that mainly exhibited a diagonal cracking failure mode.

The last considered model is the one proposed by *Zarnic et al. (1997)*; the proposed expression for predicting the maximum shear strength of the URM infill wall was derived taking into account the mutual interaction between the RC frame and URM infill panel.

To verify the prediction of the aforementioned empirical equations against the experimental results in the database, an analytical prediction of lateral load capacity is derived (Equation 3.1), hence, the total shear capacity of the RC frame with URM infill wall can be obtained as follow:

$$F_{\max} = F_{\text{bare}} + F_{\text{urm}} \quad 3.1$$

Where, F_{bare} is the bare frame shear capacity, which can be predicted as $(4M_u/h_{\text{col}})$ in which M_u and h_{col} are the flexural capacity and height of the column, respectively. F_{urm} is the shear force that the masonry infill wall can withstand as defined in table 3.1.

Table 3.1 URM infill wall maximum strength proposals for empirical models

Empirical model	Ref.
$F_{URM} = \sigma_{min} * W_{st} * t_{URM} * \text{Cos}\theta$ $\sigma_{min} = \min \left(\begin{array}{l} \frac{1.1 * \sigma_{mo} * \text{Tan}\theta}{K_{11} + K_{22} * \lambda * H_{URM}} \\ \frac{1.12 * \sigma_{mo} * \text{Sin}\theta * \text{Cos}\theta}{K_{11}(\lambda * H_{URM})^{-0.12} + K_{22} * (\lambda * h_{URM})^{0.88}} \\ \frac{(1.2 * \text{Sin}\theta * 0.45 * \text{Cos}\theta)u + 0.3 * \sigma_{mo}}{\frac{K_{11}}{\lambda * H_{URM}} + K_{22}} \\ \frac{0.6 * \tau_{mo} + 0.3 * \sigma_{mo}}{\frac{K_{11}}{\lambda * H_{URM}} + K_{22}} \end{array} \right)$	<i>Bertoldi et al. (1993)</i>
$F_{URM} = 1.3 * l_{URM} * t_{URM} * f_{tp}$	<i>Panagiotakos & Fardis (1996)</i>
$F_{URM} = \frac{0.818 * L_{URM} * t_{URM} * f_{tp}}{C_I} * \left(1 + \sqrt{C_I^2 + 1} \right)$ $C_I = 1.925 * \frac{L_{URM}}{H_{URM}}$	<i>Zarnic et al. (1997)</i>

Notations:

W_{st} : Compression strut width, t_{URM} : Thickness of the infill wall

L_{URM} : Length of the infill wall, H_{URM} : Height of the infill wall

λ : Coefficient used to determine equivalent width of infill strut

θ : Angle whose tangent is the infill height to length aspect ratio, radians

σ_{mo} : Compressive strength of the infill wall

u : Sliding resistance of the bed joint,

τ_{mo} & f_{tp} : Shear strength from the diagonal test

Table 3.2 The parameter K_{11} & K_{22}

	$\lambda H_{URM} < 3.14$	$3.14 < \lambda H_{URM} < 7.85$	$\lambda H_{URM} > 7.85$
K_{11}	1.3	0.707	0.47
K_{22}	-0.178	0.01	0.04

3.3 Experimental Samples

3.3.1 Recorded input/output Parameters

A considerable number of tests on infilled RC frames have been carried out during the past forty years with different configuration, material properties for both the RC frame elements and URM infill panel and loading direction. In this research, only tests characterized by unreinforced masonry URM without opening and tested in the in-plane and out-of-plane direction were considered. The list of the collected specimens is presented in Appendix A. The distribution of the selected samples regarding the type of loading is depicted schematically in Figure 3.1.

The total number of samples is 84 1-bay, 1-storey tests, 51 of these tests were completely described by the authors of the experimental campaigns and used hereafter.

The main target of collecting the datasets is to assess the most widely used empirical models for URM infill panel capacity in order to select the proper equation which could be used in the calibration of the numerical models under study. Thus,

- Firstly, it is important to record the most significant parameters included in each empirical equation determined to be evaluated.
- Secondly, the necessary parameters to create the numerical models for the calibration purposes have to be included (see Appendix A).

Consequently, 16 parameters are selected in which seven are used to define the geometry of the RC frame and URM infill panel, six for the material properties and two specified the reinforcement layout (see Table 3.3). The last parameter is to define the applied vertical loads.

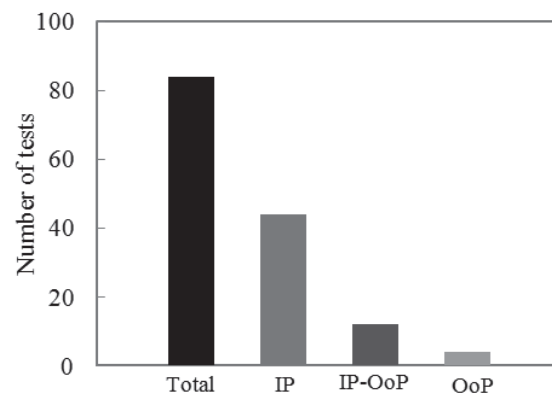


Figure 3.1 Database including all tests collected from literature

Table 3.3 Recorded input parameters

Parameter	Description	Parameter	Description
L_{URM} [m]	Length of the infill wall	f_{ck} [MPa]	Frame compressive strength
H_{URM} [m]	Height of the infill wall	f_y [MPa]	Steel yield strength
a_{cOoP} [mm]	Column width	E_c [GPa]	Modulus of elasticity of concrete
b_{cIP} [mm]	Column depth	f_{URM} [MPa]	Masonry compressive strength
a_{bOoP} [mm]	Beam width	f_{tp} [MPa]	Masonry shear strength
b_{bIP} [mm]	Beam depth	E_{URM} [MPa]	Masonry modulus of elasticity
ρ_B [%]	Beam reinforcement ratio	t_{URM} [mm]	Masonry thickness
ρ_C [%]	Column reinforcement ratio	N [kN]	Vertical loads

The output to be used in the evaluation of the adopted empirical equations and later on for the calibration/evaluation of the numerical models is as well collected. For this purpose, the maximum shear recorded for each sample is added to the database. Moreover, the force-displacement curves of the specimens are digitized in the form of force displacement vectors when needed.

3.3.2 Analytical/Experimental Results

Experimental results, namely peak strength, obtained from the collected tests performed at different laboratories as explained in the previous chapter are compared with results of theoretical expressions (Figure 3.2).

All expressions presented before are taken into account to compare the predicted shear capacity by those obtained from tests. As Figure 3.2 shows; the model presented by *Bertoldi et al. (1993)* underestimated the experimental peak strength in all cases. The average error expected to attain at 51 % and the coefficient of variation 33%. Whereas the other two models gave close results to each other as Figure 3.1 illustrates with an average error of about 25% and coefficient of variation 38 % (see Table 3.4).

Table 3.4 Calculated error and coefficient of variation

Empirical model	<i>Bertoldi et al. (1993)</i>	<i>Panagiotakos & Fardis (1996)</i>	<i>Zarnic et al. (1997)</i>
Avg.	0.51	1.26	1.24
C.o.v	0.33	0.37	0.38

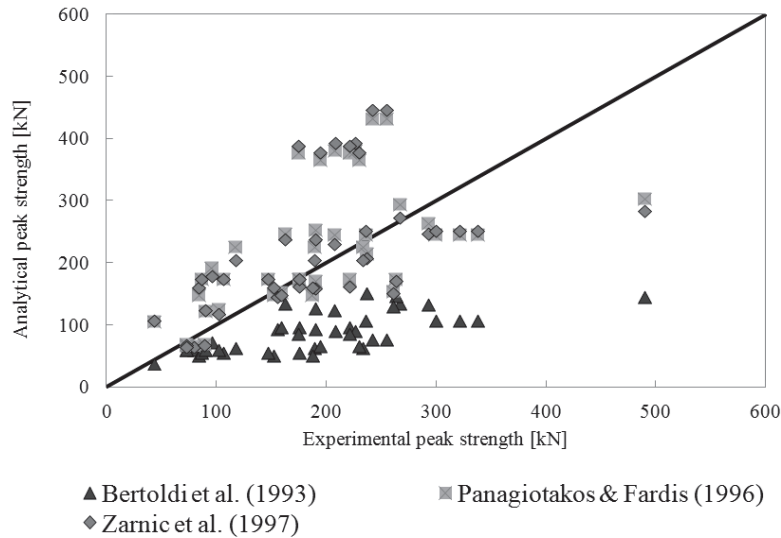


Figure 3.2 Experimental/analytical peak strength

Model by *Zarnic et al. (1997)* generally shows values of C.o.v.; that are slightly higher than those related to the other models. Furthermore, the model appears easier to apply and it has been used for the calibration of several numerical macromodels such as the model proposed by *Furtado et al. (2010)*.

Since the aforementioned model requires a very limited number of mechanical parameters and considers the interaction between the RC frame and the masonry wall, even if it is not able to predict a failure mode for the infill panel, consequently, herein, a slight modification of the model is proposed.

As shown in Figure 3.3, to obtain a simple equation to predict the maximum capacity of the URM infill panel, the parameter β is defined as presented in Table 3.5 and plotted for each sample in the database. Subsequently the minimum and maximum value is considered as a range of the parameter and the simplified Equation 3.2 is obtained. The equation will be adopted in the up following chapters to calibrate the macromodels under study.

Table 3.5 Parameter β

Parameter $\beta[-]$	Ref.
$\beta = 1.3$	<i>Panagiotakos & Fardis (1996)</i>
$\beta = \frac{0.818}{C_I} * \left(1 + \sqrt{C_I^2 + 1} \right),$ $C_I = 1.925 * \frac{L_{URM}}{H_{URM}}$	<i>Zarnic et al. (1997)</i>

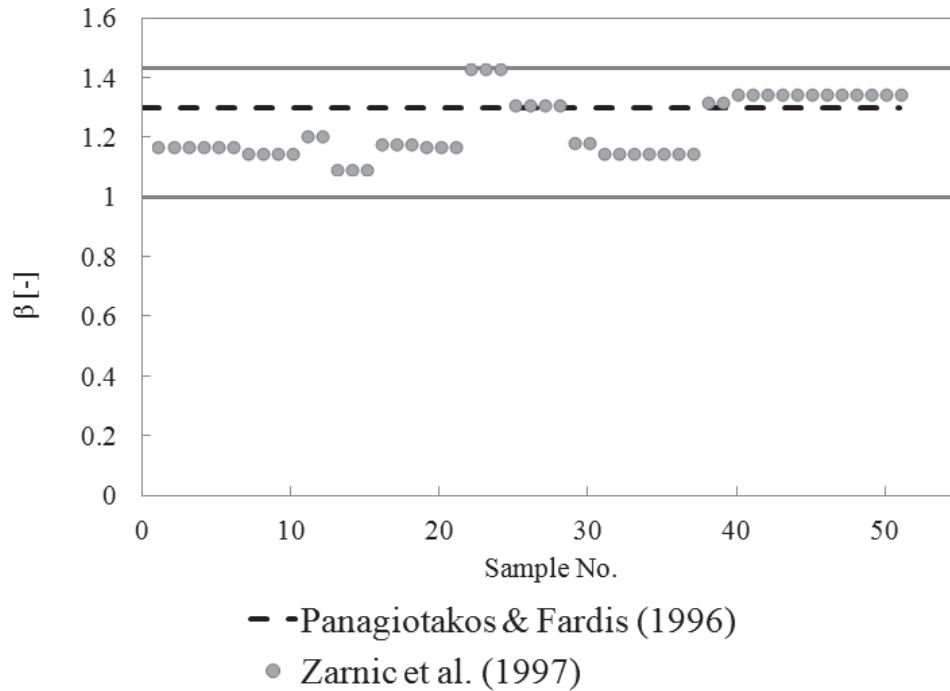


Figure 3.3 The calculated coefficient β

$$F_{max} = (1.00 \text{ to } 1.43) * l_{URM} * t_{URM} * f_{tp} \quad 3.2$$

3.4 Types of Primary and Secondary Elements due to Material Variability

From the experimental investigations that were carried out by several researchers it has been shown that the presence of infill panels improves the seismic performance of a frame. The stronger the infill and the frame, the higher is the seismic resistance and better performance than those with weak infill (*Mehrabi et al., 1996*).

To investigate the effect of considering different material properties on the structural response of RC frame with URM infill walls, *Mehrabi et al. (1996)* carried out an experimental campaign in which they considered two types of RC frame. The first was designed for moderate wind load representing older structures which doesn't meet the earthquake detailing and referred as weak frame. The second was designed due to the seismic detailing and considered as strong frame. As for infill panels both solid and hollow masonry walls were considered as a representative of strong and weak infill walls respectively. The URM material properties are included in Table 3.6.

The author concluded that the specimens with strong infill and strong panels exhibited better performance than those with weak frame and weak panels in terms

of damage distribution and energy dissipation. The dominated damage pattern in case of strong RC frame and strong infill was flexural failure of the columns and beams, whereas diagonal cracking and bed joint sliding was observed in the URM masonry walls. The weak RC frame combined with weak infill walls showed brittle shear-flexural failure of the columns and diagonal cracking accompanied with crunching of the masonry hollow concrete units. Figure 3.4 shows the observed experimental failure pattern of the specimen 4 which was designed as weak frame with weak infill. **Kakaletsis (2007)** carried out investigation on strong RC frame infilled with weak and strong brick masonry walls. The adopted masonry properties are shown in Table 3.7. It could be clearly observed from the table that the higher the masonry wall modulus of elasticity the stronger the wall.

Table 3.6 URM class according to *Mehrabi et al. (1996)*

URM class	URM type	Key parameter		
		f_m [MPa]	E_{urm} [MPa]	f_{tp} [MPa]
Strong	Solid concrete block	10	8.3	---
Weak	Hollow concrete block	15	4.5	---

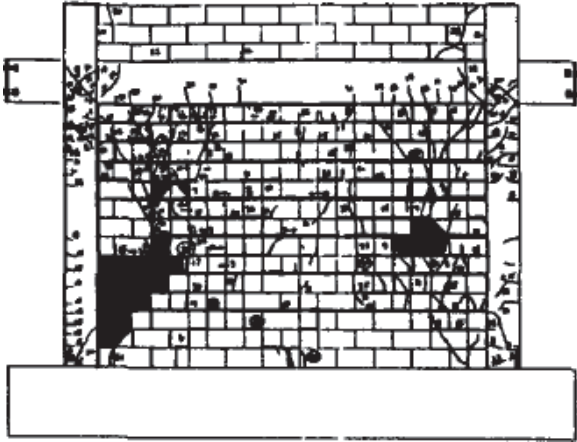


Figure 3.4 Experimental damage of specimen 4 according to *Mehrabi et al. (1996)*

Table 3.7 URM class according to *Kakaletsis (2007)*

URM class	URM type	Key parameter		
		f_m [MPa]	E_{urm} [MPa]	f_{tp} [MPa]
Strong	Vitrified ceramic bricks	15.2	2837	0.12
Weak	Hollow concrete block	2.6	660	0.08

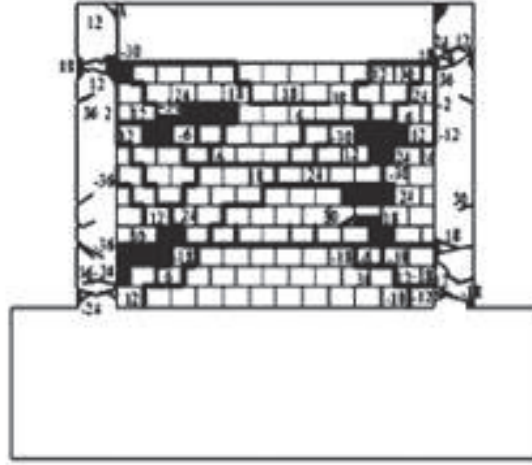


Figure 3.5 Experimental damage of specimen (S) according to *Kakaletsis (2007)*

The experimental results indicated that the RC frames exhibited flexural failure pattern and no shear-flexural failure of the column was observed. On the other hand the weak infill panel showed diagonal cracking and crushing as Figure 3.5 illustrates, whereas the strong panel suffered bed joint sliding without crushing.

In purpose to numerically check the variability of the material properties of both the RC frame element and the masonry panel on the seismic response of multi-story infilled structures, *Šipoš et al. (2018)* presented a simplified classification of the components. Accordingly the RC frame elements were considered as weak in case the column longitudinal reinforcement ratio is 1% and strong with a ratio of (1.1% - 2.7%) depending on the number of stories.

Regarding the masonry panels the material stiffness and strength was considered. Accordingly the panel with higher stiffness and strength was the strong panel as Table 3.8 shows. On one hand, the results of the numerical study referred to more preferable use of strong and medium type masonry due to lower damage suffered by both type in comparison with the weak URM infill panel. On the other hand, the RC frame with 1% reinforcement ratio suffered a heavy concentrated damage at the lower stories whereas in case of reinforcement ratio 1.1% - 2.7%, moderate damage was distributed along the height of the considered frames.

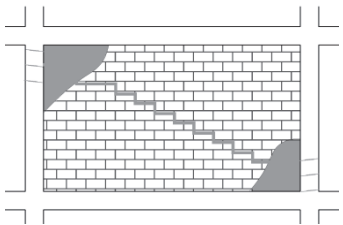
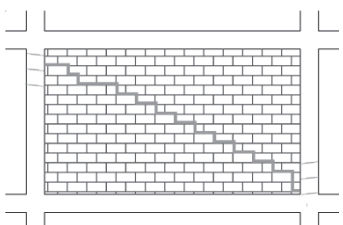
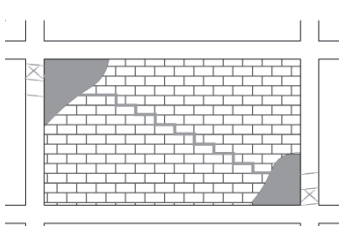
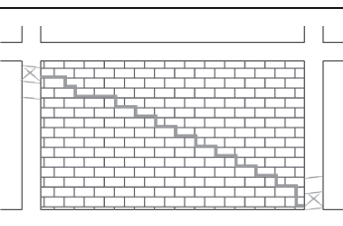
Recently, utilizing a detailed micro model, of the primary (RC frame elements) and secondary (URM infill wall), a comprehensive parametric study proposed by *Tempestti et al. (2017)*, in order to develop a consistent classification scheme.

Table 3.8 URM class according to Šipoš *et al.* (2018)

URM class	URM type	Key parameter		
		f_m [MPa]	E_{urm} [MPa]	f_{tp} [MPa]
Strong	Solid clay brick	15.2	2755	---
Medium	Euroterm	2.6	1606	---
Weak	Auto Aerated Claved	1.71	643	---

The developed classification methodology was validated using the experimental results presented by *Mehrabi et al. (1996)*; *Stavridis (2009)*. Thus, the investigated structural system, due to the variability of the material, was categorized into four classes with a distinct failure mechanism for each (see Table 3.9).

Table 3.9 Typical damage of the RC frame with URM infills for the defined frame and wall classes according to *Tempestti et al. (2017)*

RC	URM	Expected failure pattern	
Strong	Weak	Flexural cracking of the RC frame elements.	
		Diagonal cracking, bed joint sliding and crushing of the URM infill panel.	
Strong	Strong	Flexural cracking of the RC frame elements.	
		Diagonal cracking and bed joint sliding of the URM infill panel.	
Weak	Weak	Flexural-shear cracking of the RC frame elements.	
		Diagonal cracking, bed joint sliding and crushing of the URM infill panel.	
Weak	Strong	Flexural-shear cracking of the RC frame elements	
		Diagonal cracking and bed joint sliding of the URM infill panel.	

3.5 Classification Scheme for Primary and Secondary Elements

For the purpose of RC frame with URM infill panel classification one parameter is considered to represent each part of the classified system.

- The first parameter is strength ratio, i.e. the ratio of the column's section nominal shear strength to the shear force required to develop two plastic hinges in the column, (see Tables 3.10, 3.11). Consequently, the RC frame is categorized as non-ductile (weak) or ductile (strong).
- The second adopted parameter is the normalized modulus of elasticity of the URM infill walls which is considered as a quantity to represent the stiffness ratio of the URM infill wall. Thus, the infill wall is characterized as weak or strong.

The aforementioned quantities are calculated for each sample in the database utilizing the parameters in Table 3.11.

Figure 3.6 shows the relationship between the strength ratio (V_n/V_p) of each specimen and the normalized modulus of elasticity of the URM infill panels. Each sample on the plot with a strength ratio less or equal to one is classified as weak RC frame and strong in case the ratio is larger than.

The URM infill walls are as well classified as weak or strong according to the calculated stiffness ratio (E_{URM}/E_{URM_max}). Accordingly the higher ratio refer to a stronger infill wall. However one exception is the experimental models proposed by **Mehrabi et al. (1996)** which is classified to have a weak wall at a ratio of ($E_{URM}/E_{URM_max} = 0.2$) due to the high value of the modulus of elasticity for URM infill panels in the experimental campaign in comparison with the other specimens (see Table 3.6 and Figure 3.6).

Table 3.10 Classification scheme

RC	Non-Ductile (weak)	Ductile (strong)
	$(\frac{V_n}{V_p} \leq 1)$	$(\frac{V_n}{V_p} > 1)$
URM	Weak	Strong
	$\frac{E_{URM}}{E_{URM,max}} = [0.1 - 1]$	

Notations:

V_n : Column shear strength accounting for the shear resistance of concrete and transverse reinforcement ACI 318 (see Table 3.11).

V_p : Column shear force corresponding to the development of plastic hinges at the column edges (Table 3.11).

E_{URM} : Infill wall modulus of elasticity.

$E_{URM,max}$: Maximum infill wall modulus of elasticity recorded in the database.

Table 3.11 RC frame classification parameters

Parameter	Value
V_p	$\frac{2M_p}{H_{Col}}$
V_n	$\Omega(V_c + V_s)$
V_c	$0.17 \left(1 + \frac{P}{14 * A_g} \right) \sqrt{f'_c} A_g$
V_s	$\frac{A_v f_{yv} d}{s} \leq 0.66 \sqrt{f'_c} A_g$

Notations:

M_p : RC column plastic moment capacity.

H_{Col} : RC column height.

$\Omega = 0.85$: Shear strength reduction factor.

V_c : Concrete shear strength, P : Applied vertical loads

A_g : RC column cross section area

V_s : Transverse steel shear strength.

A_v : Area of transverse steel, d : cross section depth

s : Spacing between transverse steel

f'_c : Compressive strength of concrete.

f_{yv} : Yielding strength of the transverse steel.

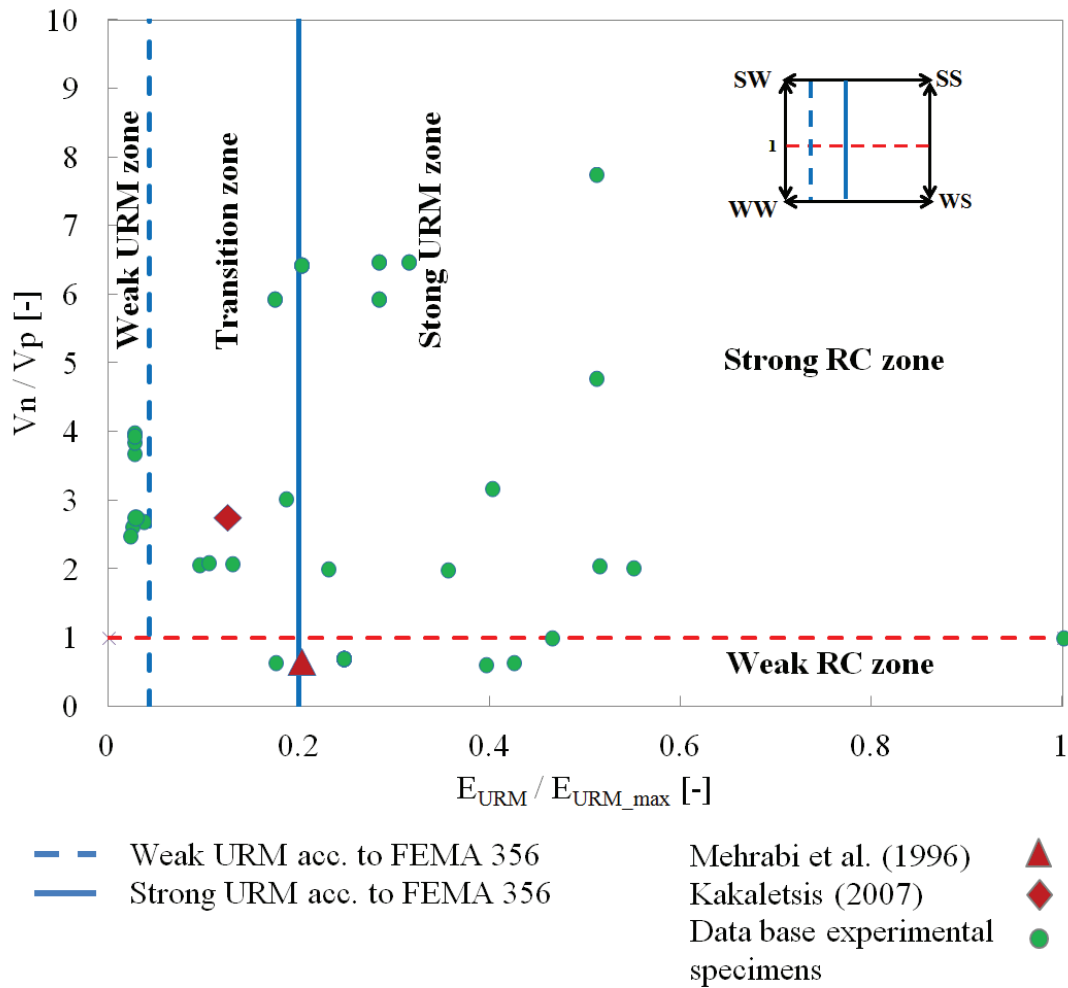


Figure 3.6 The database classified samples

3.6 Summary

In this chapter, a homogenous extensive database of experimental tests on RC frames infilled with unreinforced masonry panels without openings is collected and presented. The main and widely used empirical models existing in literature for infills in the context of single-strut models have been investigated and compared with the experimental results in order to select a model to be used for the calibration of the numerical macromodel with minimum error. In particular, predicted-to-experimental ratios related to the main parameters that describe the empirical model, i.e. the maximum strength, of the infill response are obtained and analysed for models by *Bertoldi et al. (1993)*, *Panagiotakos & Fardis (1996)* and *Zarnic et al. (1997)*.

It was observed that the model by *Bertoldi et al. (1993)* significantly underestimates peak strength with an average value of 51%. The other two models give similar results with an average overestimate of the maximum strength attained 25%.

The latter model proposed by *Zarnic et al. (1997)* has been used by different researchers to calibrate their macromodels, e.g., (*Furtado et al. 2010*).

Consequently the model was chosen and slightly modified utilizing the results of the database samples. Thus a simple practice oriented equation is proposed (Equation 3.2).

To investigate the material variability of both the RC frame and URM on the resulting seismic performance the available experimental and numerical studies were presented.

The aforementioned review indicates the strong influence of the combination of RC frame and URM panel on their performance, basically in term of load resistance, stiffness and damage mechanism. Subsequently an up to date classification methodology, of the structural system in hand, was selected and applied on the database samples. The results again referred to the strong influence of the strength and stiffness of the RC frame elements and URM infill walls on the class of the system which in turn has a direct influence on the predicted failure pattern.

Chapter 4: Primary Macromodel

Assessment

4.1 Experimental Review (Multi-Story RC Systems)

Several scaled and full-scale experimental studies on RC frame structures are utilized to calibrate and assess the models in hand.

Compared to component tests, i.e. 1 story - 1 bay experimental model, literature on scaled and full scale RC buildings/structures with masonry infill wall tests is rather limited.

To investigate the effect of the masonry infill walls on the behaviour of concrete frames, *Bertero et al. (1983)* carried out an experimental test in which a series of quasi-static cyclic and monotonic loads were applied on a 1/3 scale experimental model. It was a representative of the first three stories of an eleven story-three bay reinforced concrete structure infilled in the two external bays.

The researchers concluded that the existence of the masonry infill walls have the influence to increase the stiffness, strength, the demands for a given earthquake and subsequently the horizontal design forces.

To check the influence of the boundary conditions between the RC frame and the URM infill walls on the performance of the infilled RC frame structures, *Liauw et al. (1985a)* conducted an experimental campaign in which a scaled four story infilled frames were tested due to the application of a harmonic load on the top of each frame. Three types of connection between the RC frame and infill wall were considered.

1. Frame/infill wall without connectors around the interface.
2. Frame/infill wall with connection along the beam/infill.
3. Frame/infill wall with connection along the entire edges.

The authors concluded that the frame/infill wall with connections around the entire interface dissipate more energy than the other types. Furthermore, it proved to have more stiffness, strength and ductility.

To investigate the behaviour of RC frame with URM infill walls *Manos et al. (1990)* utilized different loading techniques; these were static, low level impulse loading, and earthquake excitations. Two story scaled RC frames infilled with solid clay bricks were tested. The authors stated in their report that the presence of masonry infill walls altered significantly the seismic performance of the tested RC frame.

An experimental campaign on a four-story full scale reinforced concrete frame was carried out at the European Laboratory for Structural Assessment (ELSA) in Ispra, Italy by *Negro et al. (1994)*, aiming the global information on dynamic response by comparing structural behaviours of a bare frame and infilled one. Pseudo Dynamic (PsD) analysis was conducted utilizing the 1976 Friuli earthquake accelerogram. Three different configurations of the tested structure were considered: namely bare (BR), uniformly infilled (UNI) and soft story (SS) frame.

Fardis et al. (1999a) tested a 3-story full scale RC infilled building with open top storey. The structure was designed following/according to Eurocodes 2 and 8 rules. The RC frames were detailed to fulfil the requirements of medium ductility and a peak ground acceleration of 0.3g. The ground motion used in the test was scaled up to 0.45g and applied twice. After the first test, minor cracks were observed in the URM infill walls, whereas no damage occurred at the RC frame. On the other hand, repeating the test once more lead to visible cracks of the top story's beams and columns.

Buonopane et al. (1999) examined a test on (1/2) scale two story, two bay infilled RC frame with window openings in the second story. The reported damage state was bed joint shear cracking in the first story's URM infill panels whereas, the infill walls in the second story suffered a diagonal cracking failure mechanism.

To evaluate the effect of plaster on the URM infill walls, *Marjani et al. (2002)* applied cyclic loading on a two story one bay brick infill RC frames. The authors concluded that the presence of plaster has the effect to increase the strength of the tested frame of about 25%.

Varum (2003), carried out an experimental campaign on two representative full-scale four story, three-bay RC frames. The first frame was a bare one and the second was infilled frame with opening. Both frames were separately subjected to IP pseudo

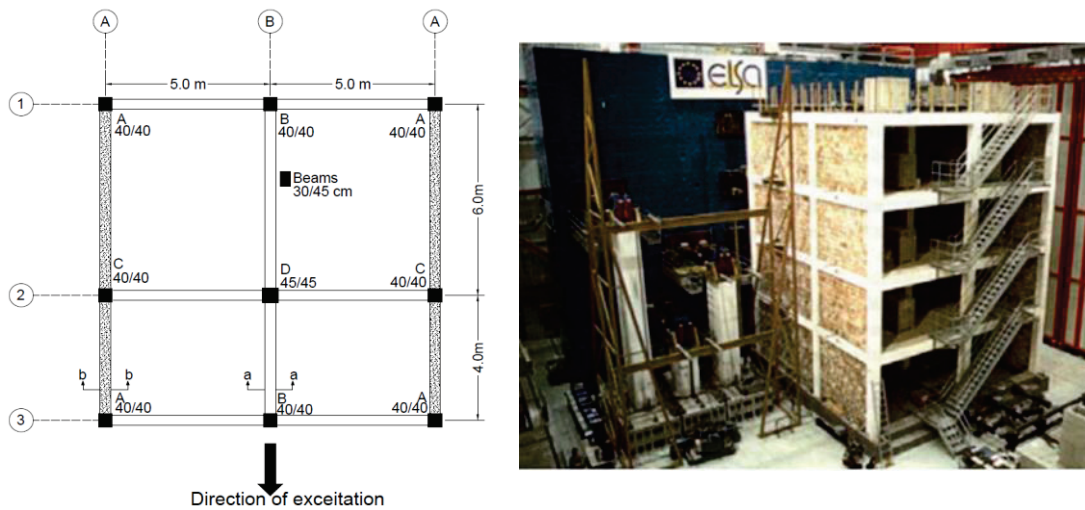
dynamic test (PsD) to assess their seismic performance. Subsequently the both damaged frames, i.e. the bare and infilled, were retrofitted and further excited to evaluate the efficiency of different retrofitting solutions.

One very important concern about the up-to-date presented experiments is the lack of considering the OoP failure pattern. Recently *Sigmund et al. (2014)* examined an experiment on a 1:2.5 scaled 3D building infilled RC structure. The specimen consists of three stories, two bays in the longitudinal direction and one bay in the transverse direction.

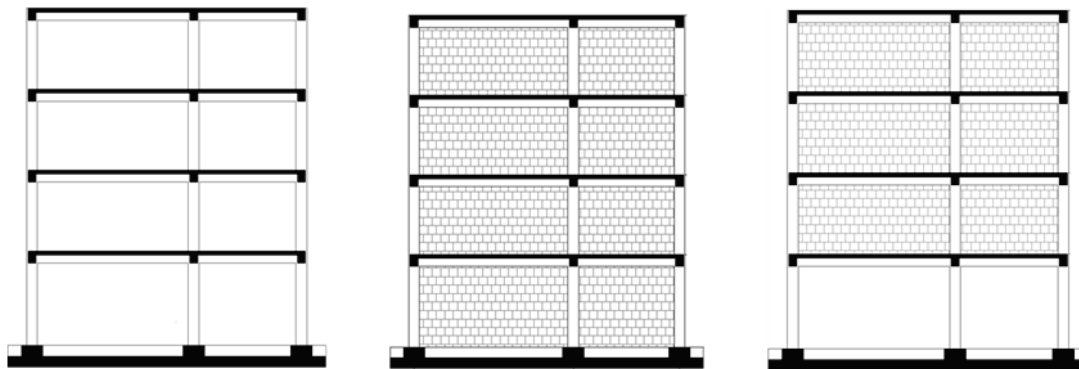
The structure was subjected to ten incremental earthquake sequences in the longitudinal direction, thus the longitudinal URM infill walls were excited IP and the transverse once responded OoP. The experimental model experienced ground shaking up to 1.2g. Heavy damage was observed at the first and second story URM infill panels, whereas the failure mechanism of the RC frame element was recognized as minor cracks.

4.2 Reference Object Description

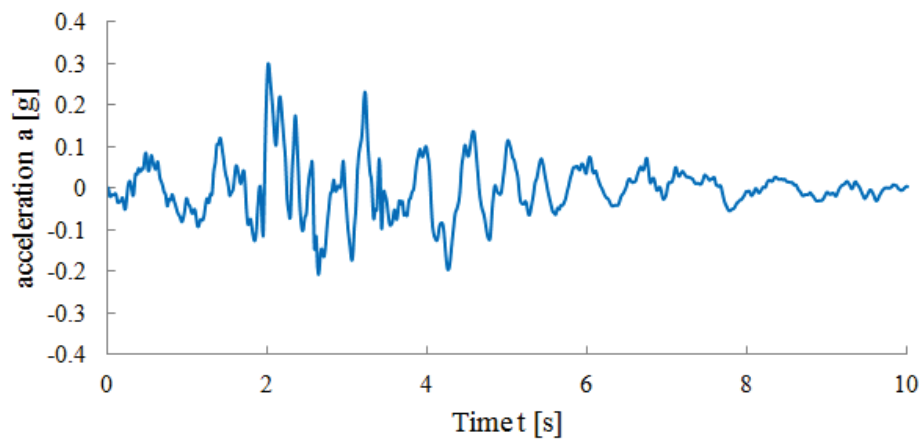
An experimental campaign on a four-storey full scale reinforced concrete frame was carried out in the European laboratory for structural assessment (ELSA) at Ispra, Italy by *Negro et al. (1994)*. Figure 4.1 a, shows the general layout of the tested structure. The structure was designed adopting high ductility RC frames requirements according to Eurocode 2 and 8, for a peak ground acceleration $a_g=0.3g$ and soil type B. The structure consists of two bays in both directions, two 5m span in the transverse direction and two of 6m and 4m span in the longitudinal direction, i.e., direction of excitation. The inter storey height is 3.5m for the first story, 3m for the other stories and the slab thickness is 0.15 m. The thickness of masonry infill is 11.2 cm. The resulting masses, which were taken into account in the pseudo-dynamic tests, were: 87t, 86t and 83t for the bottom, second and third, and top storeys, respectively. Full details about the structure geometry, the cross sections dimensions, reinforcement detailing and the used material mechanical properties are available in Appendix B. Pseudo-dynamic tests were performed on the full scale structure with different configuration. The accelerogram used in the test was generated from a real accelerogram which was recorded during the 1976 Friuli Earthquake. Figures 4.1 b & c, bdepict the plane, vertical layout and the used accelerogram.



a) Experimental layout



b) Experimental configuration



c) Used time history record

Figure 4.1 Experimental specimen according to *Negro et al. (1996)*: a) plane and experimental layouts, b) elevation view and c) used time history.

4.3 Implemented Numerical Modeling Approaches

4.3.1 Primary Element Models

According to the previously discussed nonlinear modeling approaches and utilizing the concept of lumped plasticity, 3D finite element models of the reference object are created in SAP2000.

In the first model, concentrated rigid plastic hinges are assigned at beam-column end sections. As for beams, localized moment plastic hinges (MPHs) can be used whereas, to account for the axial-force/biaxial-moment interactions, axial-force/biaxial-moment PMM plastic hinges are assigned to the columns. In a MPH, post-yield behaviour is typically described by a moment–plastic rotation relationship as shown in Figure 4.2 a. Likewise, in a PMM plastic hinge, a 3D interaction yield surface is first defined, as shown in Figure 4.2 b, and then, the post-yield behaviour of the element will be interpolated from moment-rotation curves.

In the second model, nonlinearity is considered at elements end sections by using PMM fiber hinges modeling approach. The hinge length is adopted to be as half of the higher cross section dimension according to *Furtado et al. (2015)*.

As for the constitutive models, the uniaxial *Mander et al. (1983)* concrete material model was used for both unconfined and confined concrete fibers considering tensile strength of concrete with a linear decay. The uniaxial ‘Reinforcing Steel’ material model according to the work of *Chang & Mander (1994)* is also adopted for the stress–strain relationship of steel fibers. Uniaxial stress–strain relationships of concrete and reinforcing steel fibers are depicted in Figures 4.3 a and b.

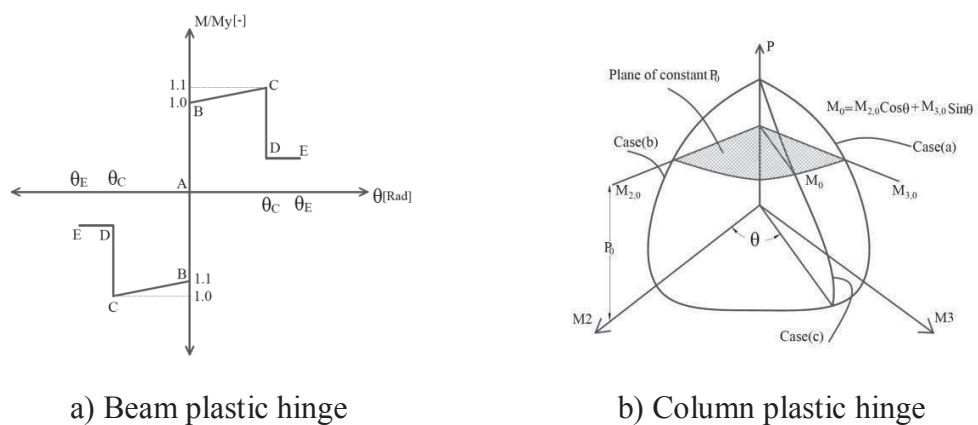


Figure 4.2 Plastic hinge definition: a) Moment–plastic rotation relationship in a typical MPH, b) A typical 3D interaction yield surface for the axial-force/biaxial-moment interaction in a PMM plastic hinge

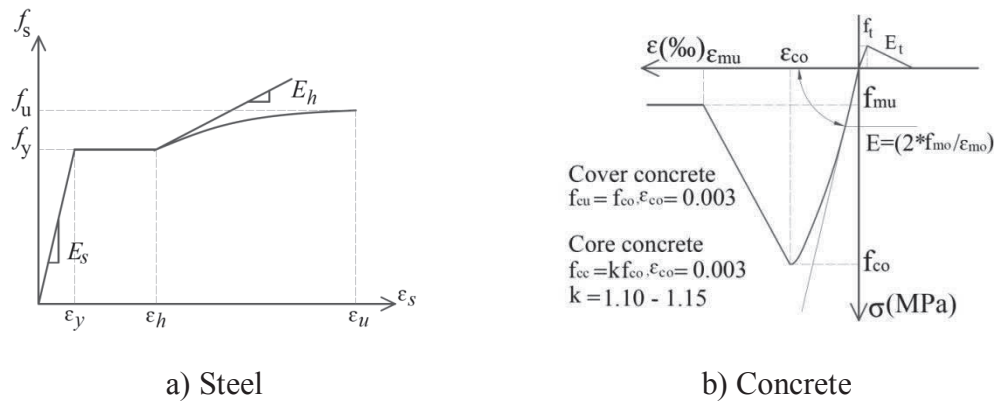


Figure 4.3 Uniaxial stress–strain relationships: a) steel, b) concrete

In both considered models, appropriate effective flexural rigidity are assigned to the cracked beam and column sections to account for redistribution of forces due to cracking.

To assess the validity of the above proposed modeling strategy for RC frame elements and URM equivalent macro elements, representative numerical macromodels of the aforementioned 4 story RC structure are created with different configuration, namely bare, uniformly infilled and soft story structure by using SAP2000. Dynamic analysis is performed on adopting the accelerogram used in the pseudo dynamic test.

4.3.2 Secondary Element Models

Many models have been developed to describe the cyclic nonlinear behavior of diagonal struts equivalent to infill walls. However, in order to perform dynamic nonlinear analyses for RC structures with URM infill walls, a flexible hysteretic model requiring few parameters and a low computational effort, with sufficient reliability in the results, has been proposed by *Cavaleri et al. (2014)*. The model is further used to validate the shear link elastic strut macromodel by *AL Hanoun et al. (2018)*. The advantage of using the Pivot model is essentially due to the fact that this model is based mainly on geometrical rules that define loading and unloading branches rather than analytical laws. It is nevertheless capable to represent observed features of real hysteresis cycles. This reduces not only the computational effort but also the number of hysteretic parameters involved. Moreover, the Pivot model has great flexibility in modeling unsymmetrical tension–compression behaviors, as in the case of infill equivalent struts which are considered resistant only to compression stresses (see Figure 4.4).

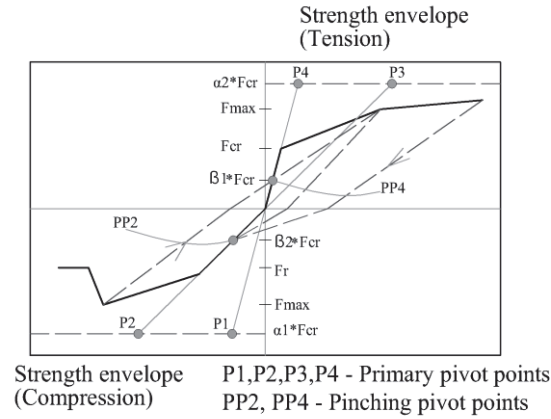


Figure 4.4 Pivot model used as a representative of URM wall

The following values are adopted for the parameters of the URM infill panel envelop curve:

- The maximum strength (F_{max}) can be calculated through Equation 4.1, in which f_{tp} is the masonry crack strength obtained according to *Negro et al. (1996)*, while t_{URM} , L_{URM} are the thickness and the length of the URM infill wall respectively. The maximum deformation (δ_{max}) occurs approximately between ($0.25\%H_{URM}$ and $0.75\% H_{URM}$).
- The ratio of the cracking to maximum strength is about ($0.45 < F_{cr} / F_{max} < 0.8$) and the cracking deformation (δ_{cr}) is given between the values ($0.05\%H_{URM}$ and $0.15\%H_{URM}$) (*AL Hanoun et al., 2018*).
- The residual strength (F_r) is estimated as 30-60% of (F_{max}) and the post-peak deformation (δ_r) is a bout ($1\%H_{URM}$ to $1.5\%H_{URM}$) (*AL Hanoun et al., 2018*).

$$F_{max} = (1.00 \text{ to } 1.43) * f_{tp} * L_{URM} * t_{URM} / \cos\theta \quad 4.1$$

The above assumptions and experimental data are used to calculate the envelope parameters of the URM panel (see Appendix B).

4.4 Dynamic Analysis and Simulation Results

Nonlinear dynamic analyses are performed for both of the structural models and for the ground motion record presented in Figure 4.1 c, which was used in the pseudo-dynamic tests. The considered peak ground accelerations were 0.15g and 0.45g.

In general, quite good agreement was observed between the calculated and experimental results in the case of fiber hinges for RC elements. However, it was

recognized, as expected, that in the cases of rigid plastic hinges models are not appropriate for simulating seismic response, in particular, in the post peak displacement range, since the moment-rotation relationship of the plastic hinges was modeled only with the bi-linear (bi-linear with steep softening, Figure 4.2 a) moment-rotation relationship. Besides, neither MPHs nor PMM plastic hinges account for the axial–flexural deformation interactions (Figures 4.5 a to d).

Contrary to the concentrated plasticity approach using MPHs, fiber-based modeling approach accounts for the plasticity distribution as well as axial–flexural deformation interaction at sectional level. Furthermore, force redistribution due to cracking and crushing of concrete fibers as well as yielding or rupturing of reinforcing steels can be robustly reflected by assigning realistic uniaxial stress-strain relationships to the concrete and steel fibers at beam-column cross-sections.

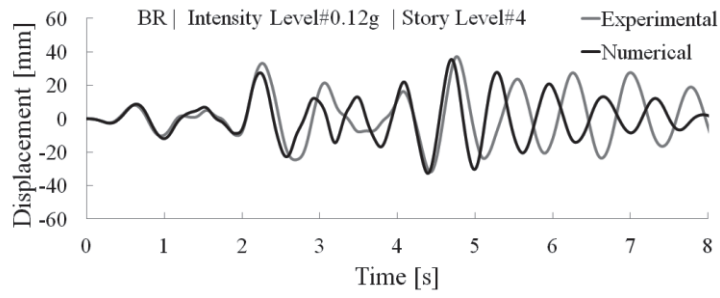
Figures 4.6 a to d show the resulting numerical and experimental top displacement for both uniformly infilled structure and the soft story one due to 0.45g excitation level. It can be clearly observed that in the case of uniformly infilled structure not a big difference in the resultant numerical response exists between both considered model that is due to the less contribution of the beam and column elements to the total response in comparison to the URM infill panels. On the other hand, likewise for the bare model, better agreement was obtained in the case of soft story model utilizing the fiber section approach, since the global response is mostly due to the participation of the first story beams and column elements.

4.5 Quality assessment of the Primary Macromodels

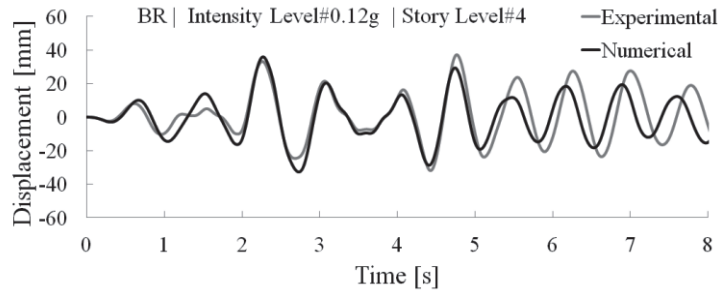
Quality assessment measures are those quantities we calculate to demonstrate the accuracy of the utilized forecasting models (how close to the real results the predicted ones are).

For the assessment of the RC frame element models in hand, the correlation matrix between the predicted numerical and measured experimental time history displacement at the different story levels is adopted/determined, thus the normalized correlation indices are calculated by means of Equation 4.2.

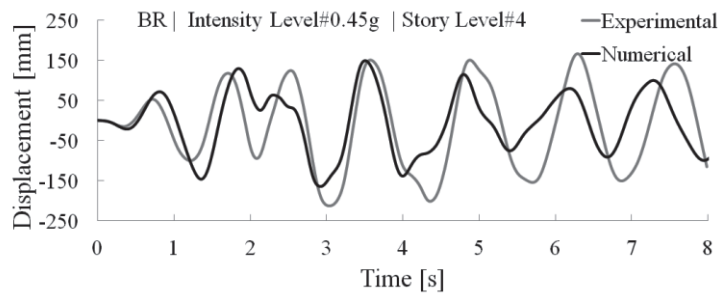
$$Corr_{norm} = \frac{\sum_{i=1}^N D_{exp,i} * D_{num,i}}{\sqrt{\sum_{i=1}^N D_{exp,i}^2 * \sum_{i=1}^N D_{num,i}^2}} \quad 4.2$$



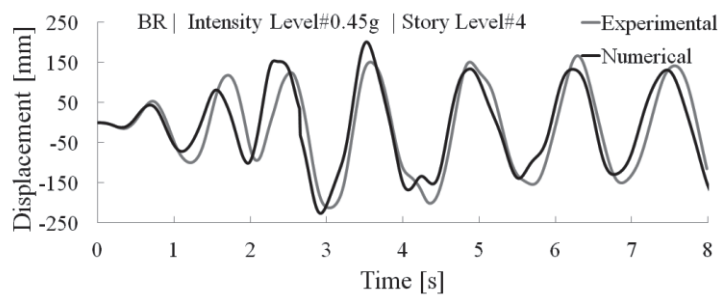
a) Low intensity level & lumped plastic hinges



b) Low intensity level & fiber plastic hinges

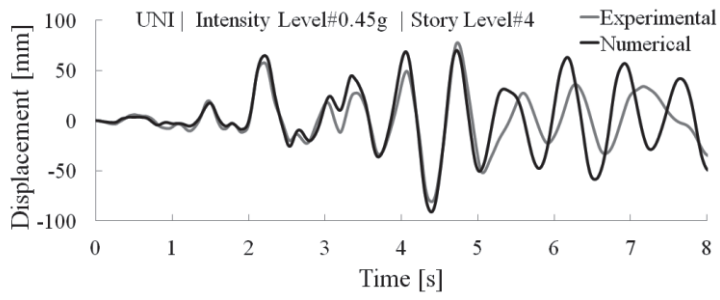


c) High intensity level & lumped plastic hinges

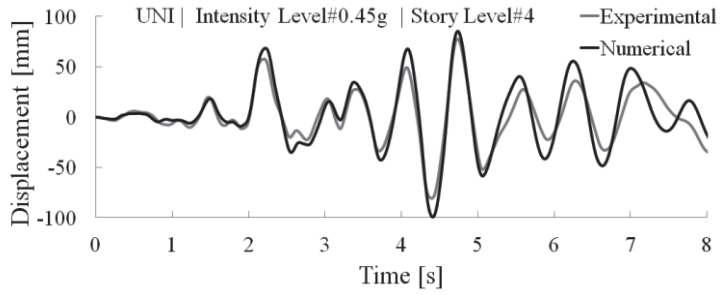


d) High intensity level & fiber plastic hinges

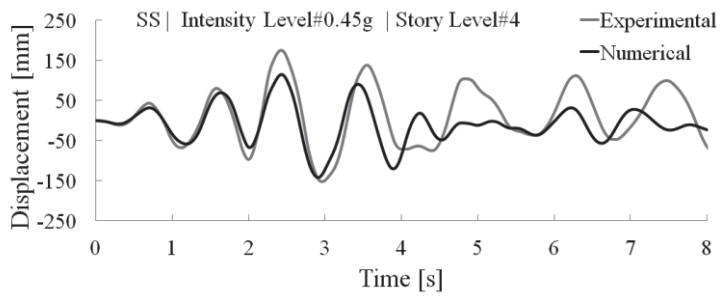
Figure 4.5 Bare frame top storey displacement: numerical vs. experimental



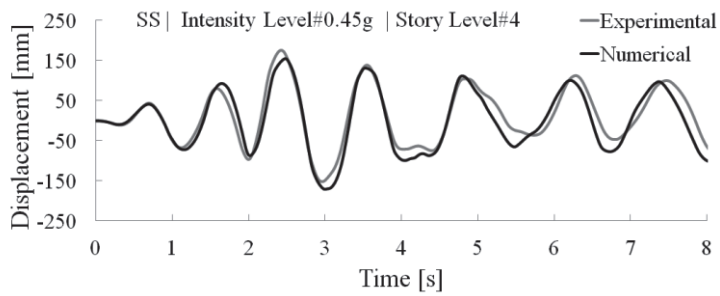
a) Full infill & lumped plastic hinges



b) Full infill & fiber plastic hinges



c) Soft story & lumped plastic hinges



d) Soft story & fiber plastic hinges

Figure 4.6 Infilled frames top storey displacement: numerical vs. experimental

The correlation values are calculated for all considered macromodels. Table 4.1 includes the calculated correlation quantities which are schematically shown in Figure 4.7;

- It is obvious, that depending on the chosen model, the correlation percentage is of different values. Higher values are obtained in case of plastic hinges with fiber section approach, however, just in case of uniform infill frame (since the overall response is dominated by the URM infill panels contribution) the use of rigid plastic hinges leads to correlation percentage approximately likewise for the case of the fiber plastic hinges.
- Global fiber section-type models proved to be sufficiently accurate to predict the dynamic nonlinear behavior of RC frame structures. This is demonstrated for the case of bare RC frames, and RC frames with masonry infills. These results are of particular importance, since no simple yet reliable evaluation methods exist to include the panels in account. The use of nonlinear fiber hinges approach proved to be particularly effective for irregular structures such as the case of ground open story structure.
- In spite of the enormous progress in the development of nonlinear computer models, professional engineers are not using these models for the analysis of RC structures. Fiber hinge type models are simple and robust; therefore, their use as an alternative to standard lumped plastic hinge models could be advocated.

Table 4.1 Correlation between experimental & numerical displacement time histories

RC frame model	Assumptions	Achieved correlation [%]				
		Story No.	BR 0.12g	BR 0.45g	UNI 0.45g	SS 0.45g
Lumped plastic hinge	<i>Beams:</i>	1st	84.8	86.0	91.2	91
	• Moment-Rotation	2nd	84.5	87.0	94.0	91.2
	<i>Columns:</i>	3rd	85.0	88.0	93.0	91.3
	• Moment-Rotation	4th	86	90	92	92
Fiber plastic hinge	• Axial force-Bending moment interaction curve.	1st	68.8	68.0	88.2	68.2
	<i>Beams and Columns:</i>	2nd	66.1	69.1	87.0	69.1
	• Stress-Strain relationship For the concrete and steel bar fibers;	3rd	68.1	67.1	86.0	67.1
	• Axial-flexural deformation interaction at sectional level.	4th	67.6	69.6	88	70.6

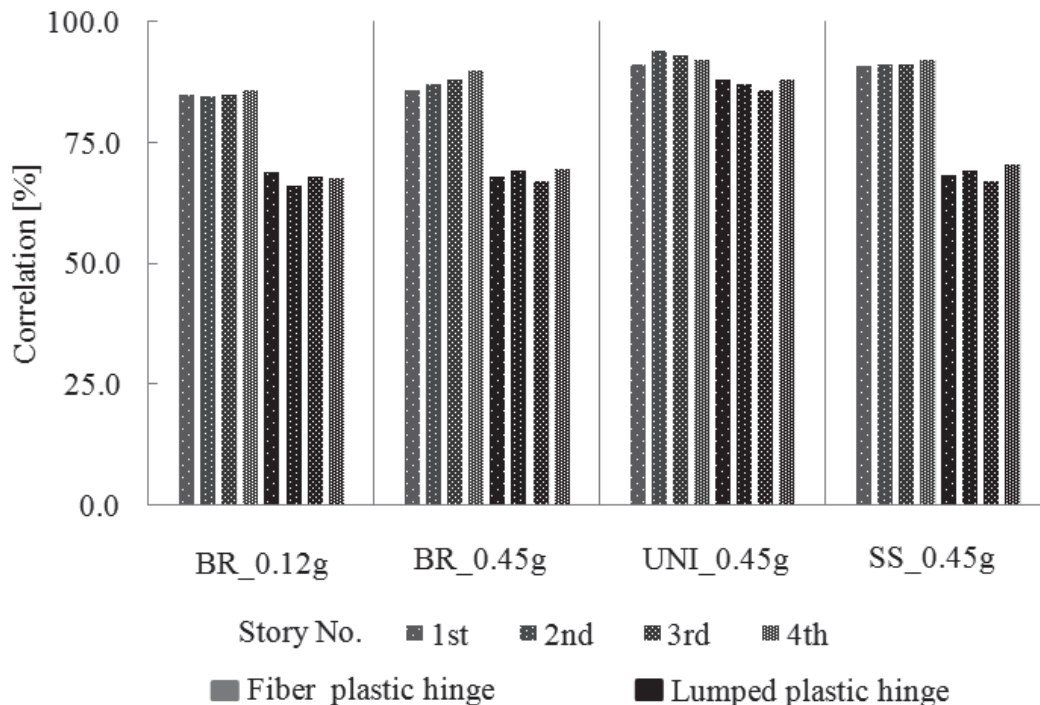


Figure 4.7 Correlation between experimental and numerical displacement time histories

Chapter 5: Macromodel for URM Infill

Walls

5.1 Introduction

In the previous chapter, nonlinear dynamic analysis is performed adopting the choice of concentrated plasticity (lumped models). Two different types of modeling the nonlinearity of the structure are tested to achieve the numerical simulation of the experimental reference object under study. The nonlinearity is considered adopting Plastic Hinges with hysteretic relationships based on FEMA 356 tables or applying Plastic Hinges with fiber elements, where a material constitutive relationship is assigned to each fiber.

In this chapter, on purpose to consider the in- and out-of-plane response of the unreinforced masonry (URM) infill panels as well as the interaction between both components, a set of URM macromodels are calibrated and later on validated against experimental results of 1:2.5, 1:1 scaled three story and four story RC structures with URM infill walls respectively.

5.2 Primary Elements Model

Beams and columns in the computational model are represented by nonlinear Beam Column elements, which are based on force formulation, and consider the lumped plasticity concept at the elements edges. Cross sections are defined using fiber discretization with distinct fibers for reinforcement. As for the constitutive laws of concrete and steel rebar the same models are adopted as they have been described in chapter 4.

5.3 In-Plane Secondary Element Model

Several 2D models, i.e. IP models, are proposed in literature to map/to represent the behavior of masonry infills. In this study the equivalent strut model with different configuration is considered, as well as the shear link element with four elastic strut elements proposed by *Rodrigues et al. (2010)* (see Section 5.6.1).

To calibrate the first considered model for URM infill panel with a single diagonal strut in each direction, “Concrete01” material, available in OpenSees library, is used to represent the nonlinear behaviour of the infill wall. It has no tensile strength and parameters are required to define is maximum stress, strain corresponding to maximum stress, ultimate strain and stress corresponding to ultimate strain ($f_{mo}, \epsilon_{mo}, f_{mu}, \epsilon_{mu}$). The initial slope (E_{URM}) of the curve is considered as two times of the secant modulus corresponding to maximum stress and strain corresponding to maximum stress ($E_{URM} = 2f_{mo}/\epsilon_{mo}$) (Figure 5.1).

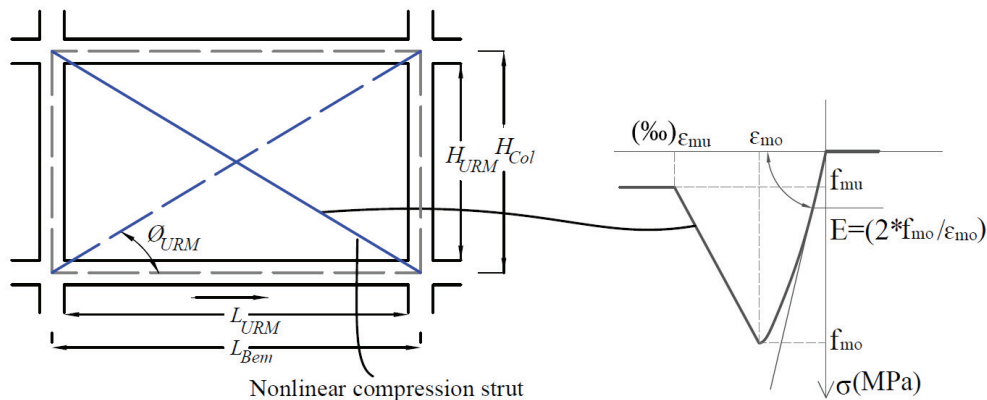


Figure 5.1 Equivalent strut model with concrete material

The FEMA 356 provisions estimate the effective area of the compression zone in the panel by the thickness of the masonry infill panel (t_{URM}) times the strut width (W_{st}) given by Equation 5.1, in consistent units. Note that the term in parenthesis in Equation 5.1 is dimensionless. The modulus of elasticity of the strut material is assumed to be the same as the expected vertical modulus of elasticity of the infill wall material. The expected in-plane shear strength (V_{URM}) of the URM infill wall is calculated by Equation 5.3, derived from the database (Chapter 3).

$$W_{st} = 0.175 d (\lambda H_{URM})^{-0.4} \quad 5.1$$

$$\lambda = \sqrt[4]{\frac{E_{URM} t_{URM} \sin(2\theta)}{4E_c I_{Col} H_{URM}}} \quad 5.2$$

$$V_{URM} = 1.3 * f_{tp} * L_{URM} * t_{URM} \quad 5.3$$

Using the above calculated parameters, the material and geometric properties of the diagonal strut model, namely the area of the diagonal struts (A_{st}), maximum equivalent diagonal strength of masonry (f_{mo}) and its corresponding strain (ϵ_{mo}), and the masonry ultimate strain (ϵ_u) can be determined as shown in Equations 5.7, 5.8, respectively.

$$A_{st} = W_{st} t_{URM} \quad 5.4$$

$$V_d = \frac{V_{URM}}{\cos \theta} \quad 5.5$$

$$f_{mo} = \frac{V_d}{A_{st}} \quad 5.6$$

$$\epsilon_{mo} = \frac{2f_{mo}}{E_{URM}} \quad 5.7$$

$$\epsilon_u = (3 \text{ to } 8) \epsilon_{mo} \quad 5.8$$

$$f_{mu} = (0.3 \text{ to } 0.6) f_{mo} \quad 5.9$$

For the calibration of the infill wall model, two samples from the database in Appendix A are utilized, namely (S1C-2) and (Unit2) specimen. Table 5.1 depicts the required parameters and Table 5.2 shows the calculated ones.

Table 5.1 Geometric and Material Properties of the Infill Walls

Spec.ID	L_{URM} [m]	H_{URM} [m]	t_{URM} [mm]	E_c [GPa]	E_{URM} [GPa]	λ_h [-]	W_{st} [mm]
S1C-2	1.6	1.6	250	25.5	4.565	0.00145	260
Unit2	2.5	2.4	90	25.2	11.55	0.00318	270

Table 5.2 Material Properties of Diagonal Struts

Spec.ID	f_{ip} [MPa]	V_d [N]	f_{mo} [MPa]	f_{mu} [MPa]	ϵ_{mo} [%]	ϵ_{mu} [%]
S1C-2	0.29	164048.8	2.52	0.50	0.111	0.553
Unit2	0.41	128630.5	5.29	1.06	0.092	0.458

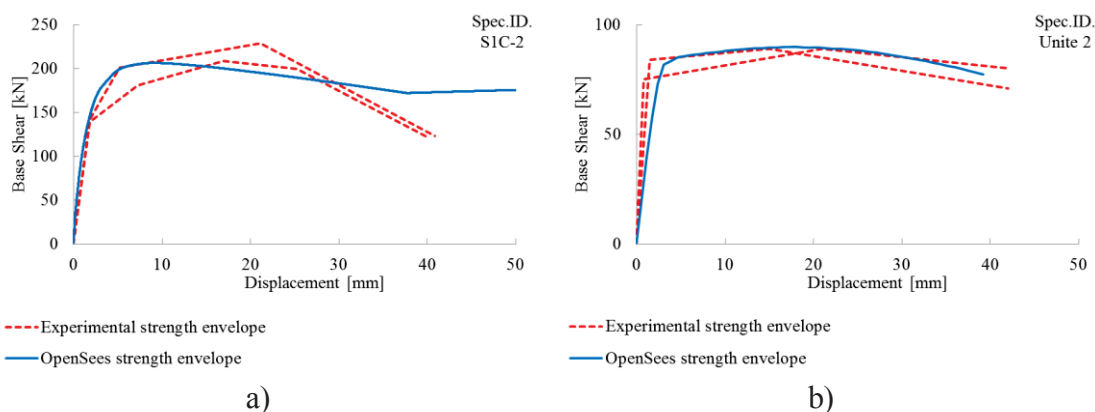


Figure 5.2 Experimental/numerical envelope curve: a) specimen S1C-2, b) specimen Unit2

For both considered specimens, the strength envelope is digitized in order to be compared with the numerical results. Figures 5.2 a and b, show the comparison between the IP experimental and numerical force-displacement response. The models fit the experimental data with a good approximation.

5.4 Developed In & Out-of-Plane Secondary Element Model

Recently, the URM out-of-plane behavior and its effect in the global seismic response on the existing structures, has been of great interest for several researchers. A conducted study on the observed damage after L'Aquila earthquake in 2009 had shown that collapse due to OoP component was specifically observed in the upper stories as a direct influence of the expected higher accelerations at the upper parts of the structures. Motivated by the OoP observed damage and targeting to characterize the OoP performance, several experimental studies have been executed (e.g., *Furtado et al., 2016*). It was reported that a mutual effect between the OoP and IP damage exist (one in one direction reduces the other in the other direction). Parallel to the field observations and experimental studies there have been similar exerted efforts to simulate the OoP response and the reciprocal IP-OoP interaction.

As mentioned in chapter 2, the first trial to simulate the OoP response and IP-OoP mutual interaction was proposed by *Mosalam et al. (2007)*. Subsequently the 3D strut and tie (SAT) model was investigated in detail by *Kadysiewski et al. (2009)* and as a conclusion they reported the model suffer some problematic behaviour. One of the fundamental issues was the instability under some load combinations. On the light of the previous check, *Kadysiewski et al. (2009)* introduced a new single beam column element with weighted fibres hinges at the mid span. Simplified Elastic-Perfectly Plastic (EPP) constitutive law was assigned to the weighted fibers as a representative of the URM infill wall behaviour. The assumed simplification lead to fundamental limitations in the post elastic range, i.e., post cracking phase. First, the current model is unable to predict whether the performance is hardening, softening, and flat or some combination of the three, (*Kadysiewski et al., 2009*). Second, since the utilized EPP constitutive law maintains strength and stiffness in the post yielding stage and after crossing the collapse limit state, this will lead to unrealistic distribution of forces in the structure. The reason behind is, the collapsed panel will continue bearing loads which will negatively influence the carried loads by the other panels and the surrounding frame elements, i.e. underestimate the load carrying capacity of the other secondary elements and subsequently the transmitted forces to the surrounding primary elements.

On one hand, as discussed, using EPP material model to represent the URM behaviour will lead to unrealistic bearing load capacity without any degradation after the peak strength capacity. On the other hand, the proposed single strut model reduces the required number of elements and consequently modeling complexity. However, such a simplification may lead to different force distribution in the surrounding RC frame member, but in cases of rigid diaphragm floors, as it is often the case; the influence of such simplification is expected to be negligible.

5.4.1 Proposed Development

Given the problems associated with the model under study a modified calibration procedures is introduced due to the following basics requirements:

1. The model configuration is the same as the one in *Kadysiewski et al. (2009)*.
2. The model has to consider the post cracking stage by using more accurate constitutive law than the EPP one.

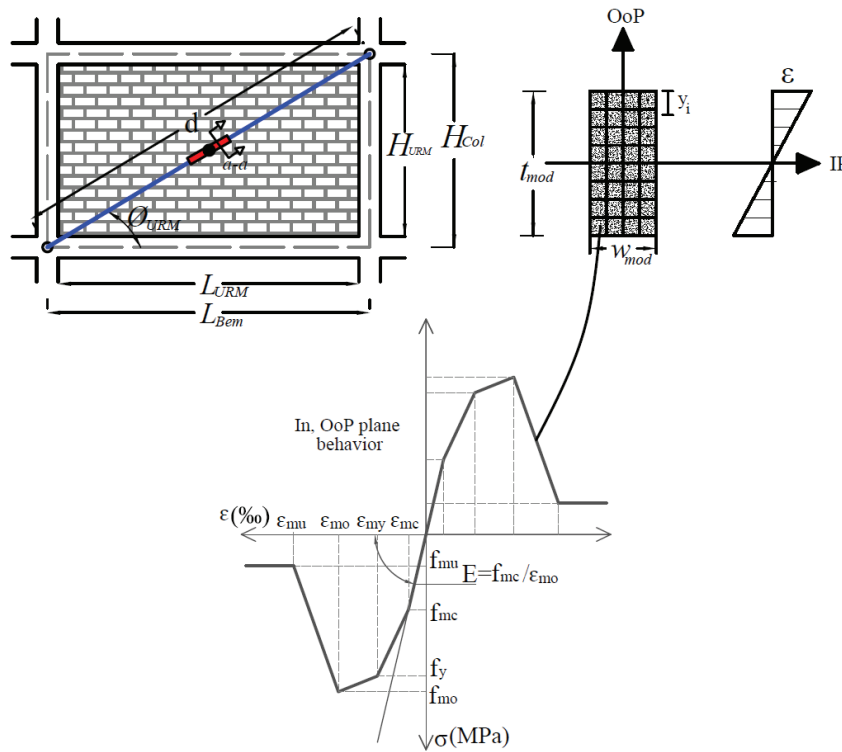


Figure 5.3 Proposed URM infill wall model

3. The proposed macromodel has to provide the same first natural frequency as the URM infill panel. To this purpose the model is calibrated with the available experimental data as an alternative to the simplified equation proposed by *Kadysiewski et al. (2009)*.
4. The model has to represent the IP-OoP interaction depending on the inherent property of fiber modeling technique which considers naturally the interaction between axial load and bending moment.

Figure 5.3 depicts the model schematic view for the case of the fiber section. Uniaxial pinching material, instead of EPP, is defined numerically (stress-strain relationship) and combined into a fiber section where moment-curvature and axial force-deformation characteristics and their interaction are calculated computationally.

The uniaxial pinching material is identified by eight parameters: cracking, yielding, maximum and residual strength and the accompanied strains.

To determine the out-of-plane equivalent stiffness of the beam-column element, *Kadysiewski et al. (2009)* used the unique dynamic characteristic of the infill panel, i.e. the first OoP frequency, accordingly, they assumed that the URM infill wall

spans vertically with pinned connections at the top and bottom edges. Consequently the OoP frequency was calculated utilizing Equation 5.10.

$$f_{ss} = \frac{\pi}{2 * H_{URM}^2} \sqrt{\frac{E_{URM} * I_{URM} * g}{W_{st}}} \quad 5.10$$

Following detailed procedures available in *Kadysiewski et al. (2009)* the vertically spanned beam was converted to a diagonal element.

In this research and due to the fact, that the URM infill wall behaves in the out of plane direction as a two-way bending slab confined vertically and horizontally (*Rivera et al., 2011*), the OoP frequency is instead modeled using a structured mesh with square shell elements of 4 nodes and six degrees of freedom per node. Each shell element is 30 by 30 cm long, so that numerical results are not sensitive to element size. To this purpose the computer program SAP2000 is used.

Knowing the mass and the frequency of the shell elements model (f_{OoP_FEM}), the stiffness of the equivalent diagonal macromodel and the OoP moment of inertia are determined utilizing Equations 5.11 and 5.12, respectively (*Kadysiewski et al., 2009*).

$$K_{OoP_macro} = (2\pi f_{OoP_FEM})^2 \frac{0.81 M_{URM}}{g} \quad 5.11$$

$$I_{OoP_macro} = \frac{K_{OoP_macro} * (d_{URM}^3)}{48E_{URM}} \quad 5.12$$

Thus, strut width and thickness have to be modified in a way to maintain the same strut area as it is calculated from in-plane calibration and enhance the out-of-plane inertia to comply with the aforementioned calculation. This can be achieved by solving Equations 5.13 and 5.14.

$$A_{st} = w_{st} t_{URM} = w_{mod} t_{mod} \quad 5.13$$

$$I_{OoP_macro} = \alpha_{cr} \frac{W_{mod} t_{mod}^3}{12} \quad 5.14$$

It is worth noting that, modifying the strut diminution will not affect the in-plane strength but it has an effect to reproduce the out-of-plane strength and stiffness to match the real URM infill wall behaviour/properties. The constitutive model parameters, ($f_{mo}, f_{mu}, \epsilon_{mo}, \epsilon_{mu}$) are calculated on the same basis as in the in-plane calibration parameters (f_{mc}, f_{my} are about $0.55 f_{mo}$ and $0.75 f_{mo}$ respectively).

To determine the OoP resisting moment of the URM infill wall the modified cross section is used along with the equivalent URM compressive strength. As discussed earlier, the modified cross section maintains the same cross sectional area and accordingly the IP strength. The applied/introduced procedure has just the effect to reproduce the OoP strength accurately. Hence, the resisting moment can be found with respect to its centroid by multiplying the force in each fiber by that fiber's centroidal distance to the section centroid and summing these moments over all the concrete fibers (Equations 5.15 to 5.21).

$$M_{OoP} = 2 \sum_{i=1}^{i=numfib/2} f_{mo} A_i \left(\frac{t_{mod}}{2} - y_i \right) \quad 5.15$$

$$M_{OoP} = f_{mo} A \frac{t_{mod}}{4} \quad 5.16$$

$$A = \sum_{i=1}^{i=numfib} A_i = w_{mod} * t_{mod} \quad 5.17$$

$$P_{OoP} = \frac{4M_{OoP}}{d_{URM}} \quad 5.18$$

$$P_{OoP} = \frac{f_{mo}}{d_{URM}} w_{mod} * t_{mod}^2 \quad 5.19$$

$$q_{OoP} = \frac{P_{OoP}}{L_{URM} * H_{URM}} \quad 5.20$$

$$q_{OoP} = \frac{f_{mo} w_{mod} t_{mod}^2}{d_{URM}} * \frac{1}{L_{URM} * H_{URM}} \quad 5.21$$

The final requirement of the developed model is set to represent the interaction phenomena between the IP and OoP response, i.e., the IP damage of the URM infill wall has to be reflected on the OoP behaviour and vice versa.

For the fiber section beam-column element shown in Figure 5.4, the element and section force and deformation vectors are given by Equations 5.22 and 5.23.

$$Q_{(x)} = [N_{(x)}, M_x]^T \quad 5.22$$

$$D_{(x)} = [\varepsilon_{(x)}, \theta_x]^T \quad 5.23$$

The section force and deformation can be linked through the section stiffness matrix $K_{(x)}$. Before cracking, i.e., in the linear elastic phase of the analysis the axial force and bending moment are uncoupled and the section stiffness matrix is diagonal given by Equations 5.24 and 5.25.

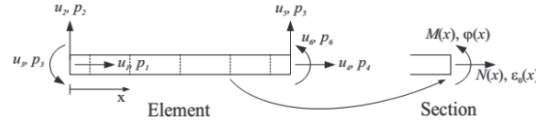


Figure 5.4 End forces and displacements in a generic beam-column element

$$Q(x) = K(x)D(x) \quad 5.24$$

$$K(x) = \left[\sum_{i=1}^{numfib} E_{(i)}A_{(i)} \quad 0, \quad 0 \quad \sum_{i=1}^{numfib} E_{(i)}A_{(i)} y_i^2 \right]^T \quad 5.25$$

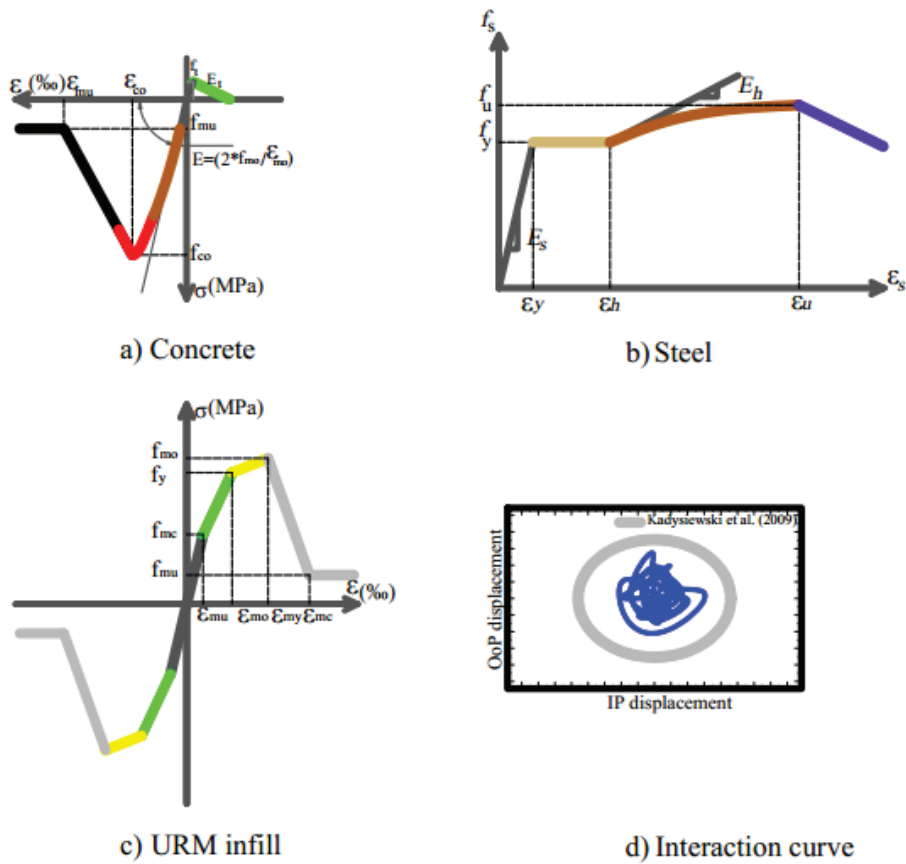
Proceeding with the analysis after cracking, the non-linearity will start to propagate all over the fiber section. The elastic section stiffness matrix is replaced with a tangent non-diagonal stiffness matrix that couples the axial force $N(x)$ and bending moment $M(x)$ in Equation 5.26.

$$K_{(Tx)} = \begin{matrix} \sum_{i=1}^{numfib} E_{(i)}A_{(i)} & - \sum_{i=1}^{numfib} E_{(i)}A_{(i)}y_i \\ - \sum_{i=1}^{numfib} E_{(i)}A_{(i)}y_i & \sum_{i=1}^{numfib} E_{(i)}A_{(i)}y_i^2 \end{matrix} \quad 5.26$$

5.4.2 Damage Definition

The definition of damage grades of RC frame structures with URM infill walls has been the topic of several studies as presented in **Grünthal et al. (1998)** and **Colangelo (2013)**. Most authors identify different damage grades depending on the failure patterns observed in the previous events through linking the severity of collapse with a specific level of damage. In this research the damage limit states were defined and related with the determined material strains as stated in **Schwarz et al. (2006)**; **AL Hanoun et al. (2017)** and repeated in Table 5.3 & Figures 5.5 a to d.

Figures 5.6 a to c, illustrate typical (possible) damage patterns for RC structures with masonry infill walls in a schematic form. They show the combination of different damage grades of the infill walls and RC frame according to the damage classification scheme according to EMS-98 (**Grünthal et al., 1998**). However, different damage observations have shown that the quality and material of the infill walls have a strong impact on the interaction with the structural frame and can cause different damage grades independent of the srory class (**Abrahamczyk et al., 2010**).



- LDG_p1
- LDG_p2
- LDG_p3
- LDG_p4
- LDG_p5a
- LDG_p5b
- ▢ LDG_s1
- ▢ LDG_s2
- ▢ LDG_s3

Figure 5.5 Material limit states (schematic view)

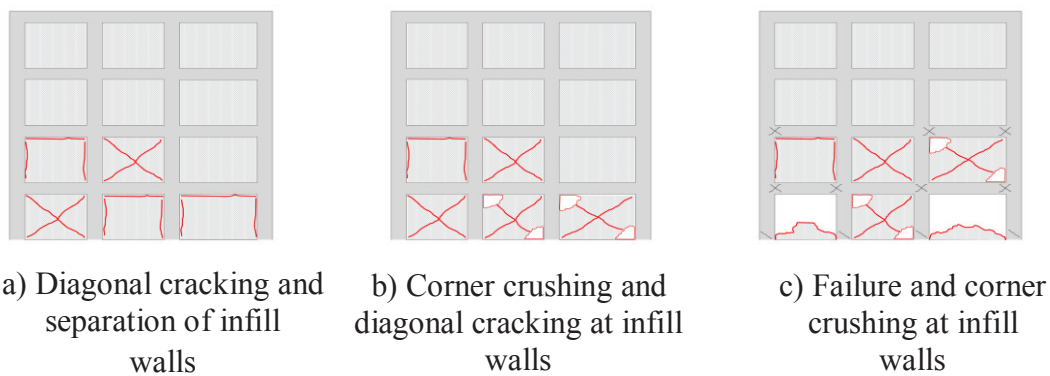


Figure 5.6 Schematic damage scenarios of infill walls on RC frame structures according to *Abrahamczyk et al. (2010)*.

Table 5.3 Definition and description of Local Damage Grades (LDG) according to Schwarz *et al.* (2006, 2015)

Element	Damage Description	Material Strains	LDG
Structural (Primary Elements)	Maximum tension strain of concrete	$\varepsilon \geq +0.0001$	LDG _p 1
	<i>Yield strain of reinforcement steel</i>	$0.002 \leq \varepsilon_s \leq 0.005$	LDG _p 2
	Spalling of concrete cover	$\varepsilon_{uc} \geq -0.001$	LDG _p 3
	<i>Moderate damage of long. steel bars</i>	$0.005 \leq \varepsilon_s \leq 0.01$	
	Strength degradation of core concrete	$-0.002 \leq \varepsilon_{cc} \leq -0.004$	LDG _p 4
	<i>Substantial damage of longitudinal steel bars (steel failure)</i>	$0.01 \leq \varepsilon_s \leq 0.02$	LDG _p 5a
	Ultimate strain of confined core concrete (transverse rebar failure)	$\varepsilon_{cc} \geq -0.004$	LDG _p 5b
Non-Structural (Secondary) Elements	Horizontal or diagonal cracking of masonry (slight to moderate damage)	$\varepsilon_{mc} \leq \varepsilon < \varepsilon_{my}$	LDGs 1
	Large cracking of masonry (heavy damage)	$\varepsilon_{my} \leq \varepsilon < \varepsilon_{mo}$	LDGs 2
	Strength degradation and extensive crushing of masonry (collapse)	$\varepsilon \geq \varepsilon_{mo}$	LDGs 3
	Collapse due to IP_OoP interaction		LDGs 3

5.4.3 Element Removal Algorithm for Secondary Element

In order to explicitly account for the failure of URM infill walls during an earthquake excitation under combined IP and OoP effects in case of multi-story structures, the above described analytical infill wall macromodel is implemented in a previously developed progressive collapse algorithm (Mosalam *et al.*, 2015). In that regard, the IP deformation is described by the relative horizontal displacement between the top and bottom nodes of the diagonal strut. The OoP displacement is determined at the midpoint node where the lumped OoP mass is attached.

The relationship between the IP and OoP displacements can be defined by an elliptical interaction curve, as shown in Figure 5.5 d, and the limits can be selected based on FEMA 356 and vision2000 with maximum IP interstory drift of 1.5% and

2.5% respectively. Whereas, the OoP drift limit is the minimum of 5% and half the thickness of the infill wall according to *Kadysiewski & Mosalam (2009)*. When the pair of IP and OoP displacements from the analysis reaches or exceeds the envelope curve, the two beam-column elements and the midpoint node, are removed to directly represent the failure of the URM infill wall. The algorithm for the removal of an infill wall is shown in Figure 5.7.

5.4.4 Macromodel Implementation

In order to explicitly account for the failure of URM infill walls during an earthquake excitation under combined IP and OoP effects, the above described numerical macromodel is implemented in the open source software OpenSees. Figure 5.8 shows a schematic flowchart for the implementation procedure. It will be explained in detail in the following section

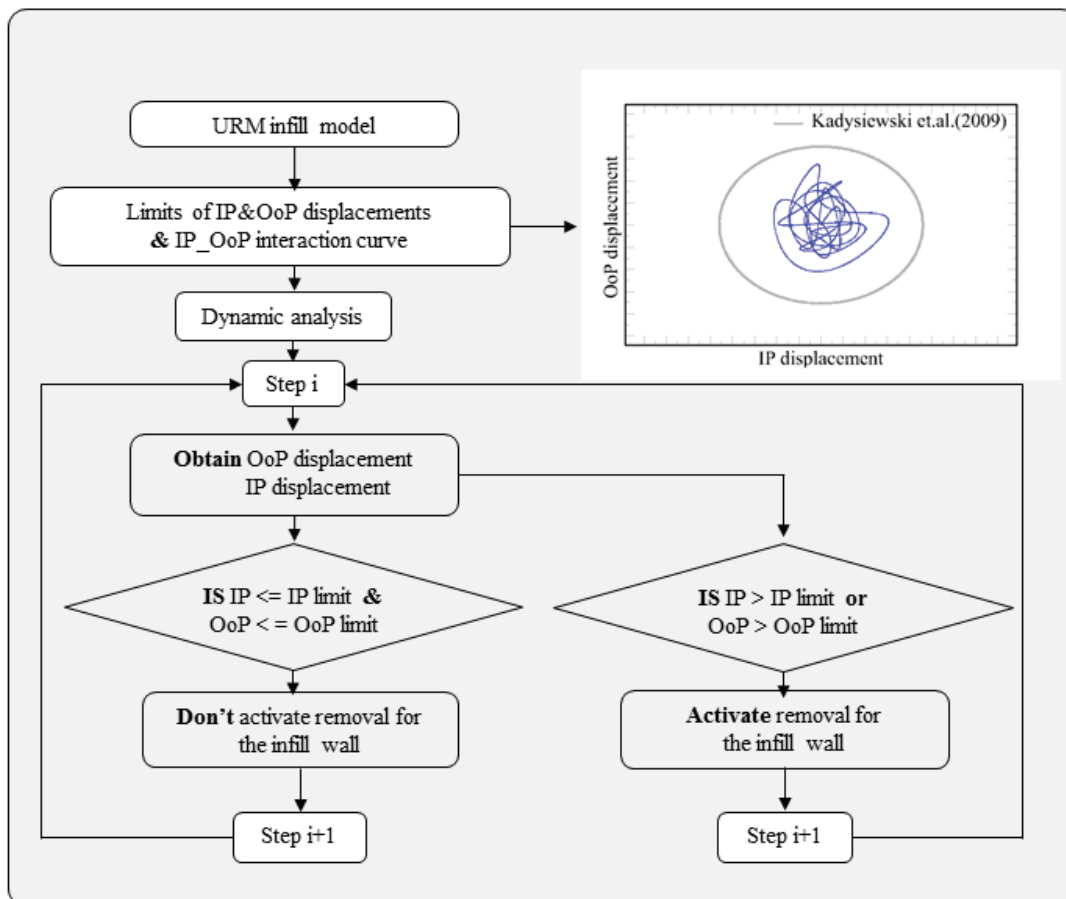


Figure 5.7 Element removal algorithm according to *Mosalam et al. (2015)*

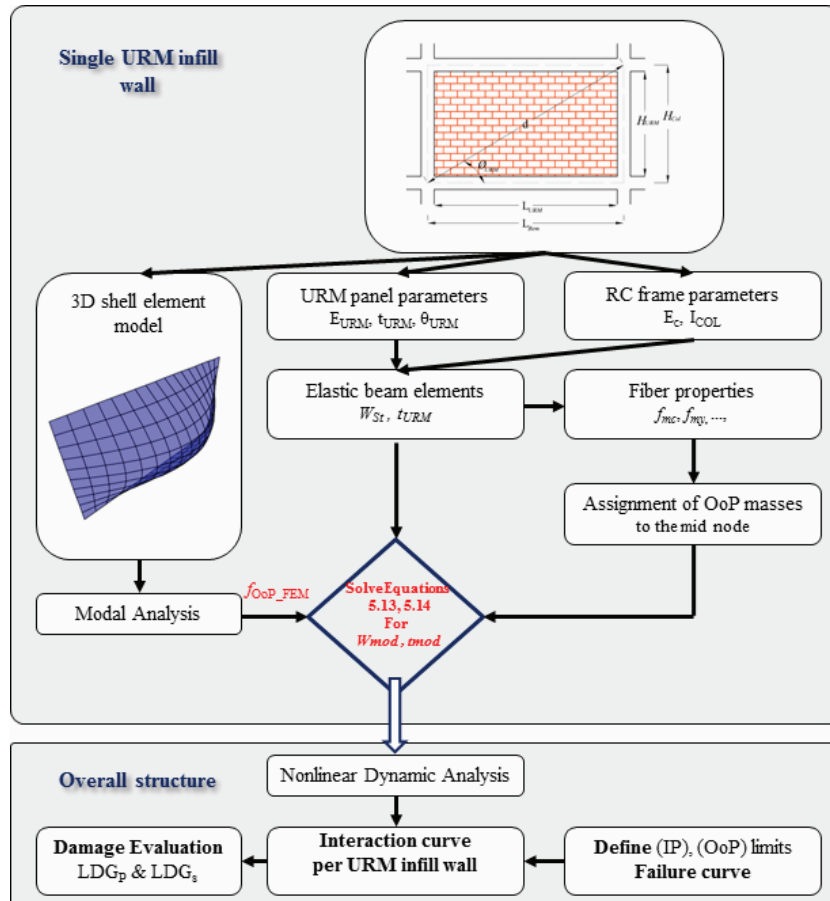


Figure 5.8 Macromodel implementation flowchart

5.4.5 In-Plane Calibration

To calibrate the model according to the aforementioned assumptions used in the current study, the S1C-2 experimental specimen from an experimental program by *Cavaleri et al. (2014)* is again selected for the comparison of the in-plane cyclic response. In this study, the IP cyclic behavior of six 1:2.5 scaled, single story, single-bay specimens having different RC frame cross section and URM material properties were investigated. The specimen S1C-2 is modeled using the above-explained approach. The numerically predicted results are compared with the reported experimental data. Figure 5.9 shows the experimental test geometry and the applied loading protocol. A comparison of the force-displacement envelope from the experimental test along with the corresponding results from the numerical model is illustrated in Figure 5.10. As it is shown, a very good agreement between the numerical and experimental results, in terms of maximum strength, initial stiffness, strength and stiffness degradation, exists. The overall level of discrepancy between the results is quite small and acceptable, hence, the modeling approach is used hereafter.

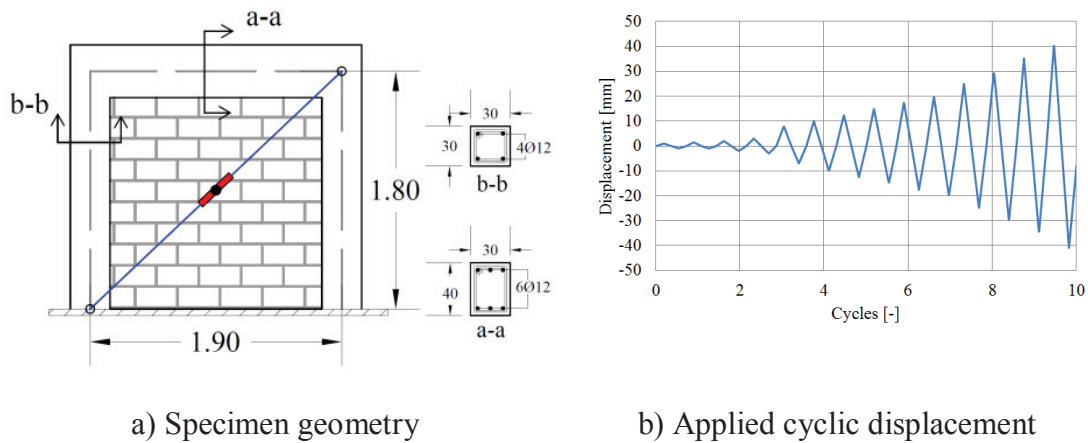


Figure 5.9 Experimental specimen S1C-2 according to *Cavaleri et al. (2014)*:
a) Model geometry, b) Applied cyclic displacements

Table 5.4 Material Properties of Diagonal Struts for Infills

Spec. ID.	f_{ip} [MPa]	V_d [N]	f_{mc} [MPa]	f_{my} [MPa]	f_{mo} [MPa]	f_{mu} [MPa]	ϵ_{mc} [%]	ϵ_{my} [%]	ϵ_{mo} [%]	ϵ_{mu} [%]
S1C-2	0.29	164048.8	1.39	1.89	2.52	0.5	0.061	0.08325	0.111	0.553

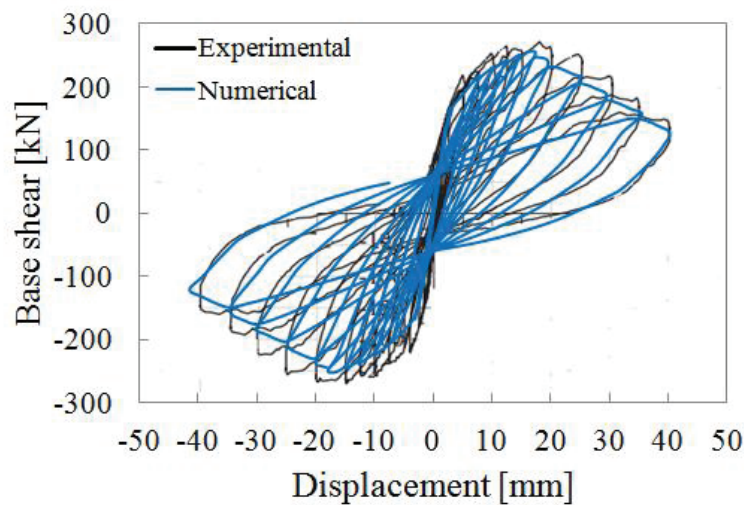


Figure 5.10 Experimental/numerical hysteretic loops (*Cavaleri et al., 2014*)

5.4.6 Out-of-Plane Calibration

To calibrate the model in the OoP direction the experimental campaign carried out by *Calvi et al. (2004)* is adopted. To investigate the effect of light surface and bed joint infill walls reinforcing, a total of ten, one to one scale single bay and single story specimens, were tested in the out-of-plane direction with previous in plane damage. Out of the ten specimens three were infilled with unreinforced masonry; consequently they are selected in this validation study since they are the main

concern of this research. Two specimens were exposed to previous in-plane cyclic loading up to 0.4 % and 1.2% interstory drift and the third one was loaded only in the OoP direction (Figure 5.11 a) shows the experimental model geometry.

The solely OoP tested specimen is used to calibrate the model in the case of OoP loading without pre IP damage, whereas the other two specimens are utilized to calibrate the model in case of OoP with pre IP damage.

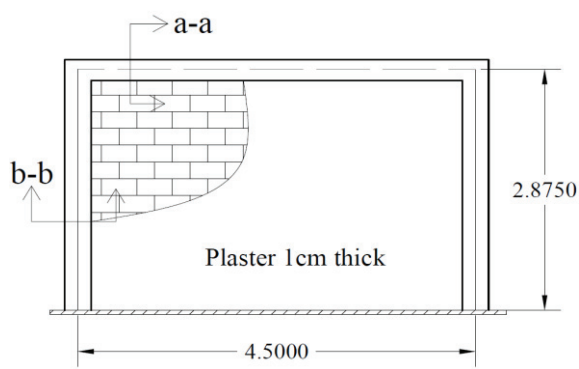
For the identification of the diagonal Beam-Column element geometrical and material properties, namely, the constitutive model parameters, OoP frequency and the modified diagonal element dimensions the following steps have to be considered.

- The first step is to calculate the IP strut width (W_{st}), compression strut area and the six pinching material model parameters as explained for IP calibration. The properties of the infilled frame and the calculated parameters due to the first step are shown in Tables 5.5 and 5.6.
- Secondly, as shown in Figure 5.11 b, a 3D linear shell element model is constructed with pinned edges connections. Consequently, the first OoP frequency is obtained and the modified diagonal element geometry calculated as explained earlier.

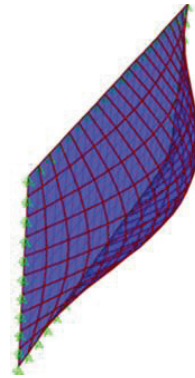
Note that the term (α_{cr}) in Equation 5.14 is equal to one since (Test 10) was tested without pre (IP) damage.

Table 5.7 shows the calculated OoP frequency utilizing the linear shell element model and the modified equivalent diagonal element dimensions. Furthermore, the OoP frequency is determined based on empirical equation as proposed in *Kadysiewski et al. (2009)*. It can be clearly observed that the URM infill panel frequency is more accurately reproduced by using the shell element model.

According to the first experimental test, i.e. (Test 10), the mid span joint was pushed in the out-of-plane direction and force-displacement values are recorded. Thus, the out-of-plane capacity curve is determined. The comparison between the numerical simulations and the OoP experimental responses showed reasonably good agreement (Figure 5.12), although the simplicity of the presented model.



a) Specimen geometry



b) Out of plane frequency of the representative shell element model of the infill wall
 $f_{\text{OoP_FEM}} = 14.5 \text{ [Hz]}$

Figure 5.11 Experimental model according to *Cavaleri et al. (2004)* of specimen Test 10

Table 5.5 Geometric and Material Properties of the Infill Wall

Spec. ID.	L_{URM} [m]	H_{URM} [m]	t_{URM} [mm]	E_c [GPa]	E_{URM} [GPa]
Test 10	4.2	2.75	135	25	1.873

Table 5.6 Material Properties of Diagonal Struts for Infills

f_{tp} [Mpa]	V_d [N]	f_{mc} [MPa]	f_{my} [MPa]	f_{mo} [MPa]	f_{mu} [MPa]	ϵ_{mc} [%]	ϵ_{my} [%]	ϵ_{mo} [%]	ϵ_{mu} [%]
0.15	101659.24	0.65	0.97	1.29	0.39	0.034	0.103	0.138	0.690

Table 5.7 Experimental/numerical comparison of the Eigen frequency for infill walls

γ [kN/m ³]	mass [kN.sec ² /m]	f_{exp} [Hz]	f_{ss} [Hz]	$f_{\text{OoP_FEM}}$ [Hz]	$f_{\text{ss}} / f_{\text{exp}}$ [-]	$f_{\text{OoP_FEM}} / f_{\text{exp}}$ [-]	W_{st} [mm]	t_{URM} [mm]	W_{mod} [mm]	t_{mod} [mm]
8.6	1.37	14.71	10	14.5	0.67	0.99	591	150	61	1400

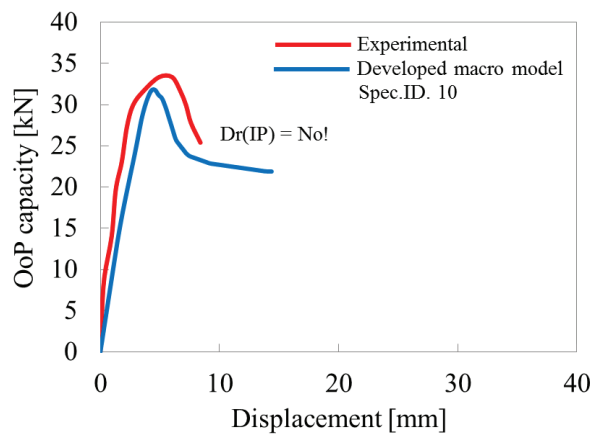


Figure 5.12 Comparison of the Experimental and Numerical OoP response

5.4.7 In-Plane and Out-of-Plane Interaction

To investigate the effect of previous IP damage on the OoP capacity reduction, Test 6 and Test 2 specimens were exposed to in-plane cyclic drift up to 0.4 % and 1.2% respectively. The calculated parameters to be used for the IP-OoP simulation are shown in Tables 5.8 and 5.9. Figure 5.13 shows the numerical results for the IP response of the specimens. As it can be clearly observed, likewise the proposed model by *Furtado et al. (2017)*, utilizing the developed model in this research the overall performance of the tested specimens is good captured in term of top displacement and base shear. The difference between the experimentally and numerically obtained maximum IP strength is between 15 and 23%. Furthermore the stiffness and strength degradation as well the pinching effect due to the cyclic loading and reloading are numerically well represented. However, it is highly significant to mention that the developed model has the capability to capture the non-linear OoP response whereas the model proposed by *Furtado et al. (2015)* responds linearly in the OoP direction. Thus, to reflect the achieved IP damage on the OoP response, subsequently after the completion of cyclic IP simulation the mid span joint of the diagonal element is pushed in the OoP direction. The numerical results for the OoP response are compared to the experimental results in Figure 5.14. The correlation between the experimental and numerical results is reasonably good in spite of the simplicity of the model. The difference between the experimentally and numerically obtained maximum OoP loads is between 15 and 20%.

Note that the term (α_{cr}) in Equation 5.14 has to be modified on the basis of the cracked OoP moment of inertia. To that purpose, in *Kadysiewski et al. (2009)* a value of (0.5) is used. Up to date there is no recommendation in the international codes about the URM infill walls cracking modifiers. Instead in this research the parameters (α_{cr}) are determined by trial and error so that the numerical OoP capacity curve matches the obtained experimental curve and a value of (0.2, 0.18) is attained for Test 6 and 2 respectively.

Table 5.8 Material properties of diagonal struts for infills

Spec. ID	f_{ip} [Mpa]	V_d [N]	f_{mc} [Mpa]	f_{my} [Mpa]	f_{mo} [Mpa]	f_{mu} [Mpa]	ϵ_{mc} [%]	ϵ_{my} [%]	ϵ_{mo} [%]	ϵ_{mu} [%]
Test 2&6	0.15	101659.2	0.65	0.968	1.29	0.39	0.034	0.103	0.138	0.690

Table 5.9 Frequency and modified geometry of the diagonal strut

Spec.ID	γ [kN/m ³]	mass [kN.sec ² /m]	f_{OoP_FEM} [Hz]	α_{crk} [-]	W_{st} [mm]	t_{URM} [mm]	W_{mod} [mm]	t_{mod} [mm]
Test 2&6	8.6	1.37	14.71	0.2-0.18	583	135	78.74	1067

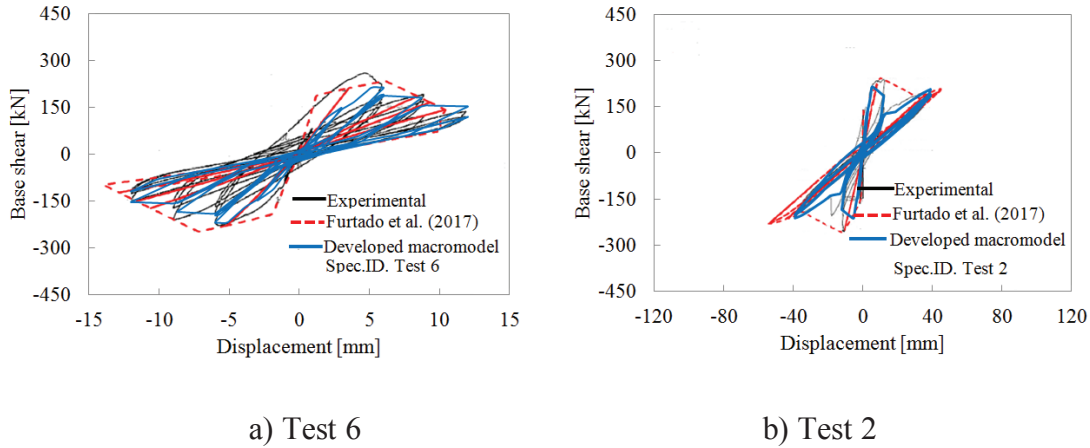


Figure 5.13 Experimental/numerical cyclic IP response
(The figure is overlapped from *Furtado et al. (2017)*)

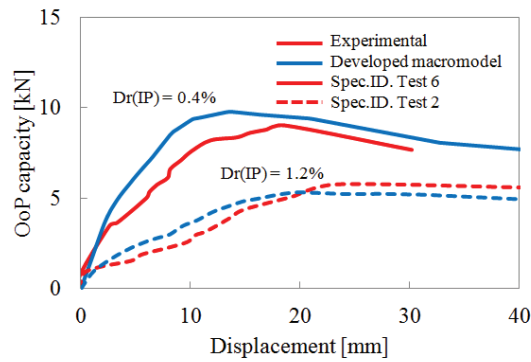


Figure 5.14 Experimental/Numerical monotonic OoP response

5.5 Model Verification

5.5.1 Considered Models

The proposed model in this research is as well verified with numerical simulation results of the two recently proposed models (i) the four elements model by *Di Trapani et al. (2017)* (see Figure 2.14) and (ii) the five elements model proposed by *Mazza (2018)* (see Figure 2.17).

The first model is validated utilizing the experimental data available in the literature. In specific three experimental campaigns are used:

The first was the RC frame with masonry URM infill walls tested first in the IP direction and subsequently in the OoP direction presented by Angel 1994, the second and third set of experiments were the data provided by *Angel (1994)* and *Flanagan*

& Bennett (1999) on infilled steel frames. The second model, proposed by *Mazza (2018)*, utilized the experimental data, on the IP-OoP response of RC frames with infill walls, by *Hak et al. (2014)* and *Furtado et al. (2015)*.

In this research the experimental data presented used by both researchers was previously collected and included in the database (see Appendix A); hence they are used in the verification study presented below.

5.5.2 Numerical Models and Verification of the Results

According to the calibration procedures adopted in the previous section, the construction of the numerical model started with the determination of the single diagonal strut parameters as a representative URM infill panel. Namely, f_{mc} , f_{my} , f_{mo} , f_{mu} , ϵ_{mc} , ϵ_{my} , ϵ_{mo} and ϵ_{mu} are determined as they represent the strength parameters. The modified diagonal strut width and thickness W_{mod} , t_{mod} are calculated to simulate the OoP response. The calculated parameters are shown in Appendix D.

Utilizing the developed macromodel in this research the numerical simulations are executed with the software platform OpenSees using fiber-section beam-column elements with lumped plasticity as a representative for the RC frame elements.

To validate their models, alternatively *Di Trapani et al. (2017)* used the concept of pushover analysis. The validation starts with the construction of the capacity curve of the numerical models using the simplified model presented by *Shing & Stavridis (2014)*. Once the pushover curves have been determined, the material properties of the diagonal struts are calculated by trial and error so that the pushover curve obtained using the four-strut model matches the results from the simplified procedures. Accordingly, to check first the IP performance of the herein presented model, the constructed models are subjected to pushover analysis and the results are compared with those presented in *Di Trapani et al. (2017)*. As Figure 5.15 illustrates the developed model reproduces the IP capacity of the tested specimens with higher values from those reported by *Di Trapani et al. (2017)*. The calculated difference between both model, i.e. the proposed herein and *Di Trapani et al. (2017)* is between 10 and 30% this is because the calculated diagonal strength is slightly higher in case of the developed model. Furthermore and for the verification in the OoP direction the cyclic IP displacement history shown in Appendix D, in which Δ_{cr} is the displacement at first cracking in the URM infills, was first applied for each specimen

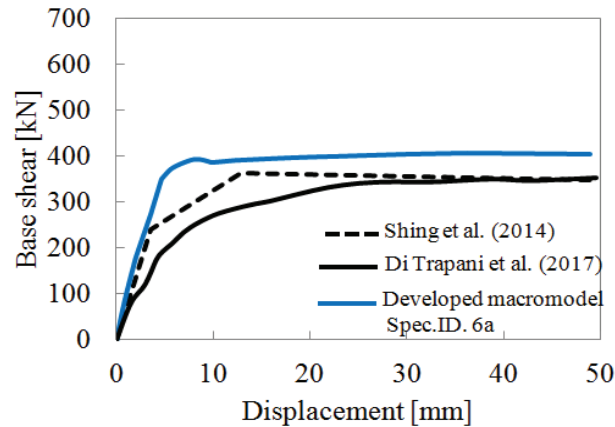


Figure 5.15 Comparison of numerical capacity curves between the proposed and *Di Trapani et al. (2017)* macromodels

and subsequently the experimental samples are subjected to monotonic OoP pushover analysis.

The numerical simulation results in the OoP direction are extracted and compared with the experimental response and the achieved results in *Di Trapani et al. (2017)*. As shown in Figure 5.16, good agreement between the accomplished results could be clearly observed by utilizing the developed model presented in this research and those achieved throughout using the model proposed by *Di Trapani et al. (2017)*. The calculated error between the numerical and experimental OoP capacity is in the range between 5 to 25% (see Appendix D for the complete results).

Due to the limit of the air bag capacity specimens 2 and 4 were not pushed to attain the maximum OoP strength of the tested URM panels. However, the achieved numerical results utilizing the proposed model refer to a good correlation between the experimental and numerical initial stiffness of the tested URM panels. The achieved maximum strength by the developed model was 20 and 50 kN less than the capacity calculated by *Di Trapani et al. (2017)* for the specimens 4 and 5, respectively. The aforementioned difference is due to the contribution of the implemented horizontal and vertical struts by *Di Trapani et al. (2017)* (see Figure 5.17). However, although the simplicity of the proposed model, on one hand, good matching between the experimental and numerical results is obtained, on the other hand, within the limitation of the model, i.e. neglecting the contribution of the horizontal and vertical OoP capacity, acceptable agreement with the results obtained by of *Di Trapani et al. (2017)* is observe

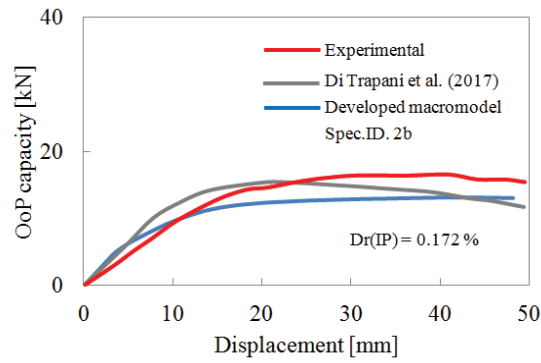


Figure 5.16 Experimental/numerical OoP response of specimen 2b

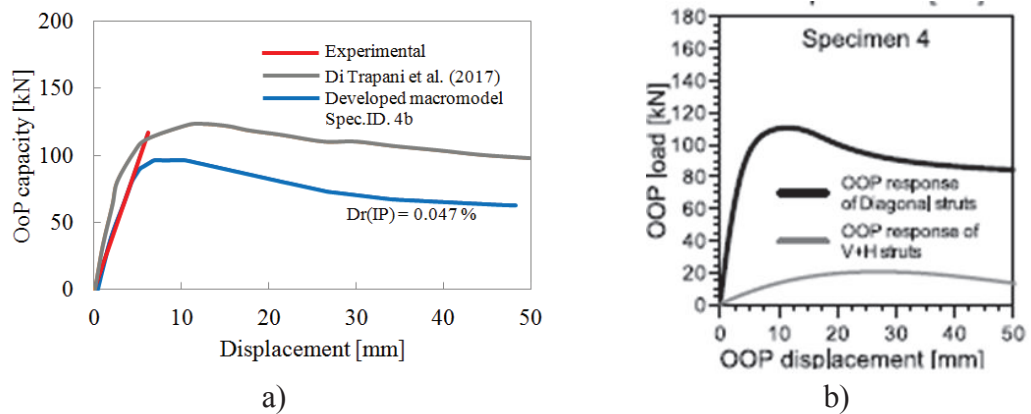


Figure 5.17 Experimental/numerical OoP response of specimen 4b:
a) current study, b) *Di Trapani et al. (2017)*

The experimental specimens which are adopted by *Mazza (2018)* to calibrate his state of the art model are numerically reproduced by the herein presented modeling technique of the RC frame elements and URM infills. The simulation results confirm the following:

- As Figures 5.18 and b, illustrate the developed model is able to represent both the experimental response and the numerical results of *Mazza (2018)*.
- The model has the ability to reproduce the response in case no previous IP damage (Figure 5.18 a)), as well as when the experimental specimen is IP damaged before the application of OoP loading (Figure 5.18 b).
- The model has the capacity to represent the OoP response due to different levels of IP damage (Figure 5.19).

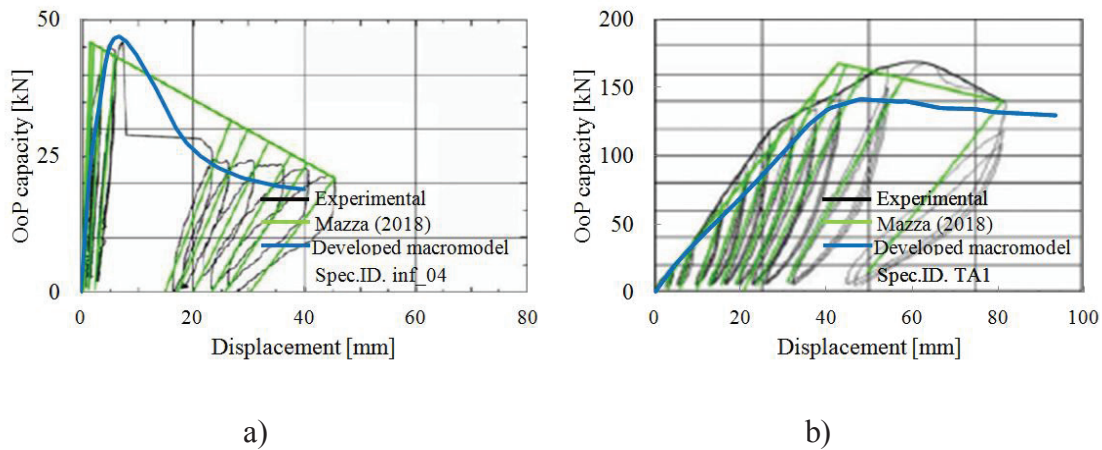


Figure 5.18 Experimental/numerical OoP response of: a) specimen inf_04 without IP damage, b) specimen TA3 after 1% pre in-plane drift ratio (The figure is overlapped from *Mazza (2018)*)

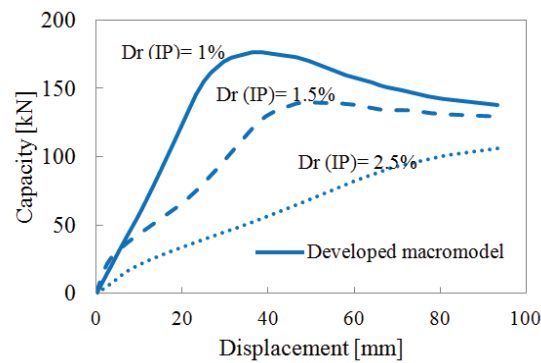


Figure 5.19 Numerical OoP response by using the developed macromodel of specimen TA3 (solid line), TA1 (dashed line) and TA2 (dotted line)

5.6 Model Validation

In purpose to validate the aforementioned macromodels the experimental results of *Negro et al. (1996)* (ELSA structure) and *FRAMA (2014)* are used. In the first experiment the URM infill walls were distributed in the direction of the test loading protocol. Subsequently the URM macromodels are validated in the IP direction. The second experiment is a three story 1:2.5 scaled structure with URM infill walls parallel and perpendicular to the excitation direction, then the macromodels of the masonry infill walls are validated in the in-plane and out-of-plane direction.

5.6.1 Comparative Study Utilizing Reference Object ELSA

The background research, described in Chapter 2, showed that a model with single strut (in each direction) is not capable of capturing the infill-frame interaction and the

correct shear and bending diagram in the frame members. *Saneinejad & Hobbs (1995)* and some other researchers have suggested that single-strut model may not be able to represent the interaction between the infill and the bounding frame and the force distribution in frame elements. In this chapter, the number and orientation of struts is varied to check the infill-frame interaction phenomenon. Namely, the considered models are (M #1) single strut, (M #2) double strut and (M #3) eccentric strut.

The fourth macromodel, (M#4) which was proposed by *Furtado et al. (2010)*, is an upgrading of the bi-diagonal compression strut model and considers the strength and stiffness degradation interaction in both directions of loading. The model is composed of four strut elements with elastic behaviour that support a central element where the nonlinear behaviour is concentrated. The nonlinear behaviour is characterized by a monotonic curve with five branches for each loading direction. The uniaxial material Pinching 04 is adopted to represent the hysteretic rule/behaviour.

Finally, the one pinned-joint diagonal beam column model with fiber hinges is used with two different uniaxial materials. The first material model is the symmetric elastic perfectly plastic model as proposed by *Mosalam et al. (2009)*, i.e., (M#5_org). Furthermore the new proposed pinching material model is utilized, i.e., (M#5_dev) (see Figure E.1, Appendix.E).

5.6.2 Discussion of the Results

In purpose to evaluate the effect of the URM infill walls on the structural response, the natural periods are calculated (see Table 5.10). It can be observed that the numerical natural periods are about (1.0 – 1.05) times larger than the predicted experimental time periods for the first four numerical models. Furthermore, the calculated time periods utilizing the models M#5_org and M#5_dev, are about 1.27 higher, which is expected due to single element modeling technique. (The considered natural time periods are in the direction of infill walls)

Table 5.10 Natural periods of the infilled structure

Model	M#1	M#2	M#3	M#4	M#5_org	M#5_dev
T_{Num} [s]	0.303	0.309	0.318	0.314	0.387	0.387
T_{Num}/T_{Exp}	1	1.02	1.05	1.04	1.27	1.27

In Figures 5.20 a and b the calculated and experimentally obtained storey displacement time histories for M#1 and M#4 are compared. As it is clearly seen, the results indicate a very good correlation between calculated and experimental values. However, the results for the other single strut models, i.e. M#2, M#3, are quite similar to the previous ones (see Appendix E). The numerical simulation results of model M#5_org and M#5_dev are shown in Figures 5.21 a and b. It is observed that the model for which the cracking of URM infill walls is neglected in the fiber plastic hinges (bi-linear stress-strain relationship with elastic-perfectly plastic branches, M#5_org), is not appropriate for simulating the case where the RC frame elements of the structure remains practically undamaged whereas the URM infill panels are heavily damaged. (A case where most of the earthquake input energy is being dissipated through the damaged infill walls and not by the RC frame elements). Moreover, Figure 5.21 b clearly illustrate the enhanced numerical response of the pinned joint one diagonal beam-column element model, i.e. M#5_dev, in case of utilizing the pinching material model, with cracking, yielding, maximum and post maximum strength, to simulate the behaviour of the URM infill panels.

5.6.3 Interaction Quality

It is worth to mention, in the experiment, only the first and second story URM infill walls were completely collapsed, the third story infill walls suffered heavy damage and the fourth story URM infill walls were intact. For a failure pattern determination, damage limit states are defined and related with the predefined material strains (see Table 5.3). Figure 5.22 displays the different observed and assigned damage states, utilizing the new calibrated pinned joint one diagonal beam-column elements with fiber hinges (M#5_dev), for the primary RC und secondary URM elements. It can be concluded:

- Moderate damages ($LDG_p 2$) at RC structural elements;
- Completely collapse at the 1st, 2nd story URM infill walls ($LDG_s 3$) and
- Heavy cracked infill walls at the 3th story ($LDG_s 2$).

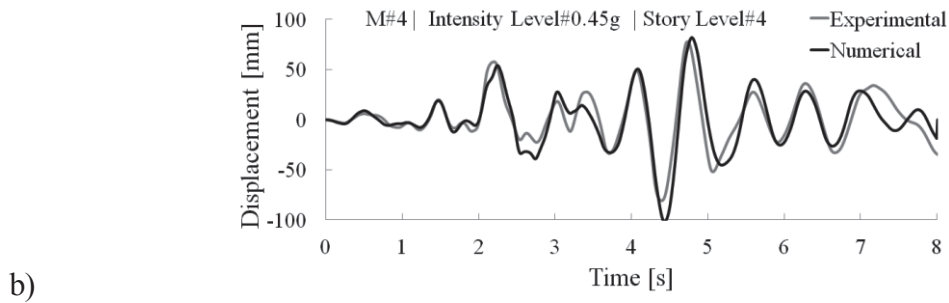
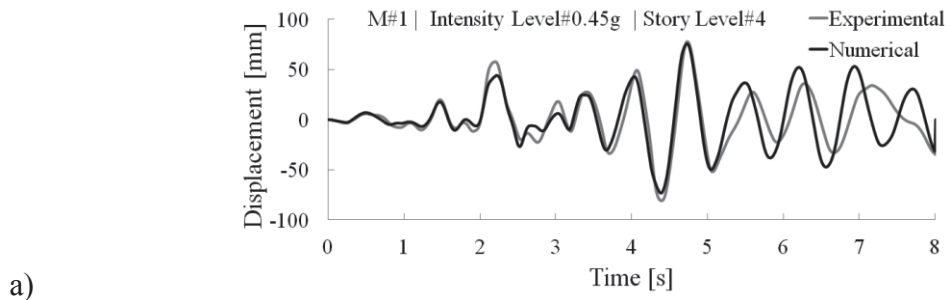


Figure 5.20 Experimental/numerical top displacement: a) M#1, b) M#4

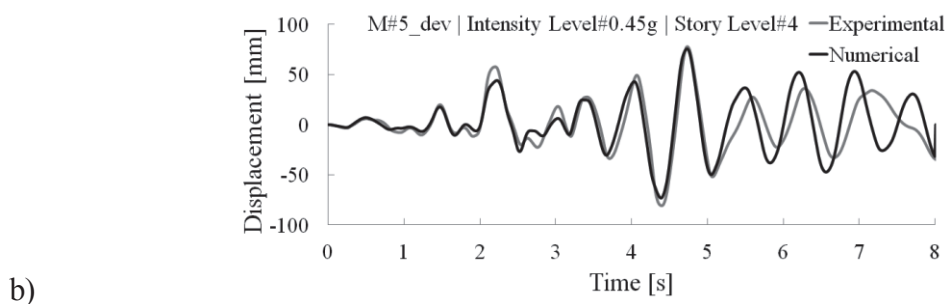
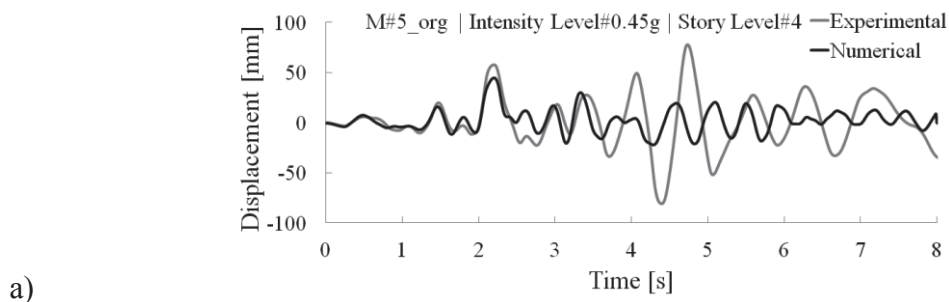


Figure 5.21 Experimental/numerical top displacement: a) M#5_org, b) M#5_dev

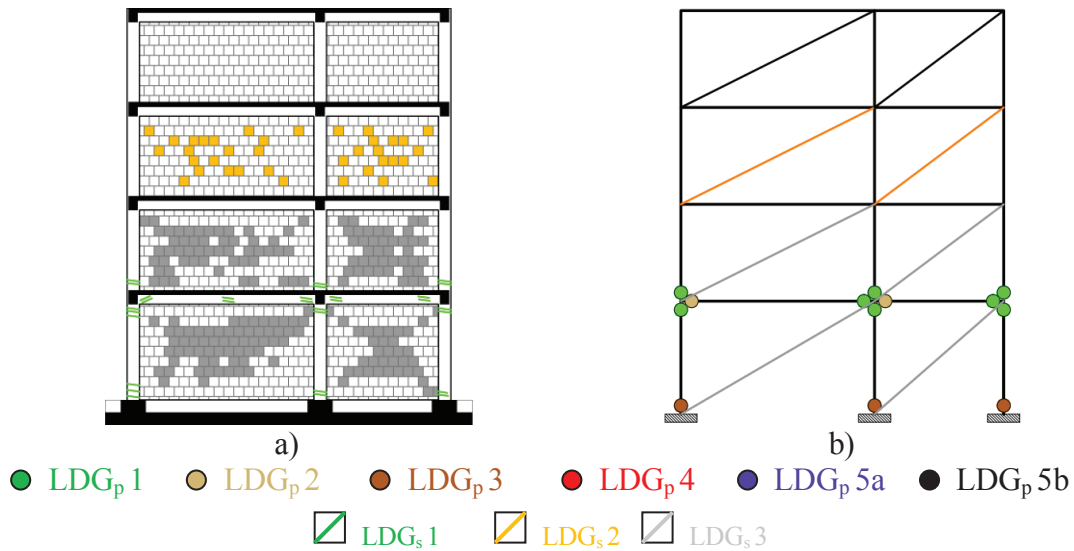


Figure 5.22 Damage distribution: a) Observed experimental, b) predicted numerical

For further investigation of the interaction between the RC frame elements and the URM macromodels under study, the maximum shear force for each column is recorded and normalized due to the column section shear capacity by using the equation proposed in ACI-318 (Chapter 3). As Figure 5.23 depicts, the higher shear demand on column is due to the one eccentric diagonal strut in each direction followed by the 2 diagonal struts and lastly the centric diagonal strut in each direction. The obtained results satisfy exactly the proposed model by FEMA 356 in which the eccentric one diagonal strut model is stated in case shear failure to the column elements is expected.

The presented results confirm the applicability of the conceptually calibrated macromodel (M#5_dev) to be used as an effective tool in the numerical modeling of the URM infill panel. Secondly, negligible force distribution between the one diagonal element in one direction (M#5_dev) and one diagonal element in each direction (M#1) is observed.

5.6.4 Reference Object FRAMA

At the University of Osijek (Croatia) and in DYNLAB the research project FRAMED-Masonry tests were carried out to study the behavior of RC frame structure with URM perforated infill walls. The experimental model was 1:2.5 scaled and tested under ten intensity increased ground motions.

The structure was designed according to the EC8 provisions and considering medium

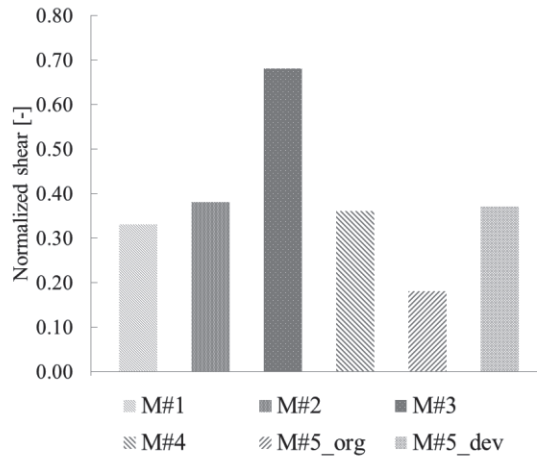


Figure 5.23 Normalized shear force applied to column

class ductility for the RC frame elements adopting the concept of over strength capacity and infilled with URM composed of hollow clay brick units has a dimension of $12 \times 25 \times 6 \text{ cm}^3$ and mortar layer with 1cm thick. As Figure 5.26 illustrates, the typical story height was 120cm, the first and second panel in the longitudinal direction were 128cm and 248cm center lines long respectively, and the length of the transverse panel was 220cm. The columns and beams cross sections were rectangular with $12 \times 16 \text{ cm}$, and the cover slab was 8cm thick.

In addition to the own weight of the structure, three sets of additional masses were placed on top of the slab at each floor (Figure 5.24). Each set contains four steel ingots with overall dimensions of $23.5 \times 14 \times 150 \text{ cm}$, with a weight of 4 kN each. The weights of the model are summarised in Table 5.11.

Table 5.11 Weight of model per element [kN]

Frame structure	74
Masonry infill	33
Foundation	47
Add. weight at the 1 st storey (12 ingots)	48
Add. weight at the 2 nd storey (12 ingots)	48
Add. weight at the roof	96
Total weight of the structure	346

As mentioned earlier, the structure was subjected to incrementally increased time history record. The adopted ground motion was recorded at the Herceg Novi station during the April 15th, 1979 Montenegro earthquake. The earthquake had a moment magnitude of 6.9 and a hypocentre depth of 12 km. The utilized peak ground acceleration levels were of 0.05g, 0.10g, 0.20g, 0.30g, 0.40g, 0.60g, 0.70g, 0.80g, 1g, 1.2g (Figure 5.25).

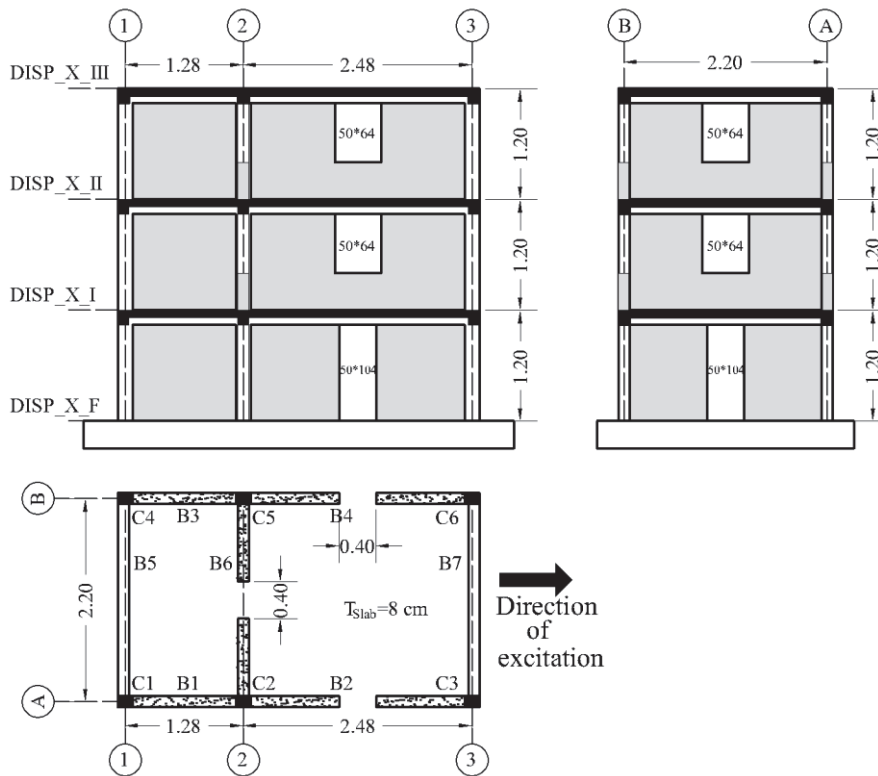


Figure 5.24 Elevation and plan view of the experimental infilled structure (Sigmund et al., 2014)

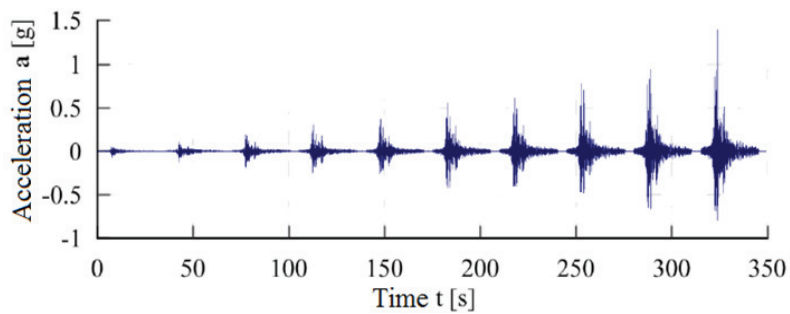


Figure 5.25 Used incremental time history in the experimental simulation

5.6.5 Considered Models and Discussion of the Results

Out of the previously six considered models four are chosen for further validation, namely (M#1, 2, 3 and M#5_dev). The results of the nonlinear time history calculations for the different models are compared with the experimental measured relative displacement of the FRAMED-Masonry experiment for the ten different intensity levels (see Appendix E).

In the second considered experiment (reference object FRAMA) the longitudinal as well as the transverse infill walls were excited, thus, the developed model (M#5_dev) is further validated in both directions.

To consider the effect of the existing openings on the capacity of the URM infill panel several experimental studies were carried out by different researches (*Calvi & Bolognini (2001)*, *Sigmund et al., 2014*) which showed that the inclusion of larger opening area will lead consequently to progressive reduction of the initial stiffness and maximum strength.

The calculated equivalent strut widths for FRAMA reference model are presented in Table 5.12 In order to calculate equivalent strut widths for the infill wall with openings, the reduction factors according to *Asteris et al. (2012)* are applied. These reduction factors reduce the strut width based on the size of the openings, thereby reducing the lateral resistance and stiffness of the infill walls.

Table 5.12 Reduced diagonal strut width [mm]

Section 1-2	Section 2-3		Section A-B	
Storey 1-2-3	Storey 1	Storey 2-3	Storey 1	Storey 2-3
164	83	105	67	88

In case of the herein proposed developed macromodel, the openings were explicitly considered through the discretization of each panel according to the doors and windows layout in the experimental model (see Appendix E).

Figure 5.26 shows the response of model (M5#_dev) compared to the experimental results. The measured peak displacement of the tested structure at the lowest intensity level is less than 1 mm. The comparison with the numerical results shows clear differences. In the case of higher intensity levels, however, satisfactory results are obtained. Higher matching between the numerical and experimental time history

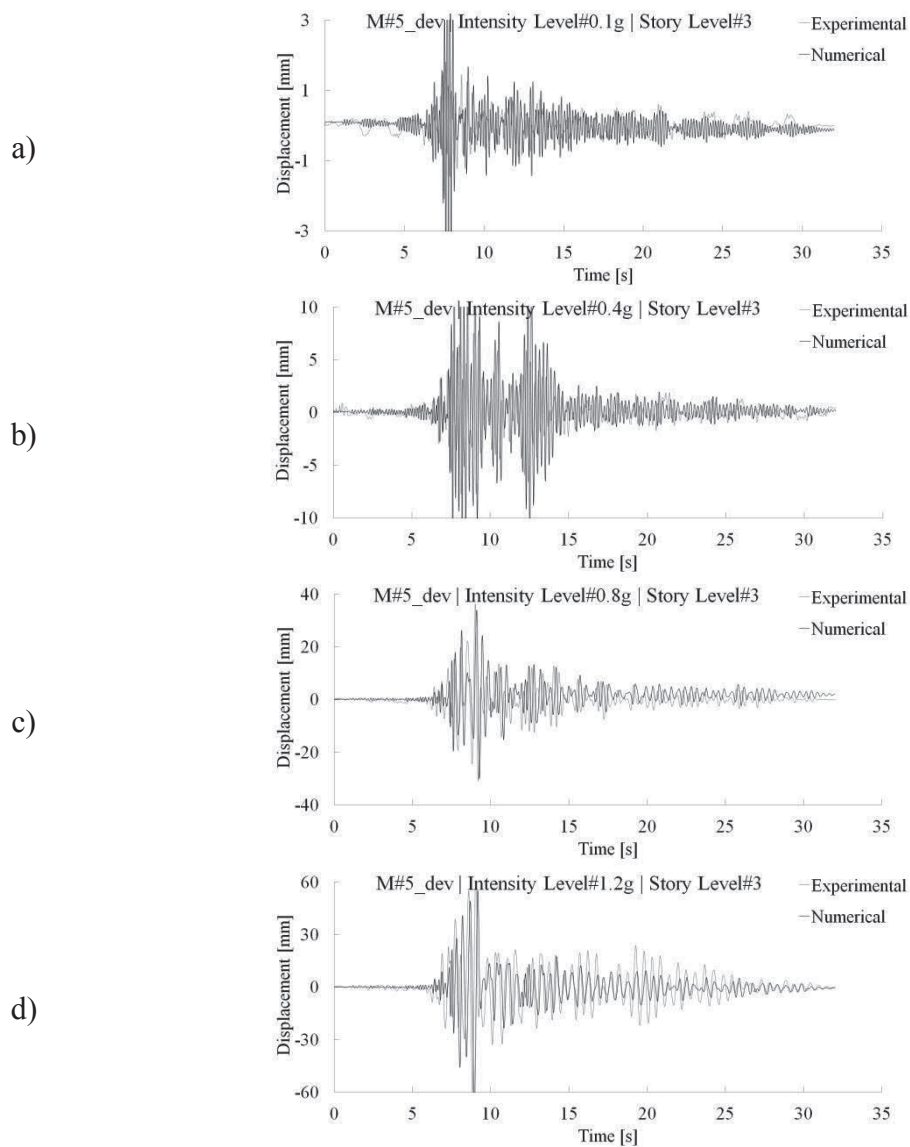


Figure 5.26 Experimental/numerical top displacement by using M#5_dev proposed macromodel at different intensity level: a) 0.1g, b) 0.4g, c) 0.8g, and d) 1.2g

displacement is attained. Figures 5.27 a to c show the growth of the experimental/numerical maximum interstory drift (IDR). It can be clearly observed that the experimental maximum IDR is considerably higher at the first story than those achieved at the second and third story. The comparison between the numerical and the experimental results at the first story and second story shows a good agreement with a difference about 8% at all intensity level. An exception are the intensity level 7 & 9 (PGA=0.7g, 1.2g), the calculated response is about two times less than the experimental one at the first story, and about two times higher at (PGA=1g, 1.2g) at the second story. A good matching of the experimental maximum interstory drift is achieved at the third story with slight differences about 4%.

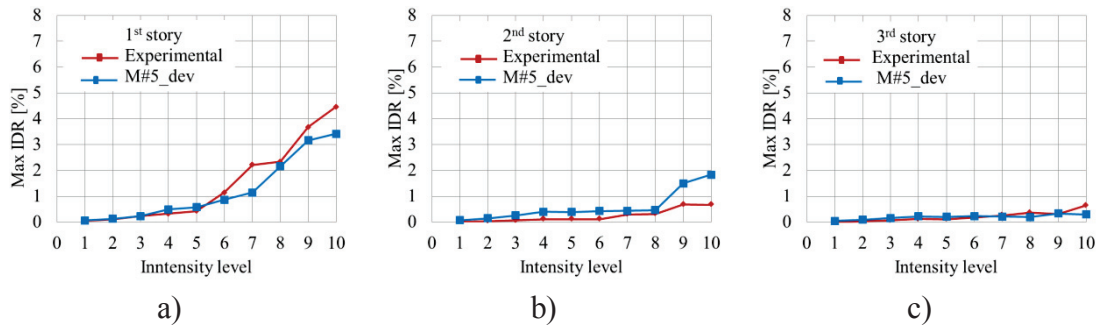


Figure 5.27 Experimental/numerical (M#5_dev) maximum interstorey drift: a) 1st story, b) 2nd and c) 3rd

For further evaluation of the models used here, the correlation between the computed numerical and measured experimental time history displacements at the top story level are determined using Equation 4.2.

As Figure 5.28 displays, depending on the chosen model and the intensity level, the correlations percentage is of a different value. At the same time, it should be noted that the results do not allow a clear ranking of the model quality. Furthermore, it can be concluded that models with different complexity are available for the damage prognosis. Hence, the choice of the "preferred model" would have to be made depending on the relevant expected damage. E.g, considering the OoP damage of the URM infill walls.

In the FRAMA blind prediction competition, to predict the expected seismic response of the structure, the models were qualified based on three different index errors (Equations 5.27, 5.28 and 5.29) estimated by the comparison between the numerical displacements at three target monitored points (D_X_I, D_X_II, and D_X_III) of the structure and the experimental displacements (see Appendix B.2).

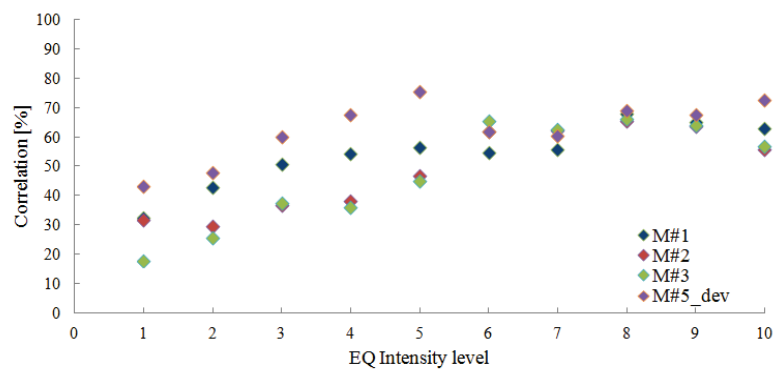


Figure 5.28 Top story correlation

$$\begin{aligned}
Error_{RMS} = & \sqrt{\frac{1}{N} \sum_{i=1}^N [|DXI_{num,i} - DXI_{exp,i}|]^2} \\
& + \sqrt{\frac{1}{N} \sum_{i=1}^N [|DXII_{num,i} - DXII_{exp,i}|]^2} \\
& + \sqrt{\frac{1}{N} \sum_{i=1}^N [|DXIII_{num,i} - DXIII_{exp,i}|]^2}
\end{aligned} \tag{5.27}$$

In expression 5.27, “num” and “exp” stand for the numerical and experimental relative displacements, respectively. N is the number of sampling points and errorRMS is the final result. The quantities D_X_I, D_X_II, and D_X_III represent the displacement, in millimetres, of the structure relative to the foundations (D_X_F) along the X-axis (longitudinal direction) (see Appendix B.2). Furthermore, an additional term that considers the area under the response curves relative to the experimental response, expressed by Equation 5.28:

$$\begin{aligned}
Error_E = & \frac{[\int_0^t |DXI_{exp,i}| - \int_0^t |DXI_{num,i}|]^2}{[\int_0^t |DXI_{exp,i}| \cdot \int_0^t |DXI_{num,i}|]} (t) dt \\
& + \frac{[\int_0^t |DXII_{exp,i}| - \int_0^t |DXII_{num,i}|]^2}{[\int_0^t |DXII_{exp,i}| \cdot \int_0^t |DXII_{num,i}|]} (t) dt \\
& + \frac{[\int_0^t |DXIII_{exp,i}| - \int_0^t |DXIII_{num,i}|]^2}{[\int_0^t |DXIII_{exp,i}| \cdot \int_0^t |DXIII_{num,i}|]} (t) dt
\end{aligned} \tag{5.28}$$

With the aim of considering the differences in the response amplitudes and the associated area under the response curves, the overall index error can be expressed by Equation 5.29.

$$Error_{RMS+E} = Error_{RMS} + Error_E \tag{5.29}$$

Table 5.13 summarizes the blind prediction errors resulting from the comparison between the numerical and experimental displacements of each storey, the individual error for each PGA level, and finally the cumulative error obtained.

Table 5.13 Cumulative Error E_{-RMS} , individual error and error for each storey

PGA [g]	Cumulative Error E_{+RMS}	Individual Error E_{+RMS}	Individual Error E_{+RMS}		
		Sum all story	1 st story	2 nd story	3 rd story
0.05	1.48	1.48	0.794	0.297	0.392
0.1	3.39	1.91	1.1824	0.304	0.428
0.2	5.85	2.45	0.620	0.784	1.045
0.3	9.98	4.13	0.691	1.591	1.8496
0.4	14.46	4.48	0.850	1.701	1.931
0.6	21.11	6.65	1.698	2.323	2.632
0.7	29.83	8.72	2.521	2.912	3.289
0.8	40.53	10.69	3.046	3.623	4.026
1.0	56.72	16.19	4.180	5.836	6.180
1.2	79.22	22.49	6.189	7.649	8.663

Figure 5.29 illustrates the obtained individual and cumulative error as reported by *Furtado et al. (2018)* and by using the developed model (M#5_dev) proposed in this study as well. It is notable that utilizing the M#5_dev model the individual error is less than 10 at the first seven intensity levels and between (10 - 22.5) at the last three intensity level.

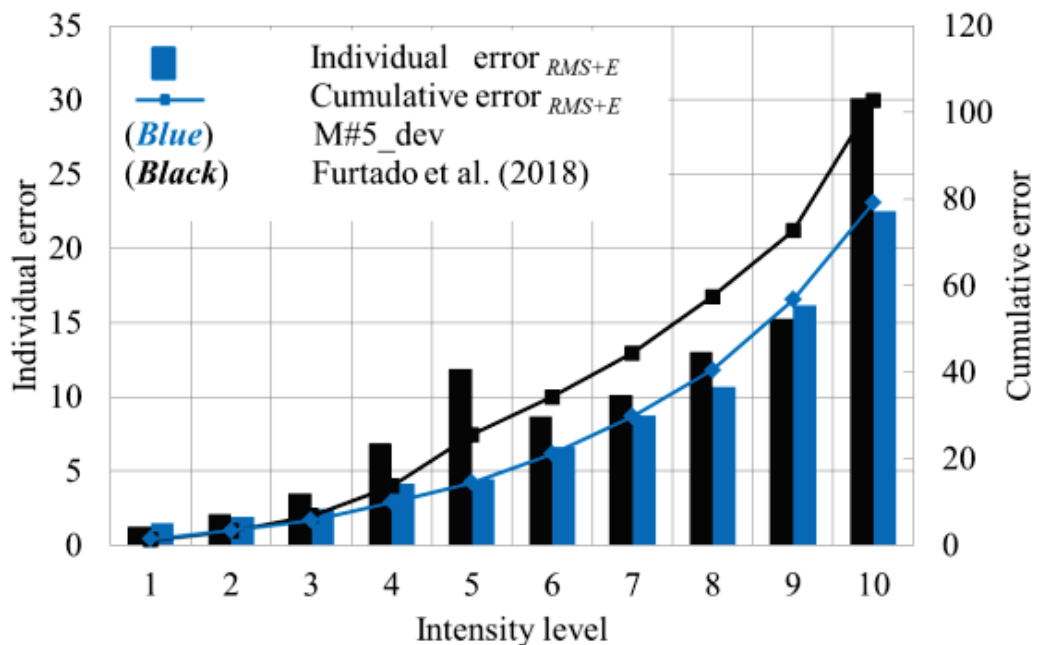


Figure 5.29 Individual and cumulative Error E-RMS results acc. to *Furtado et al. (2018)* and by using the proposed developed macromodel

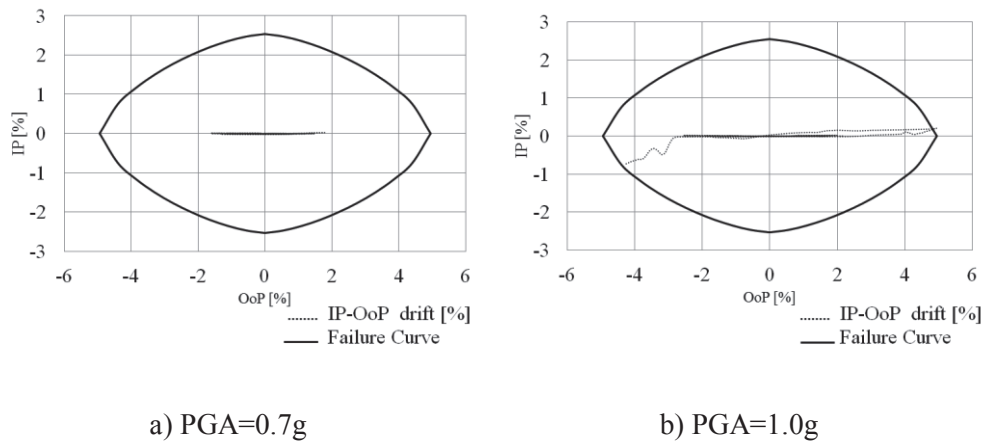


Figure 5.30 Normalized IP_OoP deformation path inside the failure curve (Story 1)

Figures 5.30 a and b show the deformation path of in-plane and out-of-plane displacement of the individual infill walls at the first story in the transverse direction due to the EQ scaled to (PGA=0.7g, 1.0g), normalized by their respective maximum IP and OoP displacements, as adopted from *VISION 2000, FEMA 356*. The failure curve is also included by red color.

In case the failure curve is exceeded, the URM infill walls are expected to be failed and will be removed by the algorithm, automatically. This is the case at PGA=1.0g, while no collapse of the URM infill walls is expected due to $PGA < 1.0g$ (Figures 5.30 a and b).

It worth to note, that the transverse walls are excited in the direction perpendicular to the URM infill panels, i.e. solely the OoP component is loaded, this justify the IP-OoP deformation path is composed of only OoP component as Figure 5.30 illustrates.

According to the reported experimental damage, the RC frame elements were slightly damaged, i.e. minor cracks, at excitation of 1.2g. The longitudinal URM infill panels subjected to IP excitation only - were heavily damaged at the first and second story. Mainly shear crack and bed joint sliding was observed (see Figure 5.31 a). The third story infill walls were intact.

As for the masonry infill walls loaded in the OoP direction, the dominated failure pattern was the separation of the URM infill panels from the surrounding RC frame elements. At 0.8g the third story infill walls were first unattached from the top beam, whereas at 1.0g the first story masonry walls were disconnected from the top beam

and subsequently at 1.2g the top row of clay block masonry was removed (*Penava et al., 2017*) (see Figure 5.31 b).

The numerical damage at intensity level 1.2g is recorded utilizing the new calibrated pinned joint one diagonal beam-column element with fiber hinges model (M#5_dev). As Figure 5.31 b illustrates, slight damages (LDG_p 1, LDG_p 2) at RC structural elements are determined, whereas, the URM infill walls, in the longitudinal direction, are completely collapsed at the 1st story (LDG_s 3), heavily damaged at the 2nd story (LDG_s 2) and intact at the 3rd story. The URM infill panels in the transverse direction, i.e. the OoP component, are proposed to fail completely.

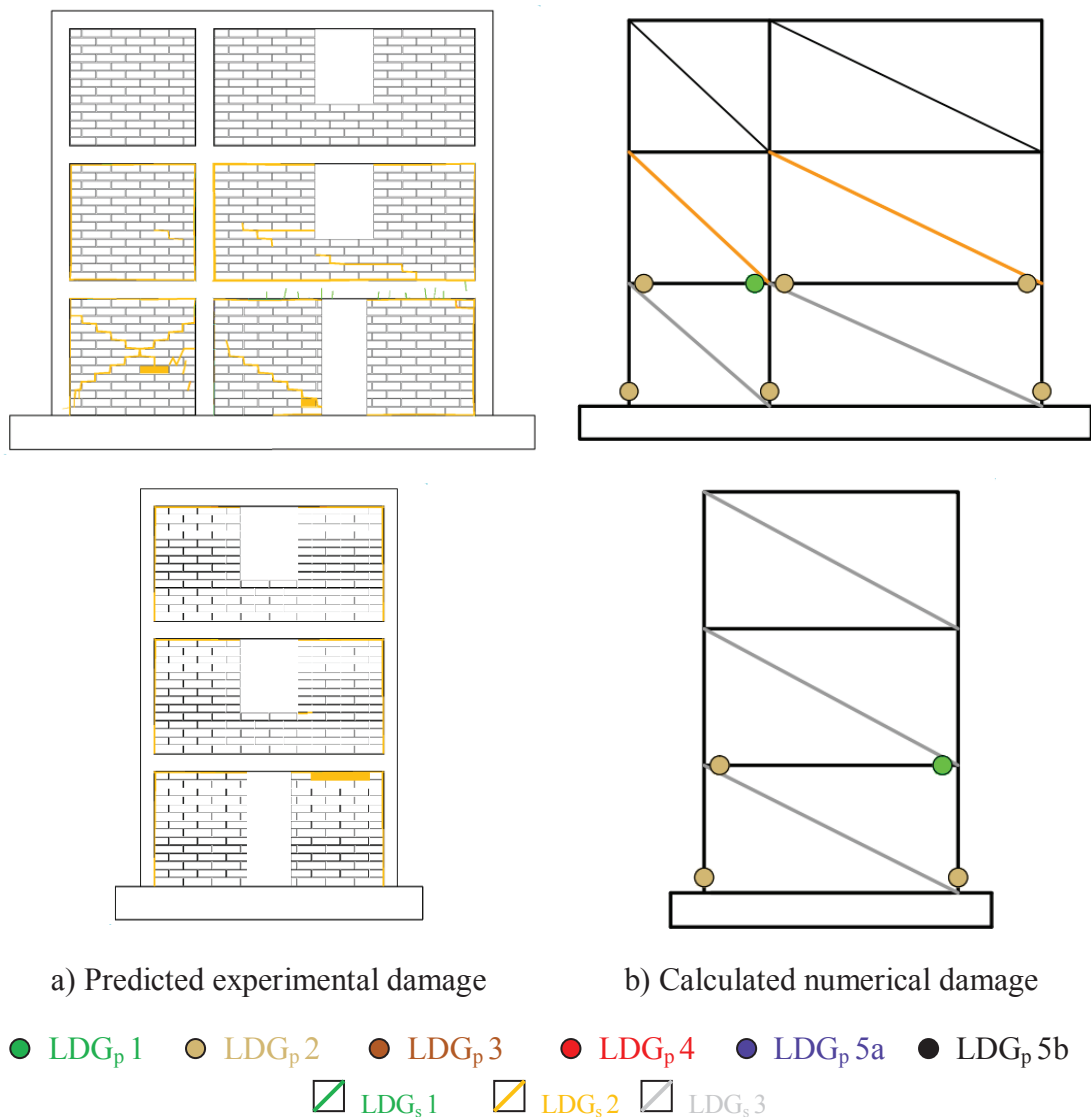


Figure 5.31 Damage prognoses: a) observed experimental, predicted, b) predicted numerical

5.7 Summary

Chapter four and five are dedicated to the introduction and elaboration of the available macromodeling strategies of RC frame structures with URM infill walls.

Chapter four is mainly concentrated to evaluate the RC frame models. Two main different macromodels of the frame elements are adopted, i.e. rigid plastic hinges and fiber based section hinges. As far as the simulation results of ELSA structure by using the fiber section is successful and gives good matching with the experimental results the concept is adopted as the source of nonlinearity of RC frame in the following chapters.

In chapter five a new simplified 3D macromodel for the assessment of both in plane and out-of-plane responses of infilled frames is developed through a process of calibration, verification and validation.

- The model provided the use of lumped plasticity fiber section beam-column elements.
- The inherent interaction between the IP and OoP responses are explicitly addressed through a coupling between axial-load and bending moment in the mathematical formulation of the discretized fiber cross section.
- The calibration is carried out performing a comparison with the results of several experimental tests provided by different authors on reinforced concrete infilled frames.
- The verification is achieved through a comparison with the results of the recently proposed macromodels for URM infill walls by *Di Trapani et al. (2017)* and *Mazza (2018)*.
- The model calibration/verification results have shown good accuracy in predicting the IP and OoP response of masonry infills. Moreover, the developed model is able to provide reliable estimations of the OoP strength and stiffness in case of infilled frame with and without pre IP damage.
- Finally, the developed model is dynamically validated utilizing the experimental data of 1:1 and 1:2.5 scaled multi-story structures. The results have shown good matching with the experimental results in term of global response (time history displacement) and local response in term of damage of both the URM infill panels and infill-frame interaction.

- To account for possible shear failure due to the local infill-frame interaction, the proposed 3D macromodel has to be eccentric in contact with columns (see Figure 5.23).

BLANK PAGE

Chapter 6: Application to 3D Multi-Story Structures

6.1 Introduction

In the previous chapter the proposed model is validated utilizing two multi story experiments. The first one, *Negro et al. (1996)* was used to validate the model in the in-plane direction. Whereas by utilizing the second experiment *FRAMA (2014)* it was possible to validate the model in the in-plane direction as well as the out-of-plane direction separately.

Due to the fact that the earthquake excites both the in- and out-of-plane direction or their combination and in purpose to investigate its behavior and capabilities, the infill model proposed in Chapter 5 is incorporated into a larger model of different-story number reinforced concrete (RC) frame building with unreinforced masonry (URM) infill walls.

1. The first group of models are constructed to investigate the effect of different number of story and different configuration of the URM infill panels. Namely, full infill and open ground storey are considered. These models are then subjected to seismic base excitation, using seven sets of ground motion generated in compliance with the German code. The used time histories are scaled at three different levels of spectral acceleration (*Schwarz et al., 2017, 2018*).
2. A second group of models are constructed targeting to check the influence of using different material type of both the RC frame elements and the URM infill walls, the numerical models are excited by using seven pair of earthquake extracted from the European database.

To evaluate the performance of the models in hand the global response quantities of the structures are determined, i.e. the maximum interstory drifts, along with the local responses of the individual RC frame elements and infill panels.

6.2 Seismic Action for Horizontal Cyclic Excitation

6.2.1 Representative Time Histories for the Site Categories of German Code

To investigate the influence of local site effects on the structural response seven sets of ground motion are selected in compliance with the German code DIN4149:2005. The German Code distinguishes between the type or consistency of soil materials of the uppermost layers and the extent of sedimentary materials. Both, the soil condition (A, B, C) and geological subsoil classes (R, T, and S) form the depth profile. In total six different combinations with different corner periods and soil factors are defined, whereas A-R represents rock and C-S soft sites (see Table F.1, Appendix F). Following the investigations by *Schwarz et al. (2017, 2018)*, sets of code spectra representative ground motion can be identified and are adopted in this study (Figure 6.1). Furthermore, the respective time history records are shown in Figure F.2 (Appendix F).

6.2.2 Representative Time Histories as per the European Database

Following recommendations from previous studies (*Iervolino et al., 2008*); the selection of natural records scaled to different levels of seismicity is accepted as a suitable solution for the numerical seismic simulation of RC structures. The records are selected from a European database using the computer software REXEL (*Iervolino et al., 2010*); the compatible records are scaled to the adopted design values of PGA (i.e., 0.05g, 0.20g, 0.35g and 0.5g) (Figure 6.2). Moreover, the representative time histories are illustrated in Figure F.4 (Appendix F).

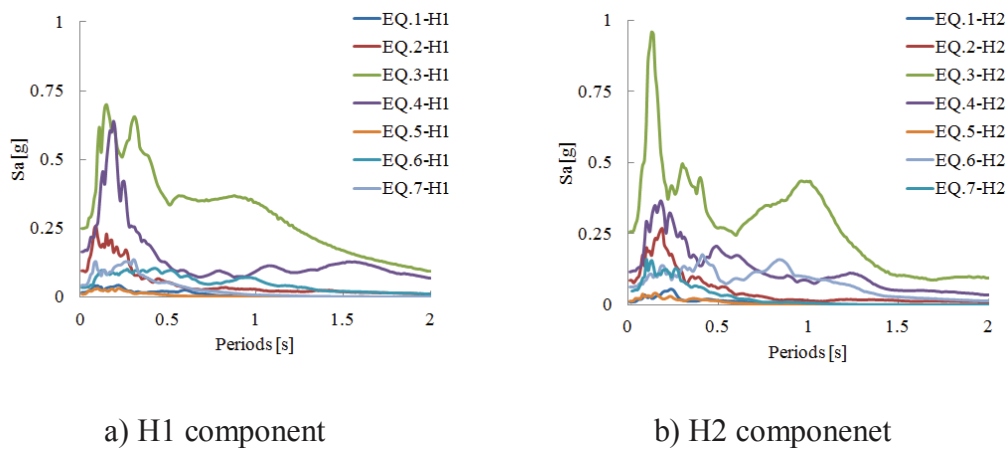


Figure 6.1 DIN4149 code spectra representative ground motion used in case study 1: a) component H1, b) component H2

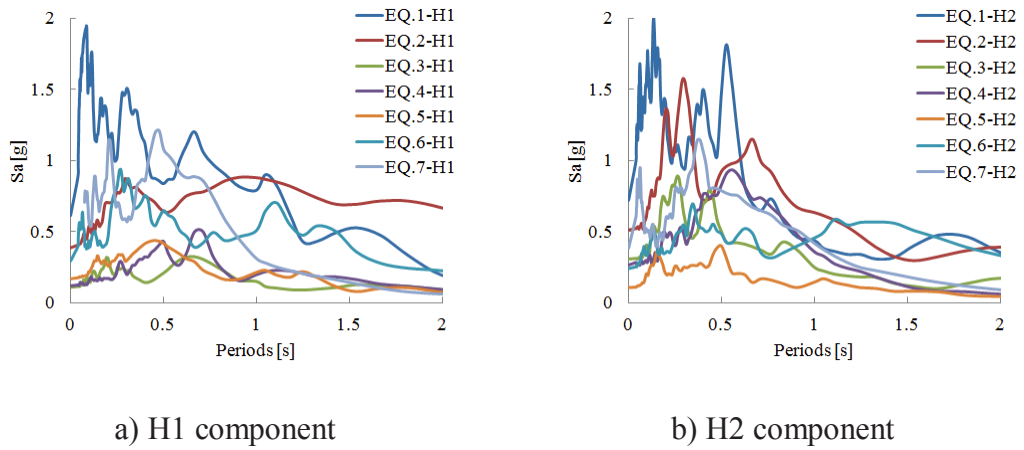


Figure 6.2 European code spectra representative ground motion used in case study 2: a) component H1, b) component H2

6.3 Definition of Assessment Criteria

Figure 6.3 illustrates a schematic view of the numerical abstraction, i.e. modeling the real structure utilizing the proposed developed numerical model, and the evaluation criteria.

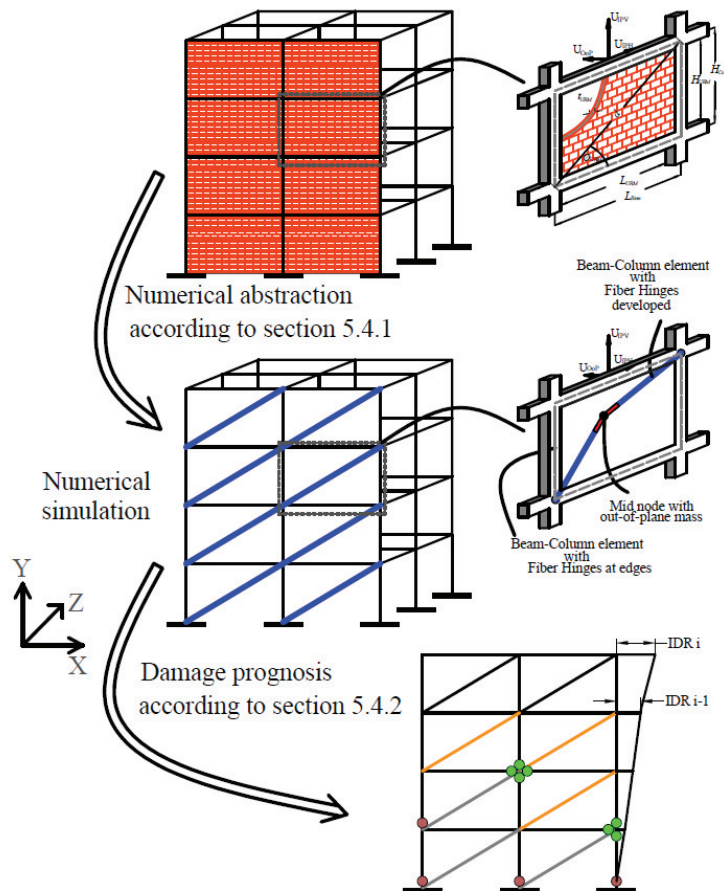


Figure 6.3 Conceptual numerical abstraction and results evaluation

6.4 Case Study 1

6.4.1 Model Description

The RC frame building has four spans in the longitudinal direction and one in the transverse direction as Figures 6.4 a and b show.

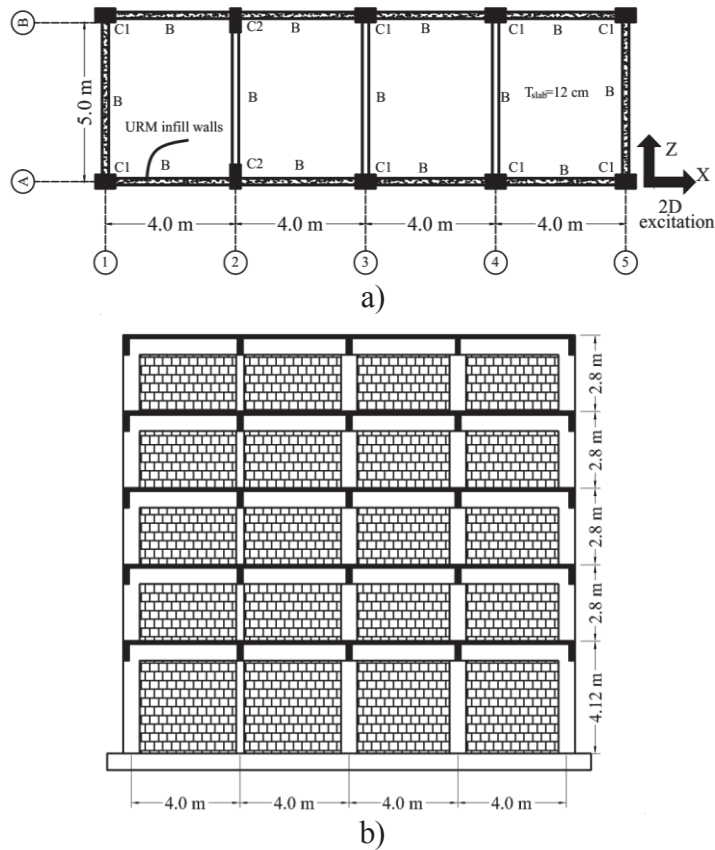


Figure 6.4 Case study 1 structure: a) plane layout, b) elevation view

Three different story height are considered, namely, 3, 5 and 7 with three different configuration for each height, in specific; (i) Bare frame without infill walls (BR), (ii) Full URM infill walls placed along the height and structure perimeter (FI) and (iii) Soft story (SS), i.e. open ground story. The RC frame and infill walls material properties are shown in Tables 6.1 and 6.2.

Table 6.1 RC frame material properties

Young modulus of concrete E_c [GPa]	29
Compression strength concrete f_c [MPa]	24
Tensile strength concrete f_t [MPa]	1.3
Weight of concrete [kN/m^3]	25
Mass density of concrete [t/m^3]	2.55
Yield strength of steel f_y [MPa]	450
Ultimate strength of steel f_u [MPa]	575

Table 6.2 URM masonry infills material properties and thickness

Young modulus of infills E_{URM} [GPa]	2.6
Diagonal cracking strength f_{ip} [MPa]	0.18
Infill wall thickness t_{URM} [mm]	150

6.4.2 Fundamental Natural Periods

The natural vibration of a structure, as one of the most important dynamic characteristics of a structure plays a significant role in the prediction of seismic behavior of a structure which is controlled by the mass and stiffness. The computed fundamental periods for the considered herein three story building models in terms of bare frame, URM infill and open first story models in X-direction have been found to be 0.195 sec, 0.146 sec and 0.165 sec, respectively. The corresponding values in Z-direction are 0.240 sec, 0.220 sec and 0.230 sec. It can be clearly observed from the results that representing the URM infill panels as equivalent beam column elements has the effect of reducing the fundamental natural period of the building. Bare frame model, in which the masonry infill walls are neglected, overestimates the induced natural period as compared to the other two models with masonry infill walls. The natural periods are calculated for all considered herein models (see Table 6.3). The same reduction in the calculated natural periods in Z-direction cannot be observed as in X-direction, since the allocation of the URM infill walls was just in the first and last span. Furthermore, it can be clearly seen from the numerical results that the open first story models provide almost the same value of the natural period provided by the bare frame models in X and Z directions and this was confirmed in *Negro et al., (1996)*. The determined results show that considering the URM infill walls significantly affect the stiffness of the structure and in turn the natural periods. In addition, the captured results indicate that the open first story building models, which are considered as partially infilled frames, provide natural period a bit lesser than the corresponding value of the bare frame models. This can be due to the presence of an open ground floor which leads to a reduction in the lateral stiffness

Table 6.3 Natural periods for the studied numerical models

No. of Stories (i)	Periods [s]					
	3		5		7	
Direction (Mode)	X	Z	X	Z	X	Z
Model 1-i (BR)	0.195	0.240	0.330	0.413	0.469	0.597
Model 2-i (FI)	0.146	0.220	0.242	0.377	0.342	0.549
Model 3-i (SS)	0.165	0.230	0.262	0.388	0.362	0.559

6.4.3 Interstory Drifts

Interstory drift, which is defined as lateral displacement of one level relative to the level above or below normalized by story height, is considered as an important indicator of the global structural behavior in performance-based seismic assessment.

In this study, the maximum interstory drift response of Models 1-i, 2-i and 3-i is extracted and compared. Figures 6.5, 6.6 and 6.7 a to c illustrate the determined interstory drift ratio at $PGA=0.3g$ for all considered models. In case of 3, 5 and 7 story structures the recorded IDR is about 0.35% for all models and due to the most used time histories. However due to soft soil (EQ.6/C-S) representative earthquake record the drift ratio attained a maximum value between (0.5-1.5%) in case of 5 and 7 story building models.

Figures 6.8, 6.9 and 6.10 a to c show the determined interstory drifts due to the different considered ground motions scaled to $PGA=0.5g$. Accordingly, Model 3-3 (SS) suffered considerably more drift magnitudes at the first story in comparison with Model 1-3 (BR) and Model 2-3 (FI). However, e.g., in case of (EQ.5/C-R, EQ.3/B-S), approximately the same interstory drift ratio for Model 1-3 (BR) and Model 3-3 (SS) in the first story is observed. Since the quantity of damage is the same for both models and no infill walls are exist in the first story of Model 3-3 (SS). Thus, the behavior of RC frames of Model 3-3 (SS) is the same as the Model 1-3 (BR). The interstory drift is smaller, i.e. less than 0.25%, for Model 3-3 (FI) with respect to all considered ground motions since the RC frame elements mostly suffered moderate damage (LDG_p 2) and the infill walls are not collapsed; consequently, that imposes more stiffness and thus smaller interstory drift ratio.

For models of the 5 story building, Model 3-5 (SS) showed the largest inter-story drift ratio when compared with Model 1-5 (BR) and Model 2-5 (FI) as depicted in Figure 6.9. However, concentration of the large inter-story drift at the first story is noticed for all considered EQ's, due to the vertical irregularities imposed by the open ground story which lead to less stiff story. Similar interstory drift are obtained in the first and second story for Model 1-5 (BR) and Model 2-5 (FI) in case of soft soil (EQ.6/C-S) code spectra representative EQ since the infill walls are collapsed and removed from the model and the damage quantity of RC frame elements in both model are the same. Whereas in case of (EQ.3/B-S) ground motion and because of

more damage imposed on RC frame elements, Model 1-5 (BR) suffers higher interstory drift in comparison with Model 2-5 (FI).

The same behavior, as for the models of five stories, can be noticed for models of the 7 story building with the exception that in case of (EQ.6/C-S) and for Model 2-7 (FI), solely the infill walls in the first story were collapsed and removed during the analysis which in turn lead to the formation of soft story mechanism and similar response as for Model 3-7 (SS).

These presented results clearly identify that the inclusion of masonry action altered the structural response. Moreover, the simulation results showed that consideration of IP-OoP interaction linked with infill wall removal capabilities is a suited approach for the damage prognosis and damage reinterpretation in case of earthquake loading.

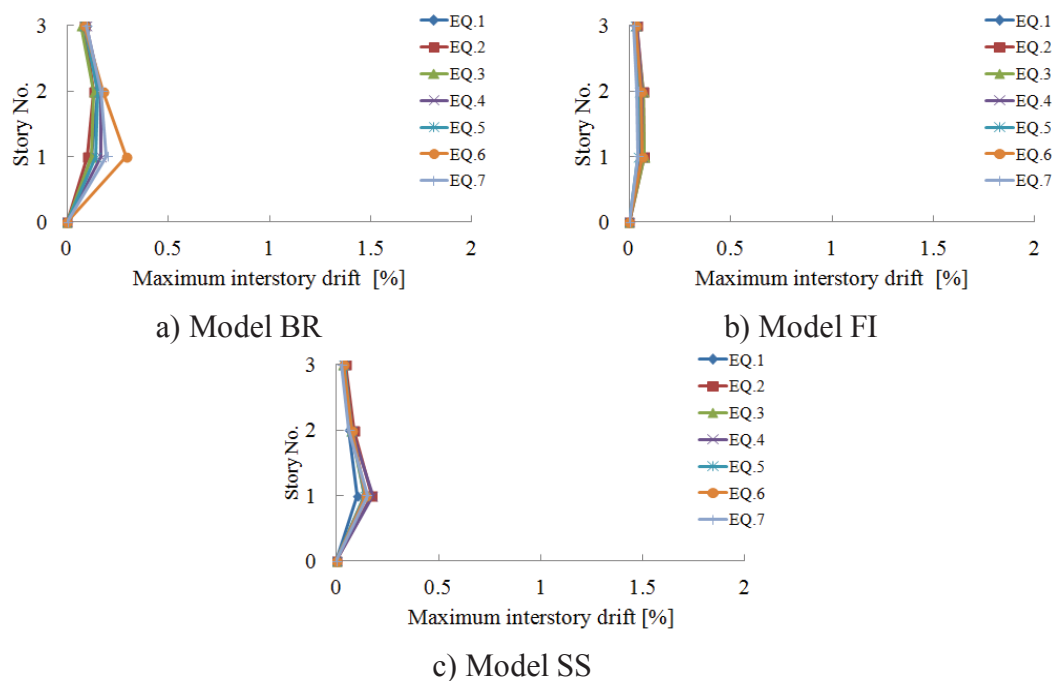


Figure 6.5 Three story models maximum interstory drift acc. to the considered ground motions at 0.3g PGA: a) bare, b) full infilled and c) soft story

It also indicates that possible soft story formation in lower stories can be simulated. Thus, IP and OoP interaction and the resultant possible collapse of URM infill walls should be addressed already in the design process of the new multi-story RC frame structures. It has also been noted that an increase in the drift profile of the model with the open ground story in case of soft soil (EQ.6/C-S) occurs at the first story. This due to stiffness irregularity which also can be a reason of failure of structures under earthquake excitations where the columns in soft story case are exposed to large deformation and formed plastic hinges at top and bottom of the vertical elements.

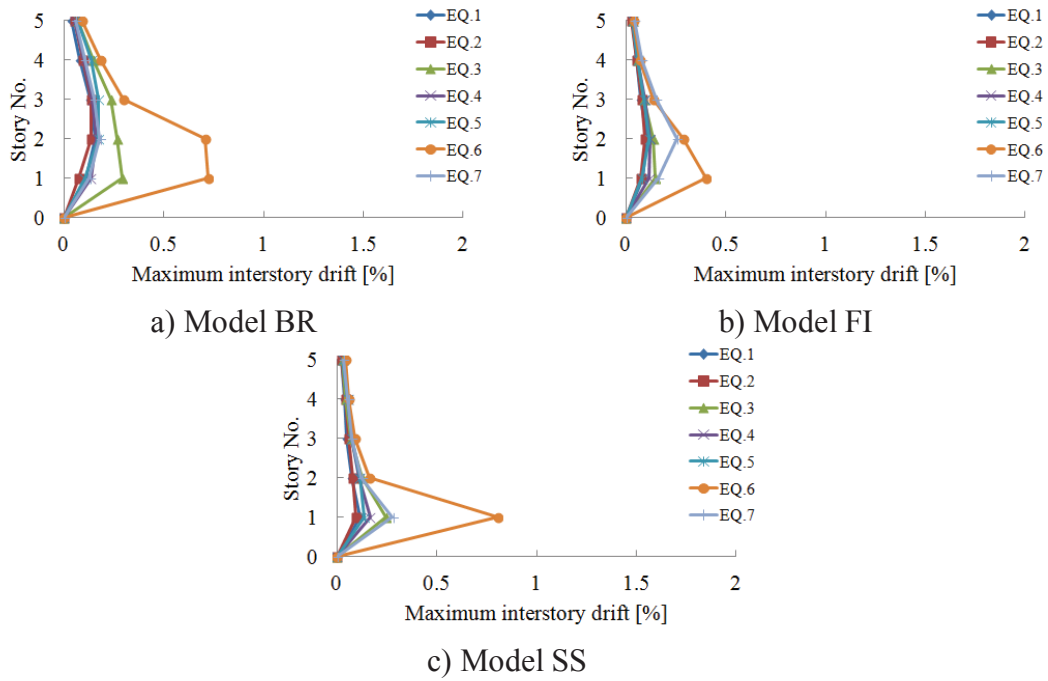


Figure 6.6 Five story models maximum interstory drift acc. to the considered ground motions at 0.3g PGA: a) bare, b) full infilled and c) soft story

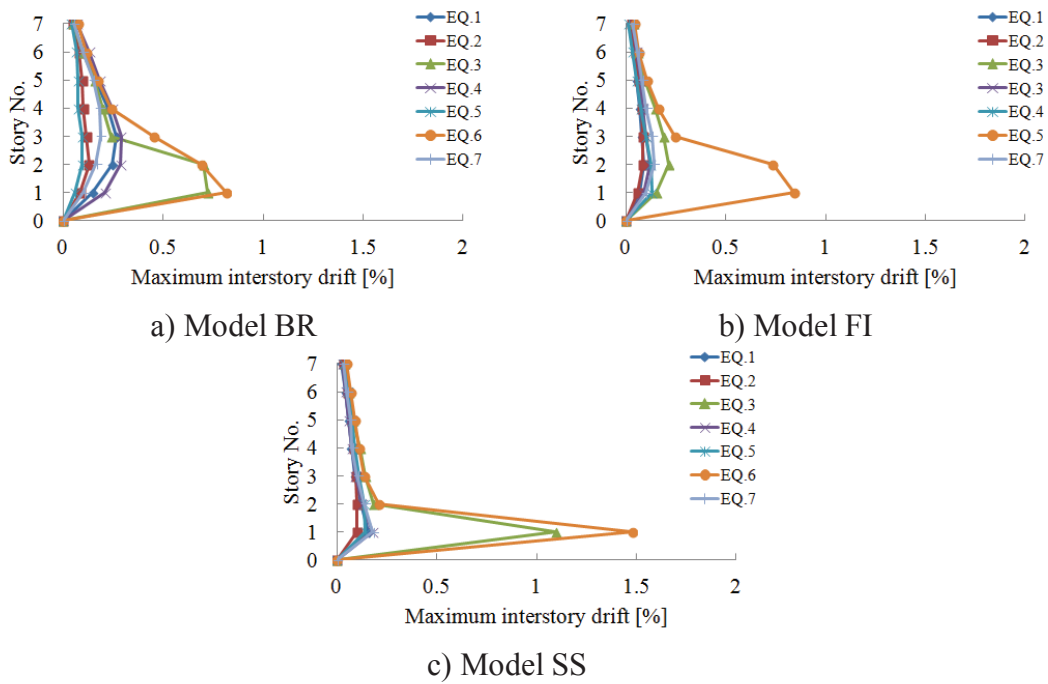


Figure 6.7 Seven story models maximum interstory drift acc. to the considered ground motions at 0.3g PGA: a) bare, b) full infilled and c) soft story

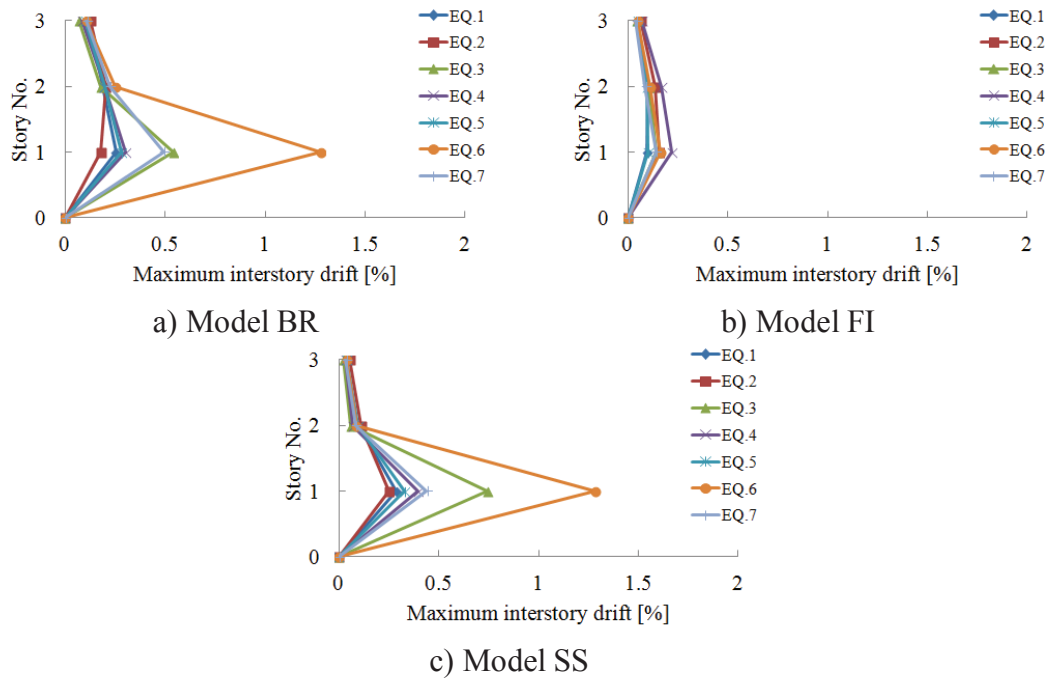


Figure 6.8 Three story models maximum interstory drift acc. to the considered ground motions at 0.5g PGA: a) bare, b) full infilled and c) soft story

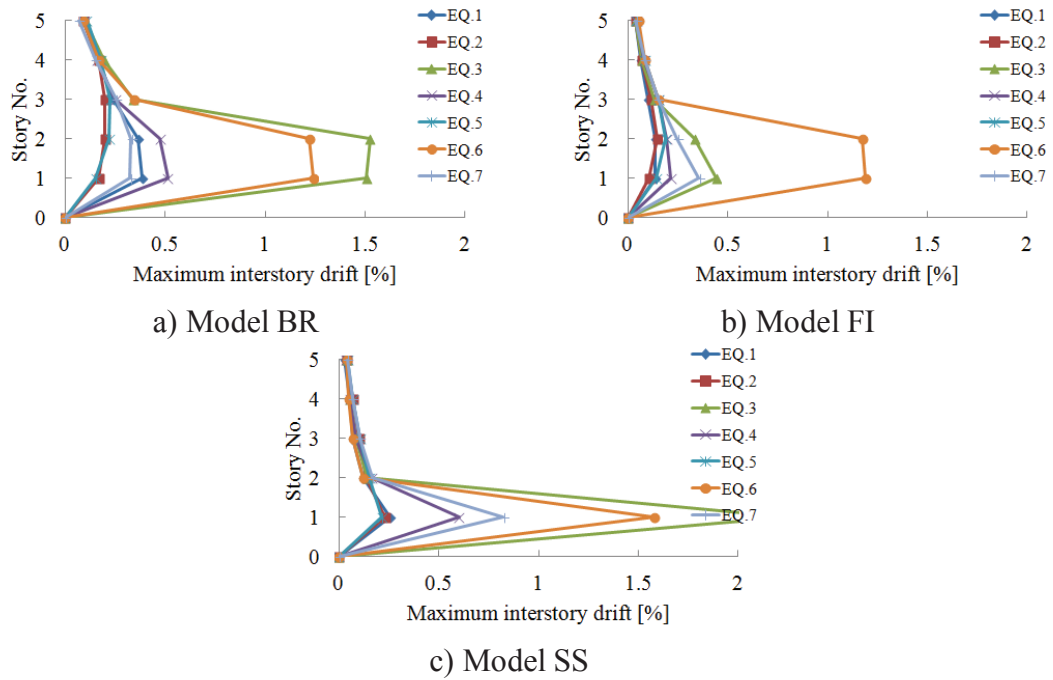


Figure 6.9 Five story models maximum interstory drift acc. to the considered ground motions at 0.5g PGA: a) bare, b) full infilled and c) soft story

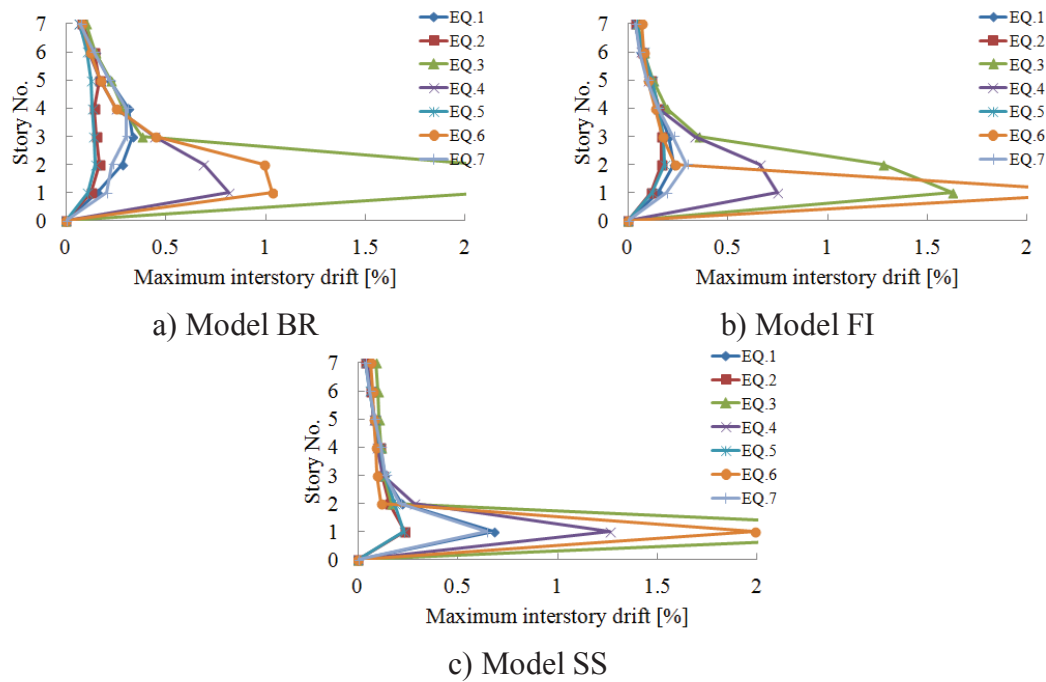


Figure 6.10 Seven story models maximum interstory drift acc. to the considered ground motions at 0.5g PGA: a) bare, b) full infilled and c) soft story

6.4.4 Damage Prognosis

In purpose to investigate the behavior of the models under study according to the local response quantities, namely recorded fiber's strains of the RC frame element and representative URM infill numerical model, the damage prognosis of the all considered models is determined and plotted according to the damage grade definitions in chapter five based on the EMS-98 for reinforced concrete frames with and without URM infill walls (see Appendix E for the complete results).

Tables 6.4 to 6.6 illustrate the numerical determined damage distribution for model BR, FI and SS with different number of story due to the (EQ.6/C-S) seismic action scaled to 0.1g, 0.3g and 0.5g respectively. As Figure 6.1 shows, the frequency contents of the used ground motions are different, accordingly different damage grades resulting from the considered earthquakes are predicted. E.g., the EQ.6 scaled to 0.1g (PGA) will cause light damage for the 3 and 5 story bare and full infilled frames whereas the 7 story structure will suffer moderate ($LDG_p 2$), severe ($LDG_s 2$) and light ($LDG_p 1$) damage level in case of the bare, full infilled and soft story numerical models respectively.

At $PGA=0.3g$, more damage to RC frame elements and URM infill panels is added. The damage of the 3 story bare frame models attained a degree of moderate damage (LDG_p 2), whereas severe damage (LDG_p 5b) is predicted for 5 and 7 story structures. Including the infill walls in the uniform pattern caused less damage to RC frame elements in the 3 and 5 story models which in turn enhance the performance of the structure. The 7 story structure suffered concentration of damage at the first story due the failure of URM infill panels. The irregularity imposed in the third group of models, i.e., the open ground story, lead to a damage grade of (LDG_p 5b) at the first story columns and subsequently the soft story failure mode for the 5 and 7 story structures whereas, the 3 story structure is protected against such a failure type. At $0.5g$ (PGA), collapse damage grade is observed in the RC columns of the 3, 5, 7 story bare model. It's worth mentioning that the failure of URM panels due to the in-plane and out-of-plane of the first story caused the so called soft story mechanism in case of 5 and 7 story buildings whereas the same is not observed for the 3 story structure and that is because most of the earthquake energy is dissipated due to the damage of masonry infill walls.

In case of open first story models, the damage was concentrated in the first story columns which in turn led to the formation of soft story mechanism.

The elaborated damage grades indicate the strong influence of the considered ground motion data for risk studies as well as the occurrence of out-of-plane failure types and show that consideration of IP-OoP interaction linked with infill wall removal capabilities is a suited approach for the damage prognosis and damage reinterpretation in case of earthquake loading. It also indicates that possible soft story formation in lower stories can be simulated.

Table 6.4 Damage prognosis for (EQ.6/C-S) seismic actions at 0.1g PGA

3 Story Model Frame	5 Story Model Frame	7 Story Model Frame
BR		
FI		
SS		
<p> ● LDG_p1 ● LDG_p2 ● LDG_p3 ● LDG_p4 ● LDG_p5a ● LDG_p5b ▧ LDG_s1 ▧ LDG_s2 ▧ LDG_s3 </p>		

Table 6.5 Damage prognosis for (EQ.6/C-S) seismic actions at 0.3g PGA

3 Story Model Frame	5 Story Model Frame	7 Story Model Frame
BR		
FI		
SS		
<div style="display: flex; justify-content: space-around; align-items: center;"> <div style="display: flex; gap: 10px;"> ● LDG_p 1 ● LDG_p 2 ● LDG_p 3 ● LDG_p 4 ● LDG_p 5a ● LDG_p 5b </div> <div style="display: flex; gap: 10px;"> ▧ LDG_s 1 ▨ LDG_s 2 ▩ LDG_s 3 </div> </div>		

Table 6.6 Damage prognosis for (EQ.6/C-S) seismic actions at 0.5g PGA

3 Story Model Frame	5 Story Model Frame	7 Story Model Frame
BR		
FI		
SS		
<div style="display: flex; justify-content: space-around; align-items: center;"> <div style="display: flex; gap: 10px;"> ● LDG_p1 ● LDG_p2 ● LDG_p3 ● LDG_p4 ● LDG_p5a ● LDG_p5b </div> <div style="display: flex; gap: 10px;"> ▤ LDG_s1 ▤ LDG_s2 ▤ LDG_s3 </div> </div>		

6.4.5 Interstory Drifts as a Function of the Scaled Seismic Records

As mentioned above 189 numerical analyses were carried out to evaluate the performance of the three considered numerical models with different story height utilizing the developed URM numerical model which considers the in-plane and out-of-plane response and the interaction between both of them. The vulnerability of the structure at different peak ground acceleration (PGA) can be obtained by plotting maximum interstory drift vs PGA. Thus, the interstory drift ratio for each model is averaged and plotted against the considered intensity level on the same graph.

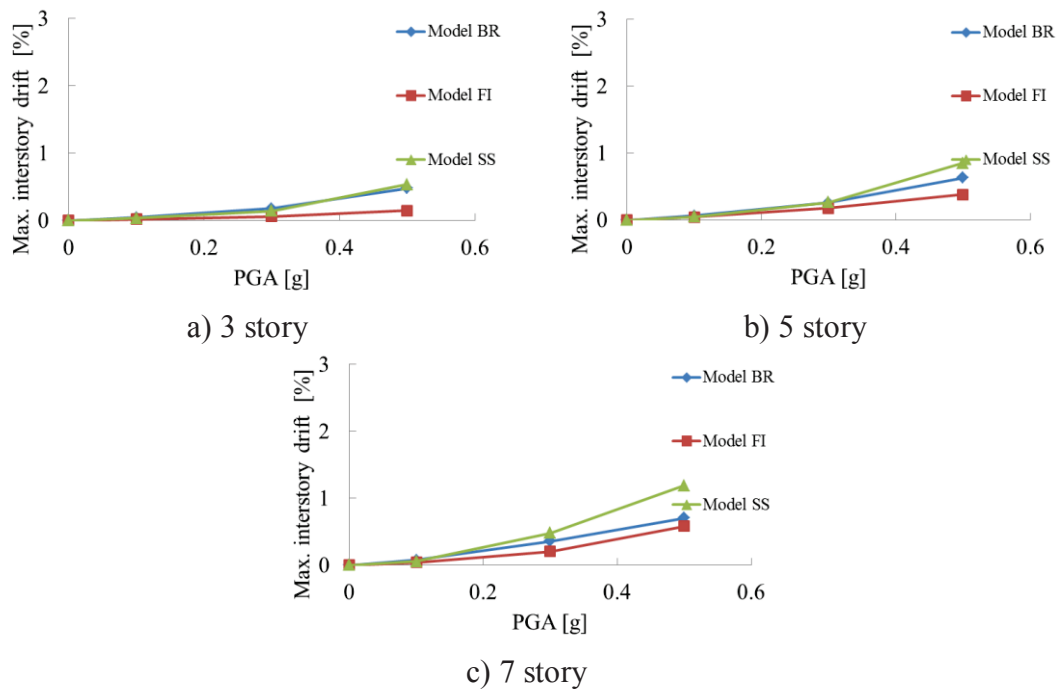


Figure 6.11 Seven ground motions average maximum interstory drift as a function of PGA: a) 3 story, b) 5 story and c) 7 story

As Figures 6.11 a to c show, it can be clearly observed that the uniformly infilled model 2-i (FI) is the less vulnerable model since it has the lowest interstory drift ratio at different intensity level and for different number of story, whereas, Model 3-i (SS) showed the largest vulnerability.

In purpose to investigate the trend of achieved global damage of the RC frame elements and masonry walls for all models and due to the utilized time history records, the damage results are presented for every earthquake with normalized scale factor in Tables 6.7 to 6.9 (The damage is described according to EMS-98).

At PGA=0.1g the bare, full infilled and soft story frame models suffered a slight damage, i.e. cracking of concrete and infill walls and by increasing the intensity level the observed damage increases. Between 0.3g-0.5g the earthquakes named (B-S, B-T, C-S and C-T) tend to give the higher response in case of 5 and 7 story buildings, the expected damage ranges from moderate to collapse in case of RC frame elements whereas the URM infill panels suffered heavy to failure damage grades. The same trend is observed in case of three story building solely at PGA=0.5g (Tables 6.7, 6.8 and 6.9).

Table 6.7 Global damage of the 3 story model

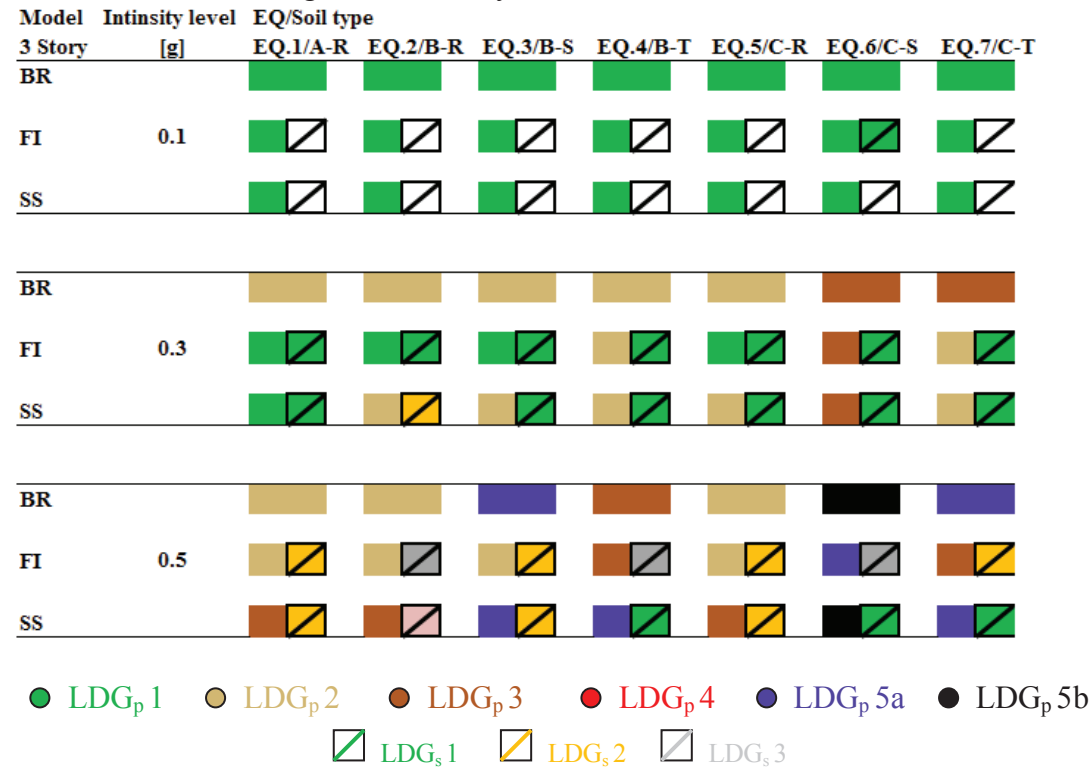


Table 6.8 Global damage of the 5 story model

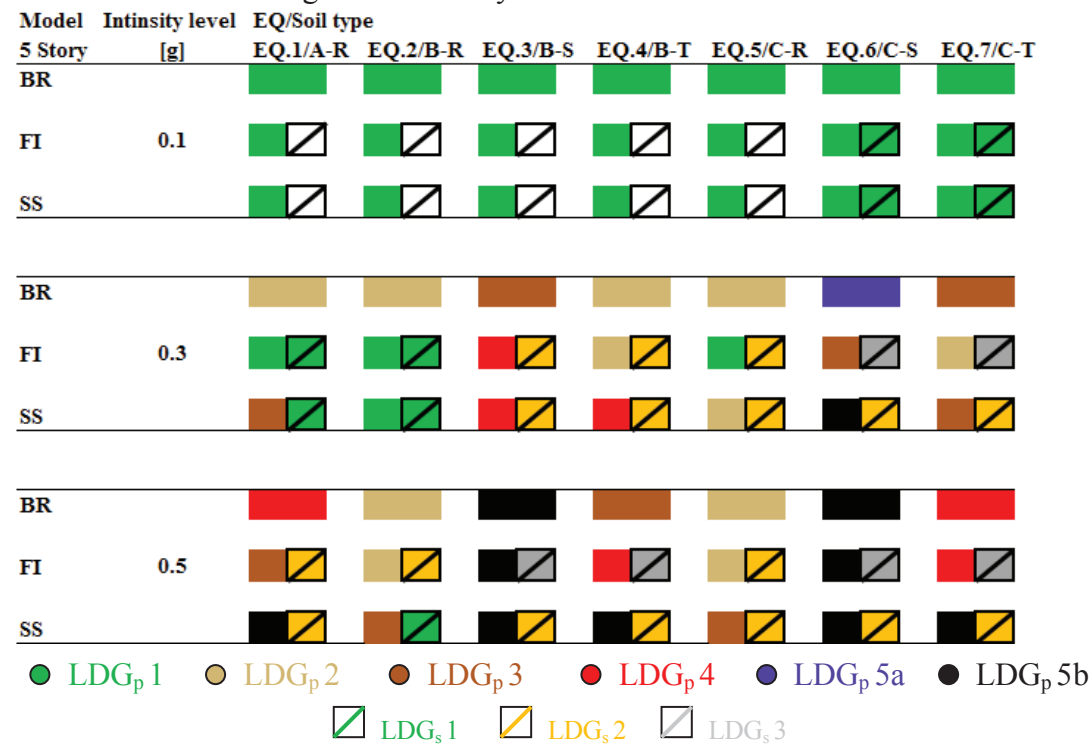


Table 6.9 Global damage of the 7 story model

Model	Intensity level	EQ/Soil type								
7 Story	[g]		EQ.1/A-R	EQ.2/B-R	EQ.3/B-S	EQ.4/B-T	EQ.5/C-R	EQ.6/C-S	EQ.7/C-T	
BR										
FI	0.1									
SS										
BR										
FI	0.3									
SS										
BR										
FI	0.5									
SS										

● LDG_p1 ● LDG_p2 ● LDG_p3 ● LDG_p4 ● LDG_p5a ● LDG_p5b
 LDG_s1 LDG_s2 LDG_s3

6.5 Case Study 2

6.5.1 Model Description

The influence of RC frame and URM infill wall types on the structural response of RC 5 story buildings subjected to seismic action is studied. Eight structural models of different classes are investigated (See Appendix F).

The RC frame structures have in-plan dimension of 15x10m² arranged in 5x5 m² modules with 3.5m story height at the first story and 3m height in the upper stories. Two different configurations are considered: (a) Bare frame without infill walls and (b) URM infill walls placed along the longitudinal building perimeter as shown in Figure 6.12. The preliminary design is carried out according to the rules of Eurocode 2 and 8, assuming typical loads (additional dead load 2.0 kN/m², to represent floor finishing and partitions, and live load 2.0 kN/m²), and high seismicity (PGA=0.3g).

The computer program OpenSees (*McKenna et al., 2000*) is used, adopting a forced-based beam-column element with lumped plasticity at both edges. four different models for each structure have been created, namely, bare, uniformly infilled and soft story model. In total eight numerical models are analyzed.

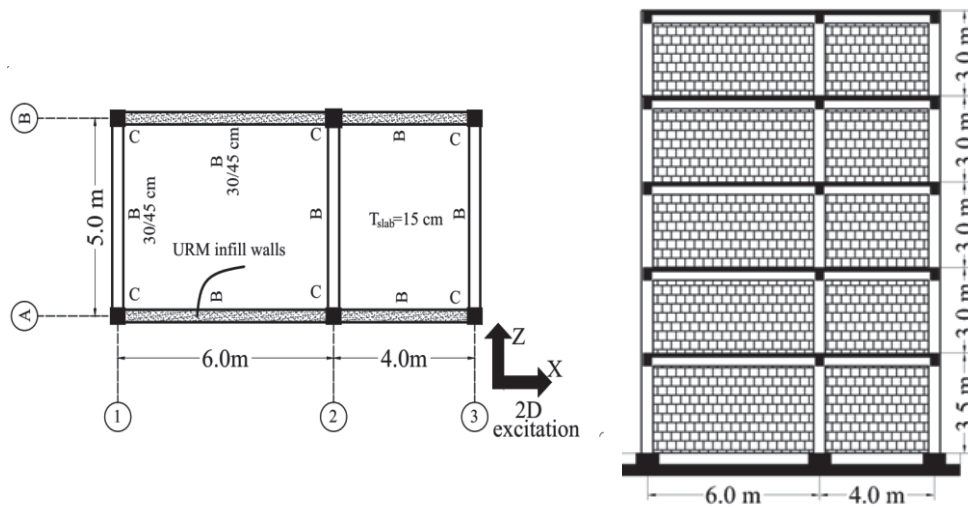


Figure 6.12 Structural layouts of the case study 2 building

The frame is characterized as weak (non-ductile) or strong (ductile) based on the ratio of the resistance to the development of a shear crack to the shear force required to develop two plastic hinges in the column as explained in chapter 3. Tables 6.10 and 6.11 show the material properties of the considered RC frame and the calculated column resistance ratio respectively.

Table 6.10 RC frame material properties

RC frame type	Weak	Strong
Young modulus of concrete E_c [GPa]	29	31
Compression strength concrete f_c [MPa]	24	33
Tensile strength concrete f_t [MPa]	1.3	2.6
Weight of concrete [kN/m ³]	25	
Mass density of concrete [t/m ³]	2.55	
Yield strength of steel f_y [MPa]	450	500
Ultimate strength of steel f_u [MPa]	575	625

Table 6.11 RC columns shear capacity

RC frame	V_p [kN]	V_n [kN]	V_n/V_p [-]
Strong	240.5	600	2.5
Weak	130	113	0.87

In the present research, three different type of masonry, whose properties are reported in Table 6.12, classified as weak infills (W), medium infills (M), and strong infills (S), as described by FEMA 356 are utilized in the analyses.

Table 6.12 URM masonry infills material properties

Masonry type	Weak	Medium	Strong
E_{URM} [GPa]	1.139	2.277	3.416
f_{tp} [MPa]	0.08	0.14	0.19

6.5.2 Fundamental Natural Period

In purpose to evaluate the effect of the RC frame and URM infill wall types on the structural response, firstly the natural periods are calculated (see Table 6.13). It can be observed that the natural periods are about 1.41-2 times smaller for the numerical models with URM infill walls in the X-direction. In Z-direction, and due to the asymmetry of infill walls configuration in both directions, the time periods are about 1.25-1.5 smaller (see Figure 6.12). The aforementioned results refer to the strong influence of the considered URM infill wall types on the natural periods of the structure, i.e. stiffer the masonry wall lesser the time period.

Table 6.13 Natural periods for the studied numerical models

RC frame		Periods [s]			
		S		W	
		X	Z	X	Z
Model	Model (iB)	0.522	0.579	0.601	0.656
	Model (iW)	0.380	0.467	0.411	0.509
	Model (iM)	0.299	0.388	0.322	0.422
	Model (iS)	0.270	0.358	0.284	0.381

i; refer to different RC frame type, S (Strong) and W (Weak).

6.5.3 Incremental Dynamic Curves

The 3D models are subjected to incremental dynamic analysis (IDA) in order to evaluate the performance of the models in hand. As aforementioned, total of seven ground motion records with two components for each record are selected from real previous seismic events and are progressively scaled, as illustrated in Figure 6.13. More than 220 analyses are carried out to check the response of the eight numerical models and evaluate the influence of two different RC frame element type combined with three different URM elements typology according to the classification procedures presented in chapter 3.

Figure 6.13 plots the evolution of the maximum interstory drift for the bare frames and for the full infilled frame with different masonry typologies (weak – W, medium – M, and strong – S).

It can be observed that the maximum drift demands are concentrated in the ground floor in case of weak RC frame models and imposed above the ground floor in the lower half of the building in case of strong one.

Since difference between the adopted models is not clearly shown from the incremental interstory drift curves (Figure 6.13), the average interstory drift resulted due to the seven pair earthquakes plotted for each model due to different PGA namely, 0.20g, 0.35g and 0.5g as Figures 6.14 a and b illustrate.

6.5.4 Average Interstory Drifts

In the following the average maximum interstory drift response of seven seismic actions was determined and plotted. As Figure 6.14 a depicts, in case of strong RC frame elements the Models (SB) show the highest interstory drift ratio in all the different considered intensity levels ranging between 0.5%-1.5% for 0.2g-0.5g PGA. Including the URM infill walls of different types i.e. Weak, Medium and Strong, has the influence to increase the stiffness of the structure and accordingly less interstory drift ratio. As Figure 6.14 a illustrates the weak URM infill walls class, give slightly less interstory drift ratio in comparison with the strong bare frame model. In fact, this response is the consequence of URM infill collapse and additionally the approximately same quantity of damage experienced by the RC frame elements. More beneficial effect is observed in case of using the medium and strong sort of URM infill walls. Hence, the interstory drifts are decreased about 50% at different considered earthquake's intensity level and subsequently lead to less degree of damage.

Figure 6.14 b depicts the resulting drift ratio in case of utilizing weak RC frame elements as a bare model and combined with different classes of URM infill walls as infilled models. At 0.2g PGA, model WB shows the higher drift ratio reaching a value of 0.6% followed by the WW model with about 0.5%. It is worth to be mentioned that:

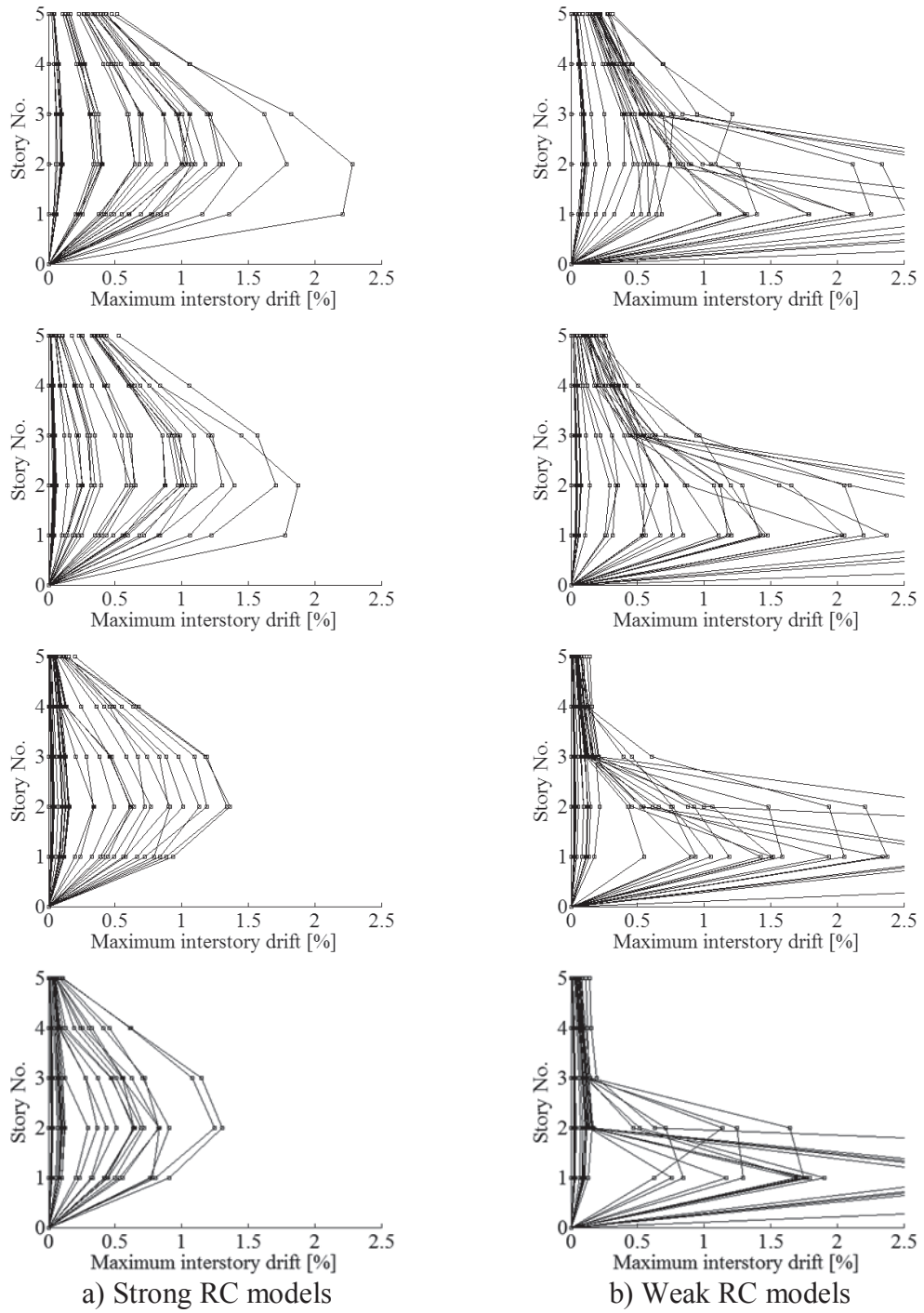


Figure 6.13 Maximum interstory drift due to incremental dynamic analysis: a) Strong RC frame models, b) Weak RC frame models

- In the case of strong RC frame structure, the implication of the URM infill walls enhance the structural response by reducing the attained values of drift ratio and in specific in case of using the type of medium and strong infill walls which in turn has an effect to reduce the expected damage grades for both RC frame elements and URM infill walls.
- Unlikely to the strong RC frame models the same is not observed by increasing the seismic intensity level in case of weak. However, as Figure 6.14 b clearly depicts the soft story effect is the dominated response which in turn leads to entire failure of the structure without a difference in the structural performance between the bare frame models and the infilled ones.

Finally, it can be clearly seen that the inclusion of URM infill walls of different classes show a positive effect at different earthquake intensity levels in case of strong RC frame elements. Whereas in case of weak RC frame elements the advantage of integrating the structure with the URM infill walls is solely noticed till $PGA=0.2g$. Further, the vulnerability of eight different models under study is determined and plotted. As Figure 6.15 shows, in case of strong RC frames the most vulnerable model is the bare frame model and followed by the model with weak URM infill walls with a slight difference between the recorded drift values for both models. Models SS, SM showed better performance and less drift ratio are obtained at different considered intensity level, with a maximum of about 1% at $PGA=0.5g$. Utilizing the weak RC frame models, up to $PGA=0.2g$, a favourable performance and similar to the case of strong frames can be observed. However, by increasing the intensity level a drastic increase is obtained which in turn refer to concentration of damage and possible occurrence by the so called soft story effect failure mechanism occurrence by the so called soft story effect.

6.5.5 Damage Prognosis

As far as, the fiber's strains for both RC frame elements and URM infill wall numerical models give closer view about the damage of the structural and non-structural elements, thus, the recorded numerical damage states are elaborated and plotted for the considered models due to the used time history records with different intensity levels (see Appendix F for the complete results)

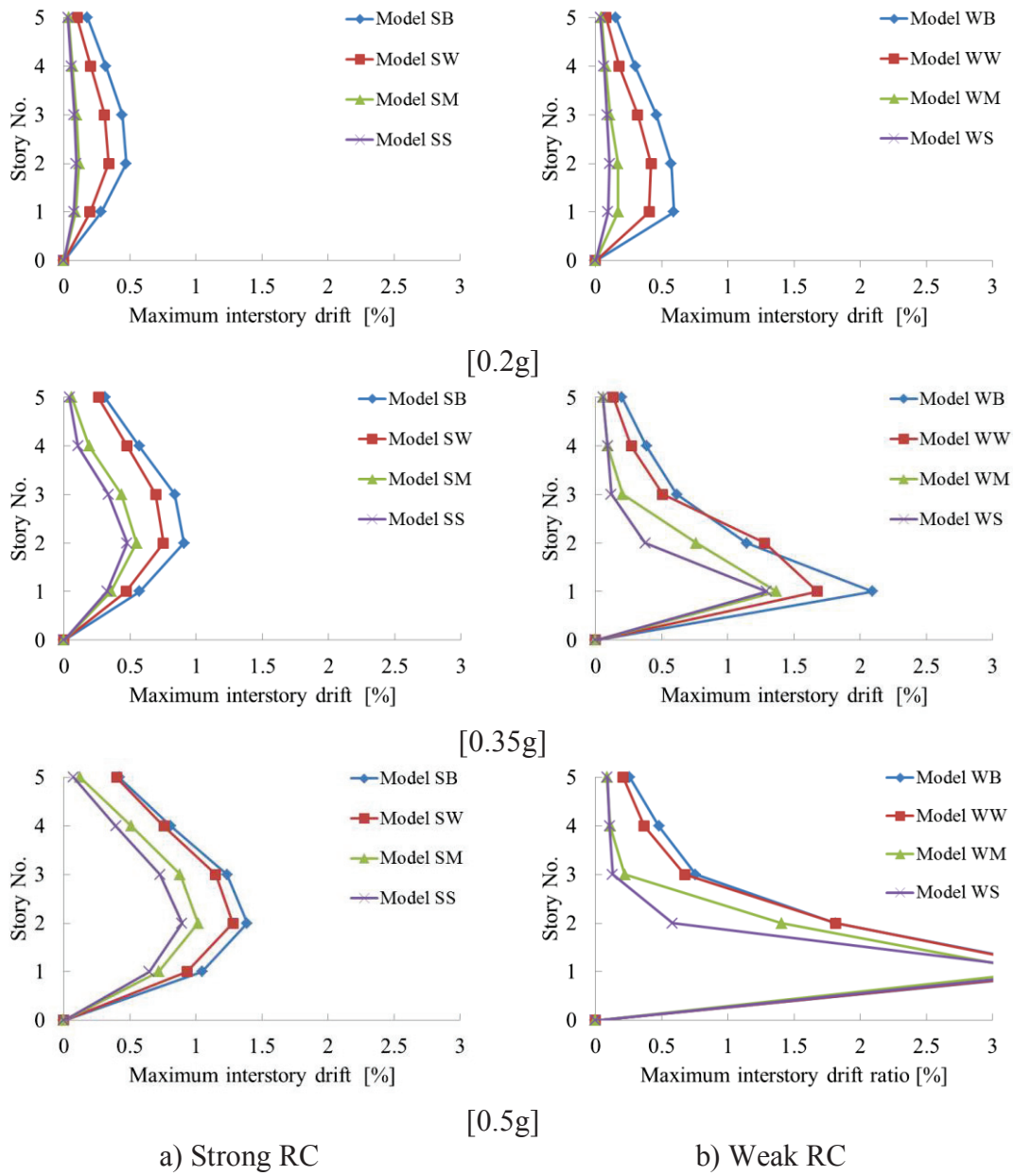


Figure 6.14 Average interstory drift

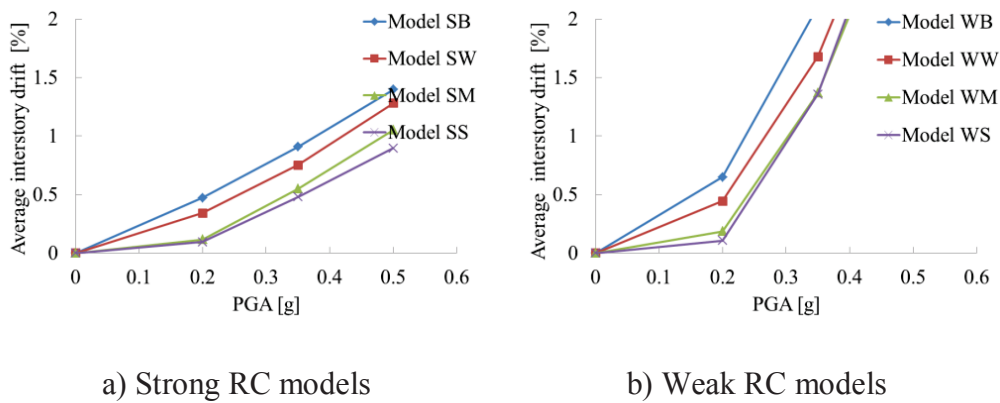


Figure 6.15 Average interstory drift as a function of PGA

Tables 6.14 and 6.15 illustrate the numerical determined damage distribution for Model SR, SW, SM and SS due to the EQ 6 seismic action (scaled to 0.2g, 0.35g and 0.5g). As Table 6.14 shows, the EQ.6 scaled to 0.2g PGA will cause light damage for the RC frame elements in case of bare frame model, however the damage is progressively increased as the intensity level increased reaching to a damage grade of (LDG_p 5b) at 0.5g PGA. The inclusion of the weak URM infill walls in the structure leads to the same damage grades as in the case of bare structure since the URM infill walls were collapsed and completely removed from the model during the analysis.

Implementing URM infill walls of type medium and strong enhance the performance of the structural elements causing less damage grades and the infill walls are protected against failure until 0.2g PGA, whereas failing of URM infill walls can be observed between 0.35g-0.5g PGA.

Unlikely to the case of bare strong frame the weak bare damages are mostly concentrated at the columns ends. The columns at the base attained to collapse (LDG_p 5b) and moderate damage of the columns heads at the second story at 0.2g PGA. However, second story damage increased as the earthquake intensity level increased. The weak type URM infill walls combined with the weak RC frame produce the same damage state as the bare model because the infill walls were completely collapsed. On the other hand, at 0.2g PGA, of including the medium and strong URM infill walls type affected the damage of the RC frame elements positively. Thus, the infill walls were protected against collapse and the frame element suffered light damage. Between 0.35g-0.5g PGA, the same response and favorable damage could not be observed. The dominated damage state is failing of the URM infill walls at the lower stories which in turn lead the non-ductile columns to be over loaded and completely collapsed. Accordingly this will cause complete failure of the lower stories. The elaborated damage grades indicate the strong influence of the considered type of RC frame element combined with URM infill walls of different typology on the damage prognosis of the structure. Thus, the utilized type of URM infill walls and the resultant possible damage state should be addressed already in the design process of new multi-story RC frame structures.

Table 6.14 Damage prognosis for (EQ.6) seismic actions for strong RC frame models

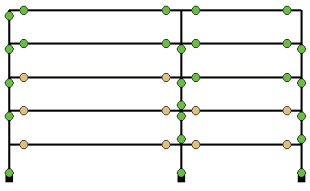
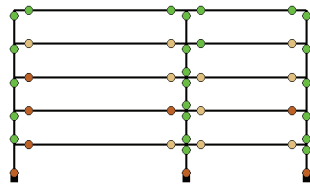
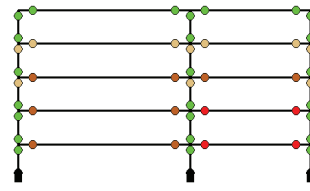
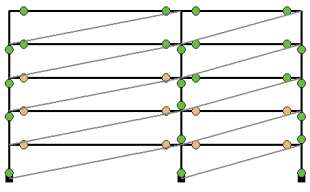
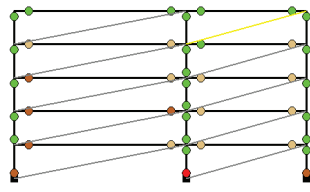
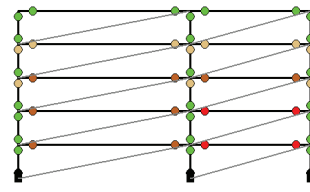
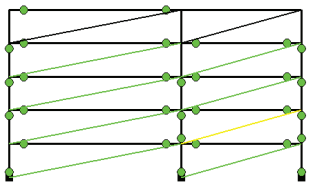
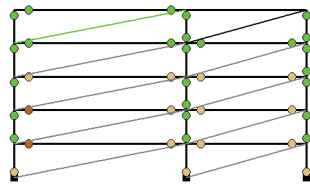
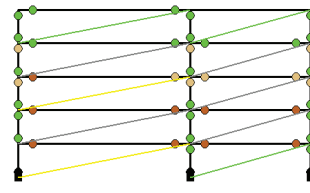
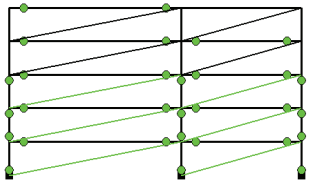
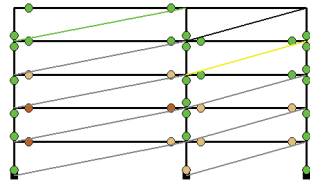
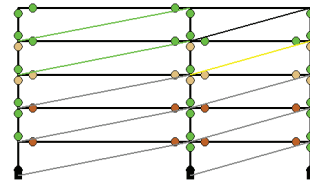
5 Story Model Frame		
0.2g	0.35g	0.5g
		
SB		
		
SW		
		
SM		
		
SS		
<div style="display: flex; justify-content: space-around; align-items: center;"> <div style="display: flex; gap: 10px;"> ● LDG_p1 ● LDG_p2 ● LDG_p3 ● LDG_p4 ● LDG_p5a ● LDG_p5b </div> <div style="display: flex; gap: 10px;"> ▧ LDG_s1 ▧ LDG_s2 ▧ LDG_s3 </div> </div>		

Table 6.15 Damage prognosis for (EQ.6) seismic actions for weak RC frame models

5 Story Model Frame		
0.2g	0.35g	0.5g
WB		
WW		
WM		
WS		
<div style="display: flex; justify-content: space-around; align-items: center;"> <div style="display: flex; gap: 10px;"> ● LDG_p1 ● LDG_p2 ● LDG_p3 ● LDG_p4 ● LDG_p5a ● LDG_p5b </div> <div style="display: flex; gap: 10px; margin-top: 5px;"> LDG_s1 LDG_s2 LDG_s3 </div> </div>		

Likewise case study 1 a global damage grade is assigned for every model and presented in Table 6.16 and 6.17. At PGA=0.2g the strong and weak RC frame model mixed with weak infills suffered slight to moderate damage of the RC frame elements whereas failing of the URM infill panels is predicted. At the same intensity level and by changing the URM material type to medium and strong respectively the performance of both RC models, i.e. the strong and weak, is enhanced and just slight damage achieved. Increasing the intensity level till 0.5g the strong RC frame models with weak, medium and strong infill walls show good performance with moderate to heavy damage concentrated mainly at the beams whereas complete collapse of the URM panels is predicted independently from the infill walls material type. It is worth mentioning that URM infill walls suffer a higher damage grade than the RC frame elements. The weak RC frame models with different type of infill walls perform poorly starting from intensity level 0.35g with heavy damage concentrated at the columns and complete failure of the infill walls (Tables 6.16 and 6.17).

Table 6.16 Global damage of the strong RC models

Model	Intensity level	EQ/Site class	EQ.1/D	EQ.2/B	EQ.3/C	EQ.4/B	EQ.5/C	EQ.6/B	EQ.7/C
5 Story	[g]								
SB			LDG _p 2	LDG _p 2	LDG _p 2	LDG _p 3	LDG _p 2	LDG _p 2	LDG _p 2
SW	0.2		LDG _s 1	LDG _s 1	LDG _s 1	LDG _s 1	LDG _s 2	LDG _s 2	LDG _s 2
SM			LDG _s 1	LDG _s 1	LDG _s 1	LDG _s 1	LDG _s 1	LDG _s 2	LDG _s 1
SS			LDG _s 1	LDG _s 1	LDG _s 1	LDG _s 1	LDG _s 1	LDG _s 1	LDG _s 1
SB			LDG _p 3	LDG _p 3	LDG _p 4	LDG _p 4	LDG _p 3	LDG _p 3	LDG _p 3
SW	0.35		LDG _s 2	LDG _s 2	LDG _s 2	LDG _s 2	LDG _s 2	LDG _s 2	LDG _s 2
SM			LDG _s 2	LDG _s 1	LDG _s 2	LDG _s 2	LDG _s 2	LDG _s 2	LDG _s 2
SS			LDG _s 2	LDG _s 1	LDG _s 2	LDG _s 2	LDG _s 2	LDG _s 1	LDG _s 2
SB			LDG _p 4	LDG _p 4	LDG _p 4	LDG _p 5a	LDG _p 3	LDG _p 4	LDG _p 4
SW	0.5		LDG _s 2	LDG _s 2	LDG _s 2	LDG _s 2	LDG _s 2	LDG _s 2	LDG _s 2
SM			LDG _s 2	LDG _s 2	LDG _s 2	LDG _s 2	LDG _s 2	LDG _s 2	LDG _s 2
SS			LDG _s 2	LDG _s 2	LDG _s 2	LDG _s 2	LDG _s 2	LDG _s 2	LDG _s 2

● LDG_p 1 ● LDG_p 2 ● LDG_p 3 ● LDG_p 4 ● LDG_p 5a ● LDG_p 5b
▣ LDG_s 1 ▣ LDG_s 2 ▣ LDG_s 3

Table 6.17 Global damage of the weak RC models

Model	Intensity level [g]	EQ/Site class						
5 Story		EQ.1/D	EQ.2/B	EQ.3/C	EQ.4/B	EQ.5/C	EQ.6/B	EQ.7/C
WB								
WW	0.2							
WM								
WS								

Model	Intensity level [g]	EQ/Site class						
5 Story		EQ.1/D	EQ.2/B	EQ.3/C	EQ.4/B	EQ.5/C	EQ.6/B	EQ.7/C
WB								
WW	0.35							
WM								
WS								

Model	Intensity level [g]	EQ/Site class						
5 Story		EQ.1/D	EQ.2/B	EQ.3/C	EQ.4/B	EQ.5/C	EQ.6/B	EQ.7/C
WB								
WW	0.5							
WM								
WS								

LDG_p1
 LDG_p2
 LDG_p3
 LDG_p4
 LDG_p5a
 LDG_p5b
 LDG_s1
 LDG_s2
 LDG_s3

6.6 Developed Model Quality Ranking

After a detailed state of the art review/investigation/analysis on the available 2D (IP) and 3D (IP_OoP) macromodel in the literature, a new model implemented in OpenSees is proposed to take into account the IP_OoP interaction in terms of IP and OoP strength and stiffness reduction during structural analysis. The URM infill wall model is composed of two equal sizes diagonal Beam-Column with Fiber Hinges and a midspan node with OoP mass (referred to as M#5_dev). The developed URM infill wall macromodel is assessed using the quality index proposed in chapter two. As Tables 6.18 and 6.19 show a $Q_{ind} = 4$ is assigned to the model due to the following;

- The proposed masonry model comprised of two diagonal beam-column elements with hinges in one direction reduces the complexity associated with the proposed model by *Di Trapani et al. (2017)* and *Mazza (2018)*. Thus, the developed model is sufficiently simple and effective tool to be used in the nonlinear dynamic analysis of multi-story structures.

- The model is integrated with the pinching material constitutive law (multi linear inelastic), with post peak strength degradation, for both in- and out-of-plane directions. It is proved that the developed model is able to capture the stiffness and strength degradation of the URM infill walls, which are generally observed in experimental tests. (See chapter 5 for detailed calibration, verification and validation). Simple calibration procedures of the fiber section properties are presented (see chapter five) as an alternative to the original method proposed by *Mosalam et al. (2008)* and further adopted by *Longo et al. (2018)*, by which the properties of the fibers (assumed having an elastic-perfectly plastic behavior) are defined with a different weight inside the cross-section.
- The herein developed URM infill wall macromodel is included in a conceptual framework to assess the damage of both RC frame and masonry infill wall, which is not considered by the other macromodels.

Table 6.18 Assigned ranking values

3D Model No.	Int. w/ RC frame	No. of elements	IP calibration	OoP calibration	Nonlinearity approach	Q_{ind}
11	0	1	0	0	1	2
12	0	0	1	0	1	2
13	0	0	0	1	0	1
14	0	0	1	1	0	2
15	0	1	0	1	1	3
16	0	0	1	0	1	2
17	0	0	1	1	1	3
18	0	1	1	1	1	4

Table 6.19 Final ranking

No.	Authors	Required elements	Interaction with RC frame	Q_{ind}
10	<i>Hashemi & Mosalam (2007)</i>	8 diagonal nonlinear compression struts and linear tension link	Joint	x
11	<i>Kadysiewski & Mosalam (2008)</i> M#5_org	1 diagonal linear strut with 2 nonlinear fiber section	Joint	2
12	<i>Furtado et al. (2015)</i> M#4	4 diagonal linear struts and nonlinear shear link	Joint	2
13	<i>Oliaee & Magenes (2016)</i>	4 diagonal nonlinear compression struts	Joint	1
14	<i>Di Trapanie et al. (2017)</i>	4 diagonal nonlinear compression struts	Joint	2
15	<i>Ricci et al. (2017)</i>	1 diagonal linear strut with 2 nonlinear zero length element	Joint	3
16	<i>Longo et al. (2018)</i>	1 diagonal linear strut with 2 nonlinear fiber section	Joint	2
17	<i>Mazza (2018)</i>	4 diagonal nonlinear beams with 1 nonlinear axial link	Joint	3
18	M#5_dev	1 diagonal linear strut With 2 nonlinear fiber section	Joint	4

6.7 Summary

This chapter is dedicated to investigate the capability of the developed URM infill model. To this purpose the model is implemented in a representative multi-story structure and two case studies are considered.

In the first case study, structures of three different story levels (3, 5 and 7 stories) and different configuration of the URM infill panels are considered. Namely, bare, full infill and open ground storey are studied by using nonlinear dynamic analysis method and explicitly consideration of the out-of-plane collapse through element removal algorithm.

The 3 story building will suffer no primary (frame system) or secondary (URM infill walls) damage under the excitation of 0.1g PGA. In case of scaled PGA to 0.3g the URM infill walls will crack and moderate damage is observed at the frame elements. Increasing the intensity level up to 0.5g a complete removal of the infill walls, i.e., collapse, at the first story and heavy damage at some columns is predicted. A complete failure of URM infill walls at the 5 and 7 story buildings will already start at the intensity level of 0.3g-scaled EQs and damage is concentrated in the lower and intermediate stories.

From the drift ratio comparison, an important difference is observed between the three considered numerical models, from which the necessity of considering the IP_OoP behavior of the URM infill walls can be confirmed. Current studies confirm that damage to masonry infill mainly occurs in the lower and intermediate stories due to the large interstory drift values.

Aiming to check the effect of using different material type for both the RC frame elements and the URM infill walls a second set of models is created. Strong and weak bare frame are considered combined with weak, medium and strong URM infill walls. Incremental dynamic analysis (IDA) is applied to investigate the seismic response of the considered models. In total 224 analyses (7 time histories, 4 intensity levels and 8 models) are conducted.

As expected, the stiffness and strength of frames increase with the introduction of the URM infill walls. In particular, the IDA curves allow to observe that the type of the considered URM infills significantly decrease interstory drift ratio.

From the average interstory drift ratio it is notable, that the possible soft story formation started at an intensity level of 0.2g, specifically in case of weak URM infills.

Vulnerability curves are determined for each URM infilled model by plotting the relationship between the intensity level and the maximum inter-story drift ratio. It can be observed that the less vulnerable model is the one infilled with strong URM walls with uniform distribution of damage. Up to $PGA=0.2g$ a favourable response is noticed utilizing the weak RC frame models mixed with different types of URM infill walls. However, by increasing the intensity level a sudden increase is obtained which lead to the concentration of damage and possible failure mechanism occurrence by the so called soft story effect.

The damage states of the eight different models due to different intensity levels of the considered ground motions, namely, 0.05g, 0.2g, 0.35g and 0.5g are plotted (see Appendix F). The main conclusions that arise from the comparison are as follow:

- The strong RC structures mixed with different URM typology shows uniform damage distribution due to the different considered intensity levels.
- In case of weak RC and up to $PGA=0.2g$, the inclusion of the URM infill walls enhance the structural performance, in specific by using medium and strong infill walls slight damage is obtained, whereas at $PGA=0.35g$, 0.5g concentration of damage is predicted at the column's edges lead to complete failure independently from the used URM class.
- In case of strong RC buildings, between 0.05g-0.2g and by changing the URM type from weak to medium and strong leads to slight damage for both the RC elements and URM infill walls instead of moderate and complete collapse for the RC and URM infills respectively. However, due the high intensity levels and starting from 0.35g a complete collapse of the URM infill walls is obtained independently from the infill wall class.
- In general the URM infill walls experience a higher damage grade than the RC frame elements specifically in case of weak URM class.

Finally, in both considered case studies, it is worth to be mentioned, that the current study did not consider the vertical and plane irregularities which are introduced into buildings because of asymmetric placement of infill walls and consequently lead to

damage pattern due to the higher mode effect. Therefore, cracking and collapse of the URM infill panels tend to occur in the lower stories of the structure and then extend to the upper stories, i.e., in none of the upper stories experience complete collapse first.

The developed beam-column macro element is used in this chapter to simulate the IP and OoP behavior of masonry infill walls. The model is represented by fiber-section beam-column elements and is able to capture OoP response of the URM infill panel wall as well as the interaction between the IP and OoP components. Furthermore, the model is sufficiently simple and efficient that it can be used for the nonlinear static or dynamic analysis of an entire structural system.

BLANK PAGE

Chapter 7: Conclusions and Outlook

7.1 Conclusions

The main purpose of this research is to develop a practical numerical model for reinforced concrete (RC) frame structures with unreinforced masonry (URM) infill walls that can be used as a practical, effective tool in a nonlinear time history analysis of the overall structure and that properly considers the interaction between the in-plane (IP) and out-of-plane (OoP) strengths and stiffness's of the infill wall. To achieve the goals of this study a comprehensive literature review on the available macromodels of both RC elements and URM panels is carried out. Subsequently, an evaluation/assessment of the main types of the RC frame models is achieved. Based on the shortcomings of the available macromodels of infill walls a new macromodel of URM panels is developed and proposed.

Depending on the results presented in this research, the following conclusions are outlined:

1. In this research, a homogenous extensive database of experimental tests on RC frames infilled with URM walls and without openings is collected and presented.
2. The main and widely used empirical models existing in literature for infills in the context of single-strut models have been investigated and compared with the experimental results in order to select a simple model to be used in the calibration of the numerical macromodels with minimum predicted error, in particular, predicted-to-experimental strength ratios.
3. The model proposed by *Bertoldi et al (1993)* significantly underestimates peak strength with an average value of 51%. Models from *Panagiotakos & Fardis (1996)* and *Zarnic et al. (1997)* overestimate the maximum strength with an average error attained 25%. To provide a simple practice equation to be used in the calibration of the numerical macromodels the model proposed by *Zarnic et al. (1997)* is selected and slightly modified utilizing the results of the database samples.

4. The available macromodels of RC frame element could be divided into two groups: rigid plastic hinges and fiber section hinges. On one hand, it is proved the superior performance of the RC element with fiber based plastic hinges, and on the other hand, the element with rigid plastic hinges present acceptable accuracy, especially in case of full infilled structures in which the earthquake energy mainly dissipates through the infill walls.

5. The URM infill macromodels fall into two classes: 2D macromodels, i.e. the strut elements models, which have the capability to represent the IP response of the infill wall; 3D macromodels, i.e. the beam-column element with fiber sections models, by which the global IP-OoP behavior of the masonry walls could be captured.

6. Utilizing the developed beam-column element with a cross section composed of nonlinear fibers linked to a pinching material model it is proved that the model is capable to capture the IP cyclic response and OoP monotonic behaviour of the URM infill panel, as well as its elastic stiffness properties. Based on the procedures proposed in this research, it is possible to specify the infill model mass, strength, and stiffness properties so that the global behavior of the overall structural model is essentially preserved.

7. It is proved that the developed herein model has the ability to capture a comparable response as the newly presented macromodels by *Di Trapani et al. (2017)* and *Mazza (2018)*.

8. The developed macromodel of URM infill walls is validated against the results of the 1:1 scale experiments carried out by *Negro et al. (1996)* and the 1:2.5 scaled experiments proposed in *FRAMA (2014)* report. Utilizing the first experimental results it is observed that the model is capable to capture the IP response accurately, whereas the second experiment gives the possibility for further IP validation of the model as well as the OoP direction.

9. Based on the results of the case studies analyses in this research, it is clear that the interaction between the IP and OoP strengths of the URM infill panels has a main influence on the observed failure mechanisms, thus the phenomena needs to be

addressed in the structural design process. This would represent a change in the typical evaluation procedure, e.g., using EC8, FEMA 356, as it is practiced today.

10. The investigated case studies proved the model capability to simulate the response of different EQ records with different frequency content.

11. The main shortcoming of the model is the inability to catch a specific type of failure pattern of URM infill walls such as bed joint sliding which involves complex phenomena and would require the use of micromodels rather than the macro models.

These local failure mechanisms of the URM infill panels are important to be addressed in case of investigating the redistributions of internal forces in the infill and the surrounding frame.

12. Finally, in this research, an innovative 3D macro element approach is employed and developed. The proposed approach for the model calibration enhances the model quality with respect to IP and OoP response. The following main points may summarize the reasons behind the quality improvement:

- The model has shown good accuracy in simulating the OoP experimental response of URM infill panels w/wo reciprocal IP-OoP damaging.
- It is illustrated that the model has the capability to represent the experimental in- and out of plane damage of the infill walls.
- The model current state shows similar results compared to the recently proposed complex macro elements, (e.g. model presented by *Mazza (2018)*).
- The model is able to reproduce the experimental response of tests with different material, scaling factors and configuration.
- The model provides effective numerical tool suitable to be used, for both engineering practice and research field, for the seismic assessment of RC structures with URM infill walls considering in and out-of-plane response of the URM infill walls.

7.2 Outlook

Critical modeling aspects for accurately simulating the interaction of the panels with the surrounding frame are: the infill type and, most importantly, the shear failure of the concrete columns interacting with the unreinforced masonry URM infill panels. Assessing the importance of these mechanisms and parameters is a key issue for creating reliable structural models for the performance assessment of non-ductile RC frames. Several works addressed the necessity of considering the inelastic shear mechanisms; therefore it should be modeled in RC members and in particular in poorly detailed columns. Thus the herein presented RC frame model has to be further enhanced to capture directly the pure shear failure and possible interaction between axial and shear forces.

On the other hand, one current limitation associates with the masonry walls is the lack of knowledge concerning the actual behavior of URM infill panels under combined IP and OoP dynamic loading. Experimental investigations, supplemented by numerical simulations, are needed to gain an understanding of this behavior, and thereby establish the goals for the practical model to meet.

Bibliography

Abrams D.P., Angel R., Uzarski J., Out-of-plane strength of unreinforced masonry infill panels, *Earthquake Spectra*, 12, 4, p.825-844, (1996).

Abrahamczyk L., Schwarz J., Lobos D., Maiwald H., Das Magnide 8.8 Manule (Chile) Erdbeben vom 27. Februar, ingenieuranalyse der erdbebenschäden, *Bautechnik* 87, 8, p.462-473, (2010).

Abrahamczyk L., AL Hanoun M.H., Penava D., Schwarz J., Model quality for RC frame with URM infill walls subjected to horizontal cyclic loading. Proc. of 12th Canadian Conference on Earthquake Engineering, Quebec, Canada, 17-20 June, (2019).

ACI 318. Building code requirements for structural concrete and commentary (ACI 318 M-5), Detroit, Michigan, American Concrete Institute, (2005).

AL Chaar G., Non-ductile behaviour of reinforced concrete frames with masonry infill panels subjected to in plane loading, Engineering Research and Development Center Champaign (IL) Construction Engineering Research Lab, (1998).

AL Hanoun M.H., Abrahamczyk L., Schwarz J., Numerical simulation of RC frames structures with infill walls under consideration of out-of-plane behaviour, Proc. 16th World Conference on Earthquake Engineering (WCEE), Santiago, Chile, 9-13 January, (2017).

AL Hanoun M.H., Abrahamczyk L., Schwarz J., Macromodeling of in- and out of plane behavior of URM infill walls. *Bull Earthquake Engineering*, 17, 1, p.519-535, (2018).

Angel R., Behavior of reinforced concrete frames with masonry infill walls. PhD. thesis, Univ. of Illinois, Urbana-Champaign, IL, (1994).

Anthoine A., Derivation of the in-plane elastic characteristics of masonry through homogenization theory, *International Journal of Solids Structures*, 32, p.137-163, (1995).

Asteris P.G., Antoniou S.T., Sophianopoulos D.S., Chrysostomou C.Z., Mathematical macromodeling of infilled frames: State of the art, *Journal of Structural Engineering*, v 137, n 12, p.1508-1517, (2011).

Asteris P.G., Kakaletsis D.J., Chrysostomou C., Symyrou E.E., Failure modes in infilled frames, *Electronic Journal of Structural Engineering*, 11, 1, p.11-20, (2011).

Atkinson R.H., Amadei B.P., Saeb S., Strue S., Response of masonry bed joints in direct shear, *Journal of Structural Engineering*, ASCE, 115, 9, p.2276-2296, (1989).

Bashandy T., Rubiano N.R., Klingner R.E., Evaluation and analytical verification of infilled frame test data. PMFSEL Report No. 95-1, (1995).

Belmouden Y., Lestuzzi P., An equivalent frame model for seismic analysis of masonry and reinforced concrete buildings, *Journal of Construction Building Material*, 23, p.4053, (2009).

Bertoldi S.H., Decanini L.D., Santini S., Via G., Analytical models in infilled frames, *Proc. of the 10th European Conference in Earthquake Engineering*, Vienna, p.1533-1538, (1994).

Bertero V.V., Aktan A.E., Charney F.A., Sause R., Earthquake simulation tests and associated studies of a 1/5th-scale model of a 7-story R/C frame-wall test structure, Report No. UCB/EERC-84/05, University of California, Berkeley, p.180, (1983).

Braga F., Manfredi V., Masi A., Salvatori A., Vona M., Performance of non-structural elements in RC buildings during the L'Aquila, 2009 Earthquake, *Bulletin of Earthquake Engineering*, 9, 1, p.307-324, (2011).

Buonopane S.G., Seismic Evaluation of a Masonry Infilled Reinforced Concrete Frame by Pseudo-dynamic Testing, M.Sc. Thesis, Cornell University, Ithaca, N.Y, (1997).

Burton H., Deierlein G., Simulation of seismic collapse in non-ductile reinforced concrete frame buildings with masonry infills, *Journal of Structural Engineering*, 140, 8, (2013).

Calderini C., Lagomarsino S., A micromechanical inelastic model for historical masonry, *Journal of Earthquake Engineering*, 10, 453, (2006).

Calvi G.M. and Bolognini D., Seismic response of reinforced concrete frames infilled with weak reinforced masonry panels, *Journal of Earthquake Engineering*, 5 02, p.153-185, (2001).

Calvi G.M., Bolognini D., Penna A., Seismic Performance of masonry-infilled RC frames, benefits of slight reinforcements, Invited lecture to "Sismica 2004-6° Congresso Nacional de Sismologia e Engenharia Sísmica", Guimarães, Portugal, April 14–16, (2004).

Cavaleri L., Di Trapani F., Cyclic response of masonry infilled RC frames: experimental results and simplified modeling, *Soil Dynamics Earthquake Engineering*, 65, p.224-242, (2014).

Calì I., Marletta M., Pantò B., A new discrete element model for the evaluation of the seismic behavior of unreinforced masonry buildings, *Journal of Engineering Structures*, 40, p.327-338, (2012).

Chaimoon K., Attard M., Modeling of unreinforced masonry walls under shear and compression, *Journal of Engineering Structures*, 29, 9, p.2056-2068, (2007).

Chang G., Mander J.B., Seismic energy based fatigue damage analysis of bridge columns: Part 1 – Evaluation of seismic capacity, Report No. NCEER-94-0006, Buffalo, NY: National Center for Earthquake Engineering Research, State University of New York, (1994).

Chiostrini S., Vignolia A., Application of a numerical method to study masonry panels with various geometry under seismic loading, Florence, Italy (1989).

Chiou Y.J., Tzeng J.Ch., Liou Y.W., Experimental and analytical study of masonry infilled frames, *Journal of structural engineering* New York, N.Y., 125, 10, p. 1109 - 1117, (1999).

Chrysostomou C.Z., Effects of degrading infill walls on the nonlinear seismic response of two-dimensional steel frames, Ph.D. thesis, Cornell University, Ithaca, NY, (1991).

Chrysostomou C.Z., Gergely P., Abel J.F., A Six-Strut model for nonlinear dynamic Analysis of steel infilled frames, *International Journal of Structural Stability and Dynamics*, 2,3, p.335-353, (2002).

Colangelo F., Pseudo- dynamic seismic response of infilled RC frames designed for gravity loading, Proc. of 13th world conference on earthquake engineering, Vancouver, B.C., Canada, August 1-6, (2004).

Crisafulli F., Analysis of infilled frame structures, seminar on masonry and earthen structures, PhD thesis, Universidade do Minho, (1997).

Crisafulli F.J., Carr A.J., Proposed macro-model for the analysis of infilled frame structures, *Bulletin New Zealand society Earthquake Engineering*, 40, 2, p.69-77, (2007).

Colangelo F., Pseudo-dynamic seismic response of infilled RC frames designed for gravity loading, Proc. of 13th World Conference on Earthquake Engineering, Vancouver, B.C., Canada, August 1-6, (2004).

Combesure D. and Pegon P., Application of the local to global approach to the study of infilled frame structures under seismic loading, Proc. of 12th (WCEE), (2000).

Di Trapani F., Shing P.B., Cavaleri L., Macroelement model for in-plane and out-of-plane responses of masonry infills in frame structures, *J Struct Eng.*, 144, 2, (2017).

Durrani A.J., Luo Y.H., Seismic Retrofit of Flat-Slab Buildings with Masonry Infills, Proc. of the NCEER Workshop on Seismic Response of Masonry Infills, National Center for Earthquake Engineering Research (NCEER), Buffalo, NY, (1994).

Dawe J.L., Seah C.K., Behavior of Masonry Infilled Steel Frames, *Canadian J. of Civil Eng.*, 16, 6, p.854-864,(1989).

Decanini L., Mollaioli F., Mura A., Saragoni R., Seismic performance of masonry infilled RC frames, 13th World Conference on Earthquake Engineering Vancouver, B.C., Canada, August 1-6, (2004).

Drucker D.C., Gibson R.I., Henkel D.J., Soil mechanics and work hardening theories of plasticity, *Transaction, ASCE*, 122 , p.338-346, (1957).

Drysdale R.G., Essawy A.S., Out-of-plane bending of concrete block walls, *Journal of Structural Engineering*, ASCE,114,1 (1998).

El-Dakhkhni W., Elgaaly M., Hamid A., Three-strut model for concrete masonry-infilled steel Frames, *Journal of Structural Engineering*, 129, 2, p.177-185, (2003).

EN 1996-1-1 Eurocode 6: Design of masonry structures-part 1-1: general rules for reinforced and unreinforced masonry structures, (2005).

Eurocode 8 (1998-1). Design provisions for earthquake resistance of structures. Brussels, Belgium: European Committee for Standardization, (2003).

Fardis M.N., Bousias S.N., Franchioni G., Panagiotakos T. B., Seismic Response and Design of RC Structures with Plan-Eccentric Masonry Infills, *Earthquake Engineering and Structural Dynamics*, 28, 2, p.173-191, (1999a).

Federal Emergency Management Agency FEMA, NEHRP commentary on the guidelines for the seismic rehabilitation of buildings, FEMA-274, Washington, DC, (1997).

Federal Emergency Management Agency FEMA, Evaluation of earthquake damaged concrete and masonry wall buildings: Basic procedures manual, FEMA-356, Washington, DC, (1998).

Federal Emergency Management Agency, Pre-standard and Commentary for the Seismic Rehabilitation of Buildings, FEMA356, Washington, D.C., (2000).

Flanagan R.D., Bennet R.M., Bidirectional behavior of structural clay tile infilled frames, *Journal of Structural Engineering*, 125, 3, p.236-244, (1999).

Furtado A., Rodrigues H., Arede A., Varum H., Simplified macro-model for infill masonry walls considering the out-of-plane behavior, *J Earthq Eng Struct Dyn*, 45, P.507-524, (2015).

Furtado A., Rodrigues H., Arede A. and Varum H., Experimental evaluation of out-of-plane capacity of masonry infill walls. *Eng Struct*, 111, p.48-63, (2016).

Furtado A., Rodrigues H., Arêde A., Varum H., Grubišić M., Prediction of the earthquake response of a three-storey infilled RC structure, *Engineering structures*, 171, p.214-235, (2018).

Gambarotta G., Lagomarsino S., Damage models for the seismic response of brick masonry shear walls. Part I: The mortar joint model and its applications, *Journal of Earthquake Engineering & Structural Dynamics*, 26, p.423-439, (1997).

Gambarotta L., Lagomarsino S., Damage models for the seismic response of brick masonry shear walls. Part II: the continuum model and its applications, *Journal of Earthquake Engineering and Structural Dynamics*, 26, 4, p.441-462, (1997).

Gambarotta K., Lagomarsino S., On dynamic response of masonry panels, *Proc. of National Conference on Masonry Mechanics between Theory and Practice*, Messina, Italy, (1996).

Giambanco G., Rizzo S., Spallino R., Numerical analysis of masonry structures via interface models, *Computer Methods in Applied Mechanics and Engineering*, 190, p.6493-6511, (2001).

Gopalaratnam V.S., Shah S.P., Softening response of plain concrete in direct tension, *ACI Journal*, 82, p.310-323, (1985).

- Griffith M., Vaculik J., Out-of-plane flexural strength of unreinforced clay brick masonry walls, *TMS J*, (2007).
- Grünthal G., Musson R.M.W., Schwarz J., Stucchi M., European Macro seismic Scale 1998, *Cahiers de Centre Européen de Géodynamique et de Séismologie*, 15, Luxembourg, (1998).
- Hak S., Morandi P., Magenes G., Out-of-plane experimental response of strong masonry infills, *Second European Conference on Earthquake Engineering and Seismology*. Istanbul, Turkey, 25–29 August, (2014).
- Hashemi A., Mosalam K.M., Seismic evaluation of reinforced concrete buildings including effects of masonry infill walls, *PEER* (2007).
- Herrmann L.R., Finite element analysis of contact problems, *Journal of Engineering Mechanics (ASCE)*, 104, p.1043-1057, (1978).
- Holmes M., Steel frames with brickwork and concrete infilling, *ICE Proc.*, 19, 4, p.473-478, (1961).
- Iervolino I., Galasso C., and Cosenza E., REXEL: Computer aided record selection for code-based seismic structural analysis, *Bulletin of Earthquake Engineering*, 8, p.339-362, (2010).
- Iervolino I., Maddaloni G., and Cosenza E., Eurocode 8 compliant real record sets for seismic analysis of structures, *Journal of Earthquake Engineering* 12, p.54-90, (2008)
- Ignatakis C., Stavrakakis E., Penelis G., Analytical model for masonry using the finite element method, in *Structural Repair and Maintenance of Historical Buildings*, Computational Mechanics Publications, p.511-523, (1989).
- Kadysiewski S., Mosalam K.M., Modeling of unreinforced masonry infill walls considering in-plane and out-of-plane interaction, *Pacific Earthquake Engineering Research Center, PEER*, p.102, (2009).
- Kakaletsis D.J., Influence of masonry strength and rectangular spiral shear reinforcement on infilled RC frames under cyclic loading, *Computational methods and experimental measurements*, 46, p.643-653, (2007).
- Karapitta L., Mouzakis H., Carydis P., Explicit finite-element analysis for the in-plane cyclic behavior of unreinforced masonry structures, *Journal of Earthquake Engineering & Structural Dynamics*, 40, 2, p.175-193, February (2011).
- Koutromanos I., Stavridis A., Shing P.B., Willam K., Numerical modeling of masonry infilled RC frames subjected to seismic loads, *Journal of Computers & Structures*, 89, 11-12, p.1026-1037, June (2011).
- Lafuente M., Molina A., Genatios C., Seismic-resistant behavior of minor reinforced concrete frames with masonry infill walls, *Proc. of 12th WCEE*, (2000).
- Liauw T.C., Kwan K.H., Nonlinear behavior of non-integral infilled frames, *Journal of Computers and Structures*, 18, 3, p.551-560, (1984).

- Liauw T.C., Kwan K.H., New development in research of infilled frames, Proc. of the eighth world conference on earthquake engineering, p.623-630, (1984).
- Liauw T.C., Kwan K.H., Static and Cyclic Behaviors of Multistory Infilled Frames with Different Interface Conditions, Journal of Sounds and Vibrations, 99, 2, p.275-283, (1985a).
- Lotfi H.R., Shing P.B., Interface model applied to fracture of masonry structures, Journal of structural engineering New York, N.Y., 120, 1, p.63-80, Jan (1994).
- Longo F., Wiebe L., Da Porto F., Modena C., Application of an in-plane/out-of plane interaction model for URM infill walls to dynamic seismic analysis of RC frame buildings. Bull Earthquake Engineering, 16, 12, p.6163-619, (2018).
- Loureno P.B., Rots J.G., On the use of micro-modeling for the analysis of masonry shear walls, em: Computer Methods in Structural Masonry - 2, Ed. G.N. Pande, J. Middleton, Books & Journals International, Swansea, UK, p.1426, (1993).
- Lourenco P.B., Computational strategies for Masonry structures, PhD. thesis. The Netherlands: Delft University of Technology, (1996).
- Lourenco P.B., Rots J.G., Multisurface Interface Model for Analysis of Masonry Structures, Journal of Engineering Mechanics, 123, 7, p.660-668, July (1997).
- Lourenco P.B., Rots J.G., Continuum model for masonry: Parameter estimation and validation, Journal of structural engineering New York, N.Y., 124, 6, p.642-652, (1998).
- Madan A., Reinhorn A.M., Mander J.B., Valles R.E., Modeling of Masonry Infill Panels for Structural Analysis, Journal of Structural Engineering ASCE, 123, 10, p.1295-1302, (1992).
- Mainstone R.J., Supplementary note on the stiffness and strengths of infilled frames, Building Research Station, Garston, UK, (1974).
- Magenes G., Calvi G.M., In-plane seismic response of brick masonry walls, Journal Earthquake Engineering and Structural Dynamics, 26, (1997).
- Magenes G., A method for pushover analysis in seismic assessment of masonry buildings, Proc. of 12th World Conference on Earthquake Engineering, (2000).
- Mander J.B., Priestley M.J.N. and Park R., Theoretical stress-strain model for confined concrete, Journal of Structural Engineering, 114, p.1804-1826, (1988).
- Marjani F., and Ersoy U., Behavior of Brick Infilled RC Frames Under Reserved Cyclic Loading, ECAS 2002 International Symposium on Structural and Earthquake Engineering, METU Publication, (2002).
- McKenna F., Fenves G., Scott M., Jeremic B., Open System for Earthquake Engineering Simulation (OpenSees), (2000), <http://opensees.berkeley.edu>.
- Mehrabi A.B., Shing P.B., Schuller M.P., Experimental evaluation of masonry-infilled RC frames, J.Struct.Eng, 122, p.228-237, (1996).

- Milania G., Lourencob P.B., Trallia A., 3D homogenized limit analysis of masonry buildings under horizontal loads, *Journal of Engineering Structures* 29, p.3134-3148, (2007).
- Milani G., 3D upper bond limit analysis of multi-leaf masonry walls. *International Journal of Mechanical Sciences*, 50, p.817-836, (2008).
- Mostafaei H., Kabeyasawa T., Effect of Infill Masonry Walls on the Seismic Response of Reinforced Concrete Buildings Subjected to the 2003 Bam Earthquake Strong Motion : A Case Study of Bam Telephone Center, *Journal of Bulletin of the Earthquake Research Institute, University of Tokyo*, 13 , p.133-156, (2004).
- Mosalam K.M., Günay S., Progressive collapse analysis of reinforced concrete frames with unreinforced masonry infill walls considering in-plane/out-of-plane interaction, *Earthquake Spectra* 31, 2, p.921–943, (2015).
- Masonry standards joint committee, *Building Code Requirements and Specification for Masonry Structures, MSJC Code*, (2008).
- Negro P., Verzeletti G., Magonette G.E., Pinto A.V., Tests on a four-storey full-scale R/C frame designed according to Eurocodes 8 and 2. Preliminary report. Report EUR 15879, European Commission, Joint Research Centre, Ispra, Italy, (1996).
- Nemati F., Macromodel for solid and perforated masonry infill frames, PhD Thesis, University of Lousiville, Louisville, KY, (2015).
- Oliaee M., Magenes G., In-Plane/Out-of-Plane interaction in the seismic response of masonry infills in RC frames, *Proc. of the 16th International Brick and Block Masonry Conference, Padova, Italy, 26–30 June*, (2016).
- Oliveira D.V., Lourenco, P.B., Implementation and validation of a constitutive model for the cyclic behaviour of interface elements, *Journal of Computers & Structures*, 82, 17-19, p.1451-1461, (2004).
- Oliveira D.V., Experimental and numerical analysis of blocky masonry structures under cyclic loading. PhD Dissertation, Universidade do Minho, Guimaraes, Portugal, (2003).
- Penava D., Sigmund V., Out-of-plane behaviour of framed-masonry walls with opening as a result of shaking table tests, *Proc. 16th World Conference on Earthquake Engineering (WCEE), Santiago, Chile, 9-13 January*, (2017).
- Penava D., Sigmund V., Kožar Iv., Validation of a simplified micromodel for analysis of infilled RC frames exposed to cyclic lateral loads, *Bulletin of Earthquake Engineering*, 14 (2016).
- Penava D., Sarhosis V., Kožar Iv., Guljaš Iv., Contribution of RC columns and masonry wall to the shear resistance of masonry infilled RC frames containing different in size window and door openings, *Engineering Structures*, 172, 1, p.105-130, (2018)
- Paulay T., Priestley M.J.N, *Seismic Design of Reinforced Concrete and Masonry Buildings*, JOHN WILEY & SONS, INC., (1992).

Polyakov S.V., *Masonry in Framed Buildings. An Investigation into the Strength and Stiffness of Masonry Infilling*, Moscow, (1957).

Puglisi M., Uzcategui M., Florez-Lopez J., Modeling of masonry of infilled frames Part I: The plastic concentrator *Journal of Engineering Structures*, 31, 1, p.113-8, (2009).

Reinhorn A.M., Mander J.B., Valles R.E., Modeling of masonry infill panels for structural analysis, *Journal of structural engineering* New York, N.Y., 123, 10, p. 1295-1302, (1997).

Ricci P., Di Domenico M., Verderame G.M., Empirical based out-of-plane URM infill wall model accounting for the interaction with In-plane demand, *Earthquake Eng. & Struct. Dynam.*, 1, 26, (2017).

Rodrigues H., Varum H., Costa A., Simplified macro-model for infill masonry panels, *Journal of Earthquake Engineering*, 14, 3, p.390-416, March (2010).

Saneinejad A., and Hobbs B., Inelastic design of infilled frames, *Journal of Structural Engineering*, 121, 4, p.634, (1995).

SAP2000. Three dimensional static and dynamic finite element analysis and design of structures. Analysis reference, version 15.1, Berkeley (CA): Computer and Structures, Inc., (2011).

Schwarz J., Lang D.H., Raschke M., Schmidt H.G., Wuttke F., Baumbach M., Zschau J., Lessons from recent earthquakes – field missions of German Task Force, Proc. of the 12th World Conference on Earthquake Engineering, Auckland, New Zealand, Jan 30-Feb 4, Special Theme Session, (2000).

Schwarz J., Abrahamczyk L., Leipold M., Swain T.M., Damage description for earthquake risk assessment, Proc. of the 1st European Conference on Earthquake Engineering and Seismology (1st ECEES), Geneva, Switzerland, (2006).

Schwarz J., Kaufmann C., Maiwald H., Seismische einwirkungen für die neue generation von erdbebenbaunomen: Gefährdungskonsistente Spektren für die Aktualisierte Erdbebenzonenkarte. Abschlussberericht. Bauforschungsvorhaben im Bauaufsichtlichen Bereich. Im Auftrag des Deutschen Instituts für Bautechnik. Zentrum für die Ingenieuranalyse von Erdbebenschäden. Scientific Technical Report 01-17, Weimar, Februar 2017; überarbeitete Fassung vom Februar 2018, Scientific Technical Report 01-18 (2017, 2018).

Shien-Beygi B., Pietruszczak S., Numerical analysis of structural masonry: mesoscale approach, *Computers and Structures*, 86, p.1958-1973, (2008).

Smyrou E., Implementation and verification of Masonry panel model for nonlinear dynamic analysis of Infilled RC frames, MSc Thesis, European School for Advanced Studies in Reduction of Seismic Risk (ROSE School), Pavia, Italy, (2006).

Smith B.S., Behavior of square infilled frames, *Journal of the Structural Division*, ASCE, 92,1, p.381-404, (1966).

Shing P.B., Stavridis A., Analysis of seismic response of masonry-infilled RC frames through collapse, *ACI Struct. J.*, 297, p.1-20, (2014).

Sigmund V. et al., FRAMed–Masonry Composites for Modeling and Standardization, FRAMA, International Benchmark within Research Project. Josip Juraj Strossmayer University of Osijek, Croatia, www.framed-masonry.com, (2014).

Sigmund V., Penava D., Influence of openings, with and without confinement, on cyclic response of infilled RC frames. An experimental study, *Journal of Earthquake Engineering*, 18, 1, p.113-146, (2014).

Stafford Smith B., Carter A., A method of analysis for infilled frames, *Proceedings of the Institute of Civil Engineers*, 44, p.31-48, (1969).

Stavridis A., Shing P.B., Finite-element modeling of nonlinear behavior of masonry infilled RC frames, *Journal of Structural Engineering*, 136, 3, p.285-296, (2010).

Stavridis A., Analytical and experimental study of seismic performance of reinforced concrete frames infilled with masonry walls, PhD Dissertation, University of California at San Diego, La Jolla, CA, (2009)

Spacone E., Ciampi V., Filippou F.C., Mixed formulation of nonlinear beam finite element. *Computers and Structures* 58, 1, p.71-83, (1996).

Soleimani D., Popov E.P., Bertero V.V., Nonlinear beam model for RC frame analysis, 7th ASCE Conference on Electronic Computation, St. Louis, (1979).

Šipoš T., Rodrigues H., Grubišić M., Simple design of masonry infilled reinforced concrete frames for earthquake resistance, *Engineering Structures*, 171, p.961-981, (2018).

Taucer F.F., Spacone, E., and Filippou F.C., A fiber beam-column element for seismic response analysis of reinforced concrete structures."UCB/EERC Report 91/17, Earthquake Engineering Research Center, University of California, (1991).

Tempestti J.M., Stavridis A., Simplified method to assess lateral resistance of infilled reinforced concrete frames, *Proc. 16th World Conference on Earthquake Engineering (WCEE)*, Santiago, Chile, 9-13 January, (2017).

Varum, H., Seismic assessment, strengthening and repair of existing buildings, PhD Thesis, Department of Civil Engineering, University of Aveiro, Portugal, (2003).

VISION2000, Performance Based Seismic Engineering of Buildings, Sacramento, CA, Structural Engineers Association of California, (2000).

Wenk T., Lacave C., Peter K., The Adana-Ceyhan Earthquake of June 27, 1998 report on the reconnaissance mission from July 6-12, 1998 of the Swiss Society of Earthquake Engineering and Structural Dynamics (SGEB). p.47, (1998).

Yorulmaz M., Sozen M.A., Behavior of single-story reinforced concrete frames filler walls, Technical report, structural research series No. 337, (1968).

Žarnic R., and Gostič S., Masonry infilled frames as an effective structural subassembly, Seismic design methodologies for the next generation of codes, P. Fajfar and H. Krawinkler, eds., A.A. Balkema, Rotterdam, Netherlands, p.335-346, (1997).

Zovkic J., Sigmund V., Guljas I., Cyclic testing of a single bay reinforced concrete frames with various types of masonry infill, Earthquake Engineering and Structural Dynamics, 42, p.1131-1149, (2013).

Appendices

Contents

List of Figures.....	139
List of Tables	142
Appendix A: Database Samples.....	143
A.1 All Samples.....	143
A.2 URM Parameters of the Studied Samples	147
A.3 RC Frame Parameters of the Studied Samples	149
Appendix B: Reference Objects Structural Details	151
B.1 Reference Object (ELSA) (<i>Negro et al., 1996</i>).....	151
B.2 Reference Object (FRAMA) (<i>Sigmund et al., 2014</i>).....	153
Appendix C: Primary Element Macromodels Assessment.....	155
C.1 Dynamic Simulation Results Utilizing Lumped Plastic & Fiber Hinges Approach ..	155
Appendix D: Verification of the Results.....	165
D.1 Developed Macromodel Parameters	165
D.2 Experimental specimens	166
D.3 In-Plane Simulation Results.....	167
D.4 Out-of-Plane Simulation Results.....	168
Appendix E: Secondary Elements Macromodels Assessment	171
E.1 Dynamic Simulation Results Utilizing Reference Object (ELSA)	171
E.2 Dynamic Simulation Results Utilizing Reference Object (FRAMA)	179
Appendix F: Application to 3D Multi-Story Structures.....	223
F.1 Structural Layouts (Case Study 1)	223
F.2 Seismic Action Based on German Code.....	224
F.3 Structural Layout (Case Study 2).....	250
F.4 Seismic Action Based on European Database	251

BLANK PAGE

LIST OF FIGURES

Figure B.1 Experimental specimen (<i>Negro et al., 1996</i>): a) plane layout, b) elevation view, c) internal columns reinforcement, d) external columns reinforcement	151
Figure B.2 Experimental specimen (<i>Negro et al., 1996</i>): a) internal beams reinforcement, b) external beams reinforcement, c) cross sections	152
Figure B.3 Experimental specimen (<i>Sigmund et al., 2014</i>): a) plane layout, b) elevation view, c) cross sections.....	153
Figure C.1 Considered macromodels in case of reference object (ELSA): a) model with lumped plastic hinges, b) model with fiber section hinges.....	156
Figure C.2 Experimental/Numerical time history displacement at different story levels for the bare (BR) structure tested at PGA=0.12g by using lumped hinges	157
Figure C.3 Experimental/Numerical time history displacement at different story levels for the bare (BR) structure tested at PGA=0.45g by using lumped hinges	158
Figure C.4 Experimental/Numerical time history displacement at different story levels for the uniformly infilled (UNI) structure tested at PGA=0.45g by using lumped hinges	159
Figure C.5 Experimental/Numerical time history displacement at different story levels for the soft story (SS) structure tested at PGA=0.45g by using lumped hinges	160
Figure C.6 Experimental/Numerical time history displacement at different story levels for the bare (BR) structure tested at PGA=0.12g by using fiber hinges	161
Figure C.7 Experimental/Numerical time history displacement at different story levels for the bare (BR) structure tested at PGA=0.45g by using fiber hinges	162
Figure C.8 Experimental/Numerical time history displacement at different story levels for the uniformly infilled (UNI) structure tested at PGA=0.45g by using fiber hinges.....	163
Figure C.9 Experimental/Numerical time history displacement at different story levels for the soft story (SS) structure tested at PGA=0.45g by using fiber hinges.....	164
Figure D.1 Infilled frame specimens tested by <i>Angel (1994)</i> : a) brick masonry infill, b) concrete unit masonry infill	166
Figure D.2 IP cyclic load protocol according to <i>Angel (1994)</i>	166
Figure D.3 Infilled frame specimens tested by: a) <i>Hak et al. (2014)</i> , b) <i>Furtado et al. (2016)</i>	166
Figure D.4 Developed and <i>Di Trapani et al. (2017)</i> macromodels in-plane response comparison of specimens tested by <i>Angel (1994)</i>	167
Figure D.5 Comparison of OoP experimental test results from <i>Angel (1994)</i> with	168
Figure D.6 <i>Di Trapani et al. (2017)</i> macromodels out-of-plane response of specimens 4 and 5 tested by <i>Angel (1994)</i>	169
Figure D.7 Developed and <i>Mazza (2018)</i> macromodels out-of-plane response comparison of specimens tested by <i>Hak et al. (2014)</i>	170
Figure D.8 Developed and <i>Mazza (2018)</i> macromodels out-of-plane response comparison of specimens tested by <i>Furtado et al. (2016)</i>	170
Figure E.1 Considered macromodels in case of reference object (ELSA):	171
Figure E.2 Experimental/numerical time history displacement at different story levels for the uniformly infilled (UNI) structure tested at PGA=0.45g	173
Figure E.3 Experimental/numerical time history displacement at different story levels for the uniformly infilled (UNI) structure tested at PGA=0.45g	174
Figure E.4 Experimental/Numerical time history displacement at different story levels for the uniformly infilled (UNI) structure tested at PGA=0.45g	175
Figure E.5 Experimental/numerical time history displacement at different story levels for the uniformly infilled (UNI) structure tested at PGA=0.45g	176
Figure E.6 Experimental/numerical time history displacement at different story levels for the uniformly infilled (UNI) structure tested at PGA=0.45g	177
Figure E.7 Experimental/numerical time history displacement at different story levels for the uniformly infilled (UNI) structure tested at PGA=0.45g	178
Figure E.8 Considered macromodels in case of reference object (FRAMA):	179
Figure E.9 Experimental/numerical (M#1) time history displacement at different story levels for the structure tested at PGA=0.05g.....	181
Figure E.10 Experimental/numerical (M#1) time history displacement at different story levels for the structure tested at PGA=0.1g.....	182
Figure E.11 Experimental/numerical (M#1) time history displacement at different story levels for the structure tested at PGA=0.2g.....	183

Figure E.42 Experimental/numerical (M#5_dev) time history displacement at different story levels for the structure tested at PGA=0.2g.....	215
Figure E.43 Experimental/numerical (M#5_dev) time history displacement at different story levels for the structure tested at PGA=0.3g.....	216
Figure E.44 Experimental/numerical (M#5_dev) time history displacement at different story levels for the structure tested at PGA=0.4g.....	217
Figure E.45 Experimental/numerical (M#5_dev) time history displacement at different story levels for the structure tested at PGA=0.6g.....	218
Figure E.46 Experimental/numerical (M#5_dev) time history displacement at different story levels for the structure tested at PGA=0.7g.....	219
Figure E.47 Experimental/numerical (M#5_dev) time history displacement at different story levels for the structure tested at PGA=0.8g.....	220
Figure E.48 Experimental/numerical (M#5_dev) time history displacement at different story levels for the structure tested at PGA=1.0g.....	221
Figure E.49 Experimental/numerical (M#5_dev) time history displacement at different story levels for the structure tested at PGA=1.2g.....	222
Figure F.1 Case study 1 structure: a) plane layout, b) elevation view, c) cross sections.....	223
Figure F.2 Respective time history records of the considered seismic action.....	225
Figure F.3 Case study 2 structure: a) plane layout, b) elevation view and	250
Figure F.4 Respective time history records of the considered seismic action.....	251

LIST OF TABLES

Table A.1 Database sources and specimens	143
Table A.2 URM parameters	147
Table A.3 RC frame parameters	149
Table B.1 RC frame material properties (<i>Negro et al., 1996</i>).....	154
Table B.2 URM infills material properties and thickness (<i>Negro et al., 1996</i>).....	154
Table B.3 RC frame material properties (<i>Sigmund et al., 2014</i>).....	154
Table B.4 URM infills material properties and thickness (<i>Sigmund et al., 2014</i>).....	154
Table C.1 Geometric and material properties of the infill walls	155
Table C.2 Force - displacement parameters for pivot model	155
Table D.1 Stress-strain parameters for pinching material model	165
Table D.2 Dynamic and geometric parameters of the developed model	165
Table E.1 Geometric and material properties of the infill walls	172
Table E.2 Stress-strain parameters for the diagonal strut models (M#1, 2, 3)	172
Table E.3 Stress-strain parameters for the shear link model (M#4)	172
Table E.4 Stress-Strain parameters for the diagonal beam-column model (M#5_dev)	172
Table E.5 Geometric and material properties of the infill walls	180
Table E.6 Stress-strain parameters for the diagonal strut models (M#1, 2, 3)	180
Table E.7 Geometric and material properties of the infill walls	211
Table E.8 Dynamic and geometric parameters of the developed model (M#5_dev).....	212
Table E.9 Stress-strain parameters for the diagonal beam-column model (M#5_dev).....	212
Table F.1 Selected ground motions for case study 1 (<i>Schwarz et al., 2017, 2018</i>).....	224
Table F.2 Predicted damage and interstory drift	229
Table F.3 Considered models	250
Table F.4 Selected ground motions for case study 2 (<i>Iervolino et al., 2010</i>)	251
Table F.5 Predicted damage and interstory drift	255

Appendix A: Database Samples

A.1 All Samples

Table A.1 Database sources and specimens

Ref.	Spec.ID.	URM type	Axial Load per Col. [kN]	Horizontal Load	Failure RC	Failure URM	Studied
<i>Mehrabi et al. (1996)</i>	1	Bare	293.7	IP(C)	F	---	X
	4	hollow brick	195.8	IP(C)	S/F	DC+CC	√
	5	solid brick	195.8	IP(C)	S/F	DC	√
	6	hollow brick	195.8	IP(C)	F	DC+CC	√
	7	solid brick	195.8	IP(C)	F	DC	√
	10	hollow brick	195.8	IP(C)	S/F	DC+CC	√
	11	solid brick	195.8	IP(C)	S/F	DC	√
<i>Kakaletsis (2007)</i>	B	Bare	50	IP(C)	F	---	X
	S	hollow brick	50	IP(C)	F	DC+CC	√
	IS	hollow brick	50	IP(C)	F	DC	√
	BS	Bare	50	IP(C)	F	---	X
	SS	hollow brick	50	IP(C)	F	DC+CC	√
	ISS	hollow brick	50	IP(C)	F	DC	√
<i>Combesure et al. (2000)</i>	I3	Bare	100	IP(C)	F	---	X
	I4	Bare	100	IP(C)	F	---	X
	I1	hollow brick	100	IP(C)	F	DC+CC	X
	I7	hollow brick	100	IP(C)	F	DC+CC	X
	I8	hollow brick	100	IP(C)	F	DC+CC	X
	I9	hollow brick	100	IP(C)	F	DC+CC	X

Horizontal load type:

IP(C): In-Plane Cyclic, IP(PsD): In-Plane Pseudo Dynamic, IP(M): In-Plane Monotonic and OoP(M): Out-of-Plane Monotonic

Failure RC:

F= Flexure, S/F= Shear/Flexure and N.R.= Not Reported

Failure URM:

DC= Diagonal Cracking, CC= Corner Crushing and SS= Shear Sliding, N.R.= Not Reported

Table A.1 Database sources and specimens (continued)

Ref.	Spec.ID.	URM type	Axial Load per Col. [kN]	Horizontal Load	Failure RC	Failure URM	Studied
<i>Colangelo (2004)</i>	U11	hollow brick	190	IP(PsD)	F	DC+CC	√
	U21	hollow brick	190	IP(PsD)	F	DC+CC	√
	V10	Bare	250	IP(PsD)	F	---	
	V11	hollow brick	250	IP(PsD)	F	DC+CC	√
	V20	Bare	250	IP(PsD)	F	---	
	V21	hollow brick	250	IP(PsD)	F	DC+CC	√
	V22	hollow brick	250	IP(PsD)	F	DC+CC	√
<i>Zovkic et al. (2013)</i>	MODEL8	hollow brick	375	IP(C)	F	CC+SS	√
	MODEL4	hollow brick	375	IP(C)	F	CC+SS	√
	MODEL3	AAC	375	IP(C)	F	DC	√
	MODEL10	Bare	375	IP(C)	F	---	X
<i>Lafuente et al. (2000)</i>	M1	N.R.	0	IP(C)	S/F	DC	√
	M2	N.R.	0	IP(C)	S/F	DC	√
	M3	N.R.	0	IP(C)	S/F	DC	√
	M4	N.R.	0	IP(C)	S/F	DC	√
	M5	N.R.	0	IP(C)	S/F	DC	√
	M6	N.R.	0	IP(C)	S/F	DC	√
	M7	N.R.	0	IP(C)	S/F	DC	√
	M8	N.R.	0	IP(C)	S/F	DC	√
	M9	N.R.	0	IP(C)	S/F	DC	√
	M10	N.R.	0	IP(C)	S/F	DC	√
<i>AL-Chaar (1998)</i>	MODEL1	Bare	0	IP(M)	S/F	---	X
	MODEL2	CMU	0	IP(M)	S/F	DC	√
	MODEL3	hollow brick	0	IP(M)	S/F	DC	√

Horizontal load type:

IP(C): In-Plane Cyclic, IP(PsD): In-Plane Pseudo Dynamic, IP(M): In-Plane Monotonic and OoP(M): Out-of-Plane Monotonic

Failure RC:

F= Flexure, S/F= Shear/Flexure and N.R.= Not Reported

Failure URM:

DC= Diagonal Cracking, CC= Corner Crushing and SS= Shear Sliding, N.R.= Not Reported

Table A.1 Database sources and specimens (continued)

Ref.	Spec.ID.	URM type	Axial Load per Col. [kN]	Horizontal Load	Failure RC	Failure URM	Studied
<i>Angel (1994)</i>	1b	hollow brick	224	OoP (M)	F	N.R.	√
	2a,b	hollow brick	224	IP(C) + OoP (M)	F	N.R.	√
	3a,b	hollow brick	224	IP(C) + OoP (M)	F	N.R.	√
	4a,b	Concrete block	224	IP(C) + OoP (M)	F	N.R.	√
	5a,b	Concrete block	224	IP(C) + OoP (M)	F	N.R.	√
	6a,b	hollow brick	224	IP(C) + OoP (M)	F	N.R.	√
	7a,b	hollow brick	224	IP(C) + OoP (M)	F	N.R.	X
	8a,b	hollow brick	224	IP(C) + OoP (M)	F	N.R.	X
<i>Crisafulli (1997)</i>	Unit 1	solid con brick	20	IP(C)	S/F	DC	√
	Unit 2	solid con brick	20	IP(C)	F	DC	√
<i>Yorulmaz et al. (1968)</i>	PF1	Bare	0	IP(M)	S/F	---	X
	PF2	hollow brick	0	IP(M)	S/F	SS	X
	F1	hollow brick	0	IP(M)	S/F	DC	X
	F2	Bare	0	IP(M)	S/F	---	X
	F3	hollow brick	0	IP(M)	S/F	SS	X
	F4	Bare	0	IP(M)	F	---	X
	FS	hollow brick	0	IP(M)	S/F	SS	X
	F6	hollow brick	0	IP(M)	S/F	SS	X
	F7	hollow brick	0	IP(M)	S/F	SS	X
F8	hollow brick	0	IP(M)	S/F	SS	X	

Horizontal load type:

IP(C): In-Plane Cyclic, IP(PsD): In-Plane Pseudo Dynamic, IP(M): In-Plane Monotonic and OoP(M): Out-of-Plane Monotonic

Failure RC:

F= Flexure, S/F= Shear/Flexure and N.R.= Not Reported

Failure URM:

DC= Diagonal Cracking, CC= Corner Crushing and SS= Shear Sliding, N.R.= Not Reported

Table A.1 Database sources and specimens (continued)

Ref.	Spec.ID.	URM type	Axial Load per Col. [kN]	Horizontal Load	Failure RC	Failure URM	Studied
<i>Cavaleri et al. (2014)</i>	S1A-1	Calcarenite	200	IP(C)	F	SS	√
	S1A-2	Calcarenite	200	IP(C)	F	SS	√
	S1B-1	Clay	200	IP(C)	F	DC	√
	S1B-2	Clay	200	IP(C)	F	DC	√
	S1C-1	Lw.C	200	IP(C)	F	DC	√
	S1C-2	Lw.C	200	IP(C)	F	DC	√
	S1C-3	Lw.C	200	IP(C)	F	DC	√
	S1C-4	Lw.C	200	IP(C)	F	DC	√
	S2A-1	Calcarenite	200	IP(C)	F	SS	√
	S2A-2	Calcarenite	200	IP(C)	F	SS	√
	S2B-1	Clay	200	IP(C)	F	DC	√
	S2B-2	Clay	200	IP(C)	F	DC	√
<i>Calvi et al. (2004)</i>	Test 10	clay blocks	0	OoP (M)	N.R.	N.R.	√
	Test 2	clay blocks	0	IP(C) + OoP(M)	F	N.R.	√
	Test 6	clay blocks	0	IP(C) + OoP (M)	F	N.R.	√
<i>Hak et al. (2014)</i>	TNT	Bare	400	IP(C)	F	N.R.	√
	TA3	Brick	400	IP(C) + OoP(C)	F	N.R.	√
	TA2	Brick	400	IP(C) + OoP(C)	F	N.R.	√
	TA1	Brick	400	IP(C) + OoP(C)	F	N.R.	√
<i>Furta- do et al. (2016)</i>	Inf_02	Brick	300	OoP(C)	N.R.	N.R.	√
	Inf_04	Brick	300	OoP(C)	N.R.	N.R.	√

Horizontal load type:

IP(C): In-Plane Cyclic, IP(PsD): In-Plane Pseudo Dynamic, IP(M): In-Plane Monotonic and OoP(M): Out-of-Plane Monotonic

Failure RC:

F= Flexure, S/F= Shear/Flexure and N.R.= Not Reported

Failure URM:

DC= Diagonal Cracking, CC= Corner Crushing and SS= Shear Sliding, N.R.= Not Reported

A.2 URM Parameters of the Studied Samples

Table A.2 URM parameters

Spec.ID.	L_{URM} [m]	H_{URM} [m]	t_{URM} [mm]	$\frac{L_{URM}}{H_{URM}}$ [-]	$\frac{H_{URM}}{t_{URM}}$ [-]	f_{URM} [MPa]	E_{URM} [MPa]	f_{tp} [MPa]
4	2.032	1.4224	92.075	1.43	15.4	10.61	4595.63	0.637
5	2.032	1.4224	92.075	1.43	15.4	13.85	8943.22	0.831
6	2.032	1.4224	92.075	1.43	15.4	10.13	4196.01	0.607
7	2.032	1.4224	92.075	1.43	15.4	13.57	9067.24	0.814
10	2.032	1.4224	92.075	1.43	15.4	10.61	3941.08	0.637
11	2.032	1.4224	92.075	1.43	15.4	11.44	9597.77	0.686
S	1.2	0.8	60	1.5	13.3	5.11	670.3	0.08
IS	1.2	0.8	52	1.5	15.4	17.68	540.19	0.12
SS	1.2	0.8	60	1.5	13.3	5.11	670.3	0.08
ISS	1.2	0.8	52	1.5	15.4	17.68	540.19	0.12
U11	1.7	1.3	77	1.31	16.9	2.24	598.6652	0.35
U21	1.7	1.3	77	1.31	16.9	2.24	598.6652	0.35
V11	2.3	1.3	77	1.8	16.9	2.24	598.6652	0.35
V21	2.3	1.3	77	1.8	16.9	2.24	598.6652	0.35
V22	2.3	1.3	77	1.8	16.9	2.24	598.6652	0.35
MODEL8	1.8	1.3	120	1.4	10.8	4.28	827.5264	0.2568
MODEL4	1.8	1.3	120	1.4	10.8	1.89	549.9091	0.1134
MODEL3	1.8	1.3	120	1.4	10.8	1.63	510.6858	0.0978
M1	1.971	1.38	120	1.43	11.5	7.42	5568	0.66
M2	1.971	1.38	120	1.43	11.5	7.42	5568	0.66
M3	1.971	1.38	120	1.43	11.5	7.42	5568	0.66
M4	1.221	1.38	120	0.88	11.5	7.42	5568	0.66
M5	1.221	1.38	120	0.88	11.5	7.42	5568	0.66
M6	1.221	1.38	120	0.88	11.5	7.42	5568	0.66
M7	1.468	1.38	120	1.1	11.5	7.42	5568	0.66
M8	1.468	1.38	120	1.1	11.5	7.42	5568	0.66
M9	1.468	1.38	120	1.1	11.5	7.42	5568	0.66
M10	1.468	1.38	120	1.1	11.5	7.42	5568	0.66
MODEL2	1.83	1.33	68.8	1.4	19.3	16.6	10500	0.9
MODEL3	1.83	1.33	37.8	1.4	35.2	15.6	22600	0.9

Table A.2 URM parameters (continued)

Spec.ID.	L_{URM} [m]	H_{URM} [m]	t_{URM} [mm]	$\frac{L_{URM}}{H_{URM}}$ [-]	$\frac{H_{URM}}{t_{URM}}$ [-]	f_{URM} [MPa]	E_{URM} [MPa]	f_{tp} [MPa]
2a,b	2.44	1.625	47.625	1.5	34.1	10.85175	8040.63	1.19
3a,b	2.44	1.625	47.625	1.5	34.1	10.1283	5208.84	1.10
4a,b	2.44	1.625	92.075	1.5	17.6	22.88169	12429.56	1.15
5a,b	2.44	1.625	142.875	1.5	11.4	21.44857	11616.54	1.11
6a,b	2.44	1.625	98.425	1.5	16.5	4.58185	2135.9	0.51
Unit 1	2.516	2.4	90	1.05	26.7	19.3	11550	0.3
Unit 2	2.516	2.4	90	1.05	26.7	19.3	11550	0.3
S1A-1	1.6	1.6	210	1	7.6	2.67	3933	0.73
S1A-2	1.6	1.6	210	1	7.6	2.67	3933	0.73
S1B-1	1.6	1.6	150	1	10.7	8.66	6401	1.07
S1B-2	1.6	1.6	150	1	10.7	8.66	6401	1.07
S1C-1	1.6	1.6	250	1	6.4	1.74	4565	0.29
S1C-2	1.6	1.6	250	1	6.4	1.74	4565	0.29
S1C-3	1.6	1.6	250	1	6.4	1.74	4565	0.29
S1C-4	1.6	1.6	250	1	6.4	1.74	4565	0.29
S2A-1	1.6	1.6	210	1	7.6	4.57	7106	0.89
S2A-2	1.6	1.6	210	1	7.6	4.57	7106	0.89
S2B-1	1.6	1.6	150	1	10.7	8.66	6401	1.07
S2B-2	1.6	1.6	150	1	10.7	8.66	6401	1.07
Test 10	4.2	2.75	135	1.5	20.4	1.11	1873	0.15
Test 2	4.2	2.75	135	1.5	20.4	1.11	1873	0.15
Test 6	4.2	2.75	135	1.5	20.4	1.11	1873	0.15
TA3,2,1	4.2	2.95	350	1.42	8.4	3.9	5299	0.29
Inf_02	4.2	2.3	150	1.8	15.3	0.531	1417	0.28
Inf_04	4.2	2.3	150	1.8	15.3	0.531	1417	0.22

L_{URM} [m]	URM infill wall length	f_{ck} [MPa]	Frame compressive strength
H_{URM} [m]	URM infill wall height	f_y [MPa]	Steel yield strength
a_{cOoP} [mm]	Column width	E_c [GPa]	Modulus of elasticity of concrete
b_{cIP} [mm]	Column depth	f_{URM} [MPa]	Masonry compressive strength
a_{bOoP} [mm]	Beam width	f_{tp} [MPa]	Masonry shear strength
b_{bIP} [mm]	Beam depth	E_{URM} [MPa]	Masonry modulus of elasticity
ρ_B [%]	Reinforcement beam ratio	t_{URM} [mm]	Masonry thickness
ρ_C [%]	Reinforcement column ratio	N [kN]	Vertical loads

A.3 RC Frame Parameters of the Studied Samples

Table A.3 RC frame parameters

Spec.ID.	a_{cOoP} [mm]	b_{cIP} [mm]	ρ_C [%]	a_{bOoP} [mm]	b_{bIP} [mm]	ρ_B [%]	f_c [MPa]	E_c [GPa]	f_y [MPa]
4	177.8	177.8	3.26	300	500	1.15	26.8	24.7	413
5	177.8	177.8	3.26	152.4	228.6	1.15	20.9	18.1	413
6	203.2	203.2	3.88	152.4	228.6	1.15	25.8	19.8	413
7	203.2	203.2	3.88	152.4	228.6	1.15	33.4	18.6	413
10	177.8	177.8	3.26	152.4	228.6	1.15	26.9	20.1	413
11	177.8	177.8	3.26	152.4	228.6	1.15	25.7	18.1	413
S	150	150	0.88	100	200	0.62	28.5	25.1	390.47
IS	150	150	0.88	100	200	0.62	28.5	25.1	390.47
SS	150	150	0.88	100	200	0.62	28.5	25.1	390.47
ISS	150	150	0.88	100	200	0.62	28.5	25.1	390.47
U11	200	200	0.75	200	250	0.63	35.6	33.2	385
U21	200	200	0.50	200	250	0.47	41.3	35.5	558
V11	200	200	0.75	200	250	0.63	39.6	33.1	385
V21	200	200	0.50	200	250	0.47	42.5	30.1	558
V22	200	200	0.50	200	250	0.47	41.7	31.7	558
MODEL8	200	200	2.36	120	200	1.31	41.2	30.2	594
MODEL4	200	200	2.36	120	200	1.31	38.8	29.3	594
MODEL3	200	200	2.36	120	200	1.31	28.0	24.9	594
M1	120	120	3.52	120	200	1.1	18.0	19.9	420
M2	120	120	3.52	120	200	0.94	18.0	19.9	420
M3	120	120	3.52	120	200	0.94	18.0	19.9	420
M4	120	120	3.52	120	200	0.94	18.0	19.9	420
M5	120	120	3.52	120	200	0.94	18.0	19.9	420
M6	120	120	3.52	120	200	0.94	18.0	19.9	420
M7	120	120	3.52	120	200	0.94	18.0	19.9	420
M8	120	120	3.52	120	200	0.94	18.0	19.9	420
M9	120	120	3.52	120	200	0.94	18.0	19.9	420
M10	120	120	3.52	120	200	0.94	18.0	19.9	420
MODEL2	127	203.2	1.10	127	196.85	0.85	42.7	31.8	438
MODEL3	127	203.2	1.10	300	500	0.85	42.7	31.8	438

Table A.3 RC frame parameters (continued)

Spec.ID.	a_{cOoP} [mm]	b_{cIP} [mm]	ρ_C [%]	a_{bOoP} [mm]	b_{bIP} [mm]	ρ_B [%]	f_c [MPa]	E_c [GPa]	f_y [MPa]
2a,b	304.8	304.8	3.27	254	304.8	2.1	56.1	35.2	400
3a,b	304.8	304.8	3.27	254	304.8	2.1	57.1	35.5	400
4a,b	304.8	304.8	3.27	254	304.8	2.1	58.1	35.8	400
5a,b	304.8	304.8	3.27	254	304.8	2.1	59.1	36.1	400
6a,b	304.8	304.8	3.27	254	304.8	2.1	60.1	36.4	400
Unit 1	150	150	1.40	150	200	0.5	22.5	22.1	323
Unit 2	150	150	2.09	150	200	1	31.2	25.2	323
S1A-1	200	200	0.79	200	400	0.59	25.0	25.5	450
S1A-2	200	200	0.79	200	400	0.59	25.0	25.5	450
S1B-1	200	200	0.79	200	400	0.59	25.0	25.5	450
S1B-2	200	200	0.79	200	400	0.59	25.0	25.5	450
S1C-1	300	300	0.50	300	400	0.57	25.0	25.5	450
S1C-2	300	300	0.50	300	400	0.57	25.0	25.5	450
S1C-3	300	300	0.50	300	400	0.57	25.0	25.5	450
S1C-4	300	300	0.50	300	400	0.57	25.0	25.5	450
S2A-1	200	200	0.50	200	400	0.59	25.0	25.5	450
S2A-2	200	200	0.50	200	400	0.59	25.0	25.5	450
S2B-1	200	200	0.50	200	400	0.59	25.0	25.5	450
S2B-2	200	200	0.50	200	400	0.59	25.0	25.5	450
Test 10	300	300	3.4	700	250	0.92	29	29	500
Test 2	300	300	3.4	700	250	0.92	29	29	500
Test 6	300	300	3.4	700	250	0.92	29	29	500
TA3,2,1	350	350	2.5	350	350	0.5	28	30	450
Inf_02	300	300	0.9	300	500	0.7	25	25	400
Inf_04	300	300	0.9	300	500	0.7	25	25	400

L_{URM} [m]	URM infill wall length	f_{ck} [MPa]	Frame compressive strength
H_{URM} [m]	URM infill wall height	f_y [MPa]	Steel yield strength
a_{cOoP} [mm]	Column width	E_c [GPa]	Modulus of elasticity of concrete
b_{cIP} [mm]	Column depth	f_{URM} [MPa]	Masonry compressive strength
a_{bOoP} [mm]	Beam width	f_{tp} [MPa]	Masonry shear strength
b_{bIP} [mm]	Beam depth	E_{URM} [MPa]	Masonry modulus of elasticity
ρ_B [%]	Reinforcement beam ratio	t_{URM} [mm]	Masonry thickness
ρ_C [%]	Reinforcement column ratio	N [kN]	Vertical loads

Appendix B: Reference Objects Structural Details

B.1 Reference Object (ELSA) (Negro et al., 1996)

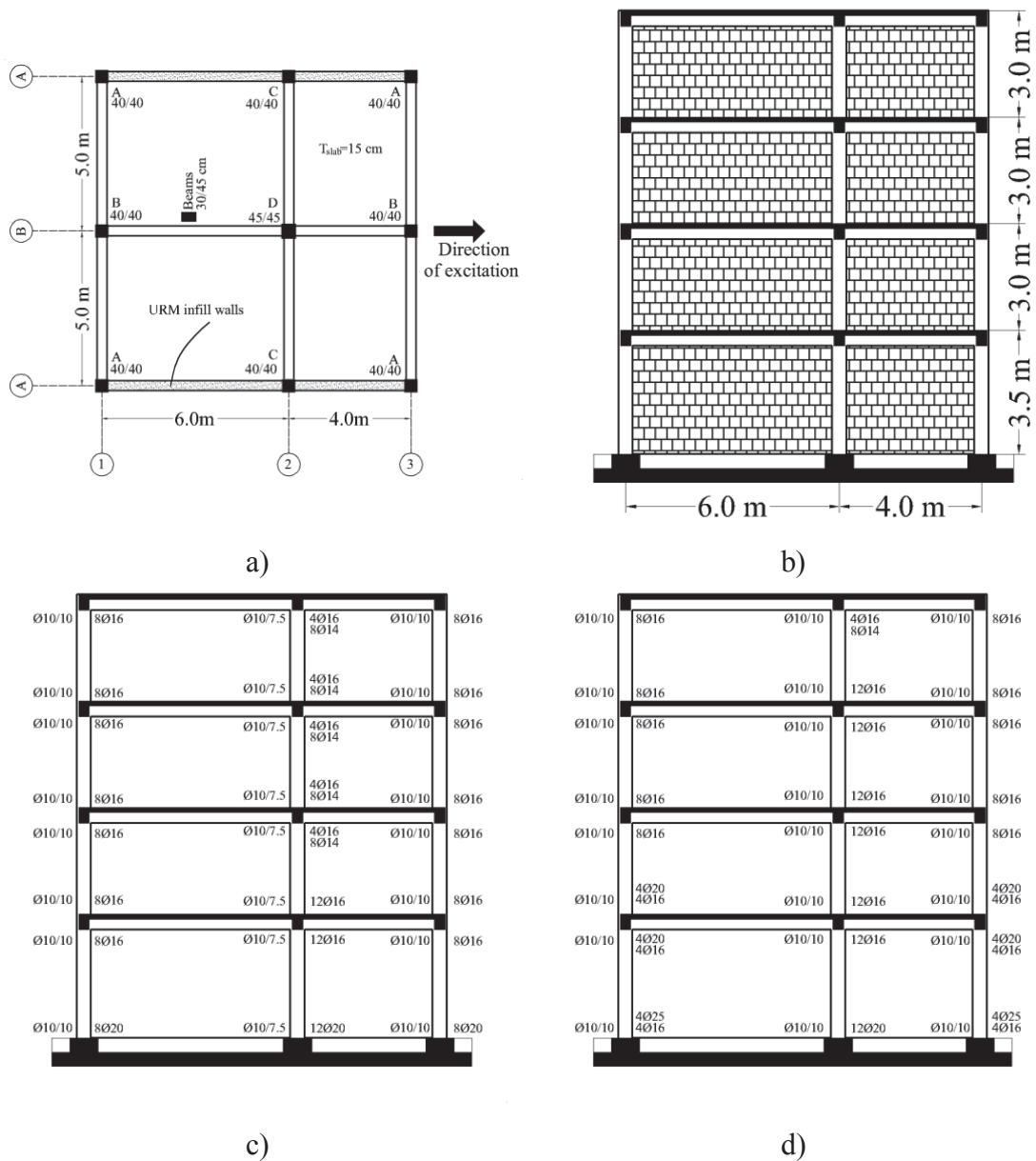
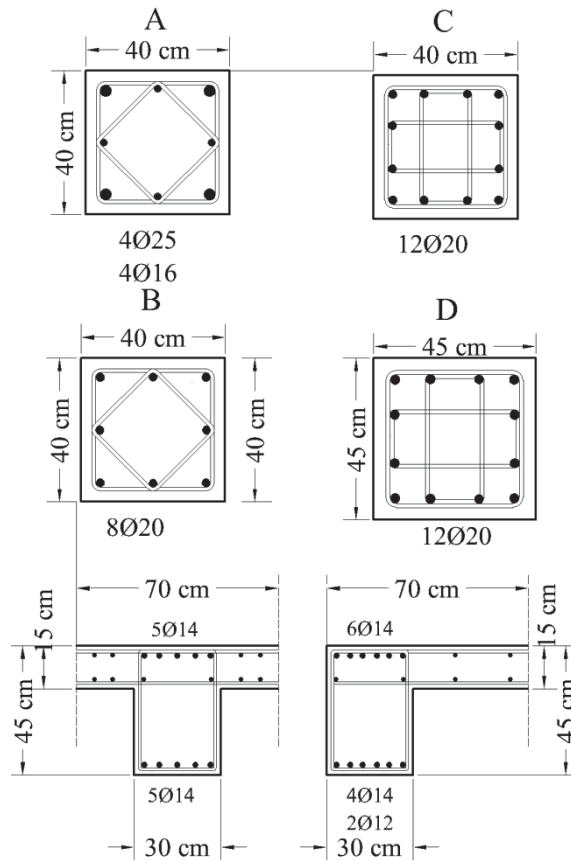


Figure B.1 Experimental specimen (Negro et al., 1996): a) plane layout, b) elevation view, c) internal columns reinforcement, d) external columns reinforcement



a)

b)



c)

Figure B.2 Experimental specimen (Negro et al., 1996): a) internal beams reinforcement, b) external beams reinforcement, c) cross sections

B.2 Reference Object (FRAMA) (*Sigmund et al., 2014*)

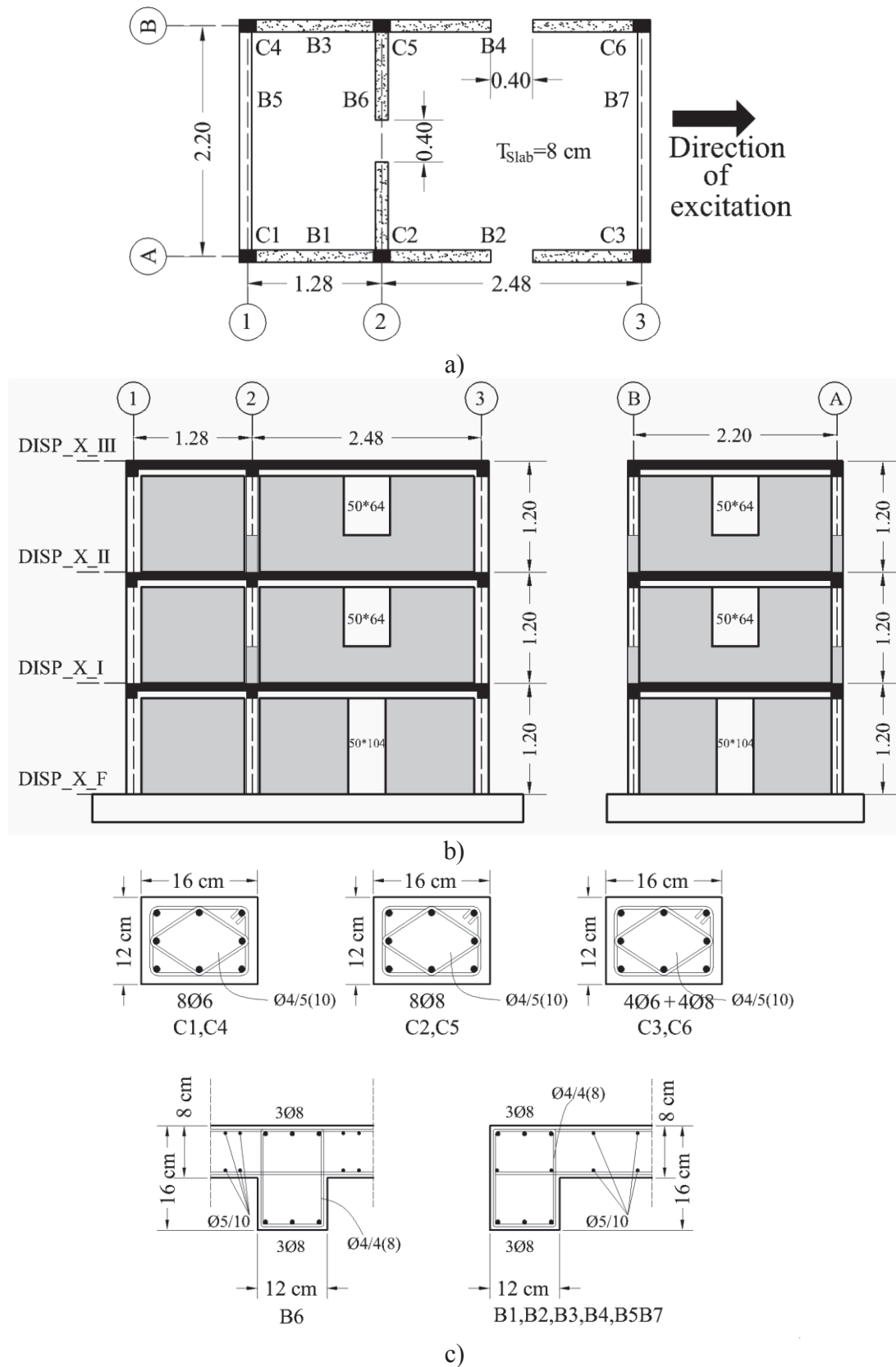


Figure B.3 Experimental specimen (*Sigmund et al., 2014*): a) plane layout, b) elevation view, c) cross sections

Table B.1 RC frame material properties (*Negro et al., 1996*)

Young modulus of concrete E_c [GPa]	31.5
Compression strength concrete f_c [MPa]	28
Tensile strength concrete f_t [MPa]	1.7
Weight of concrete [kN/m ³]	25
Mass density of concrete [t/m ³]	2.55
Yield strength of steel f_y [MPa]	450
Ultimate strength of steel f_u [MPa]	575

Table B.2 URM infills material properties and thickness (*Negro et al., 1996*)

Young modulus of infills E_{URM} [GPa]	3.6
Diagonal cracking strength f_{tp} [MPa]	0.28
Infill wall thickness t_{URM} [mm]	115

Table B.3 RC frame material properties (*Sigmund et al., 2014*)

Young modulus of concrete E_c [GPa]	38.8
Compression strength concrete f_c [MPa]	25
Tensile strength concrete f_t [MPa]	1.2
Weight of concrete [kN/m ³]	25
Mass density of concrete [t/m ³]	2.55
Yield strength of steel f_y [MPa]	500
Ultimate strength of steel f_u [MPa]	560

Table B.4 URM infills material properties and thickness (*Sigmund et al., 2014*)

Young modulus of infills E_{URM} [GPa]	2.025
Diagonal cracking strength f_{tp} [MPa]	0.28
Infill wall thickness t_{URM} [mm]	120

Appendix C: Primary Element Macromodels Assessment

C.1 Dynamic Simulation Results Utilizing Lumped Plastic & Fiber Hinges Approach

Table C.1 Geometric and material properties of the infill walls

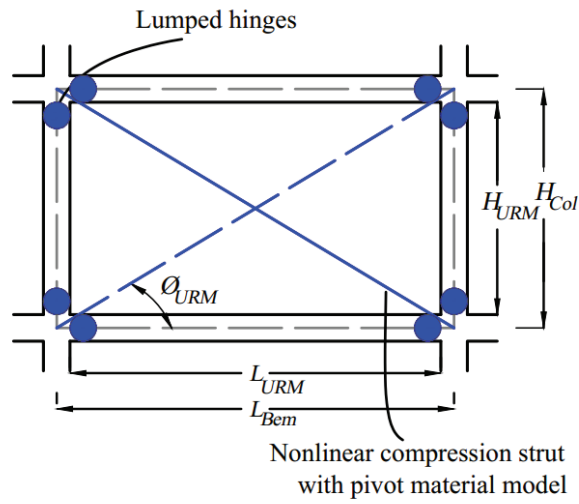
Story	L_{URM} [m]	H_{URM} [m]	t_{URM} [mm]	f_{tp} [N/mm ²]	V_{URM} [kN]	θ [deg]
1 [*]	5.6	3.05	112	0.28	175.6	28.6
2,3,4 [*]	5.6	2.55	112	0.28	175.6	24.5
1 ^{**}	3.6	3.05	112	0.28	112.9	40.3
2,3,4 ^{**}	3.6	2.55	112	0.28	112.9	35.3

*: Long span, **:Short span

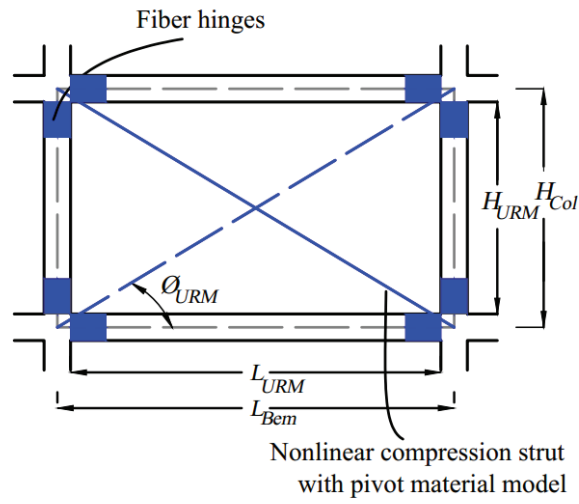
Table C.2 Force - displacement parameters for pivot model

Story	F_{cr} / δ_{cr} [kN/mm]	F_{max} / δ_{max} [kN/mm]	F_r / δ_r [kN/mm]
1 [*]	200/2.7	260/15.4	91/40.2
2,3,4 [*]	193/2.3	250/13.3	87.5/34.8
1 ^{**}	148/2.3	192/13.4	67.3/43.9
2,3,4 ^{**}	138.3/2.1	180/12	63/31.2

*: Long span, **:Short span



a) Model with lumped plastic hinges and pivot material model



b) Model with fiber section hinges and pivot material model

Figure C.1 Considered macromodels in case of reference object (ELSA): a) model with lumped plastic hinges, b) model with fiber section hinges

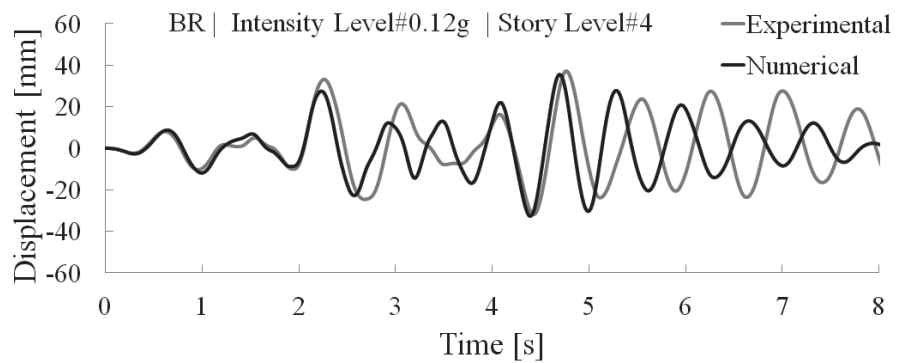
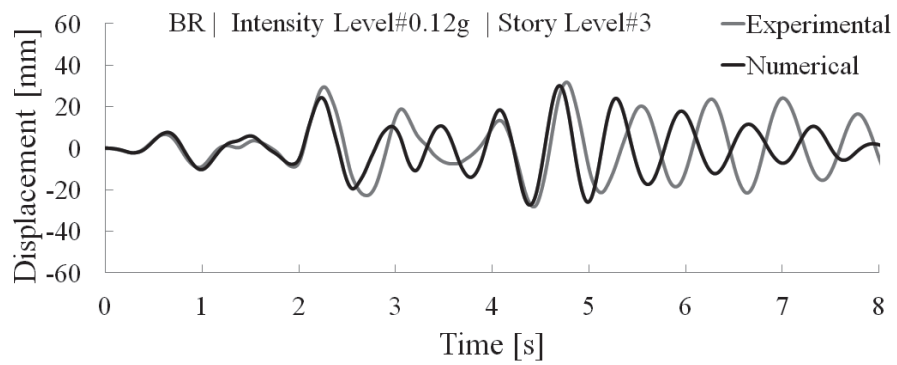
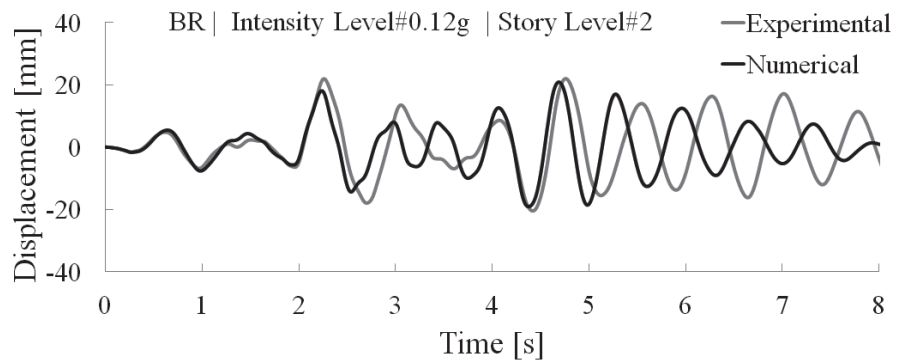
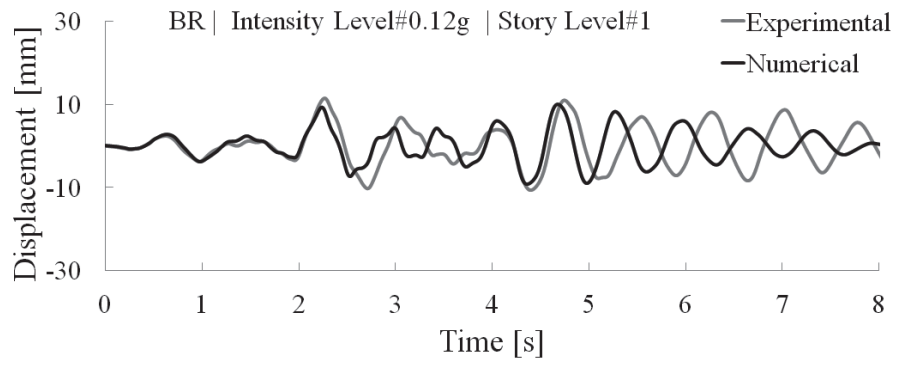


Figure C.2 Experimental/Numerical time history displacement at different story levels for the bare (BR) structure tested at PGA=0.12g by using lumped hinges

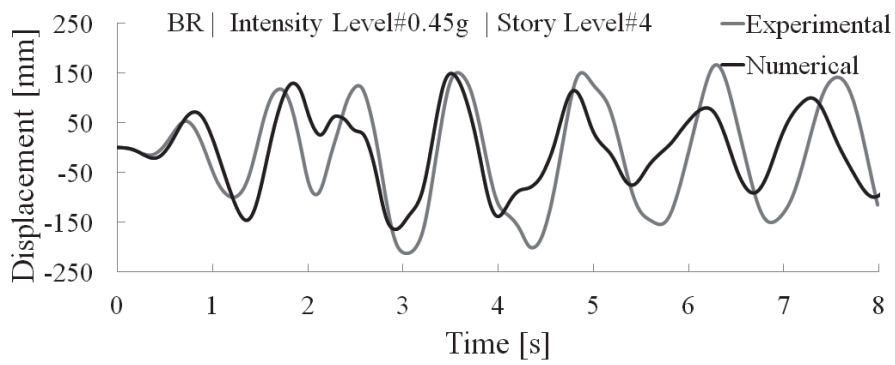
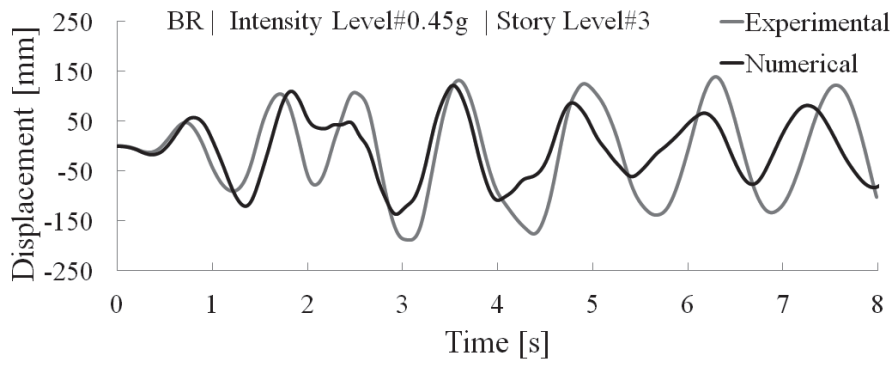
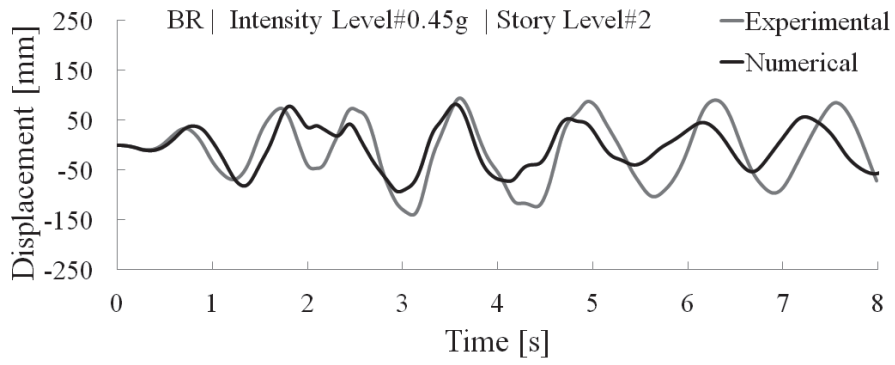
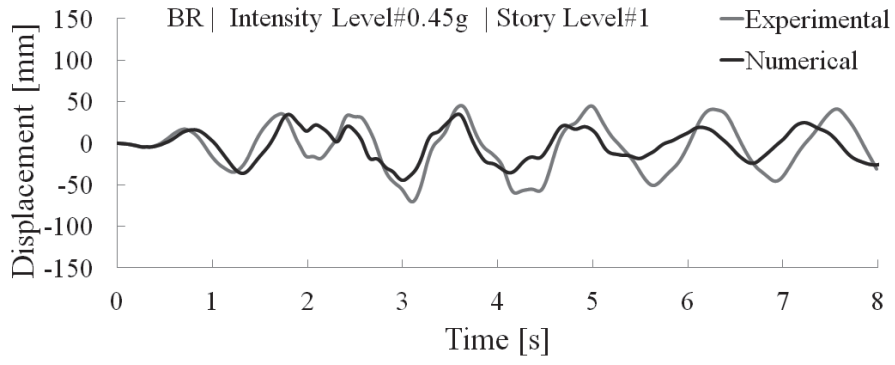


Figure C.3 Experimental/Numerical time history displacement at different story levels for the bare (BR) structure tested at PGA=0.45g by using lumped hinges

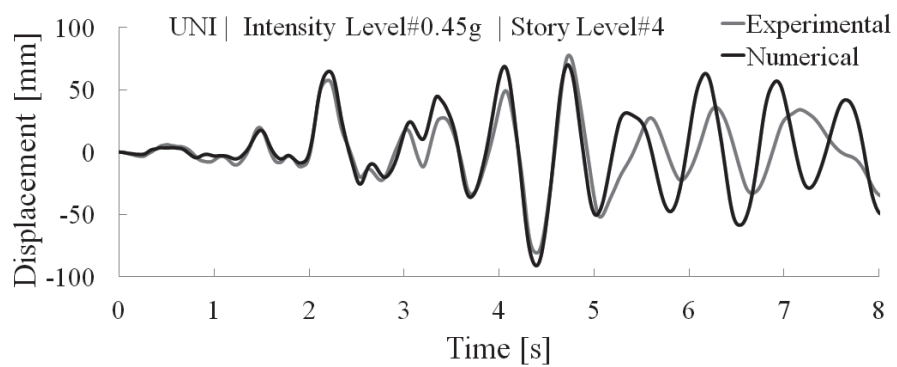
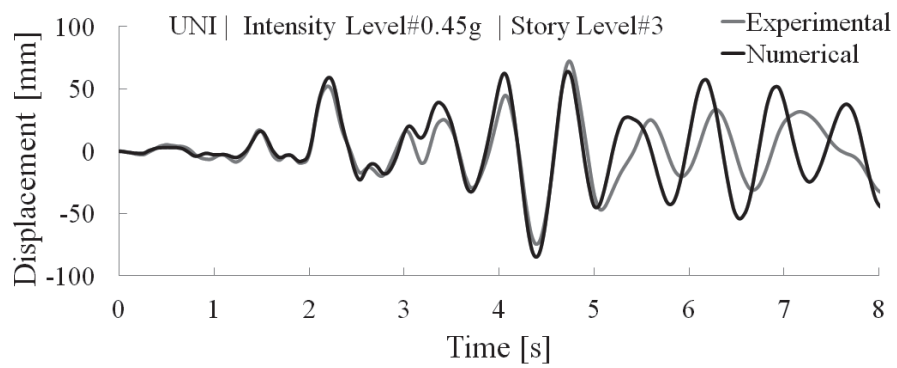
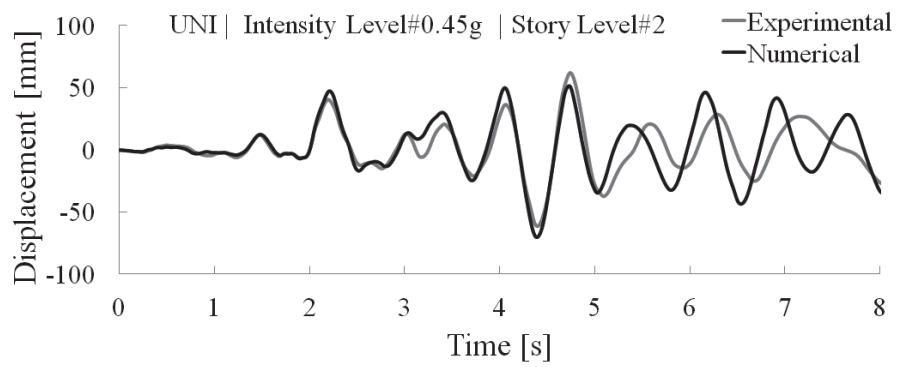
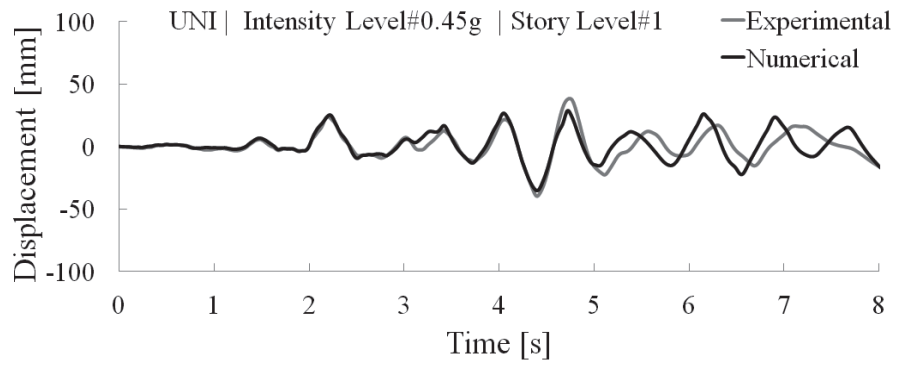


Figure C.4 Experimental/Numerical time history displacement at different story levels for the uniformly infilled (UNI) structure tested at PGA=0.45g by using lumped hinges

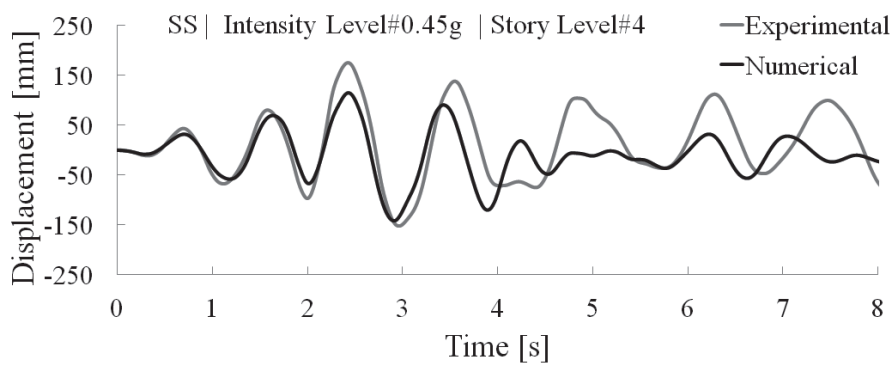
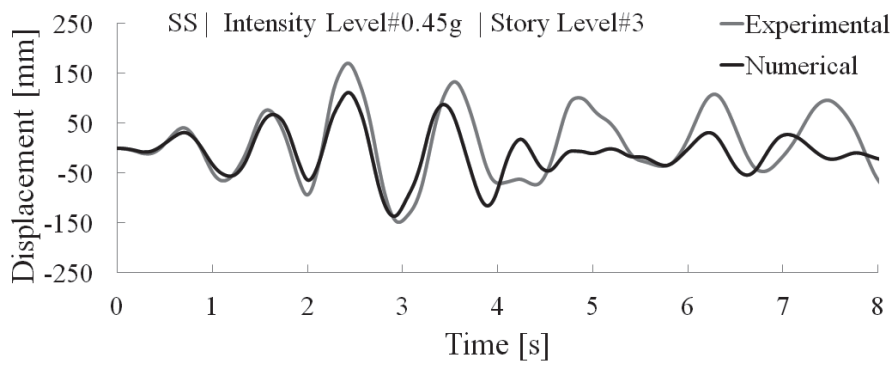
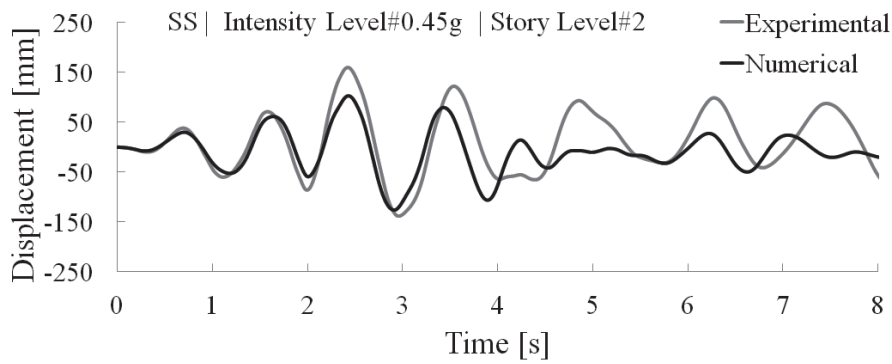
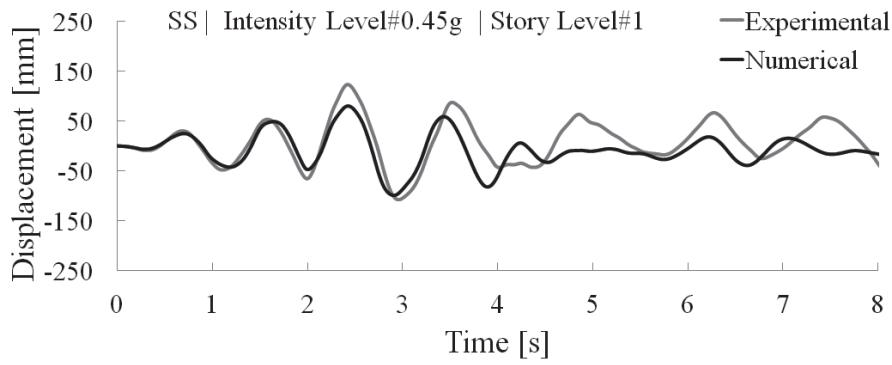


Figure C.5 Experimental/Numerical time history displacement at different story levels for the soft story (SS) structure tested at PGA=0.45g by using lumped hinges

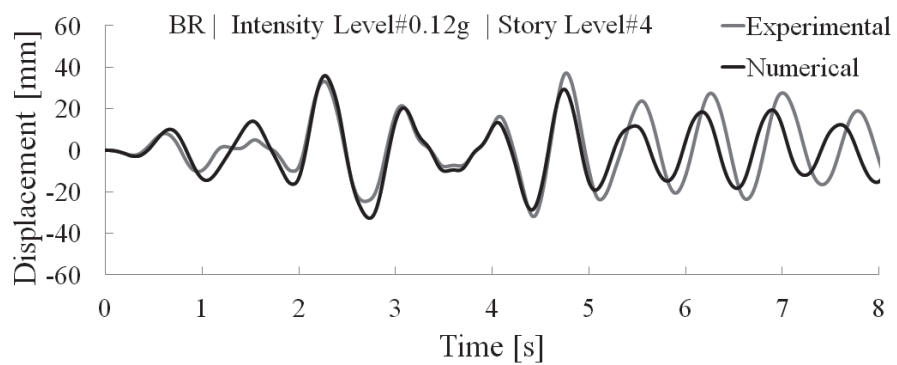
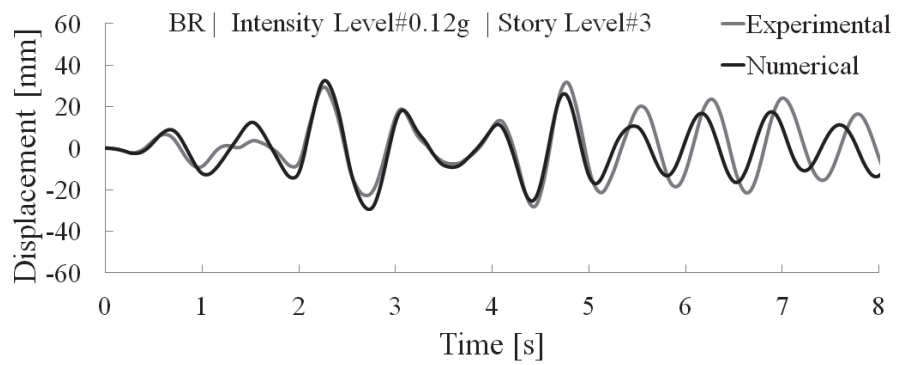
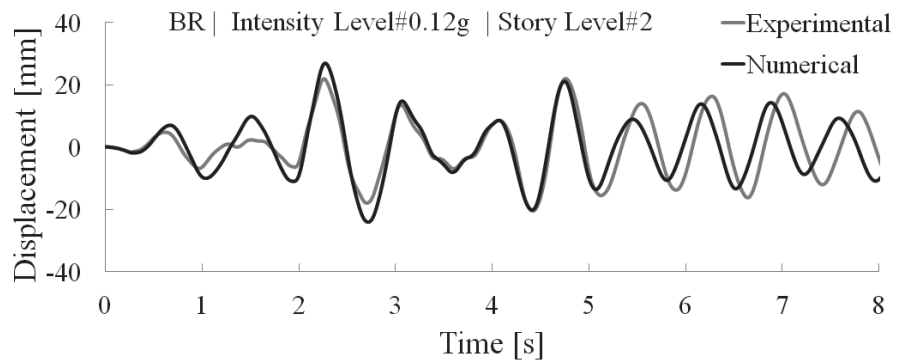
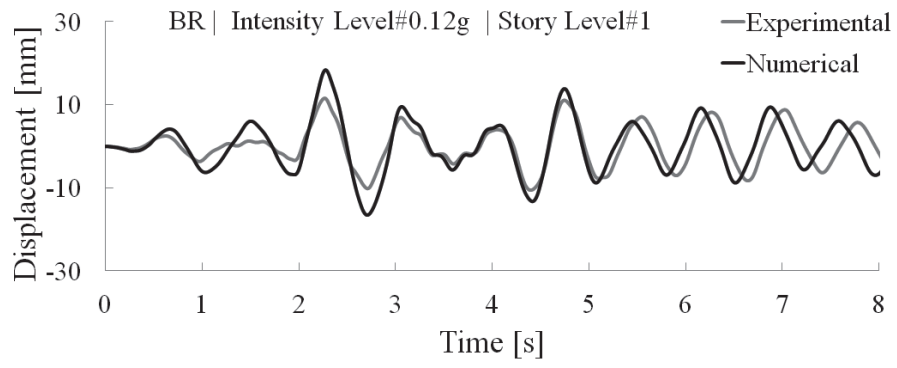


Figure C.6 Experimental/Numerical time history displacement at different story levels for the bare (BR) structure tested at PGA=0.12g by using fiber hinges

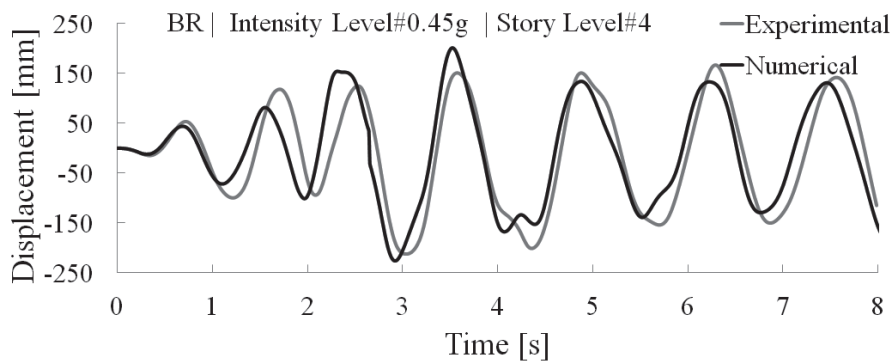
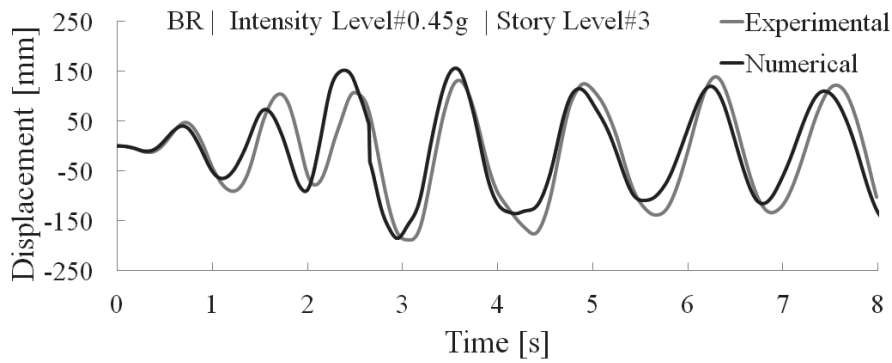
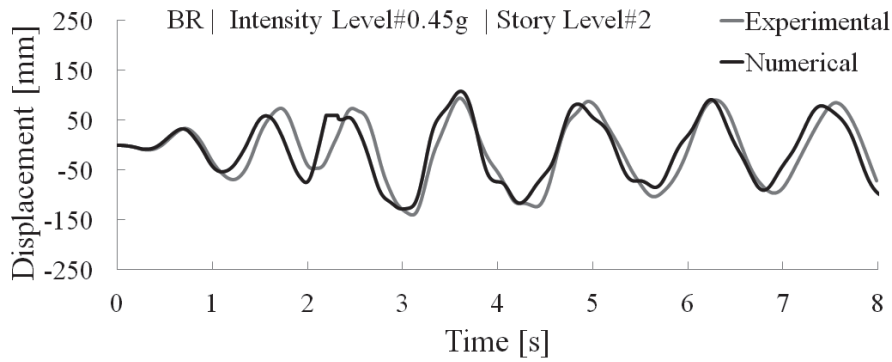
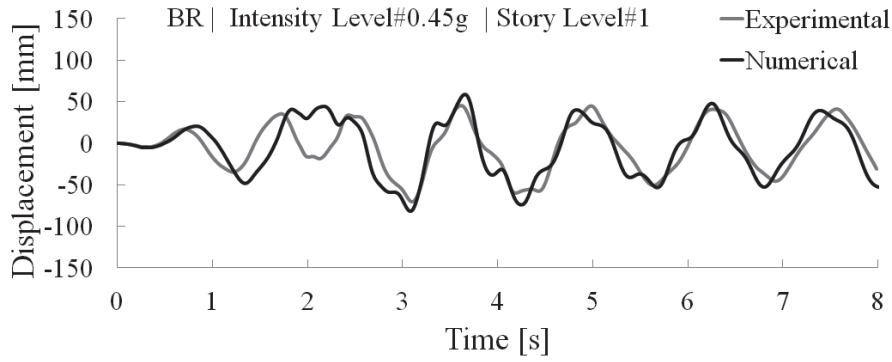


Figure C.7 Experimental/Numerical time history displacement at different story levels for the bare (BR) structure tested at PGA=0.45g by using fiber hinges

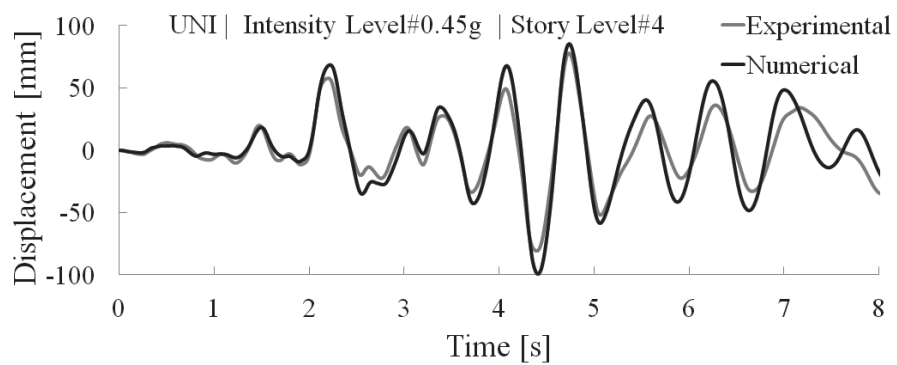
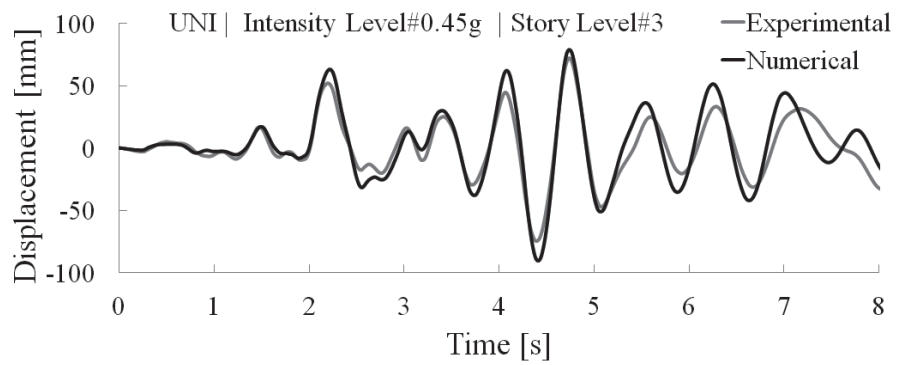
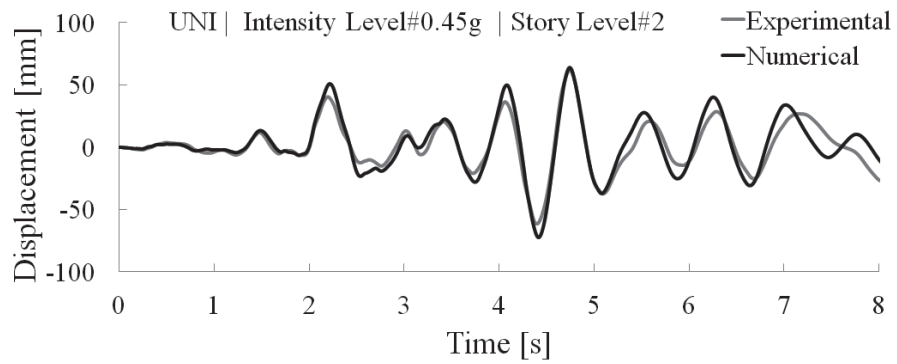
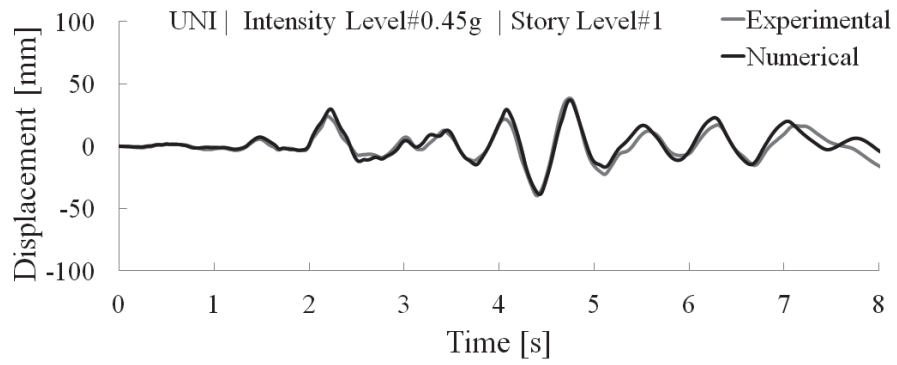


Figure C.8 Experimental/Numerical time history displacement at different story levels for the uniformly infilled (UNI) structure tested at $PGA=0.45g$ by using fiber hinges

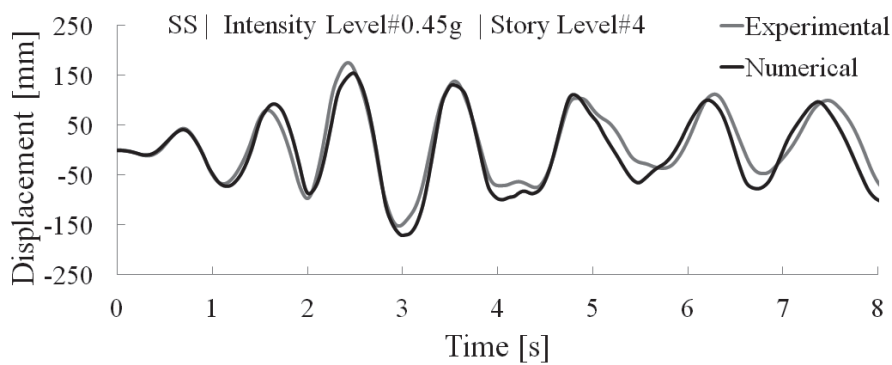
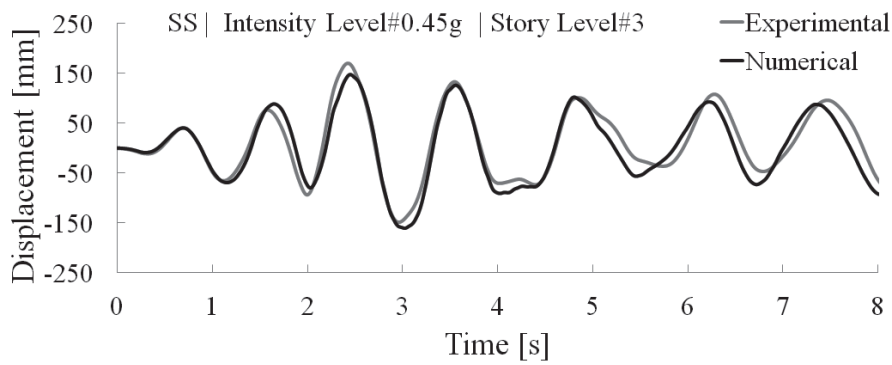
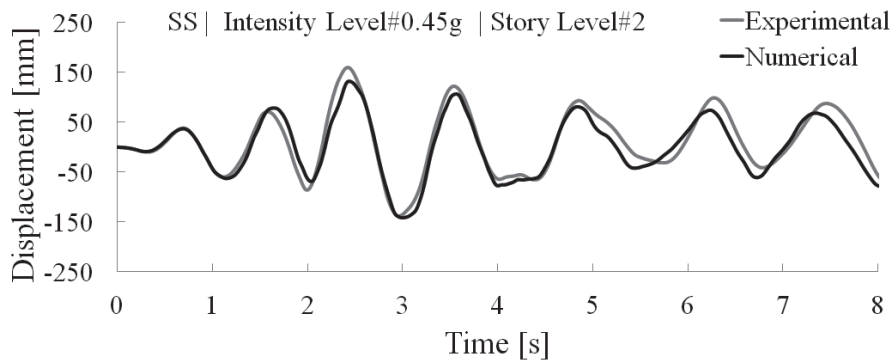
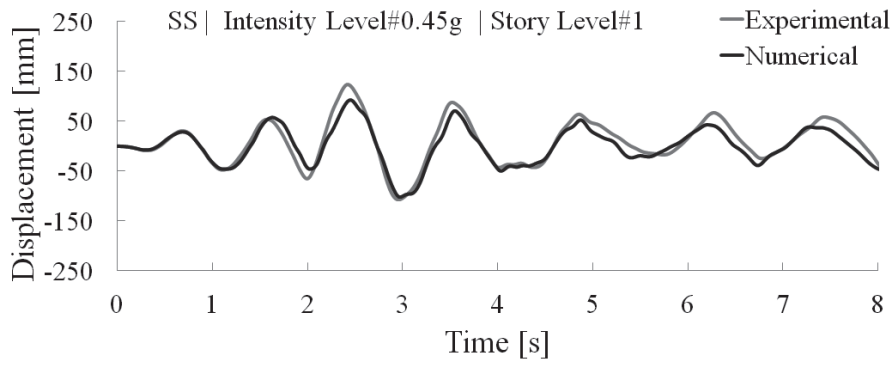


Figure C.9 Experimental/Numerical time history displacement at different story levels for the soft story (SS) structure tested at PGA=0.45g by using fiber hinges

Appendix D: Verification of the Results

D.1 Developed Macromodel Parameters

Table D.1 Stress–strain parameters for pinching material model

Spec.ID	f_{tp} [MPa]	V_d [N]	f_{mc} [MPa]	f_{my} [MPa]	f_{mo} [MPa]	f_{mu} [MPa]	ϵ_{mc} [%]	ϵ_{my} [%]	ϵ_{mo} [%]	ϵ_{mu} [%]
1b	1.27	236536.3	6.35	9.52	12.69	7.62	0.08	0.24	0.32	1.62
2b	1.19	222138.4	5.97	8.96	11.95	7.17	0.07	0.22	0.30	1.19
3b	1.10	205683.7	5.30	7.95	10.59	6.36	0.10	0.31	0.41	2.03
4b	1.15	415610.0	6.45	9.68	12.91	7.74	0.05	0.16	0.21	1.04
5b	1.11	623669.4	6.47	9.70	12.93	7.76	0.06	0.17	0.22	1.11
6b	0.51	195589.7	2.40	3.60	4.79	2.88	0.11	0.34	0.45	2.24
TA3,1,2	0.29	522610.7	1.44	2.16	2.88	1.3	0.027	0.082	0.109	0.871
Inf_02	0.28	201118.2	1.15	1.73	2.3	0.69	0.07	0.209	0.279	1.4
Inf_04	0.22	158021.4	0.9	1.36	1.81	0.54	0.055	0.164	0.219	1.1

Table D.2 Dynamic and geometric parameters of the developed model

Spec.ID	γ [kN/m ³]	mass [kN.sec ² /m]	f_{oOp_FEM} [Hz]	α_{crk} [-]	W_{st} [mm]	t_{URM} [mm]	W_{mod} [mm]	t_{mod} [mm]
1b	15	0.317	24	1	392	47.6	35.5	524.3
2b	15	0.317	24.2	0.55	391	47.6	47.9	387.9
3b	15	0.317	19.5	0.55	408	47.6	51.1	380.0
4b	15	0.612	58.2	0.55	350	92.0	40.6	792.6
5b	15	0.951	87.5	0.55	338	143	38.4	1255.8
6b	15	0.654	25	0.55	415	98.4	54.1	754.5
TA3,1,2	8.8	3.2	65	0.45	518	350	62.3	2906.1
Inf_02	6.8	0.81	24.3	1	582	150	4.6	1900.5
Inf_04	6.8	0.81	24.3	1	582	150	4.6	1900.5

D.2 Experimental specimens

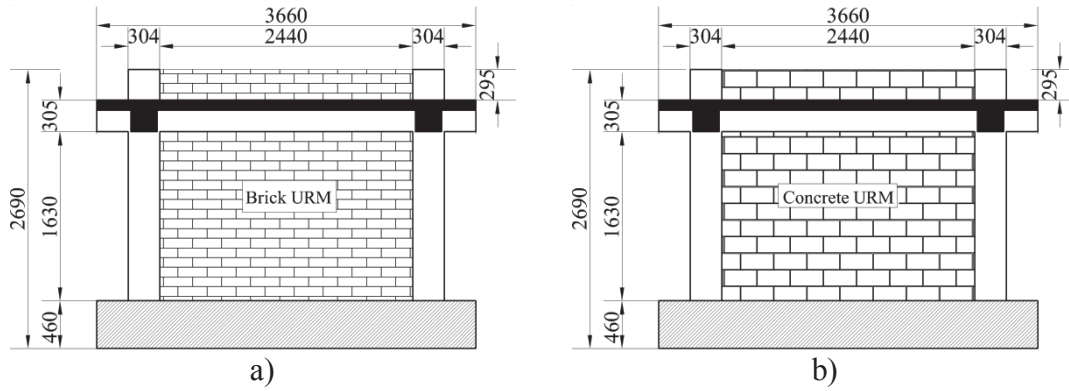


Figure D.1 Infilled frame specimens tested by *Angel (1994)*: a) brick masonry infill, b) concrete unit masonry infill

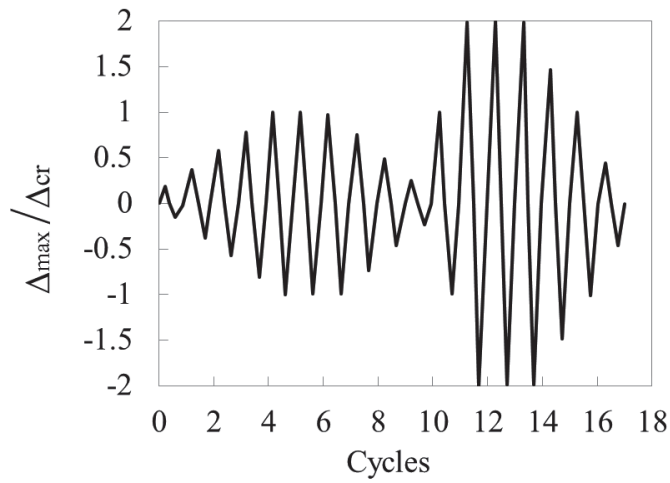


Figure D.2 IP cyclic load protocol according to *Angel (1994)*

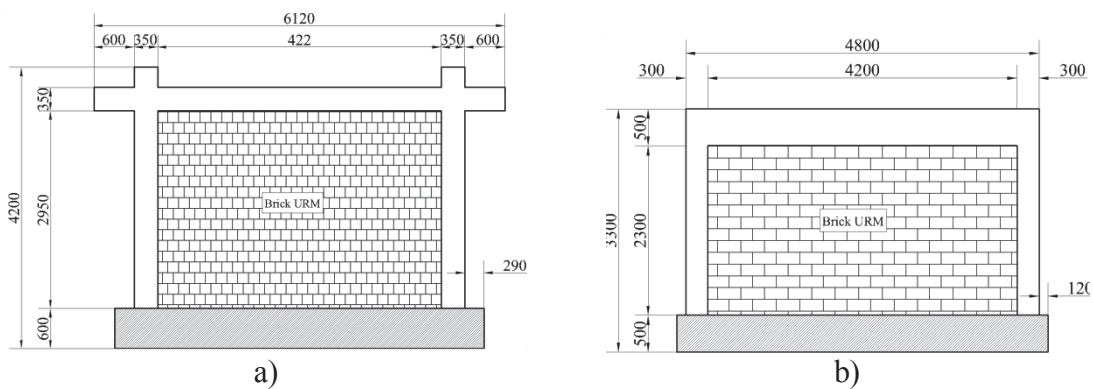


Figure D.3 Infilled frame specimens tested by: a) *Hak et al. (2014)*, b) *Furtado et al. (2016)*

D.3 In-Plane Simulation Results

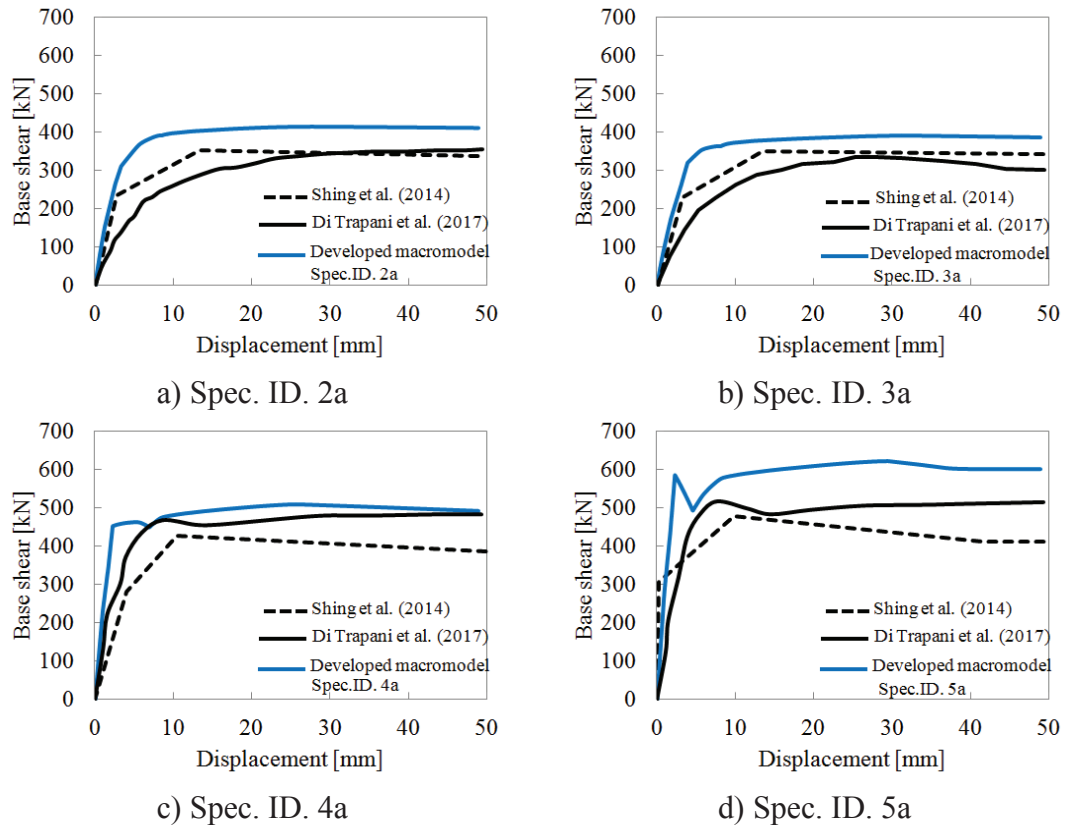
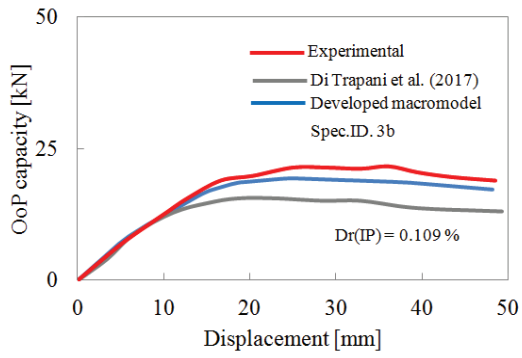
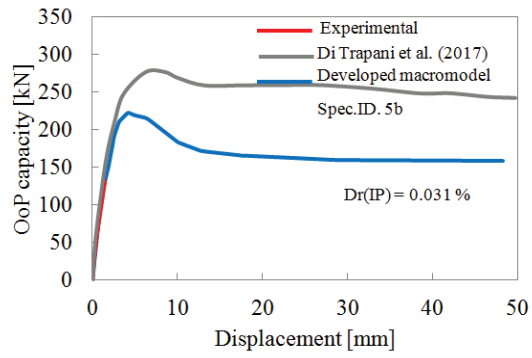


Figure D.4 Developed and *Di Trapani et al. (2017)* macromodels in-plane response comparison of specimens tested by *Angel (1994)*

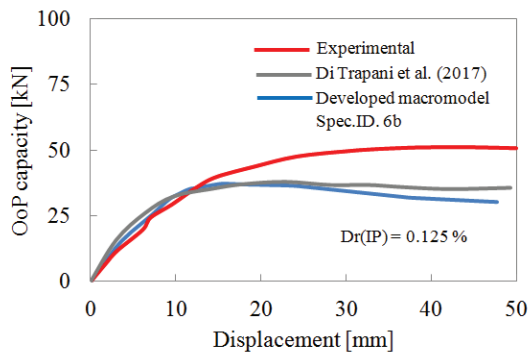
D.4 Out-of-Plane Simulation Results



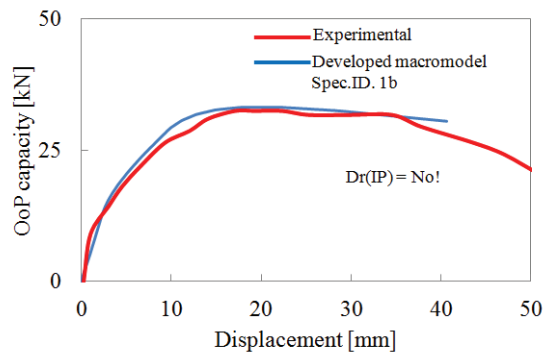
a) Spec. ID. 3b



b) Spec. ID. 5b



c) Spec. ID. 6b

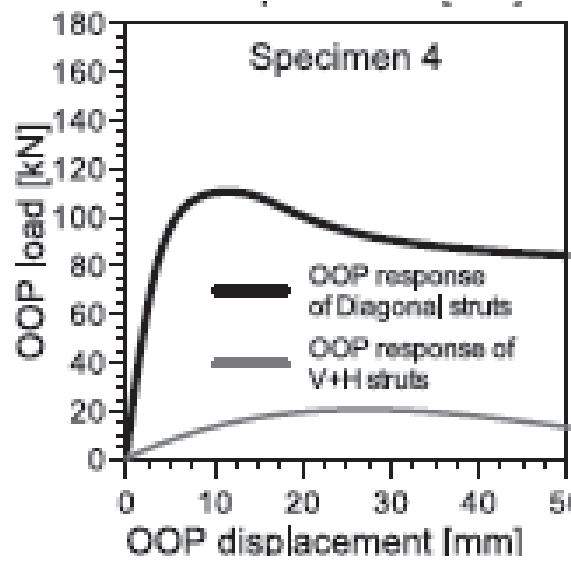


d) Spec. ID. 1b

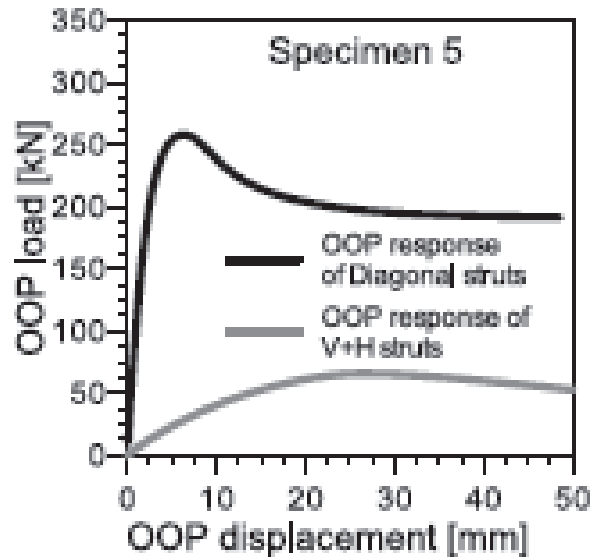
Figure D.5 Comparison of OoP experimental test results from *Angel (1994)* with numerical results applying developed and *Di Trapani et al. (2017)* macromodels

Note:

Dr(IP): Refer to the applied in-plane drift ratio before the out-of-plane test

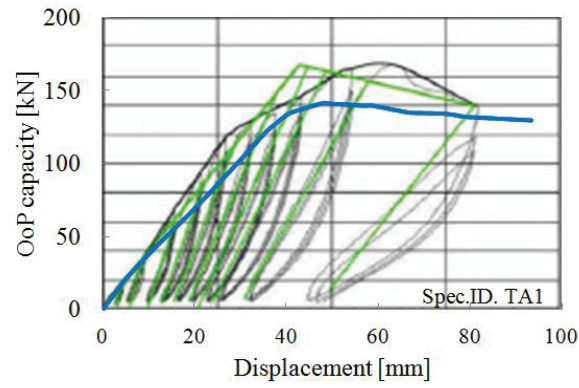


a) Spec. ID. 4b

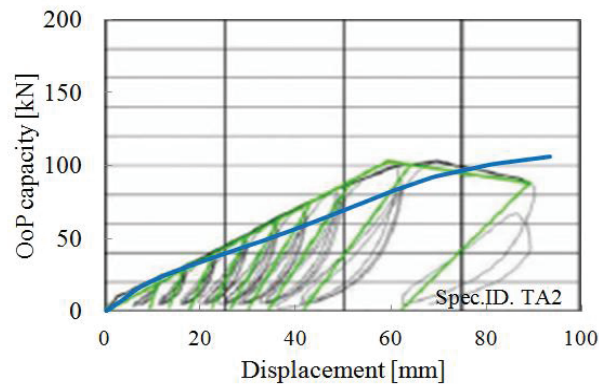


b) Spec. ID. 5b

Figure D.6 *Di Trapani et al. (2017)* macromodels out-of-plane response of specimens 4 and 5 tested by *Angel (1994)*

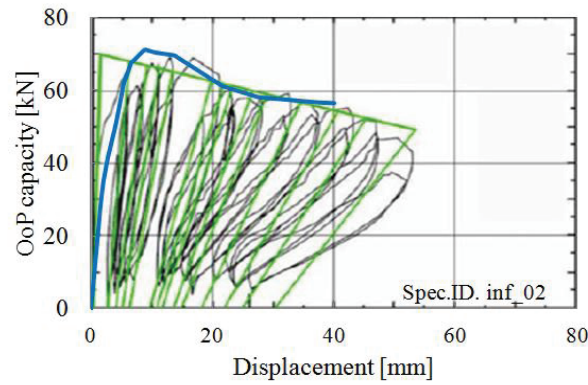


a) Spec. ID. TA1



b) Spec. ID. TA2

Figure D.7 Developed and *Mazza (2018)* macromodels out-of-plane response comparison of specimens tested by *Hak et al. (2014)*



Spec. ID. Inf_02

Figure D.8 Developed and *Mazza (2018)* macromodels out-of-plane response comparison of specimens tested by *Furtado et al. (2016)*

- Experimental
- Mazza (2018) macromodel
- M#5_dev macromodel

Appendix E: Secondary Elements Macromodels Assessment

E.1 Dynamic Simulation Results Utilizing Reference Object (ELSA)

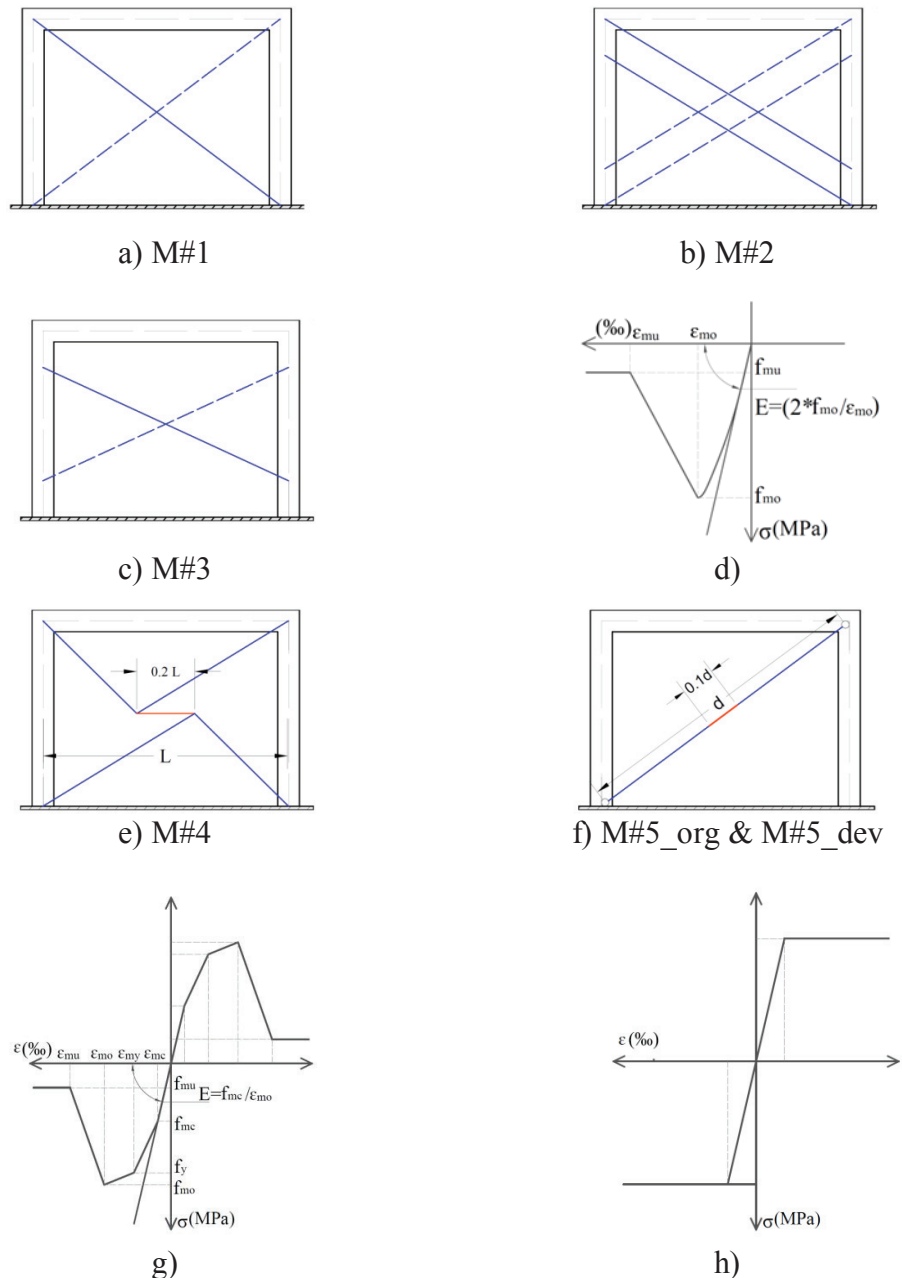


Figure E.1 Considered macromodels in case of reference object (ELSA): a), b) and c) strut models with different configuration, d) used material model in case of strut, e) shear link model, f) diagonal beam-column model, g) material model in case of shear link model and M#5_dev, h) elastic perfectly plastic material model in case of M#5_org

Table E.1 Geometric and material properties of the infill walls

Story	L_{URM} [m]	H_{URM} [m]	t_{URM} [mm]	E_c [GPa]	E_{URM} [GPa]	θ [deg]	W_{st} [mm]
1*	5.6	3.05	112	31.5	3.68	28.6	756
2,3,4*	5.6	2.55	112	31.5	3.68	24.5	778
1**	3.6	3.05	112	31.5	3.68	40.3	551
2,3,4**	3.6	2.55	112	31.5	3.68	35.3	547

*: Long span, **:Short span

Table E.2 Stress-strain parameters for the diagonal strut models (M#1, 2, 3)

Story	f_{ip} [MPa]	V_d [N]	f_{mo} [MPa]	f_{mu} [MPa]	ϵ_{mo} [%]	ϵ_{mu} [%]
1*	0.28	200022.1	2.36	0.47	0.103	0.517
2,3,4*	0.28	192992.8	2.21	0.44	0.097	0.485
1**	0.28	148027.6	2.40	0.48	0.105	0.525
2,3,4**	0.28	138329.6	2.26	0.45	0.099	0.495

*: Long span, **:Short span

Table E.3 Stress-strain parameters for the shear link model (M#4)

Story	f_{ip} [Mpa]	V_{URM} [N]	f_{mc} [Mpa]	f_{my} [Mpa]	f_{mo} [Mpa]	f_{mu} [Mpa]	ϵ_{mc} [%]	ϵ_{my} [%]	ϵ_{mo} [%]	ϵ_{mu} [%]
1*	0.28	175616.0	1.04	1.56	2.07	0.62	0.028	0.085	0.113	0.564
2,3,4*	0.28	175616.0	1.01	1.51	2.02	0.60	0.027	0.082	0.110	0.548
1**	0.28	112896.0	0.91	1.37	1.83	0.55	0.025	0.075	0.099	0.497
2,3,4**	0.28	112896.0	0.92	1.38	1.84	0.55	0.025	0.075	0.100	0.501

*: Long span, **:Short span

Table E.4 Stress-Strain parameters for the diagonal beam-column model (M#5_dev)

Story	f_{ip} [Mpa]	V_d [N]	f_{mc} [Mpa]	f_{my} [Mpa]	f_{mo} [Mpa]	f_{mu} [Mpa]	ϵ_{mc} [%]	ϵ_{my} [%]	ϵ_{mo} [%]	ϵ_{mu} [%]
1*	0.28	200022.1	1.18	1.77	2.36	0.71	0.032	0.096	0.128	0.642
2,3,4*	0.28	192992.8	1.11	1.66	2.21	0.66	0.030	0.090	0.120	0.602
1**	0.28	148027.6	1.20	1.80	2.40	0.72	0.033	0.098	0.130	0.652
2,3,4**	0.28	138329.6	1.13	1.69	2.26	0.68	0.031	0.092	0.123	0.614

*: Long span, **:Short span

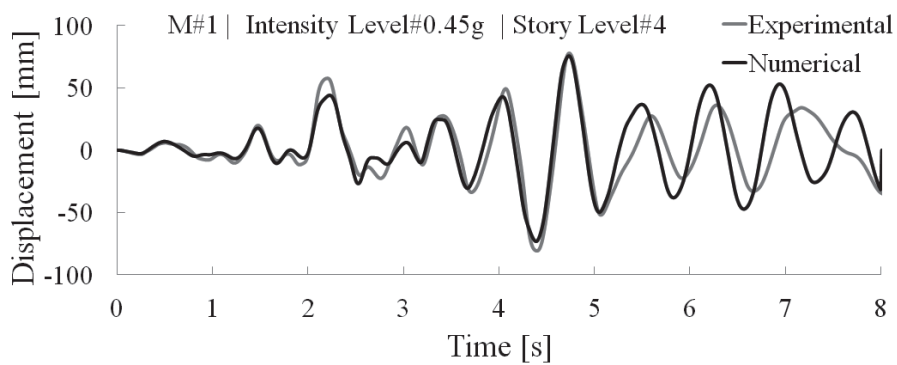
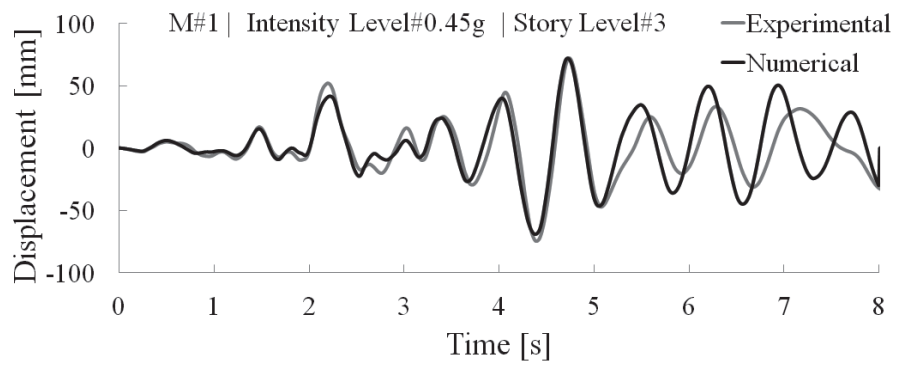
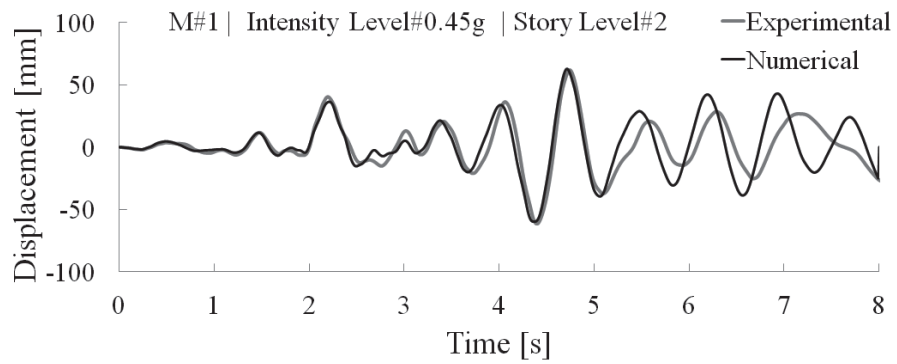
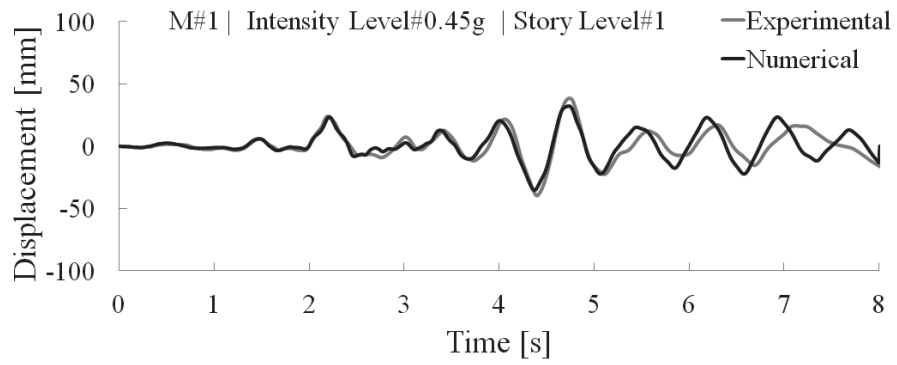


Figure E.2 Experimental/numerical time history displacement at different story levels for the uniformly infilled (UNI) structure tested at PGA=0.45g

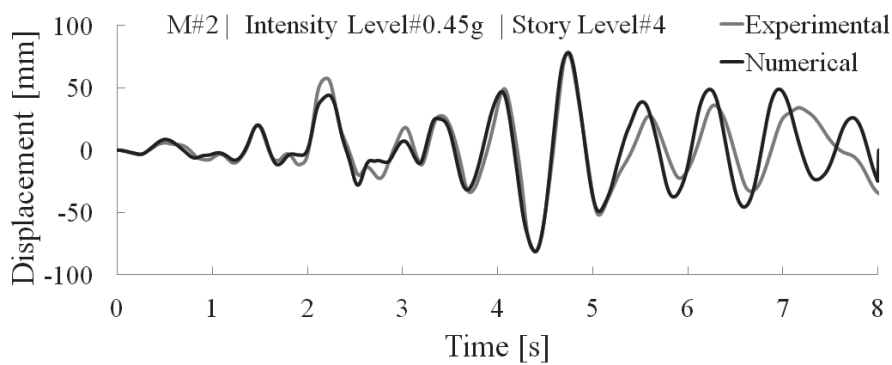
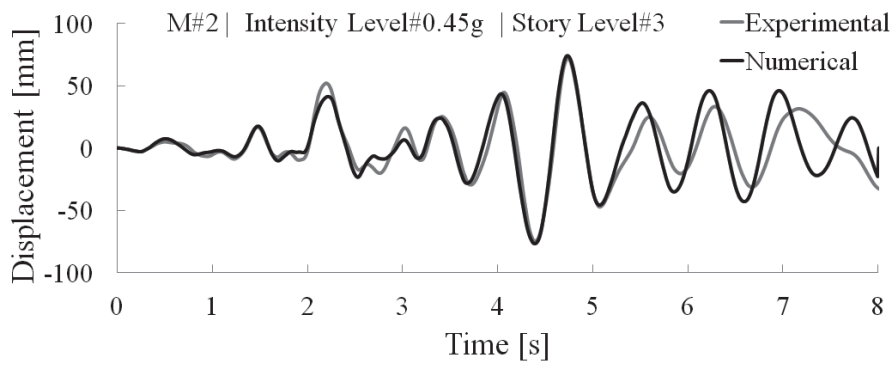
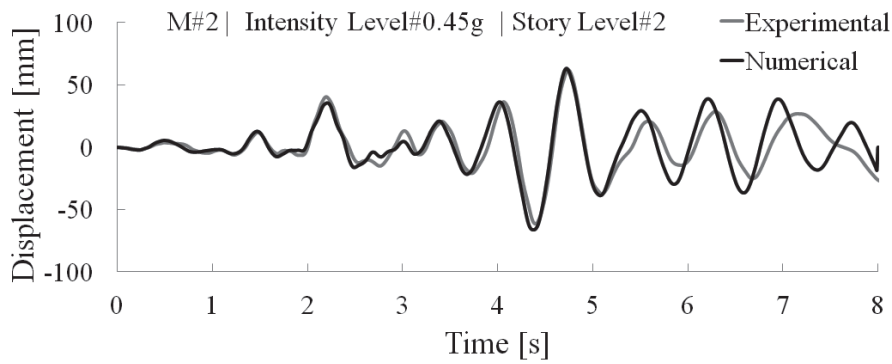
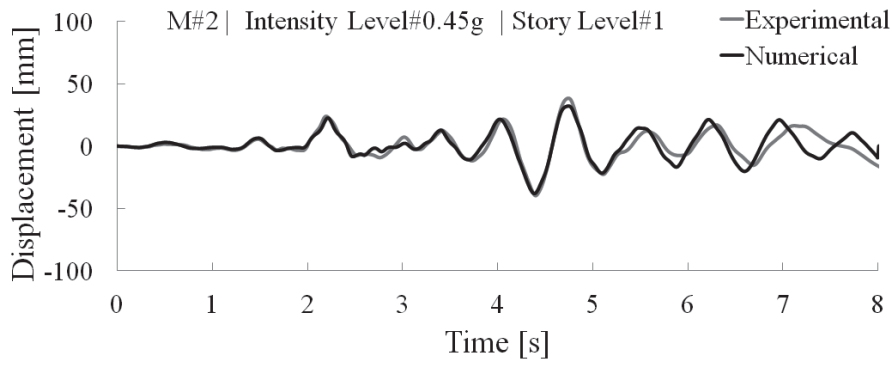


Figure E.3 Experimental/numerical time history displacement at different story levels for the uniformly infilled (UNI) structure tested at PGA=0.45g

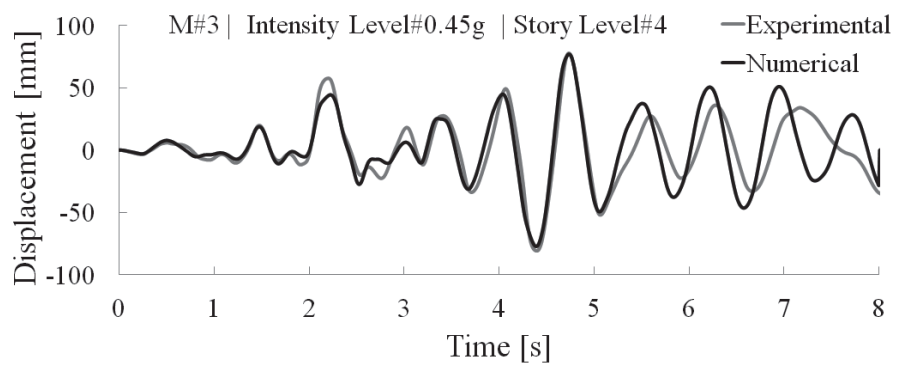
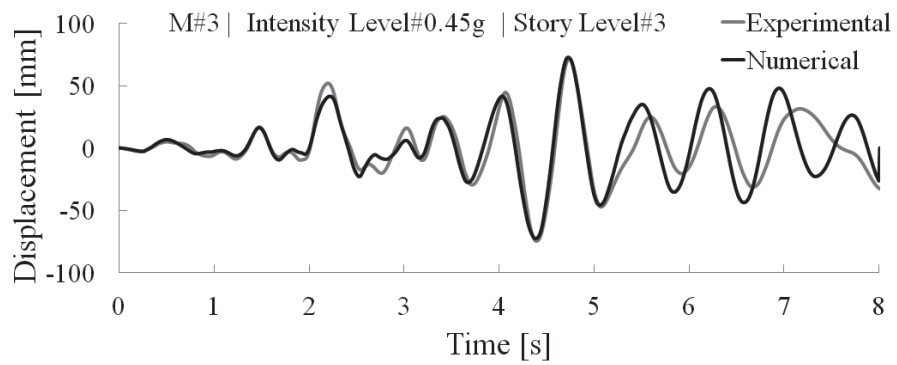
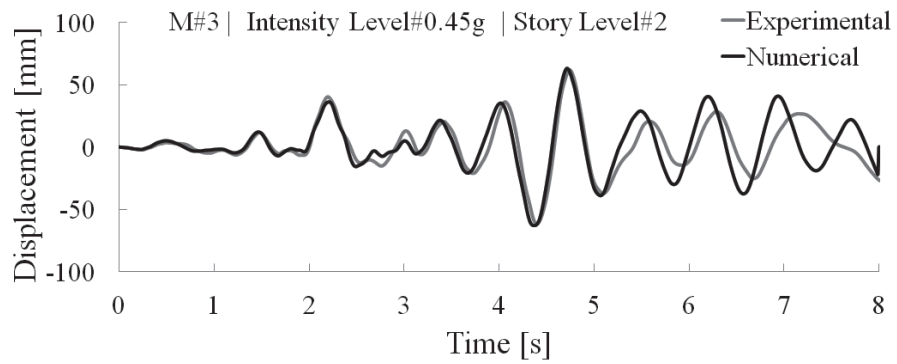
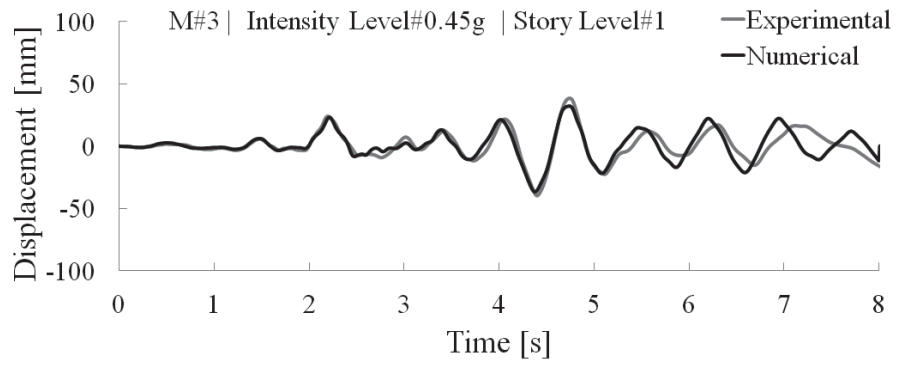


Figure E.4 Experimental/Numerical time history displacement at different story levels for the uniformly infilled (UNI) structure tested at PGA=0.45g

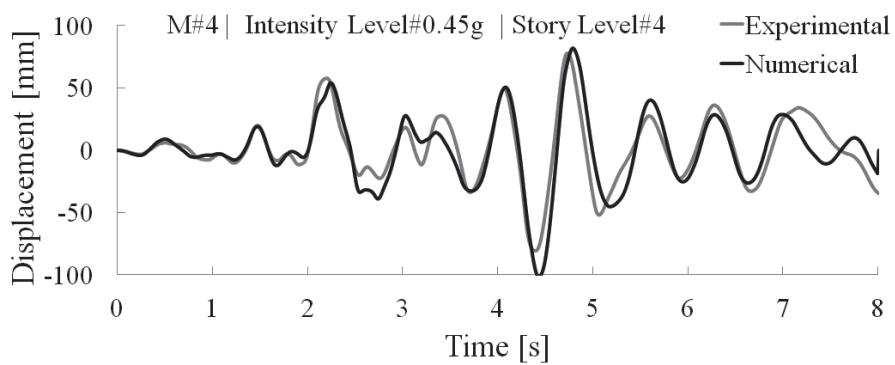
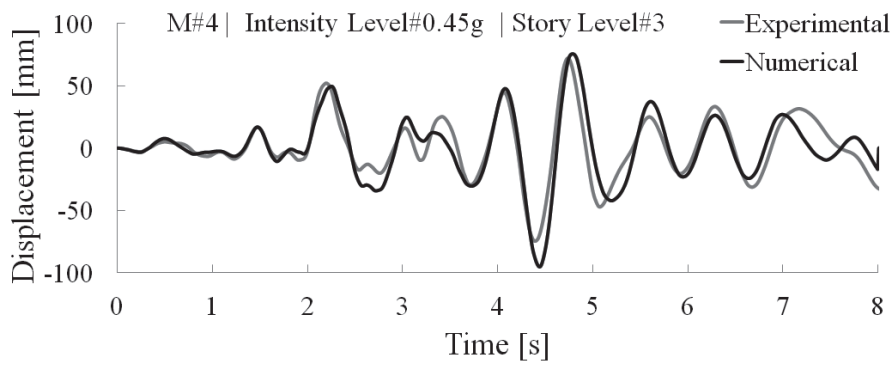
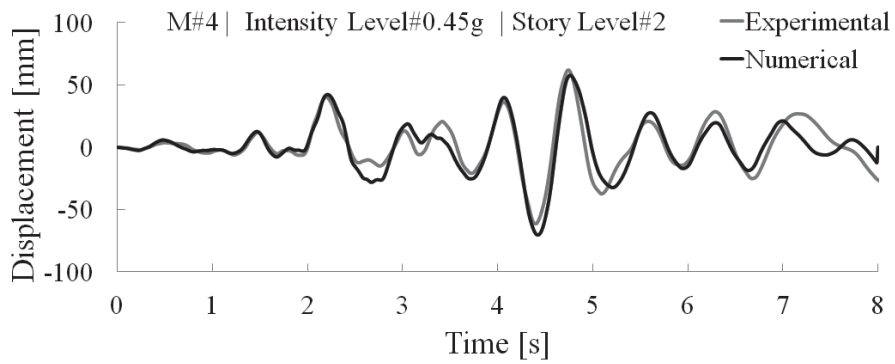
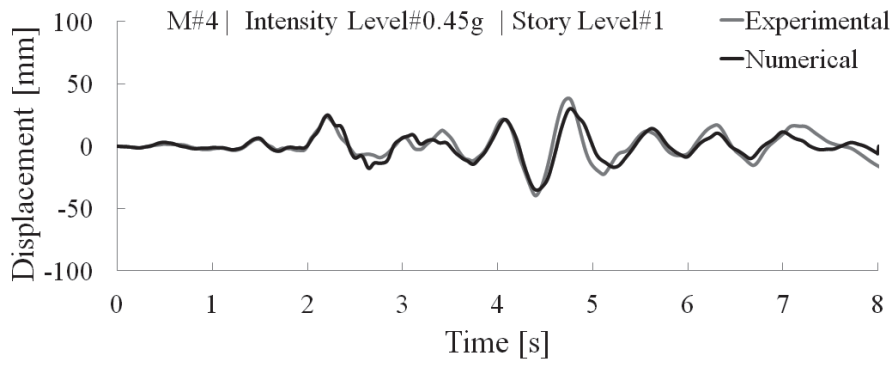
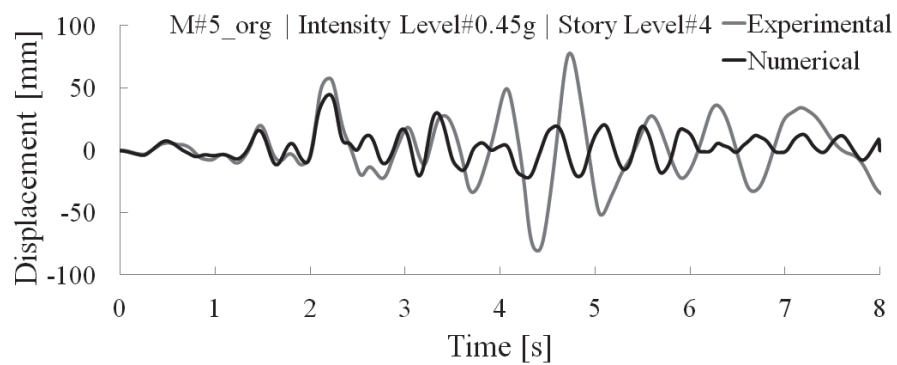
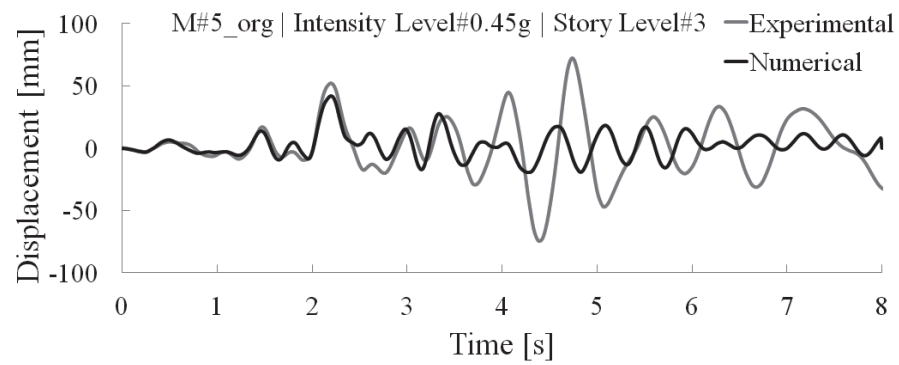
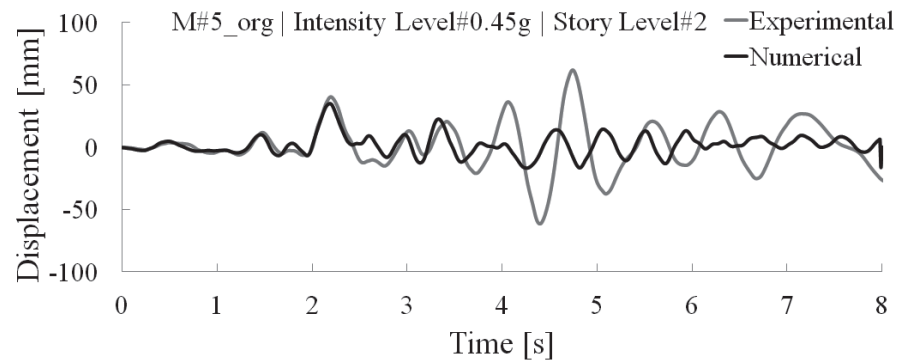
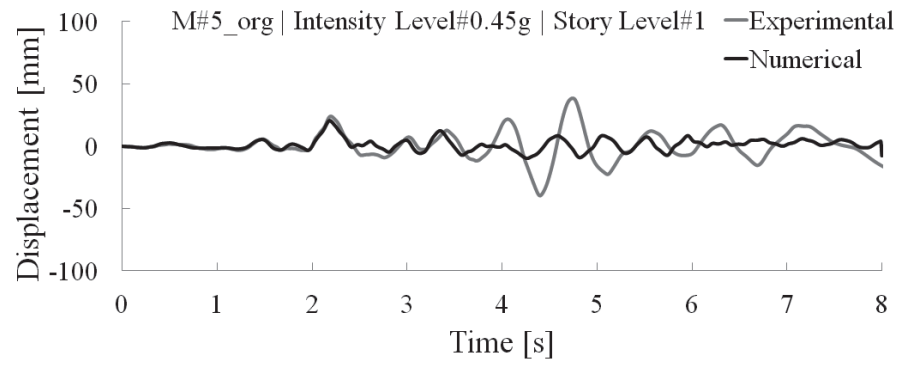


Figure E.5 Experimental/numerical time history displacement at different story levels for the uniformly infilled (UNI) structure tested at PGA=0.45g



c

Figure E.6 Experimental/numerical time history displacement at different story levels for the uniformly infilled (UNI) structure tested at PGA=0.45g

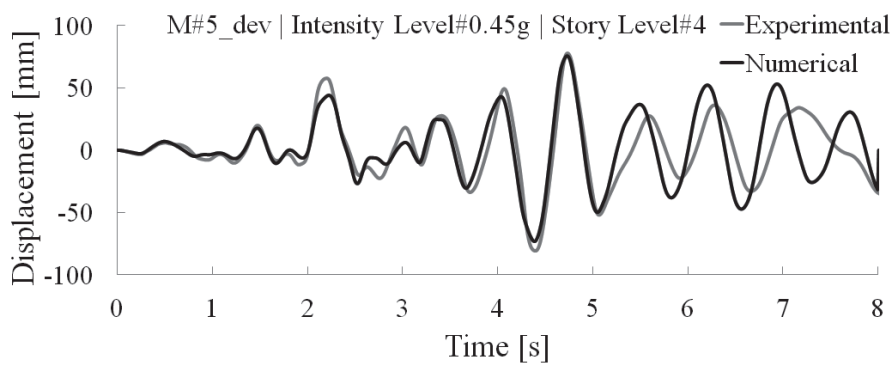
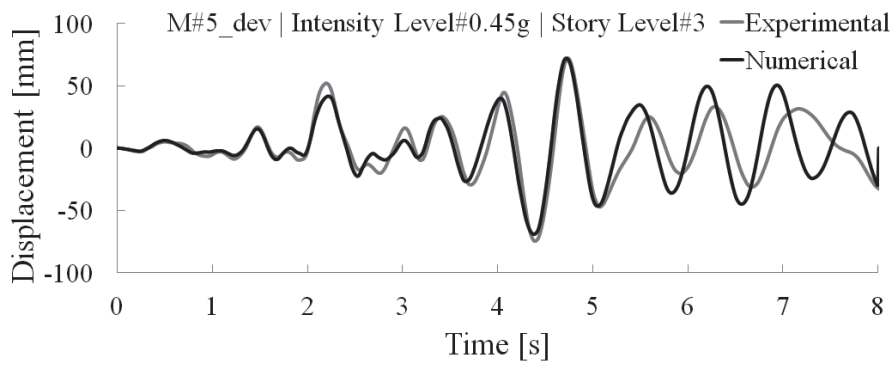
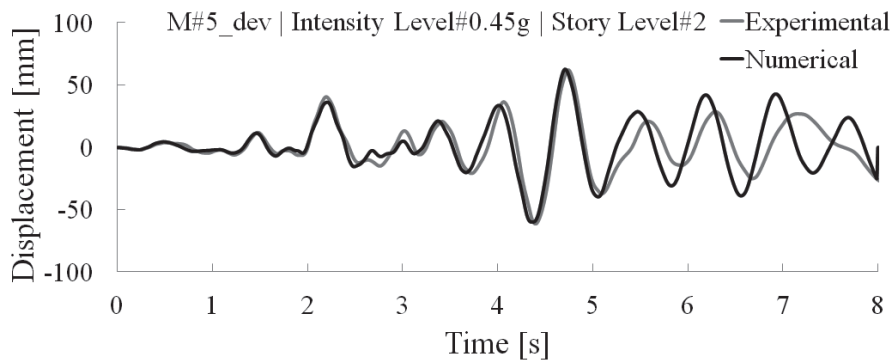
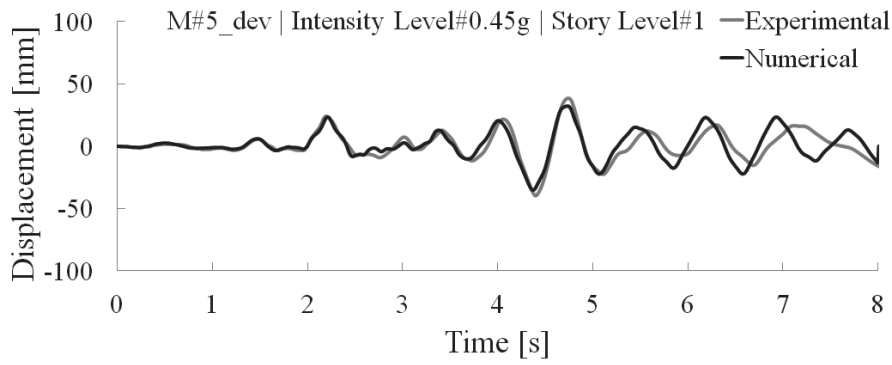


Figure E.7 Experimental/numerical time history displacement at different story levels for the uniformly infilled (UNI) structure tested at $PGA=0.45g$

E.2 Dynamic Simulation Results Utilizing Reference Object (FRAMA)

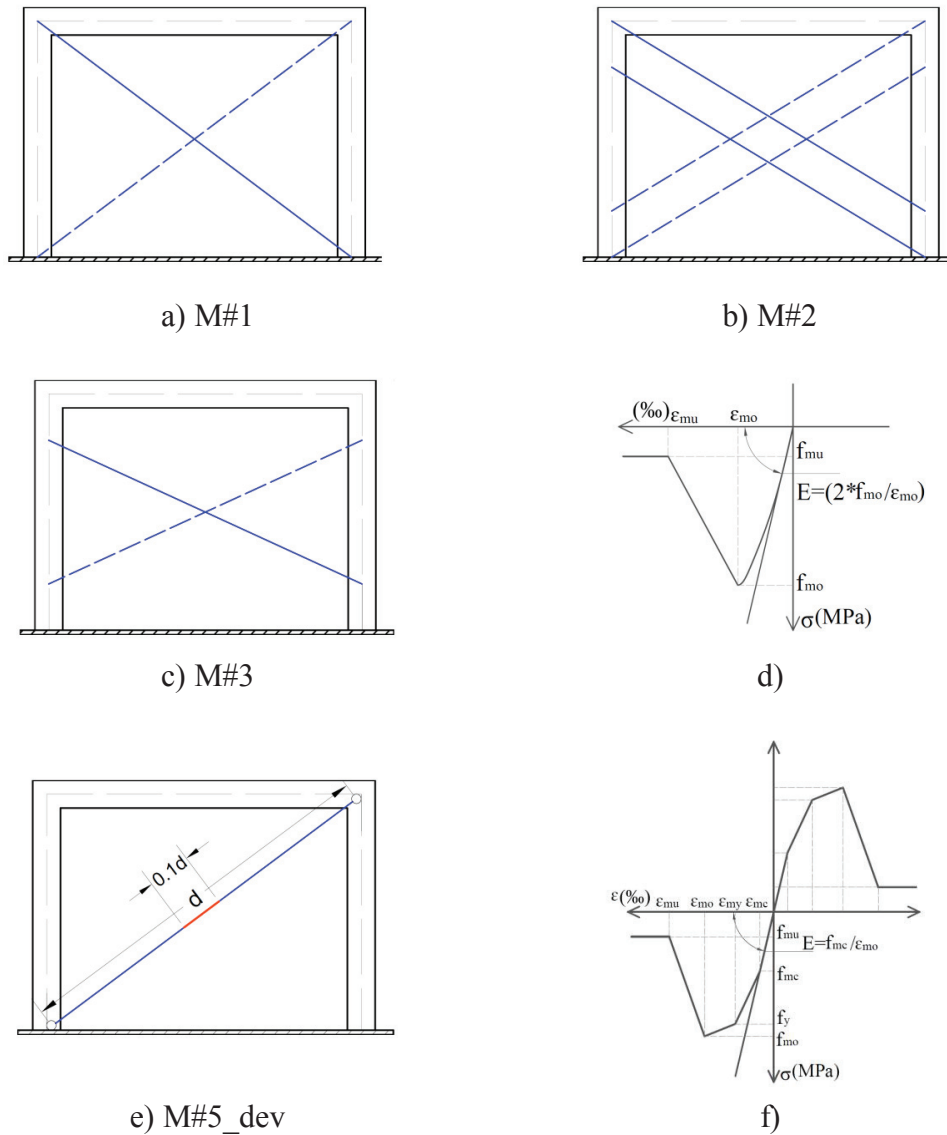


Figure E.8 Considered macromodels in case of reference object (FRAMA): a), b) and c) strut models with different configuration, d) used material model in case of strut models, e) developed diagonal beam-column model (M#5_dev), f) material model in case of and M#5_dev

Table E.5 Geometric and material properties of the infill walls

Section	Story	L_{URM} [m]	H_{URM} [m]	t_{URM} [mm]	E_c [GPa]	E_{URM} [GPa]	θ [deg]	W_{st} [mm]
1--2	1	1.12	1.12	120	38.839	2.025	45.0	164
1--2	2,3	1.12	1.04	120	38.839	2.025	47.0	164
2--3	1	2.32	1.12	120	38.839	2.025	25.8	83
2--3	2,3	2.32	1.04	120	38.839	2.025	27.3	105
A--B	1	2.08	1.12	120	38.839	2.025	28.3	67
A--B	2,3	2.08	1.04	120	38.839	2.025	30.0	88

Table E.6 Stress-strain parameters for the diagonal strut models (M#1, 2, 3)

Section	Story	f_{tp} [Mpa]	V_d [N]	f_{mo} [MPa]	f_{mu} [MPa]	ϵ_{mo} [%]	ϵ_{mu} [%]
1--2	1	0.12	22808.4	1.16	0.23	0.115	0.573
1--2	2,3	0.12	23637.1	1.20	0.24	0.119	0.593
2--3	1	0.12	37097.3	3.72	0.74	0.368	1.840
2--3	2,3	0.12	37612.4	2.99	0.60	0.295	1.475
A--B	1	0.12	34018.2	4.23	0.85	0.418	2.090
A--B	2,3	0.12	34579.2	3.27	0.65	0.324	1.618

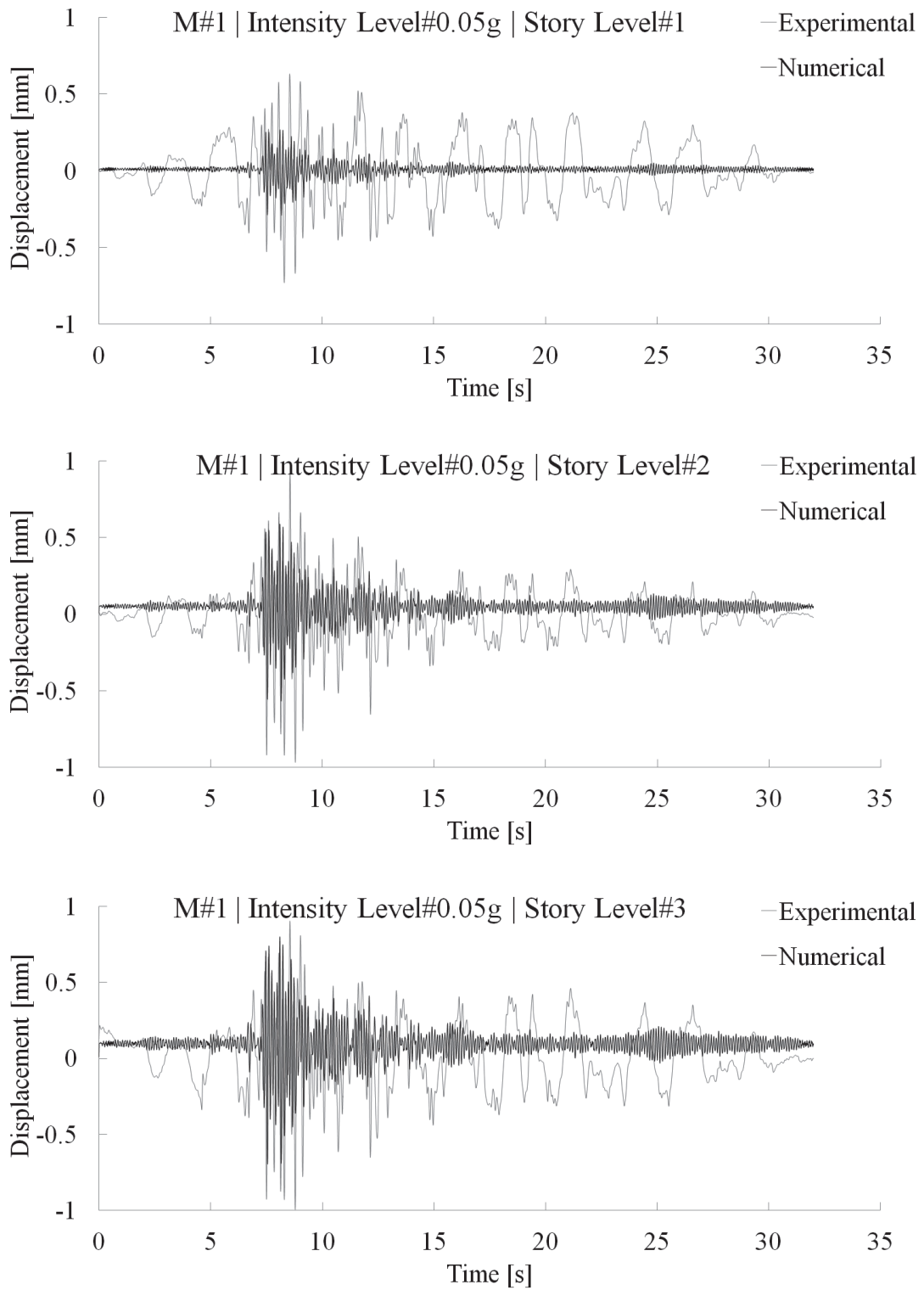


Figure E.9 Experimental/numerical (M#1) time history displacement at different story levels for the structure tested at PGA=0.05g

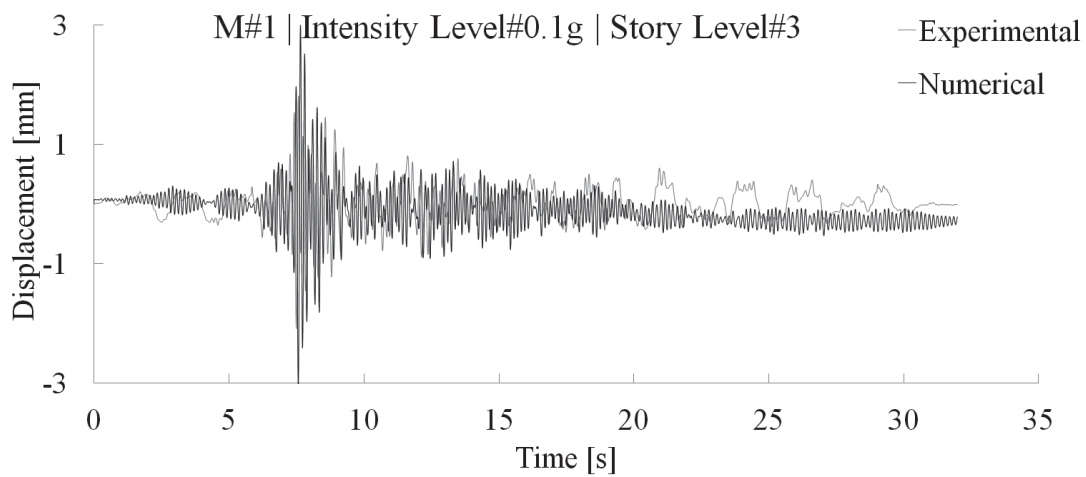
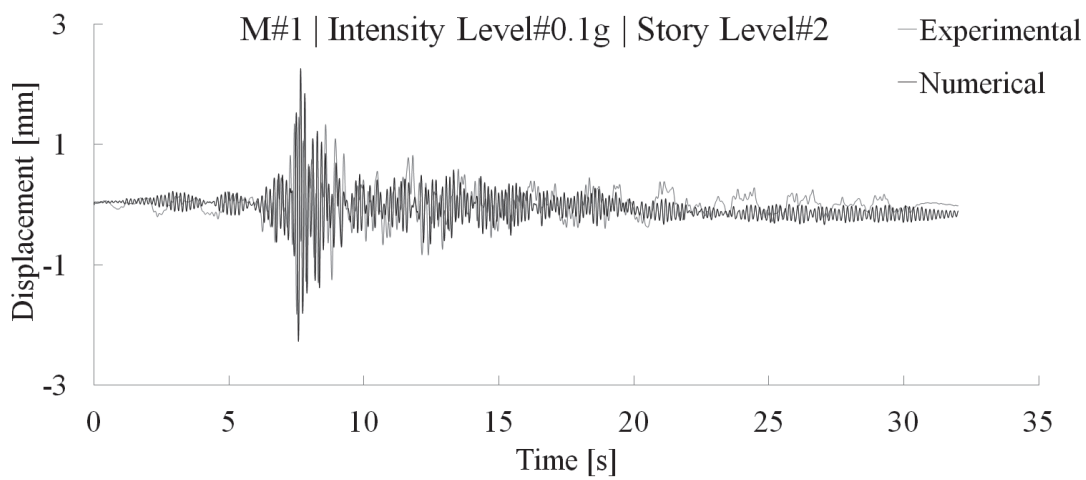
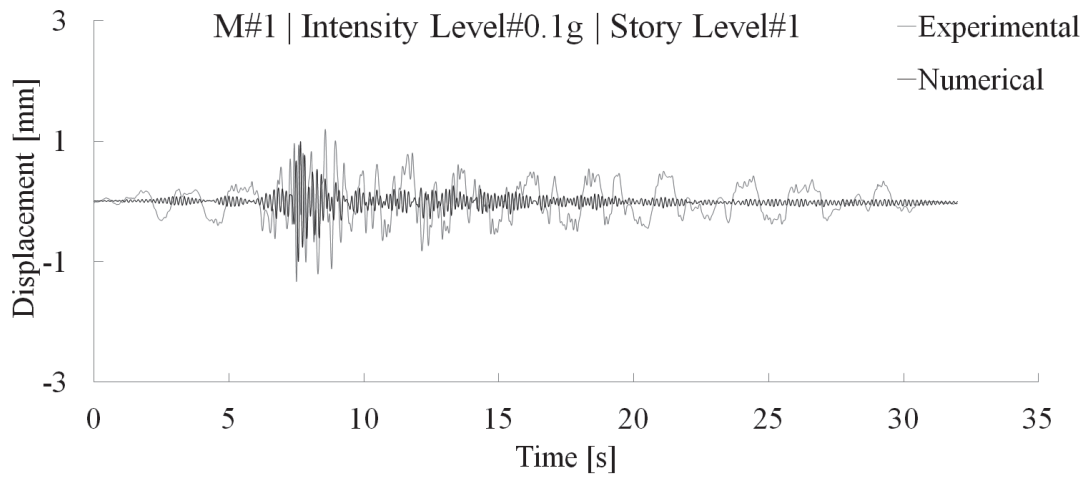


Figure E.10 Experimental/numerical (M#1) time history displacement at different story levels for the structure tested at PGA=0.1g

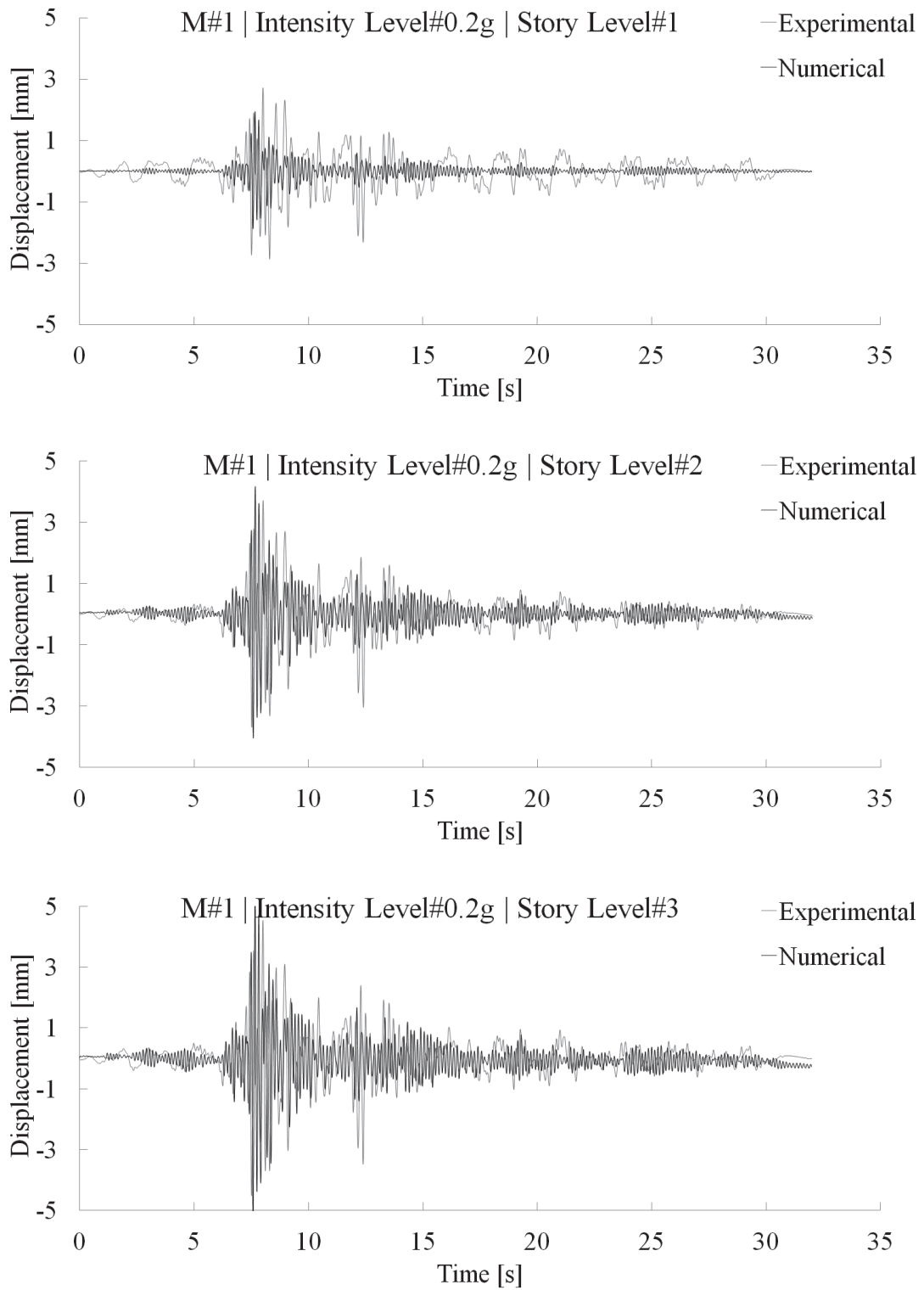


Figure E.11 Experimental/numerical (M#1) time history displacement at different story levels for the structure tested at PGA=0.2g

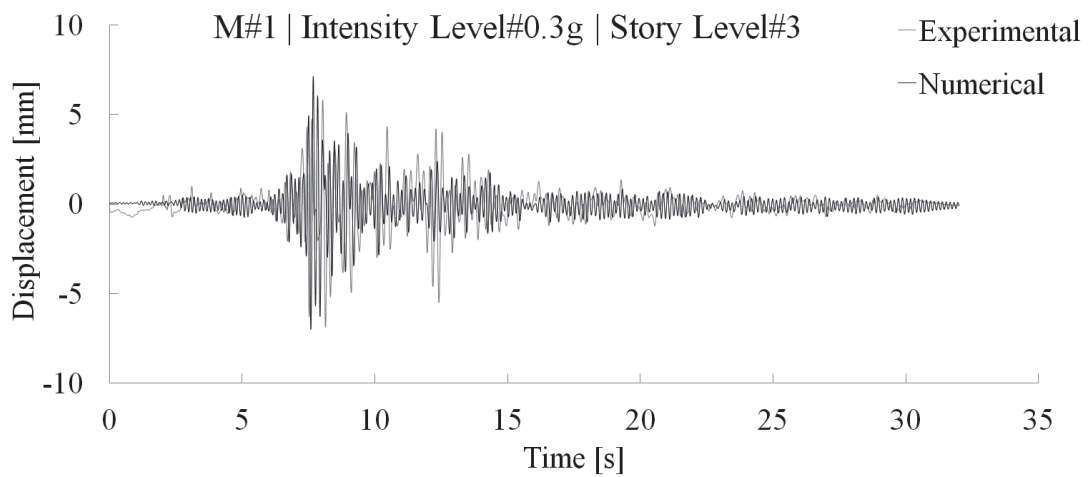
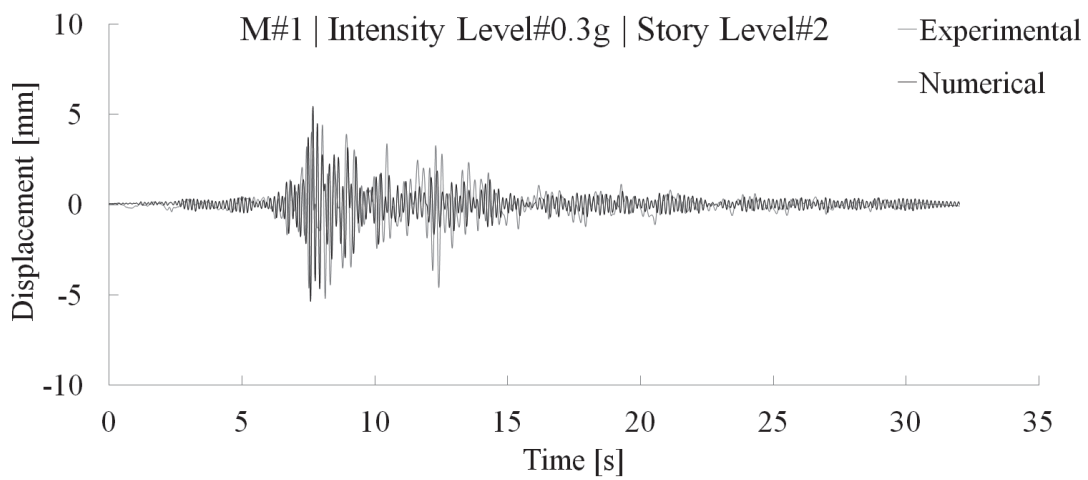
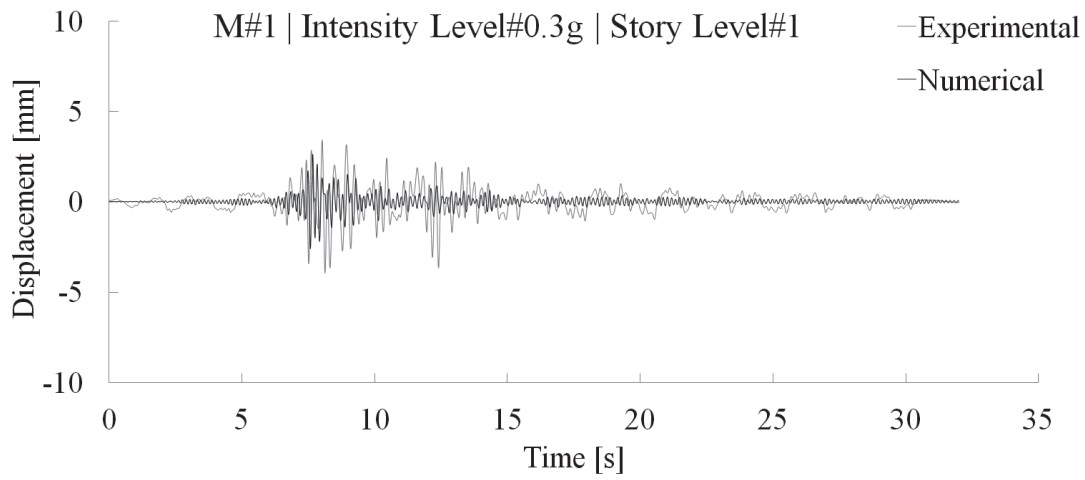


Figure E.12 Experimental/numerical (M#1) time history displacement at different story levels for the structure tested at PGA=0.3g

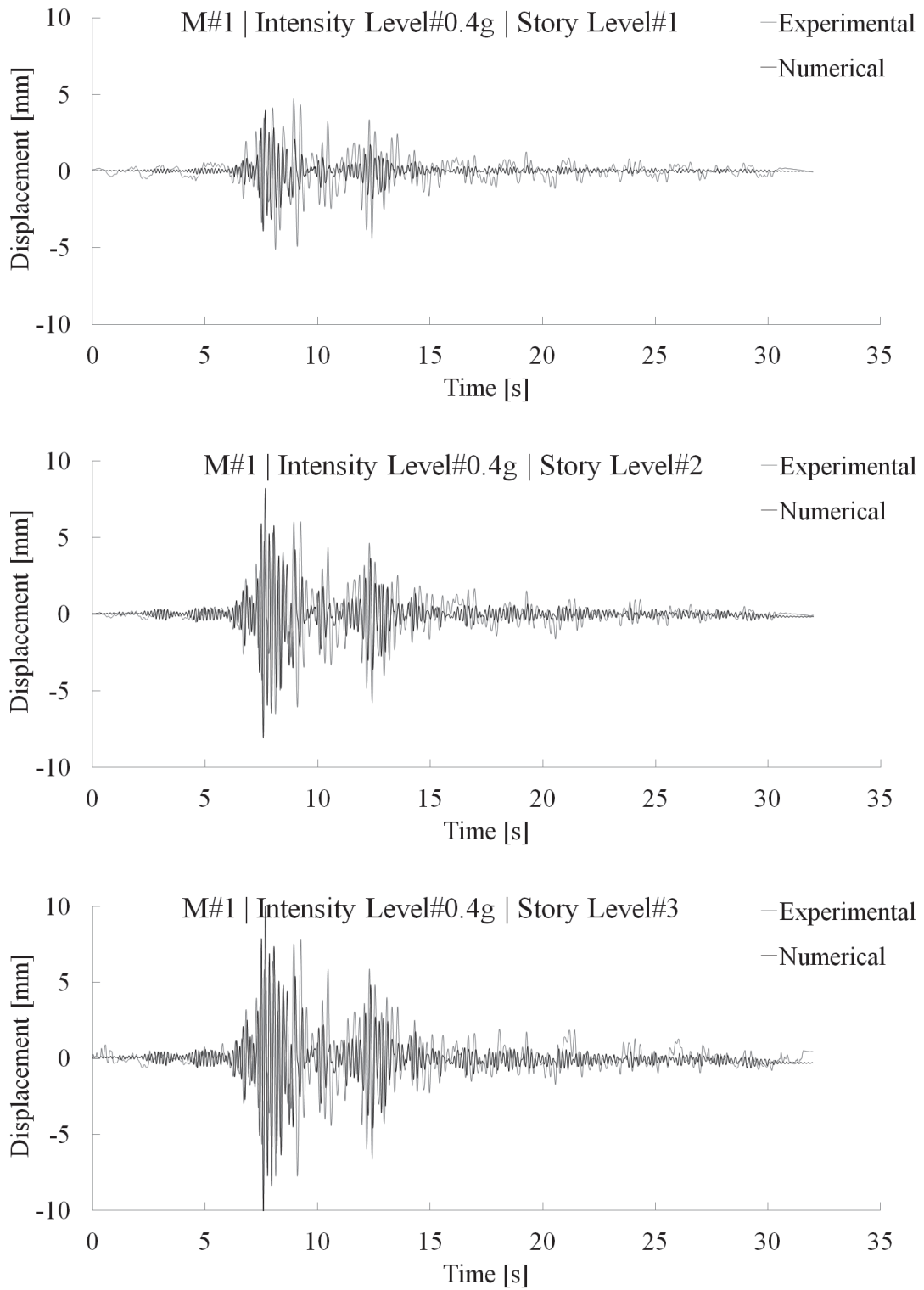


Figure E.13 Experimental/numerical (M#1) time history displacement at different story levels for the structure tested at PGA=0.4g

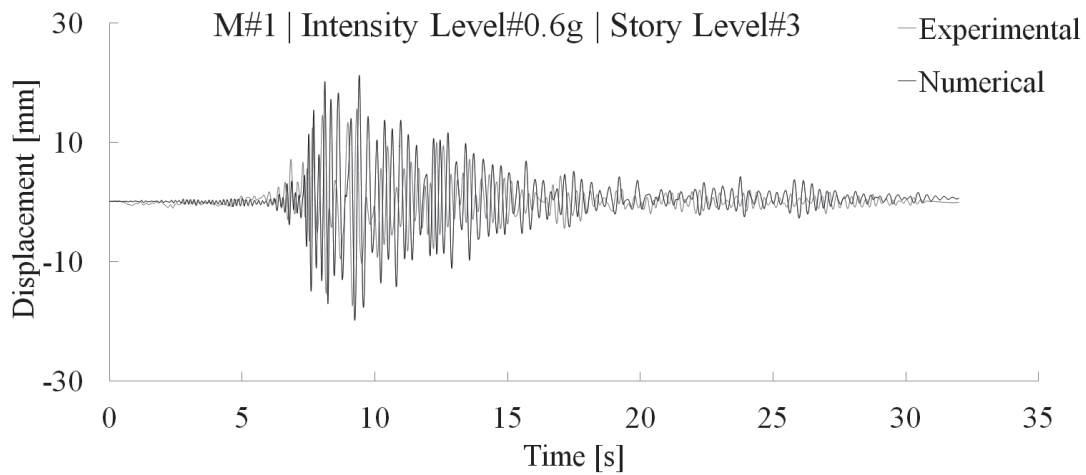
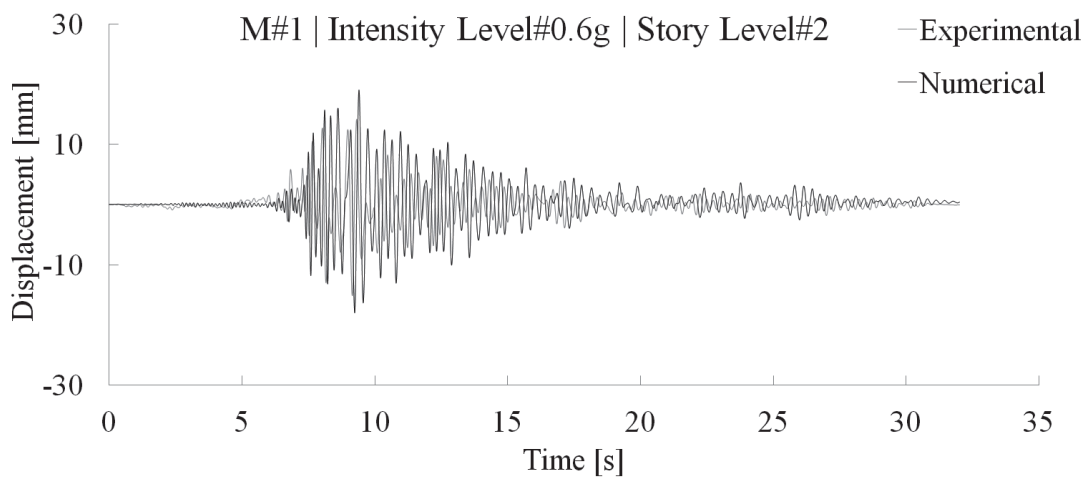
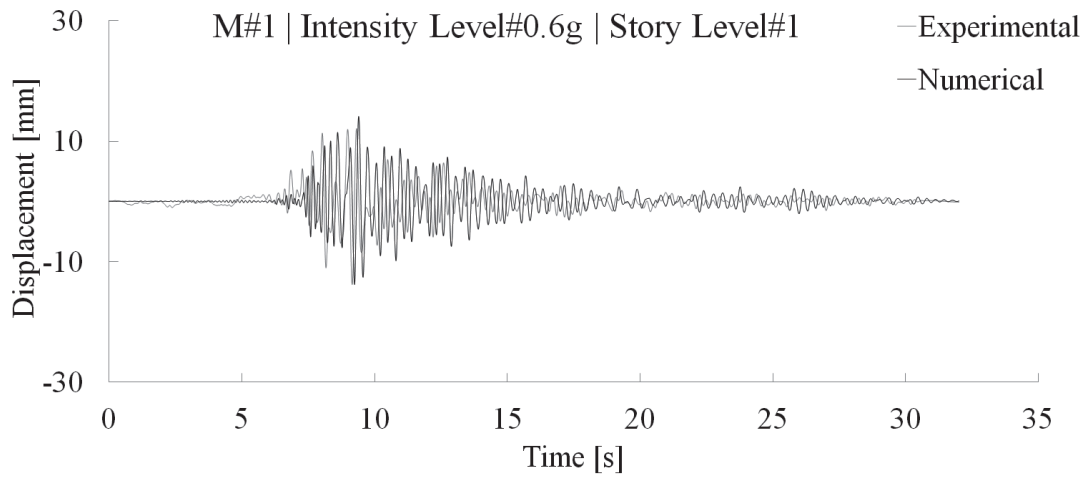


Figure E.14 Experimental/numerical (M#1) time history displacement at different story levels for the structure tested at PGA=0.6g

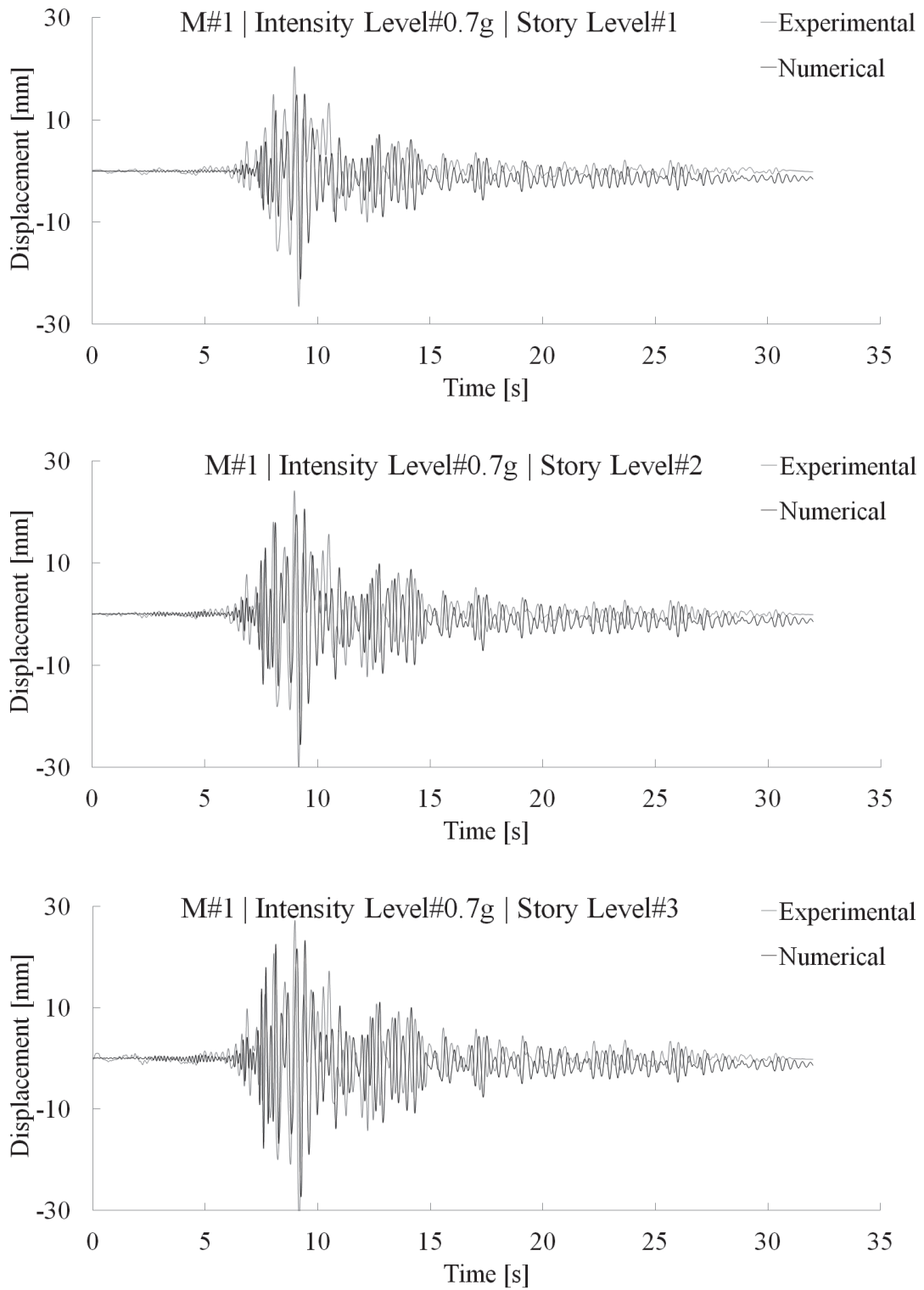


Figure E.15 Experimental/numerical (M#1) time history displacement at different story levels for the structure tested at PGA=0.7g

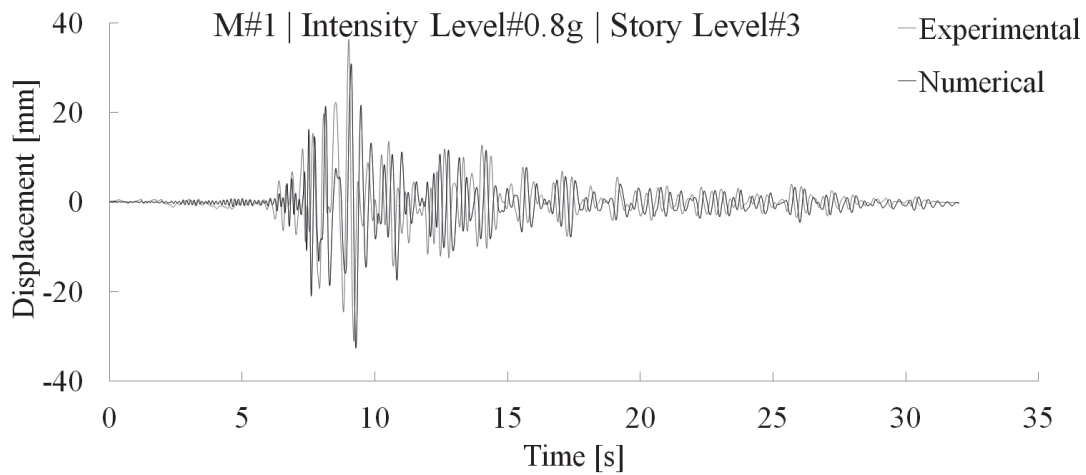
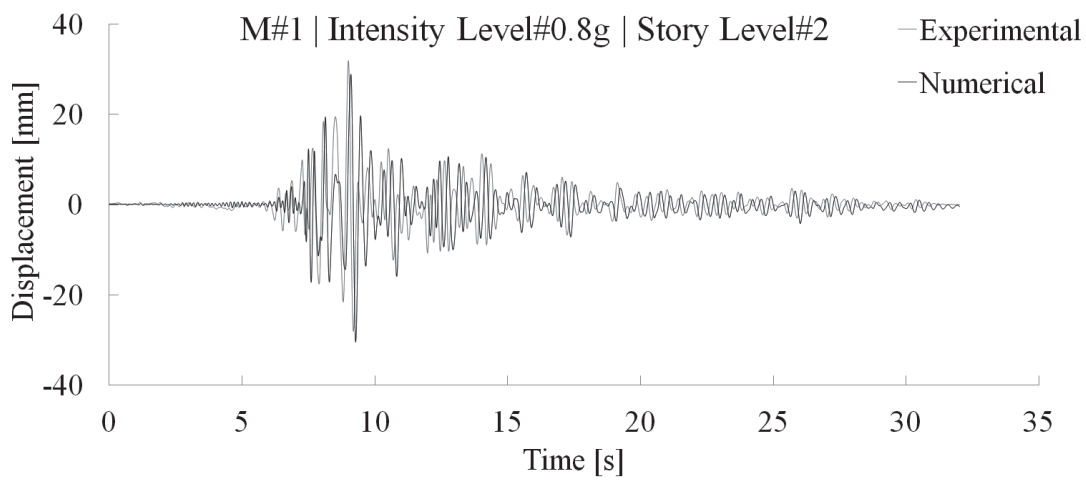
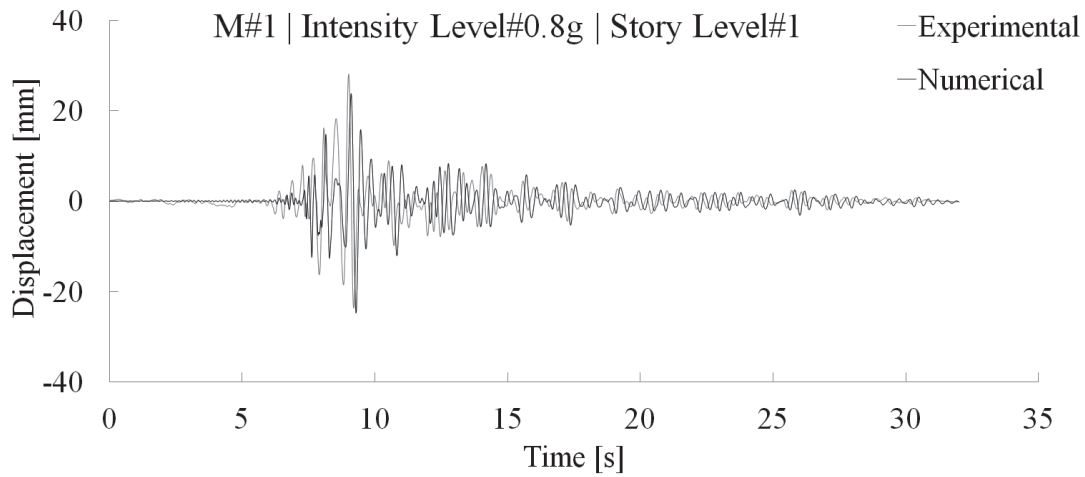


Figure E.16 Experimental/numerical (M#1) time history displacement at different story levels for the structure tested at PGA=0.8g

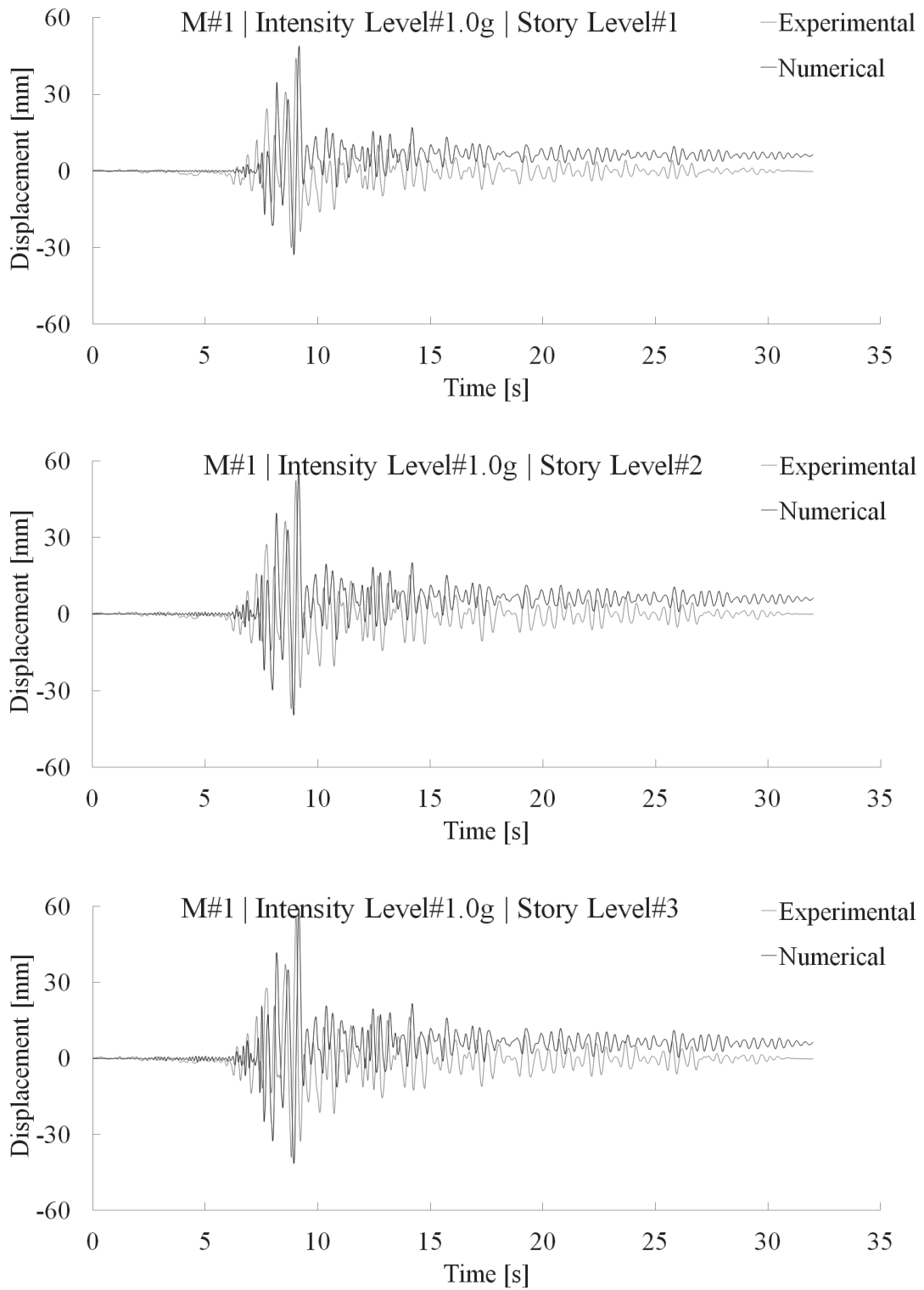


Figure E.17 Experimental/numerical (M#1) time history displacement at different story levels for the structure tested at PGA=1.0g

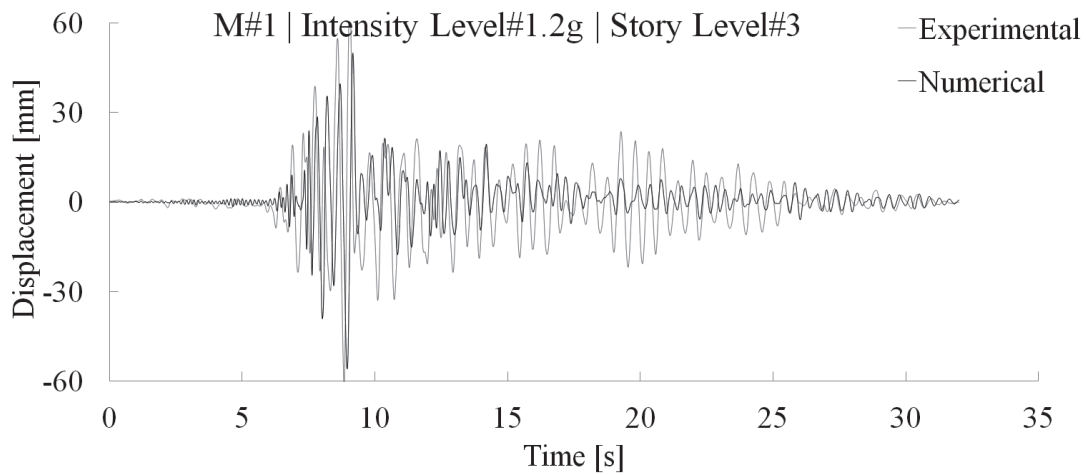
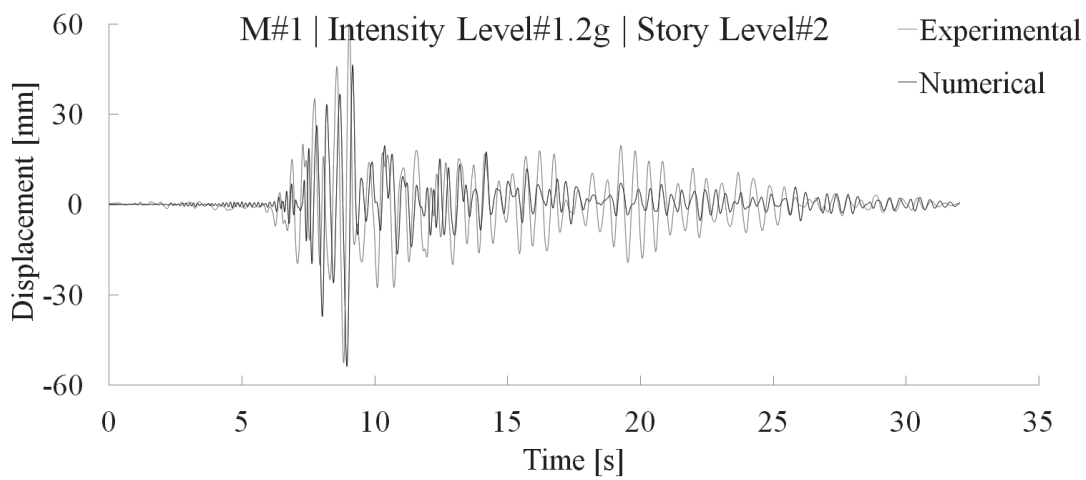
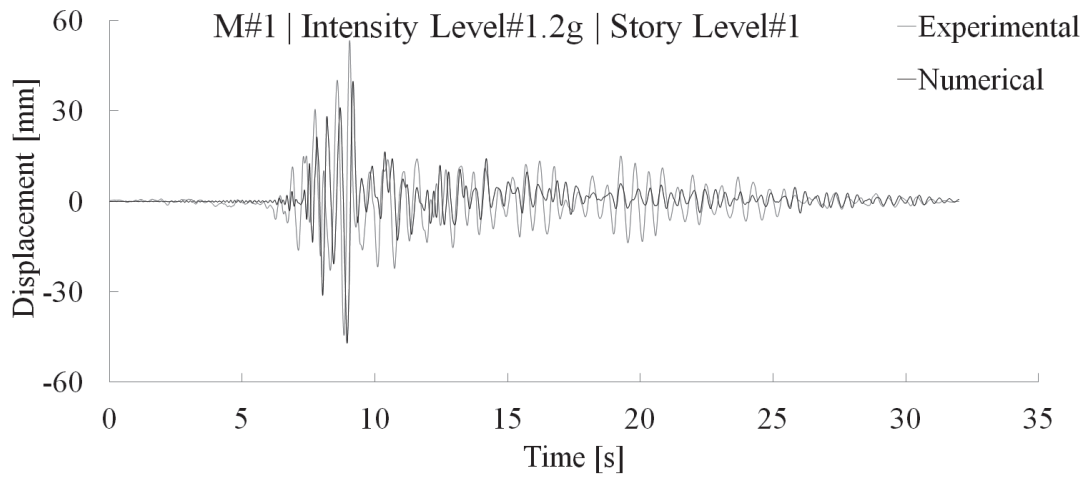


Figure E.18 Experimental/numerical (M#1) time history displacement at different story levels for the structure tested at PGA=1.2g

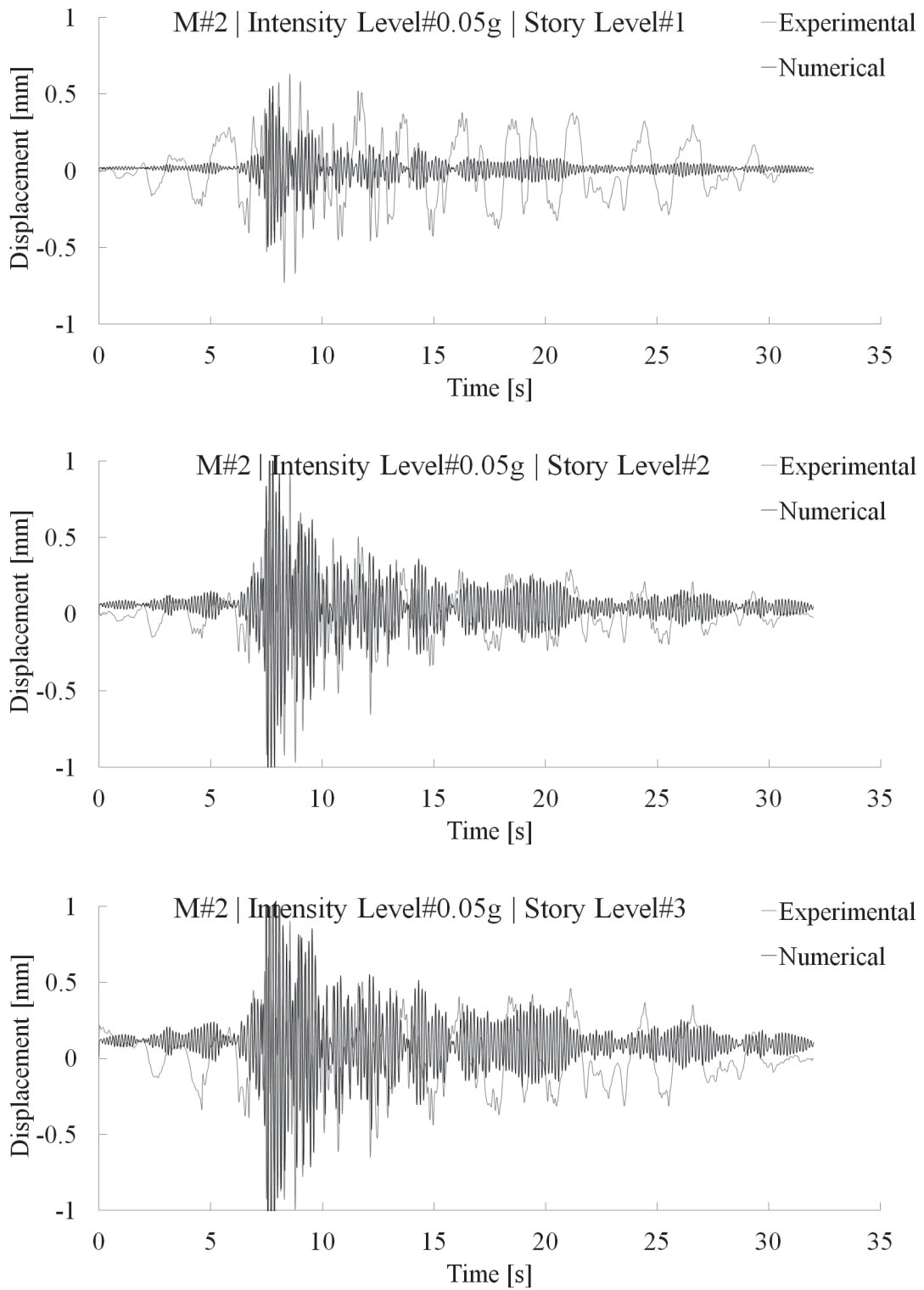


Figure E.19 Experimental/numerical (M#2) time history displacement at different story levels for the structure tested at PGA=0.05g

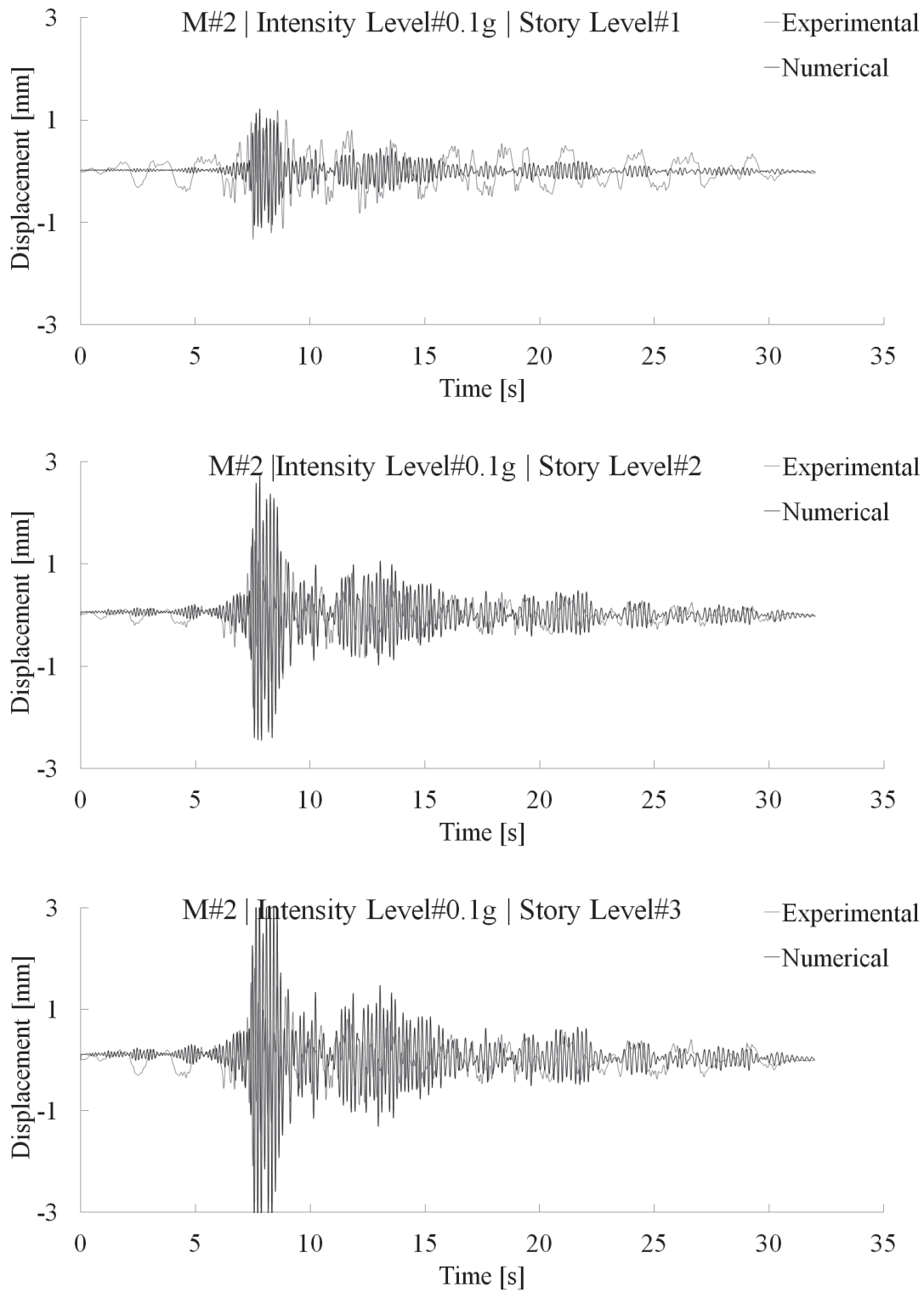


Figure E.20 Experimental/numerical (M#2) time history displacement at different story levels for the structure tested at PGA=0.1g

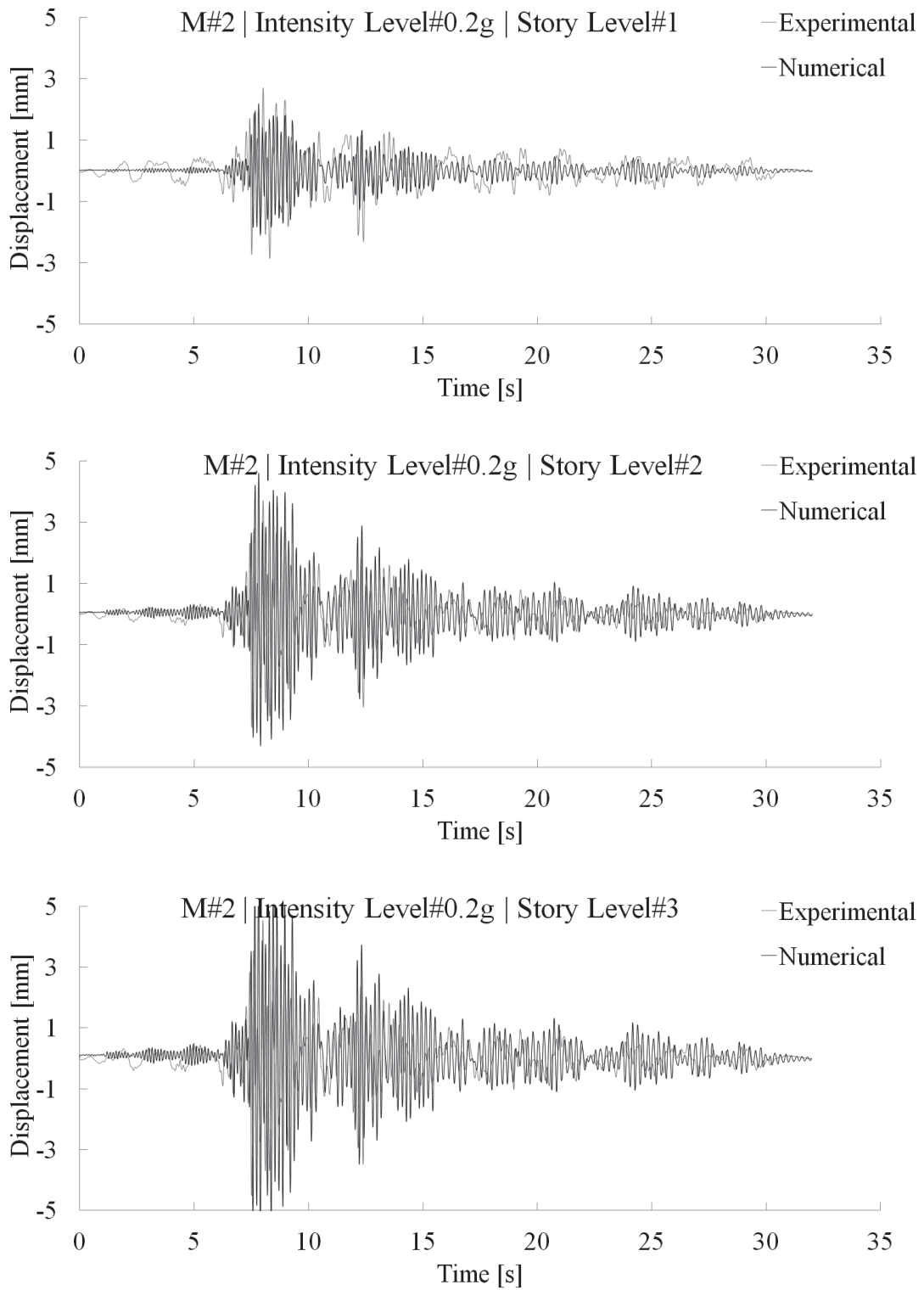


Figure E.21 Experimental/numerical (M#2) time history displacement at different story levels for the structure tested at PGA=0.2g

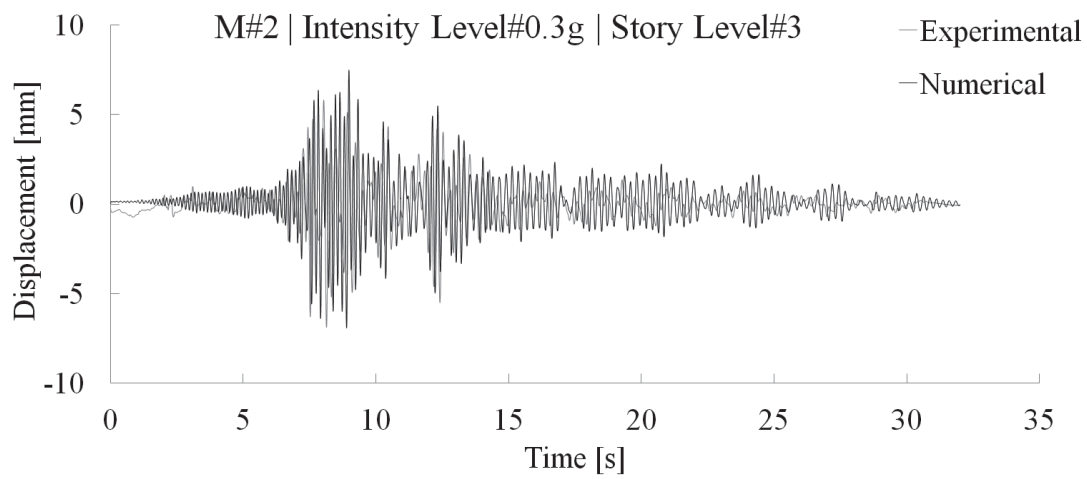
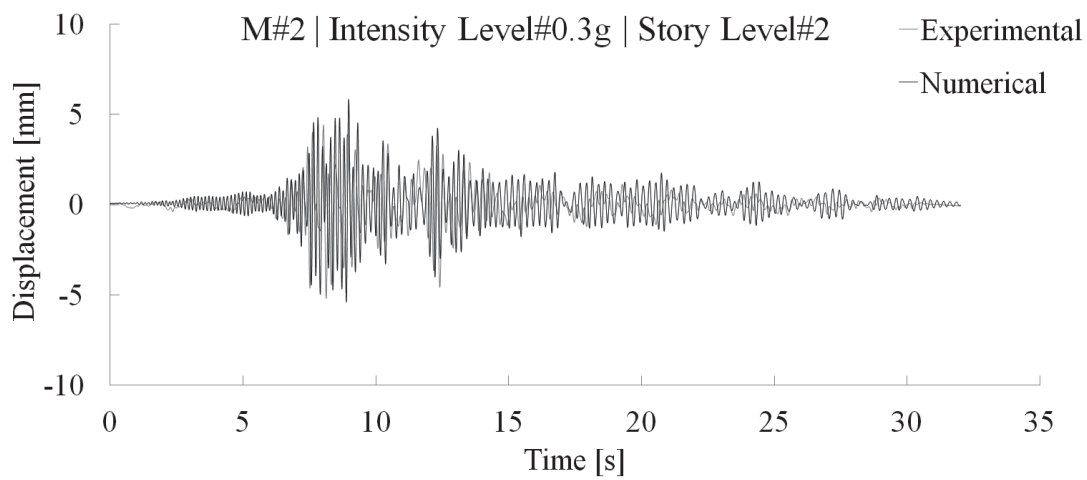
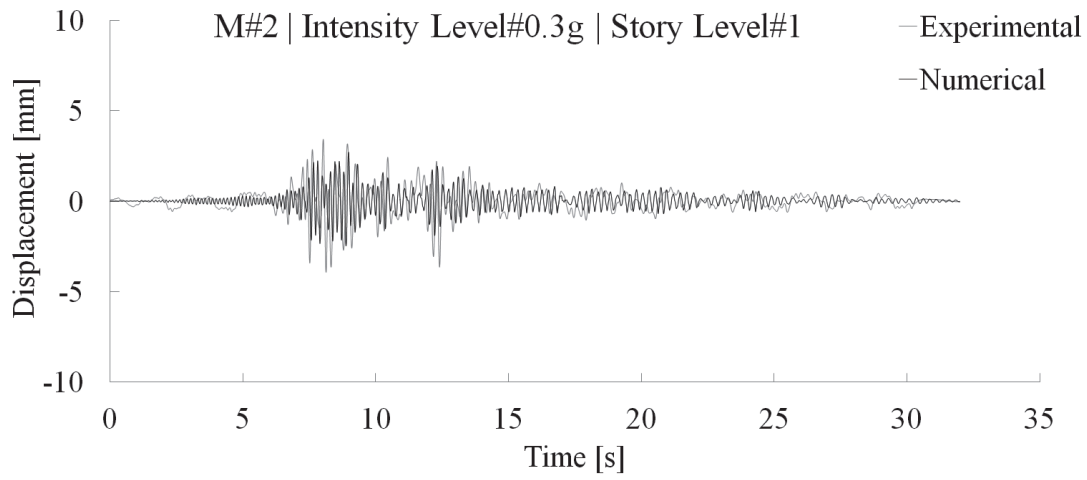


Figure E.22 Experimental/numerical (M#2) time history displacement at different story levels for the structure tested at PGA=0.3g

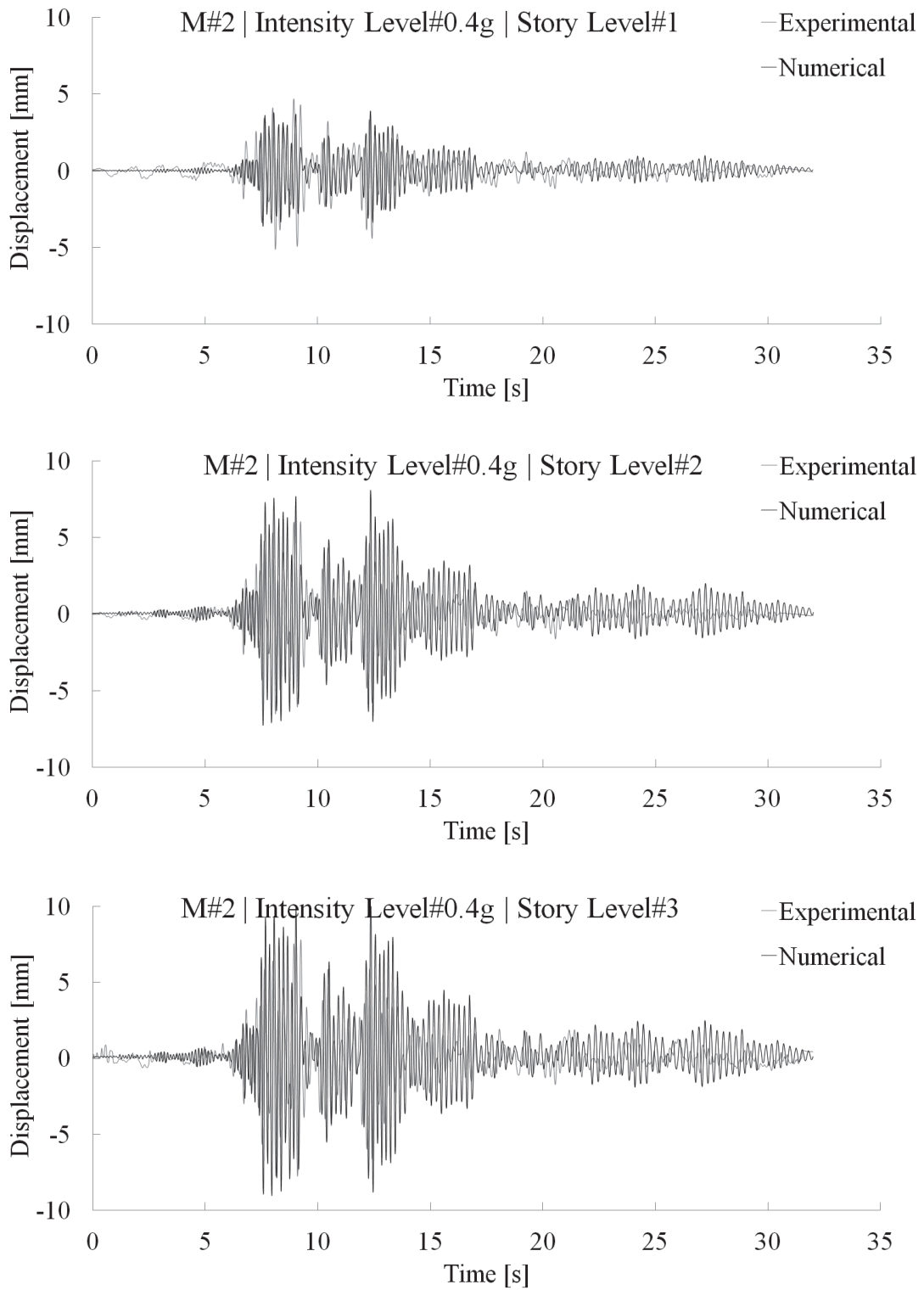


Figure E.23 Experimental/numerical (M#2) time history displacement at different story levels for the structure tested at PGA=0.4g

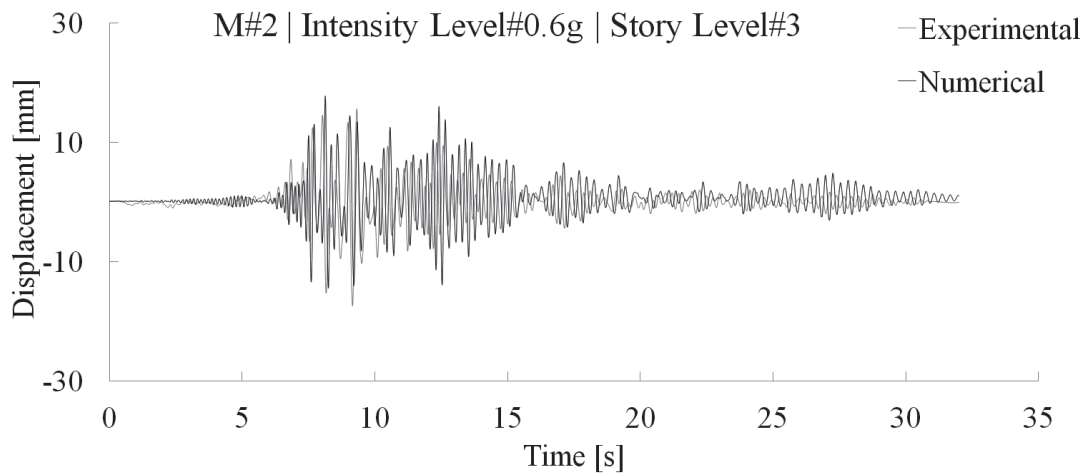
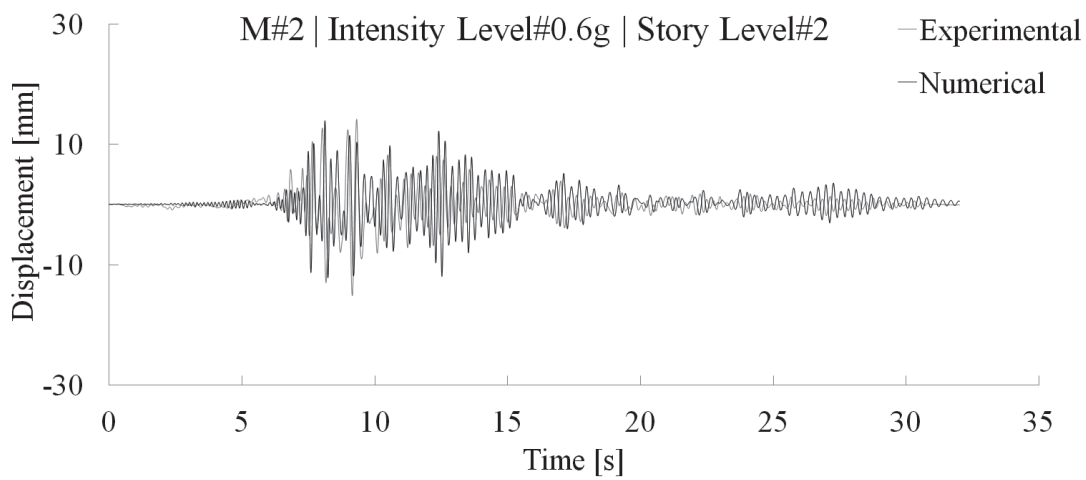
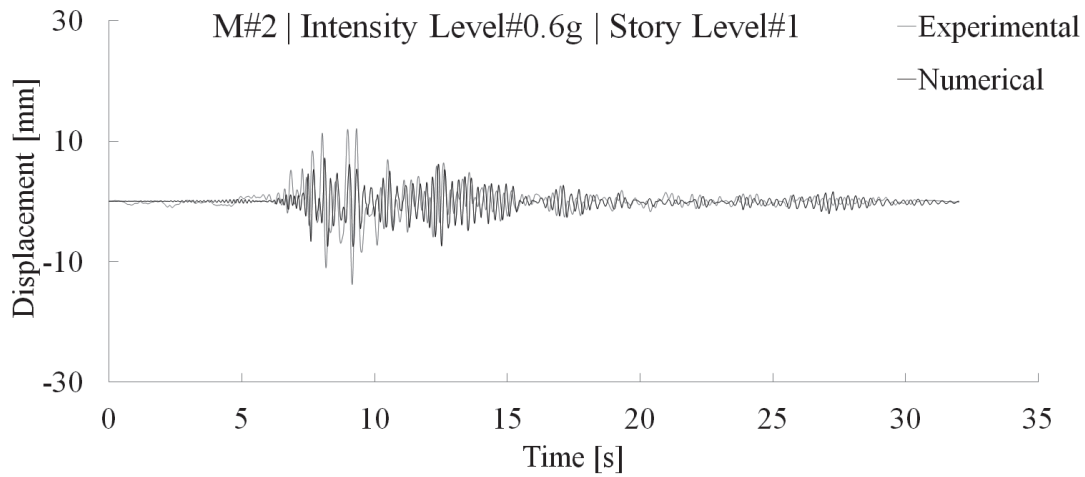


Figure E.24 Experimental/numerical (M#2) time history displacement at different story levels for the structure tested at PGA=0.6g

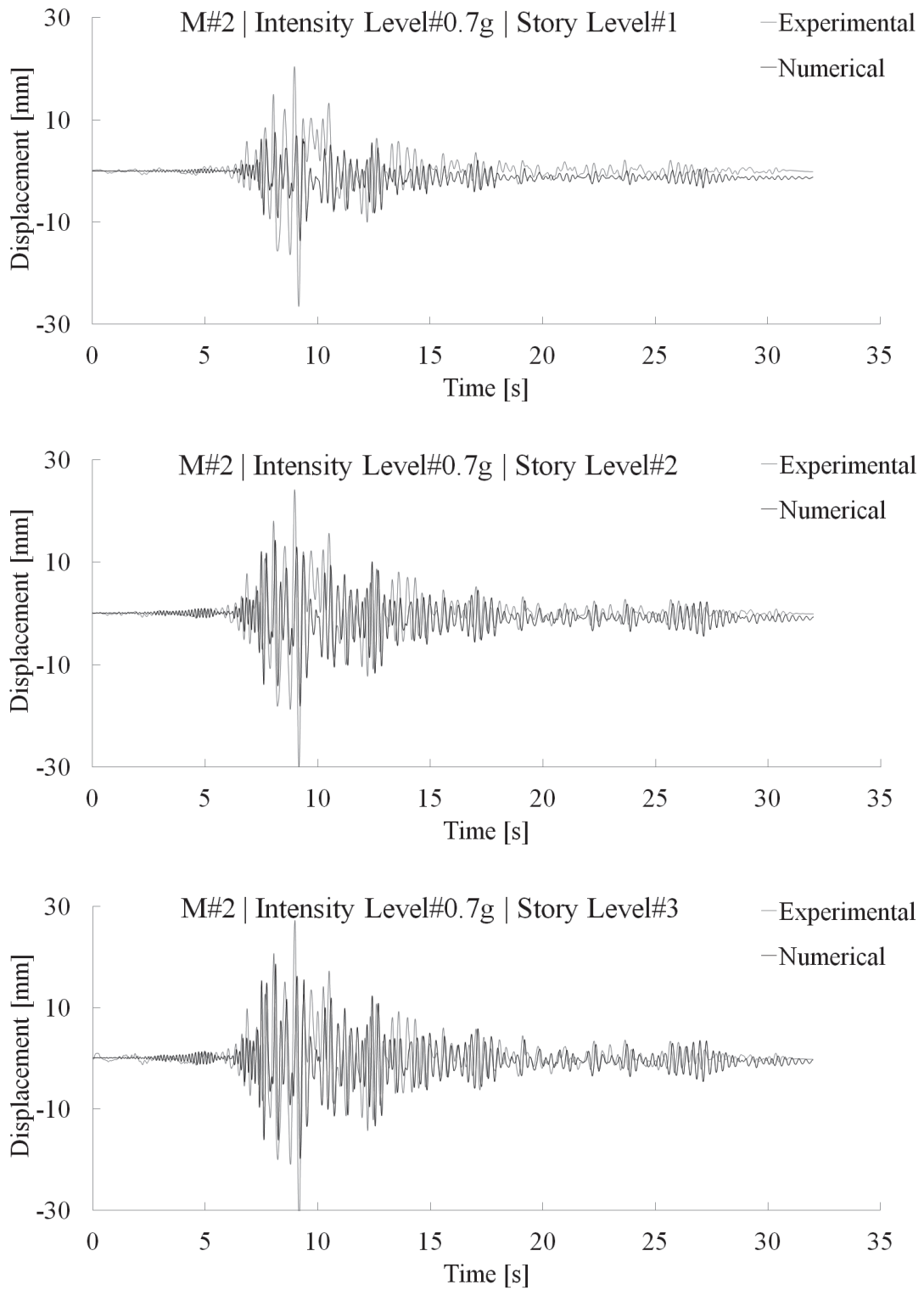


Figure E.25 Experimental/numerical (M#2) time history displacement at different story levels for the structure tested at PGA=0.7g

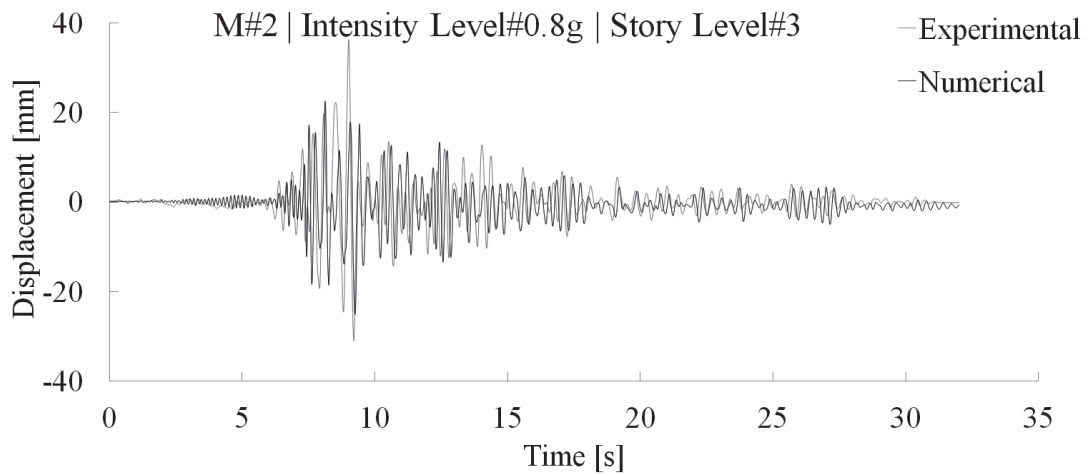
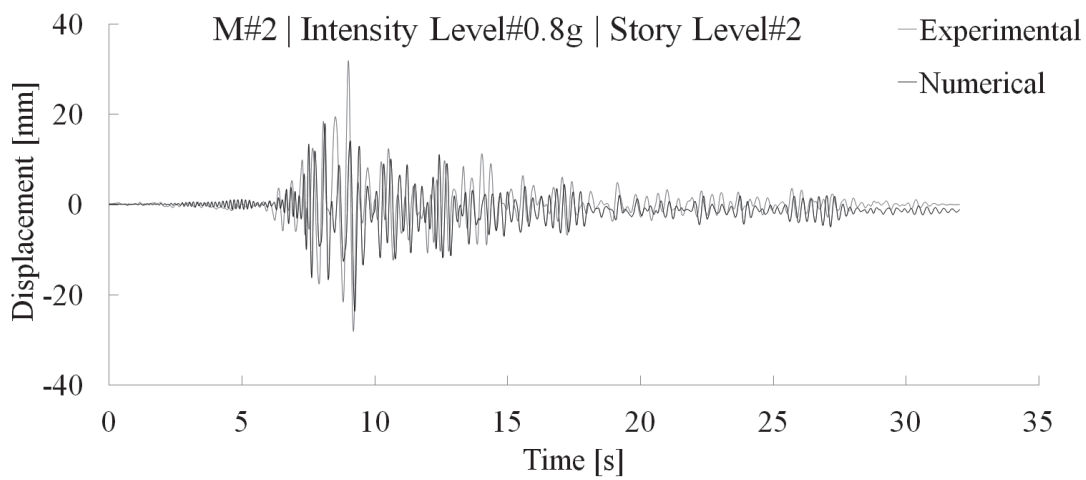
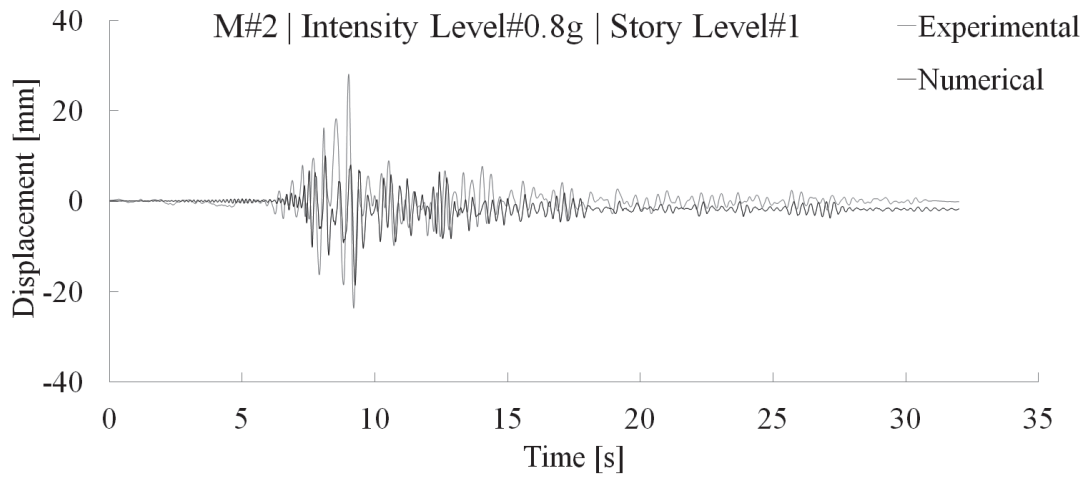


Figure E.26 Experimental/numerical (M#2) time history displacement at different story levels for the structure tested at PGA=0.8g

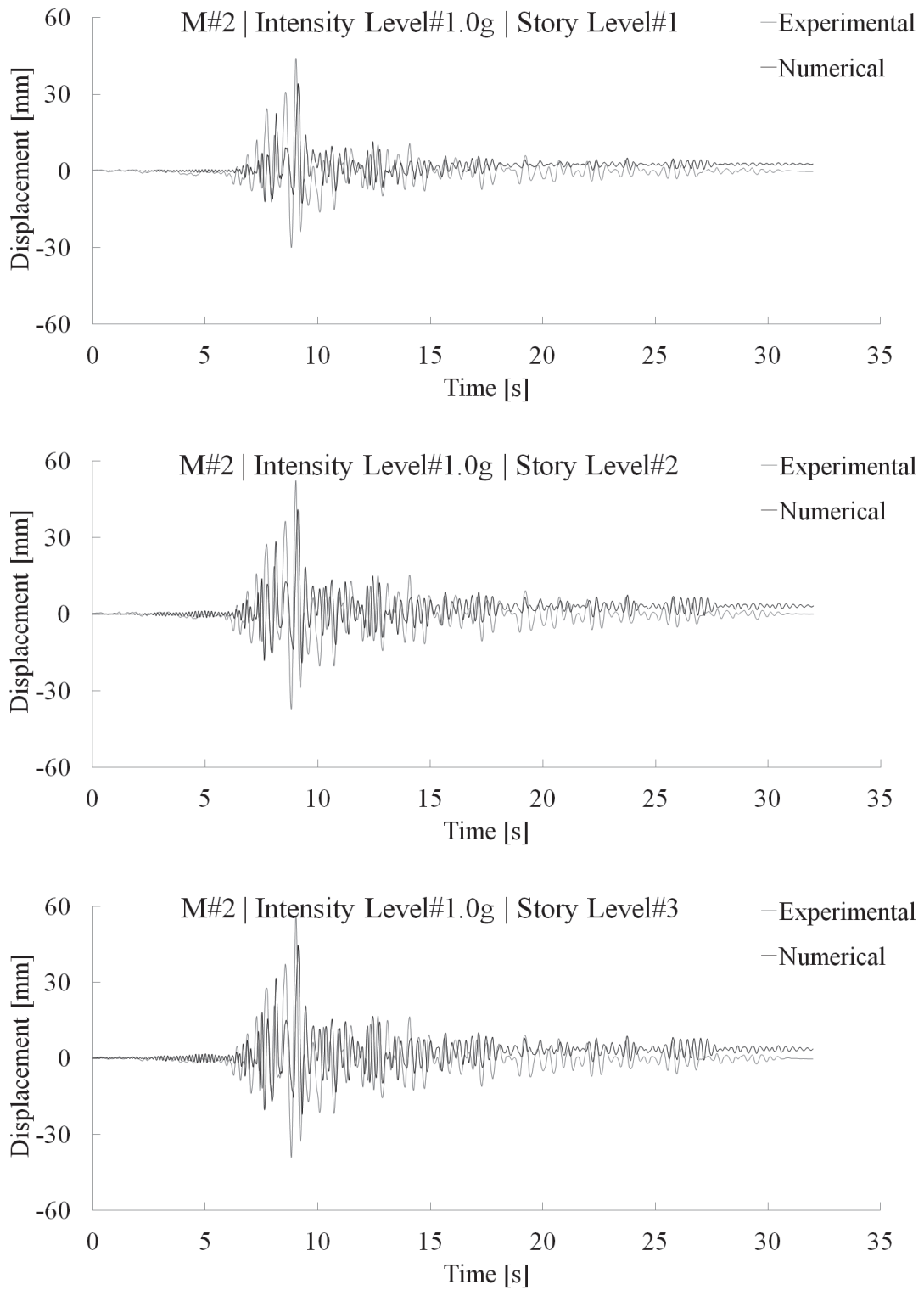


Figure E.27 Experimental/numerical (M#2) time history displacement at different story levels for the structure tested at PGA=1.0g

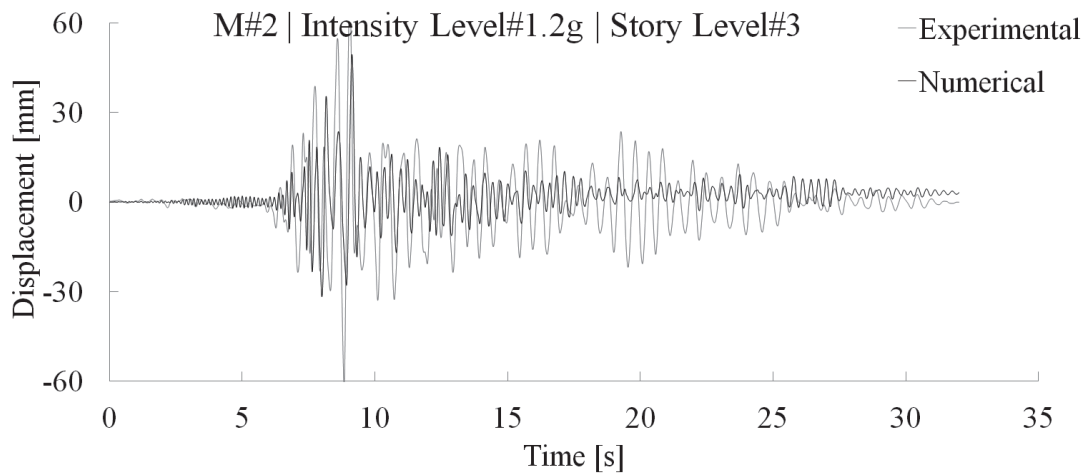
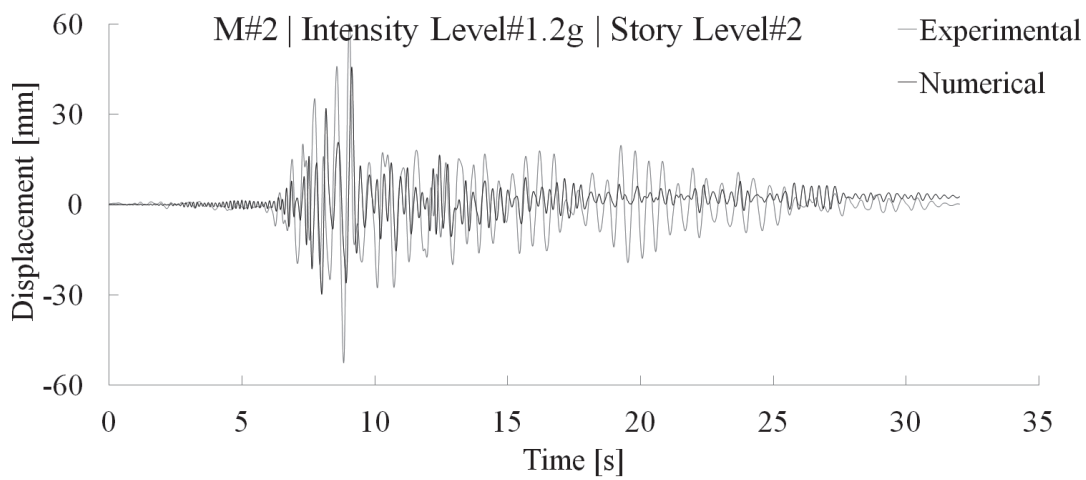
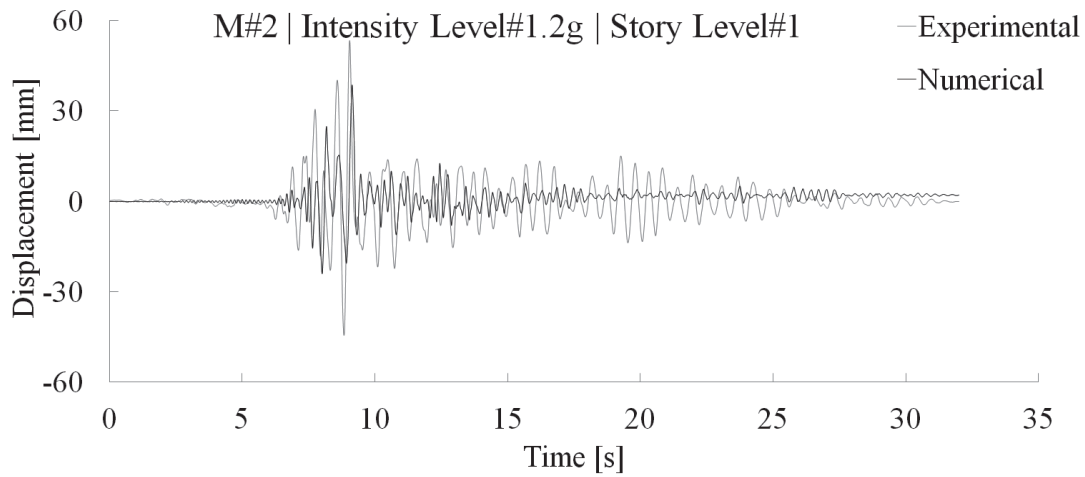


Figure E.28 Experimental/numerical (M#2) time history displacement at different story levels for the structure tested at PGA=1.2g

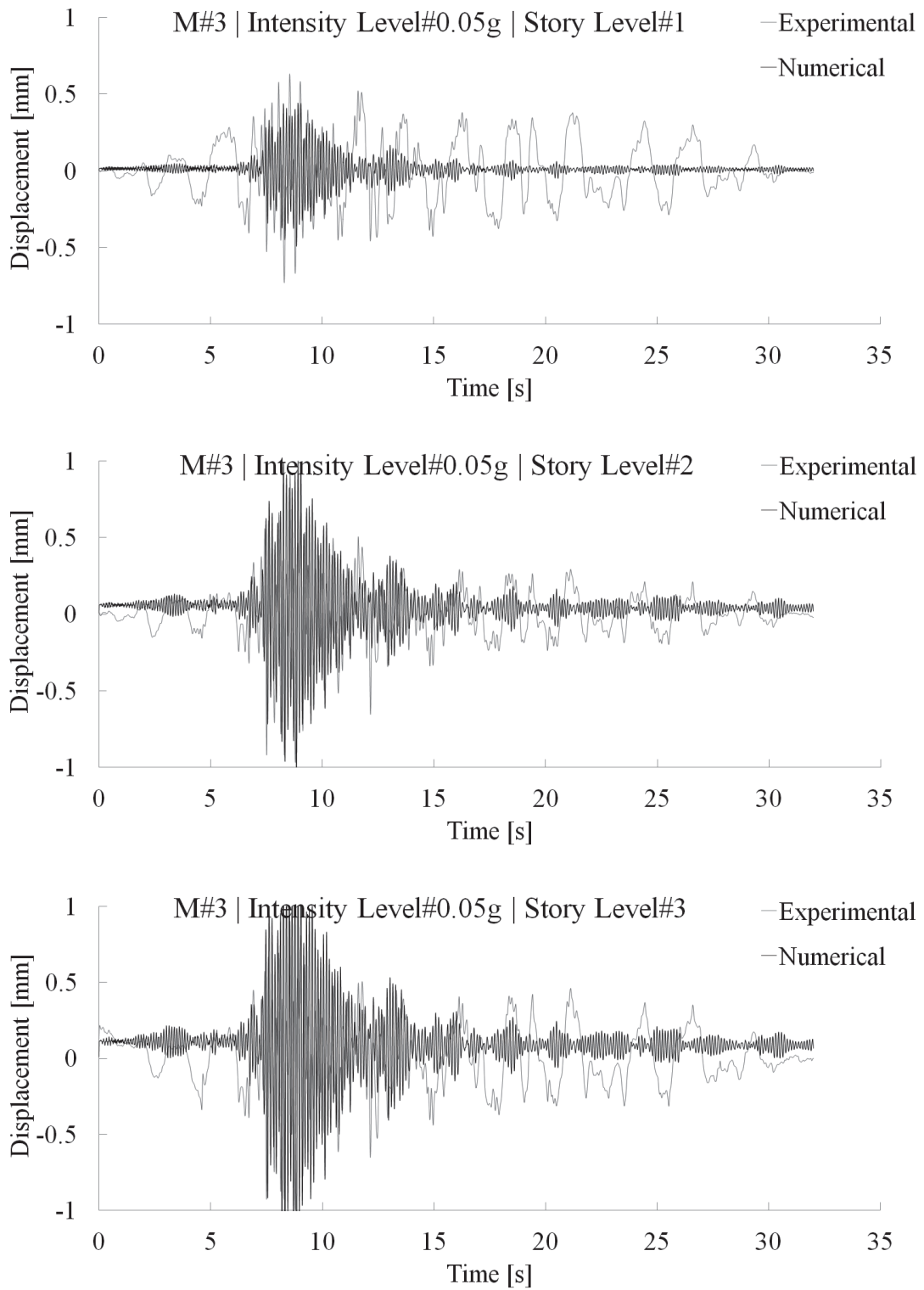


Figure E.29 Experimental/numerical (M#3) time history displacement at different story levels for the structure tested at PGA=0.05g

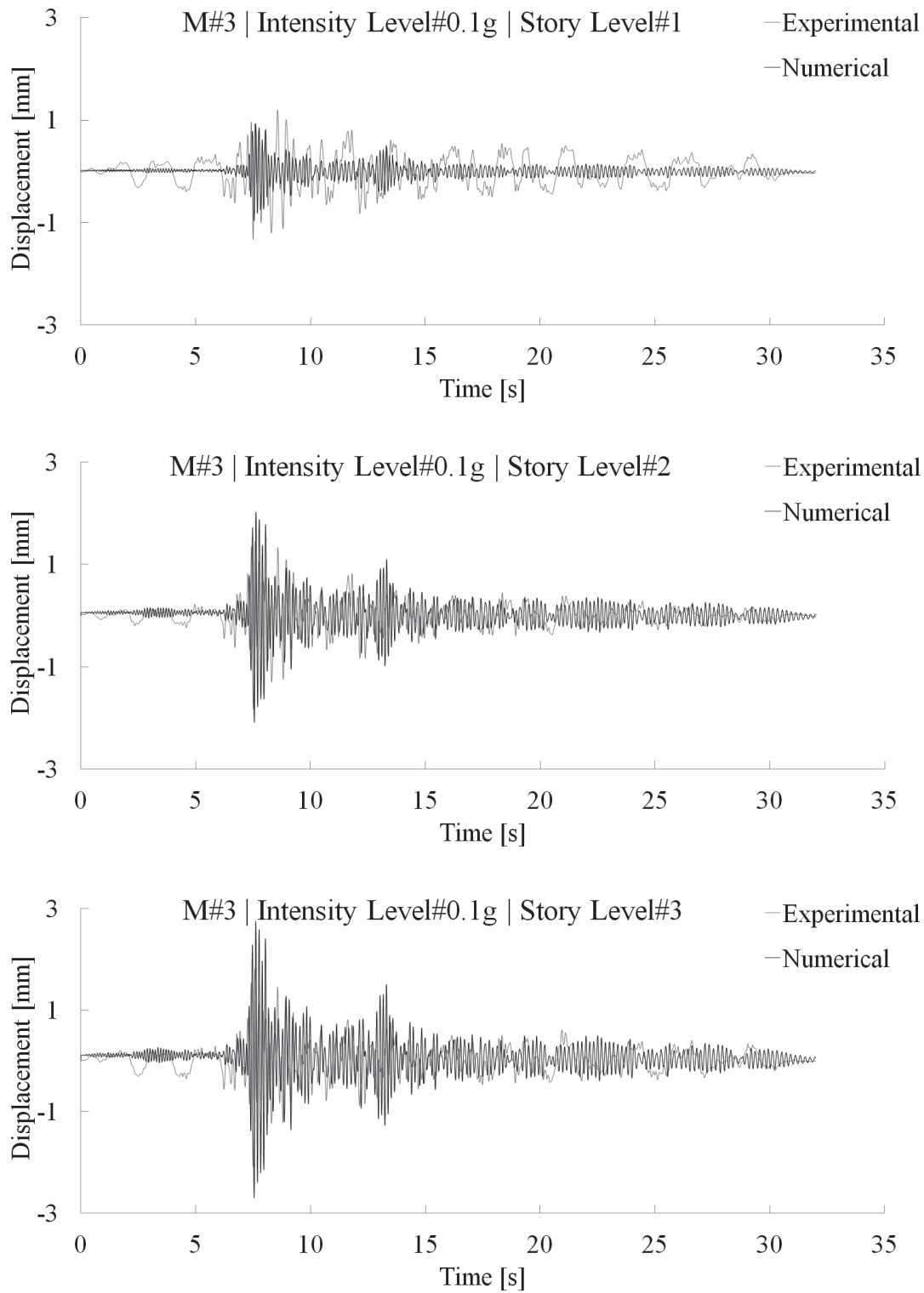


Figure E.30 Experimental/numerical (M#3) time history displacement at different story levels for the structure tested at PGA=0.1g

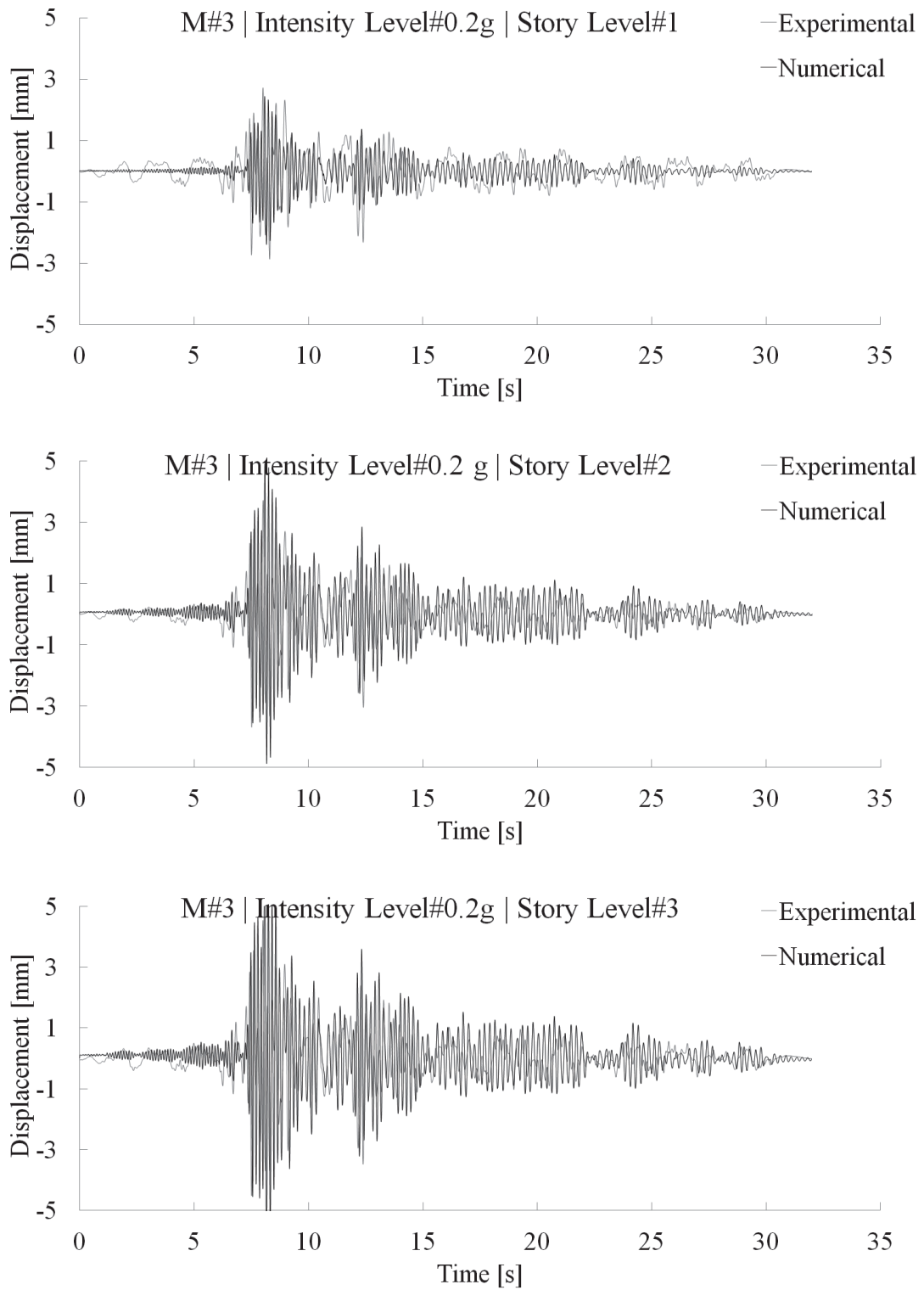


Figure E.31 Experimental/numerical (M#3) time history displacement at different story levels for the structure tested at PGA=0.2g

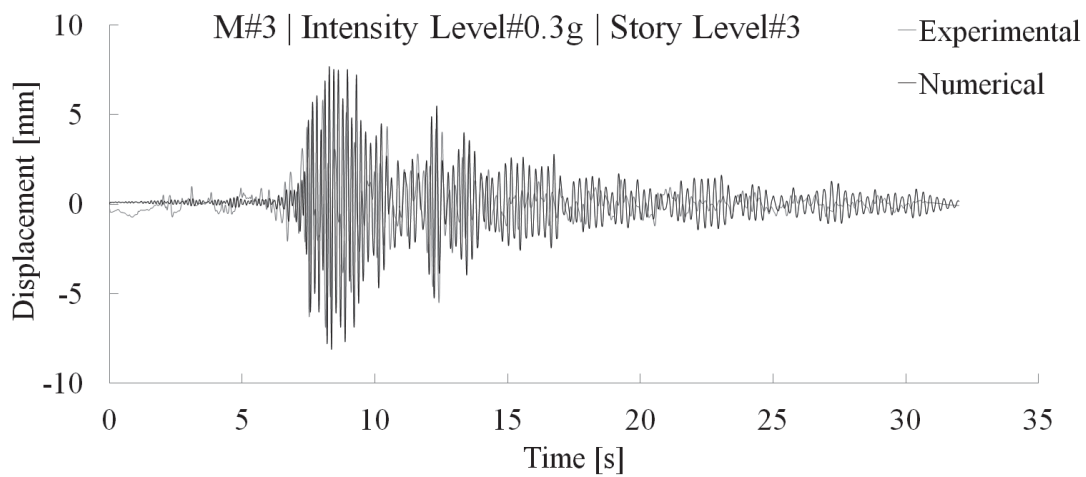
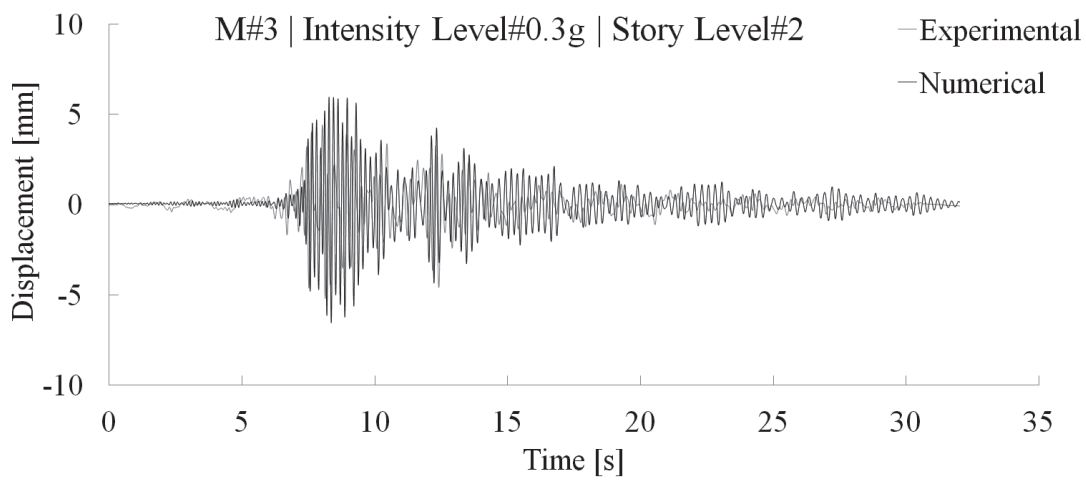
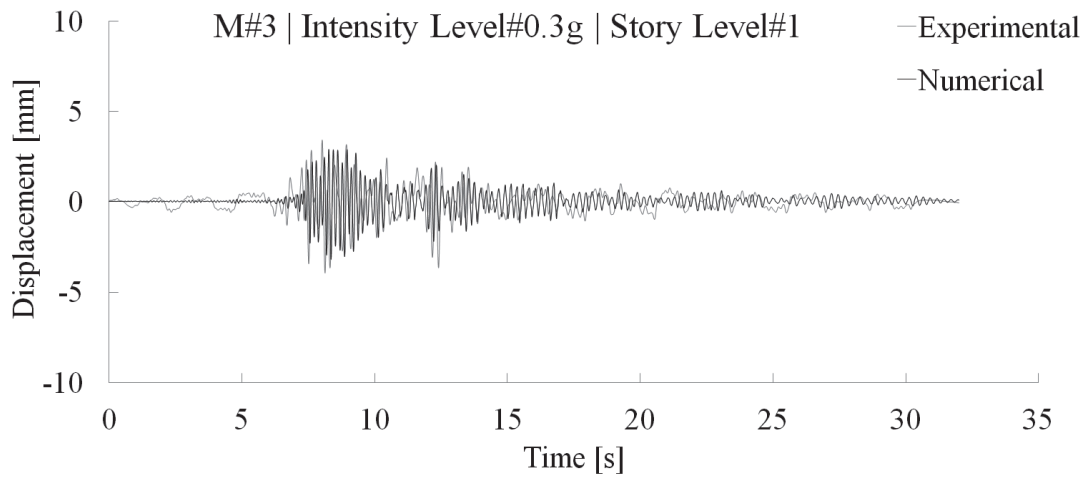


Figure E.32 Experimental/numerical (M#3) time history displacement at different story levels for the structure tested at $PGA=0.3g$

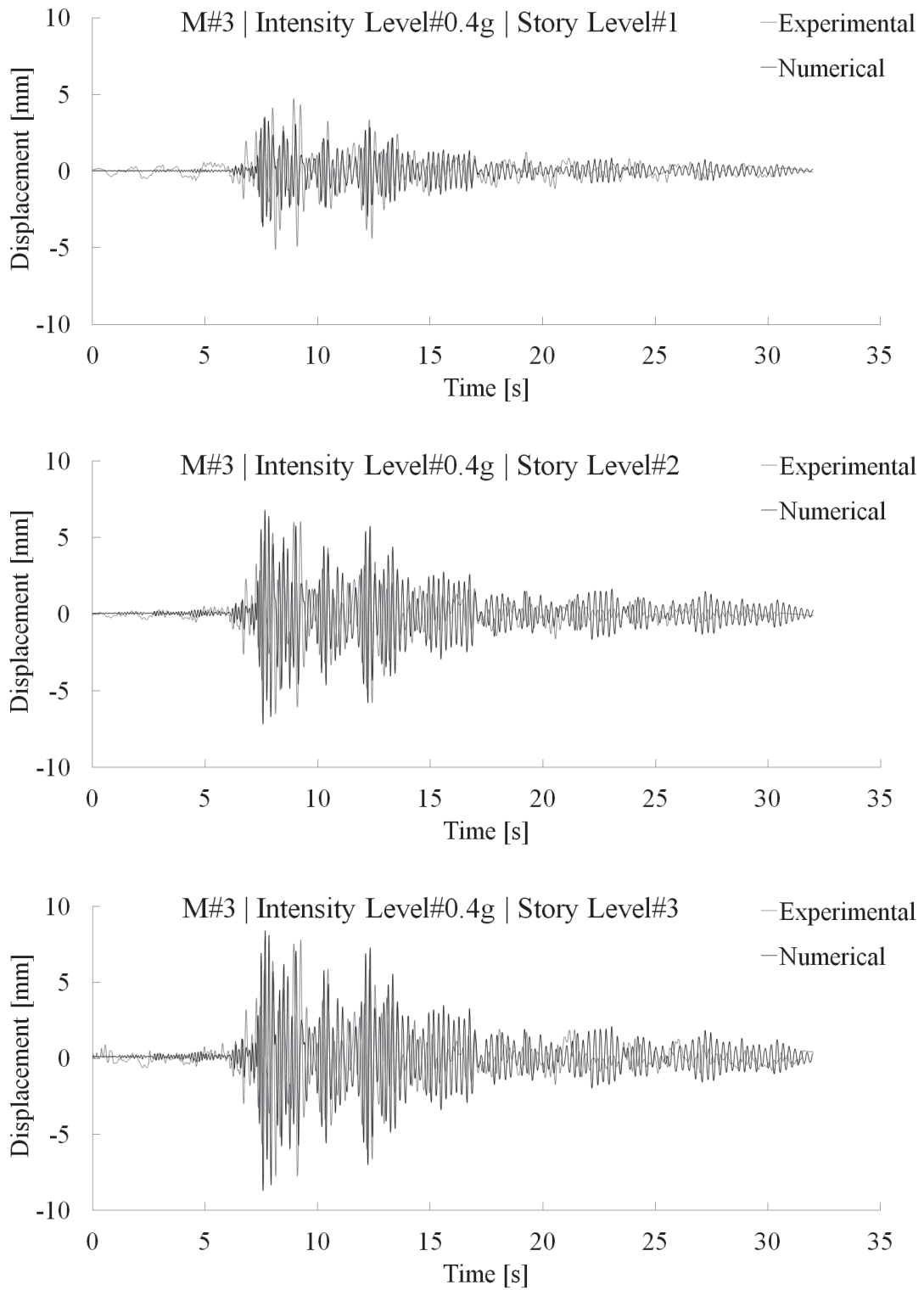


Figure E.33 Experimental/numerical (M#3) time history displacement at different story levels for the structure tested at PGA=0.4g

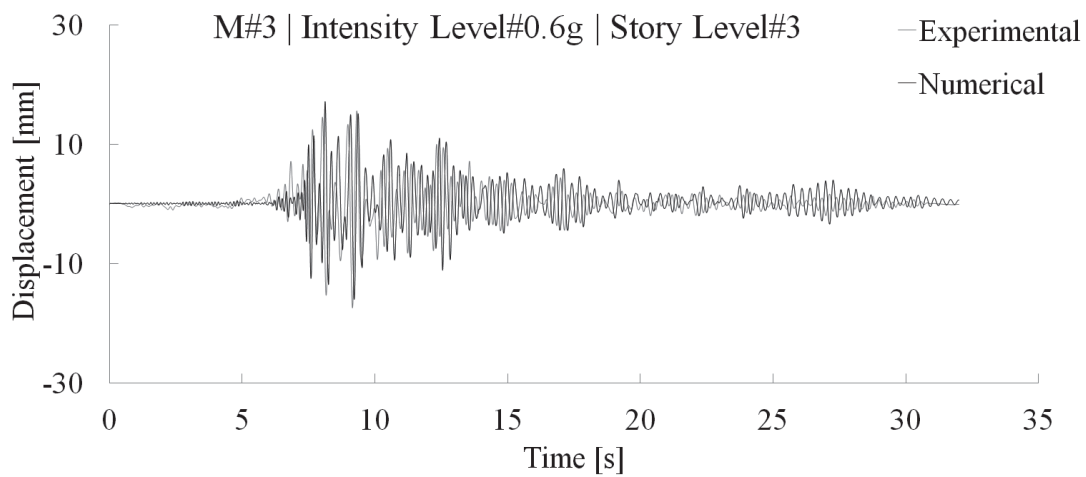
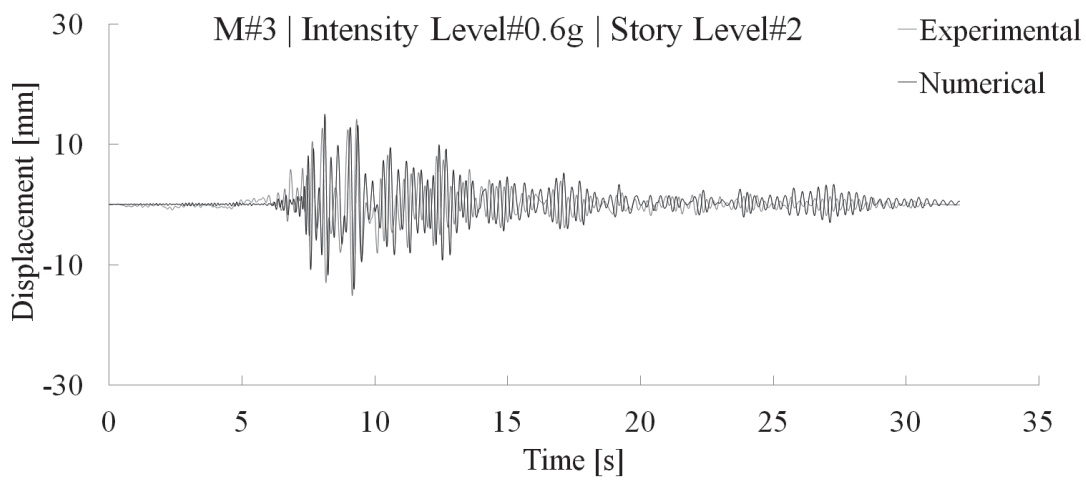
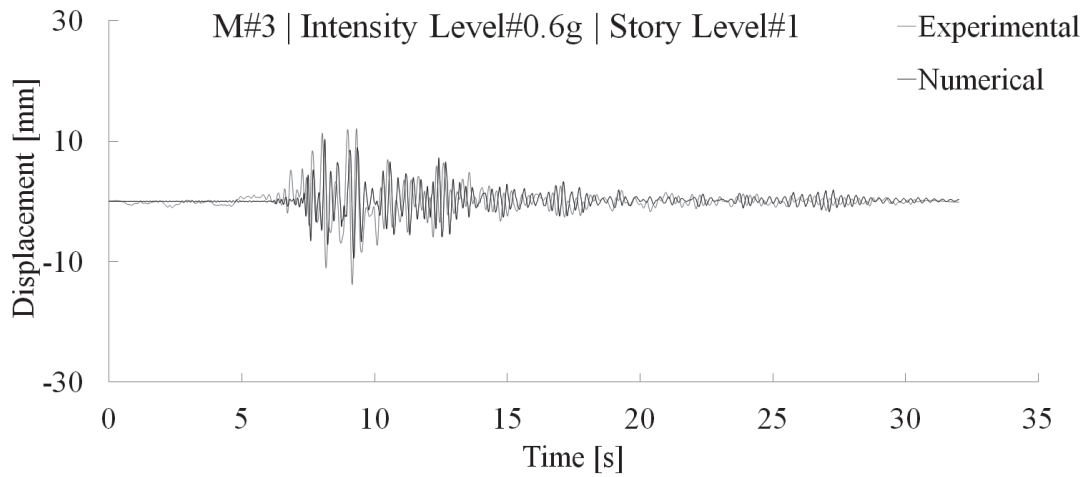


Figure E.34 Experimental/numerical (M#3) time history displacement at different story levels for the structure tested at PGA=0.6g

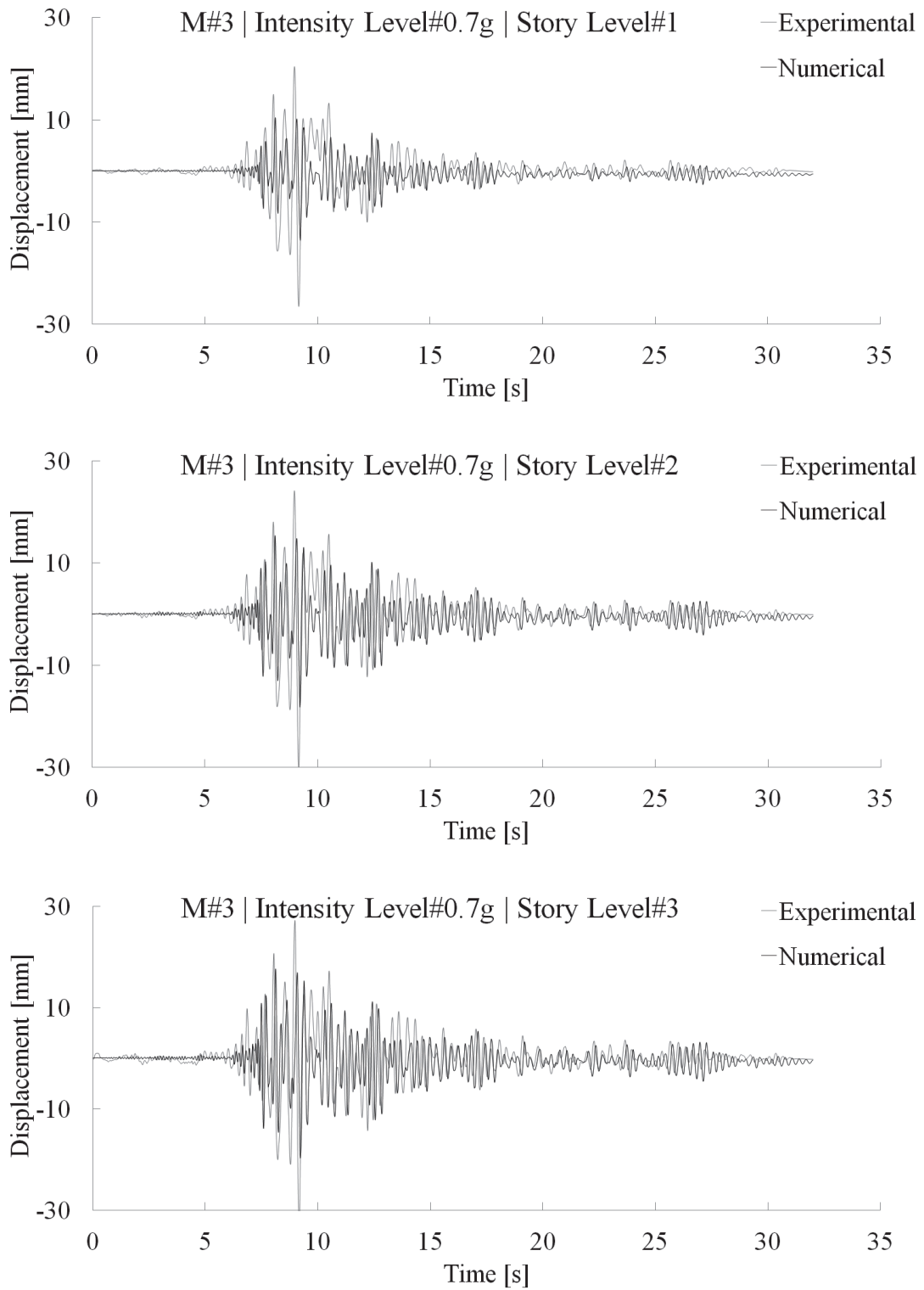


Figure E.35 Experimental/numerical (M#3) time history displacement at different story levels for the structure tested at PGA=0.7g

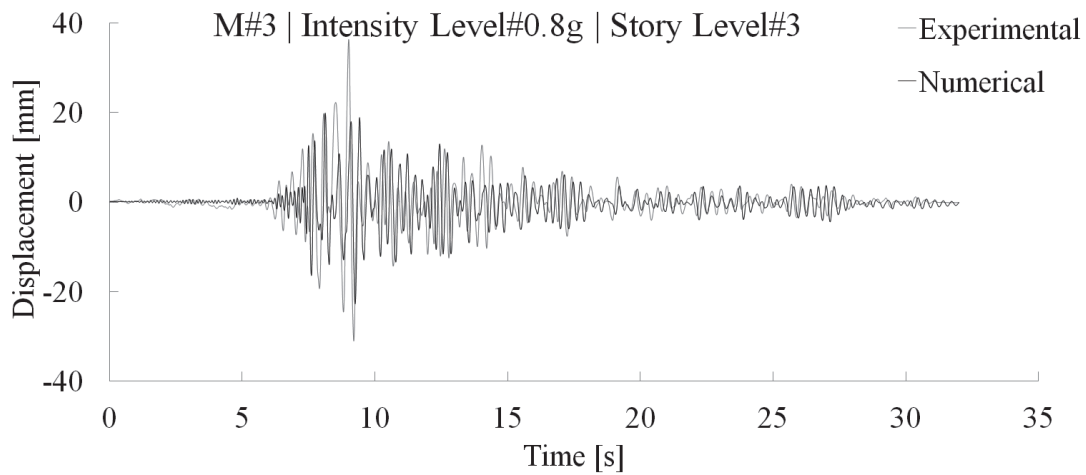
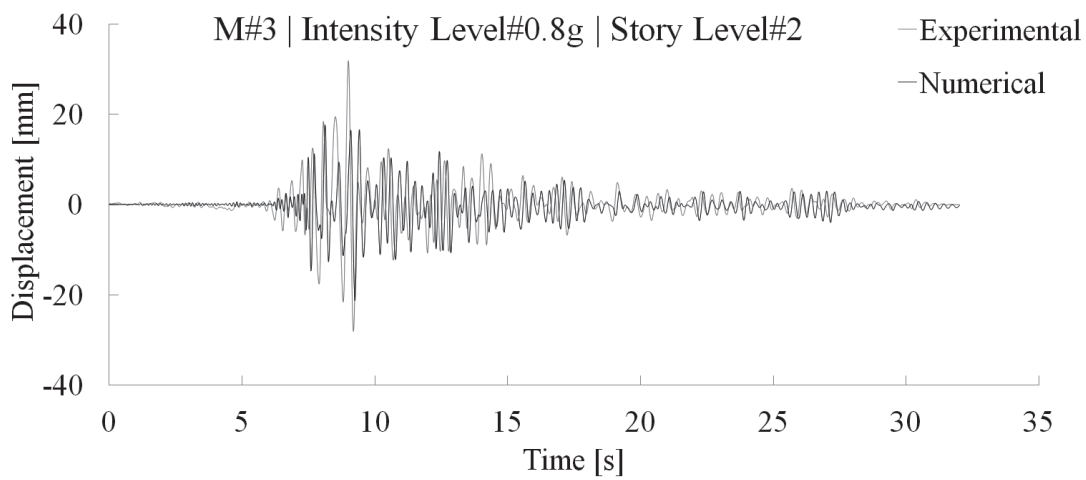
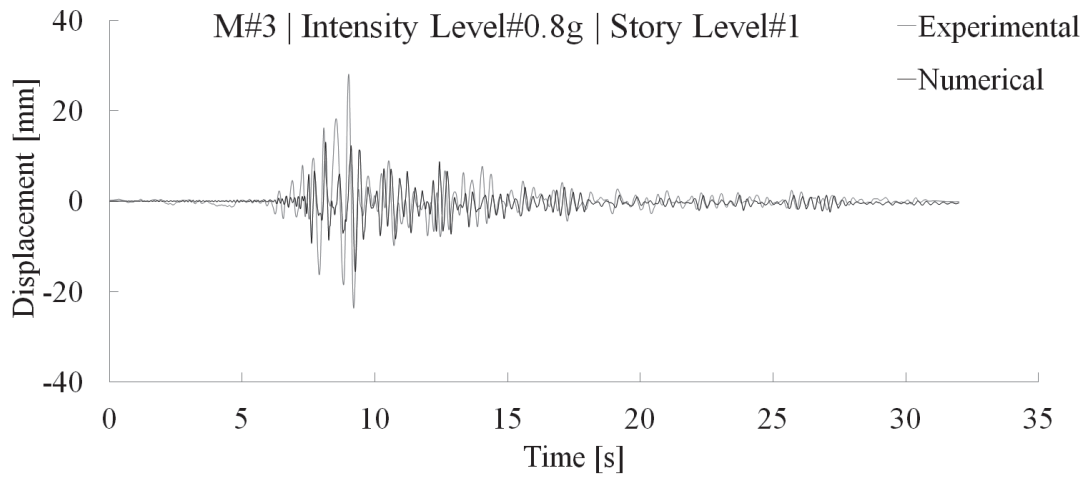


Figure E.36 Experimental/numerical (M#3) time history displacement at different story levels for the structure tested at PGA=0.8g

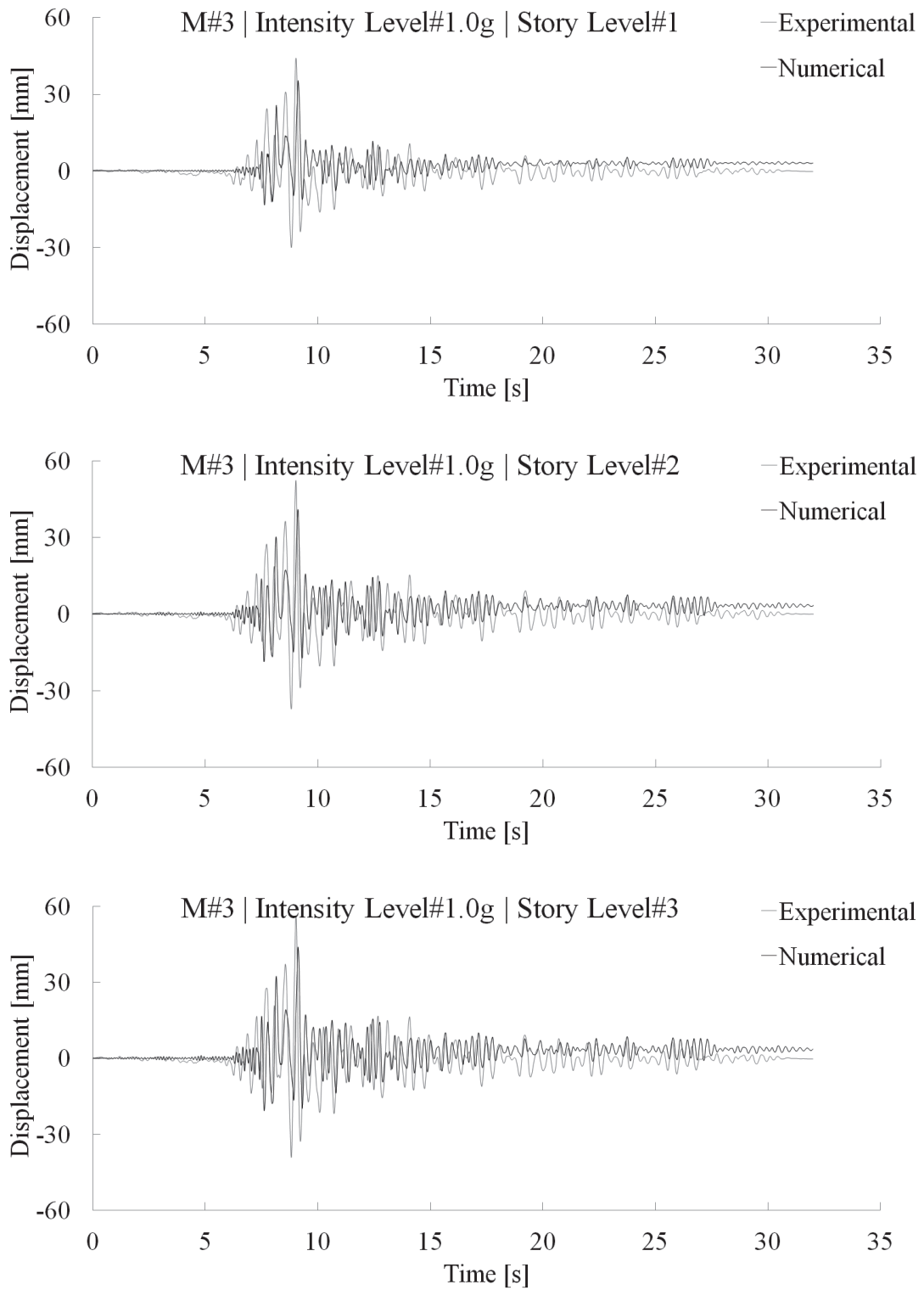


Figure E.37 Experimental/numerical (M#3) time history displacement at different story levels for the structure tested at PGA=1.0g

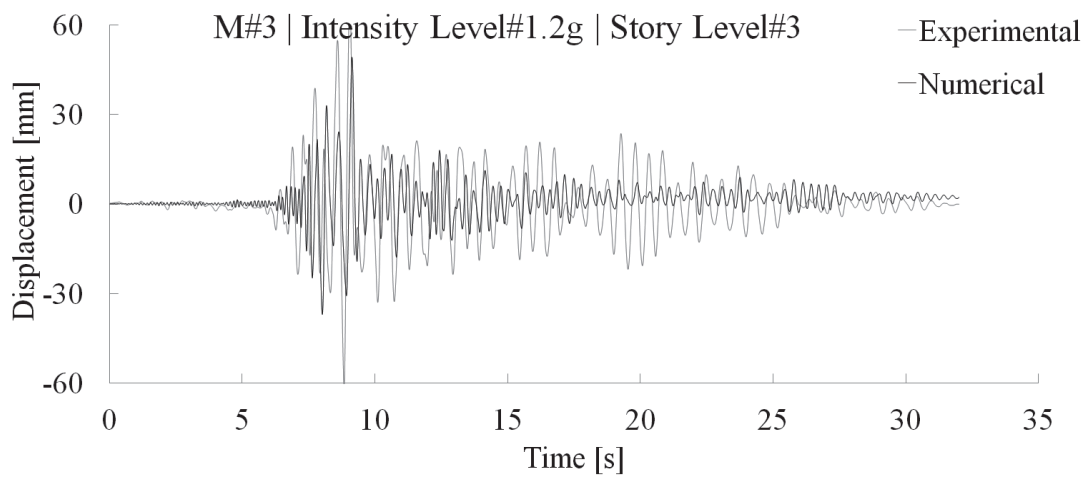
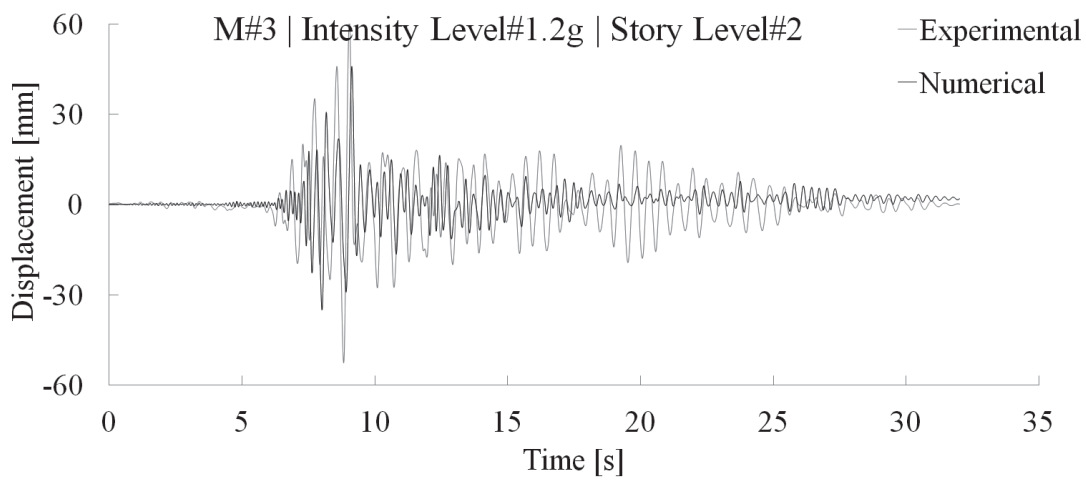
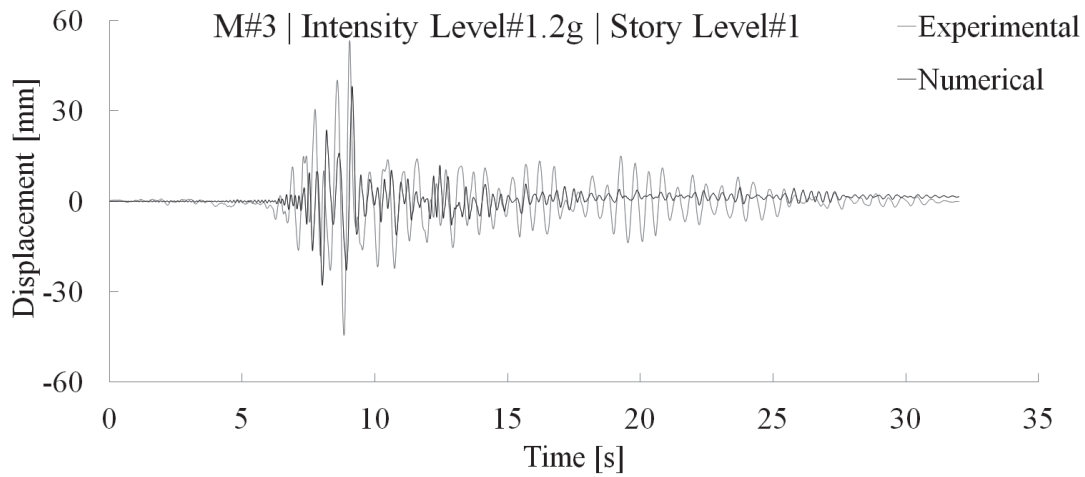
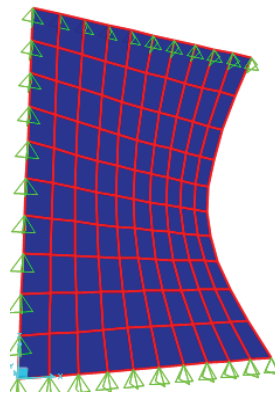


Figure E.38 Experimental/numerical (M#3) time history displacement at different story levels for the structure tested at PGA=1.2g

Table E.7 Geometric and material properties of the infill walls

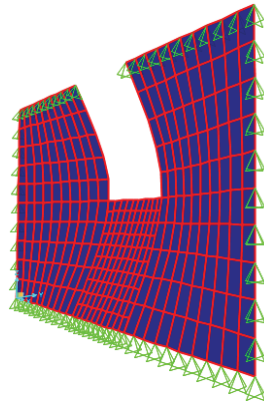
Section	Story	L_{URM} [m]	H_{URM} [m]	t_{URM} [mm]	E_c [GPa]	E_{URM} [GPa]	θ [deg]	W_{st} [mm]
1--2	1	1.12	1.12	120	38.839	2.025	45.0	164
1--2	2,3	1.12	1.04	120	38.839	2.025	47.0	164
2--3	1	0.96	1.12	120	38.839	2.025	49.4	165
2--3	2,3(1)	0.91	1.04	120	38.839	2.025	52.8	165
2--3	2,3(2)	0.64	0.56	120	38.839	2.025	41.2	115
A--B	1	0.84	1.12	120	38.839	2.025	53.1	157
A--B	2,3(1)	0.79	1.04	120	38.839	2.025	56.6	156
A--B	2,3(2)	0.64	0.56	120	38.839	2.025	41.2	120

(1), (2): See Figure B.4



- a) Shell elements linear model of the infill wall in the transverse direction (Section A--B) at the 1st story of FRAMA experimental model (see Figure B.3 b)

$$f_{OoP_FEM} = 71 \text{ [Hz]}$$



- b) Shell elements linear model of the infill wall with opening in the transverse direction (Section A--B) at the 2nd story of FRAMA experimental model (see Figure B.3 b)

$$f_{OoP_FEM} = 59.7 \text{ [Hz]}$$

Figure E.39 Transverse infill walls natural frequency

Table E.8 Dynamic and geometric parameters of the developed model (M#5_dev)

Section	Story	γ [kN/m ³]	mass [kN.sec ² /m]	$f_{\text{OoP_FEM}}$ [Hz]	W_{st} [mm]	t_{URM} [mm]	W_{mod} [mm]	t_{mod} [mm]
A--B	1	14	0.163	71.0	48	120	46.0	409.1
A--B	2,3(1)	14	0.113	59.7	49	120	53.1	355.8
A--B	2,3(2)	14	0.058	59.7	120	120	121.1	119.1

(1), (2): See Figure B.4

Table E.9 Stress-strain parameters for the diagonal beam-column model (M#5_dev)

Section	Story	f_{tp} [MPa]	V_{d} [N]	f_{mc} [MPa]	f_{my} [MPa]	f_{mo} [MPa]	f_{mu} [MPa]	ϵ_{mc} [%]	ϵ_{my} [%]	ϵ_{mo} [%]	ϵ_{mu} [%]
1--2	1	0.12	22808.4	0.58	0.87	1.16	0.35	0.029	0.086	0.115	0.458
1--2	2,3	0.12	23637.1	0.60	0.90	1.20	0.36	0.030	0.089	0.119	0.593
2--3	1	0.12	21241.8	0.54	0.80	1.07	0.32	0.027	0.080	0.106	0.530
2--3	2,3(1)	0.12	21686.7	0.79	1.18	1.57	0.47	0.039	0.116	0.155	0.776
2--3	2,3(2)	0.12	12245.9	0.32	0.49	0.65	0.19	0.016	0.048	0.064	0.321
A--B	1	0.12	20160.0	0.54	0.80	1.07	0.32	0.026	0.079	0.106	0.529
A--B	2,3(1)	0.12	20688.4	0.55	0.83	1.11	0.33	0.027	0.082	0.109	0.546
A--B	2,3(2)	0.12	12245.9	0.43	0.64	0.85	0.26	0.021	0.063	0.084	0.420

(1), (2): See Figure B.4

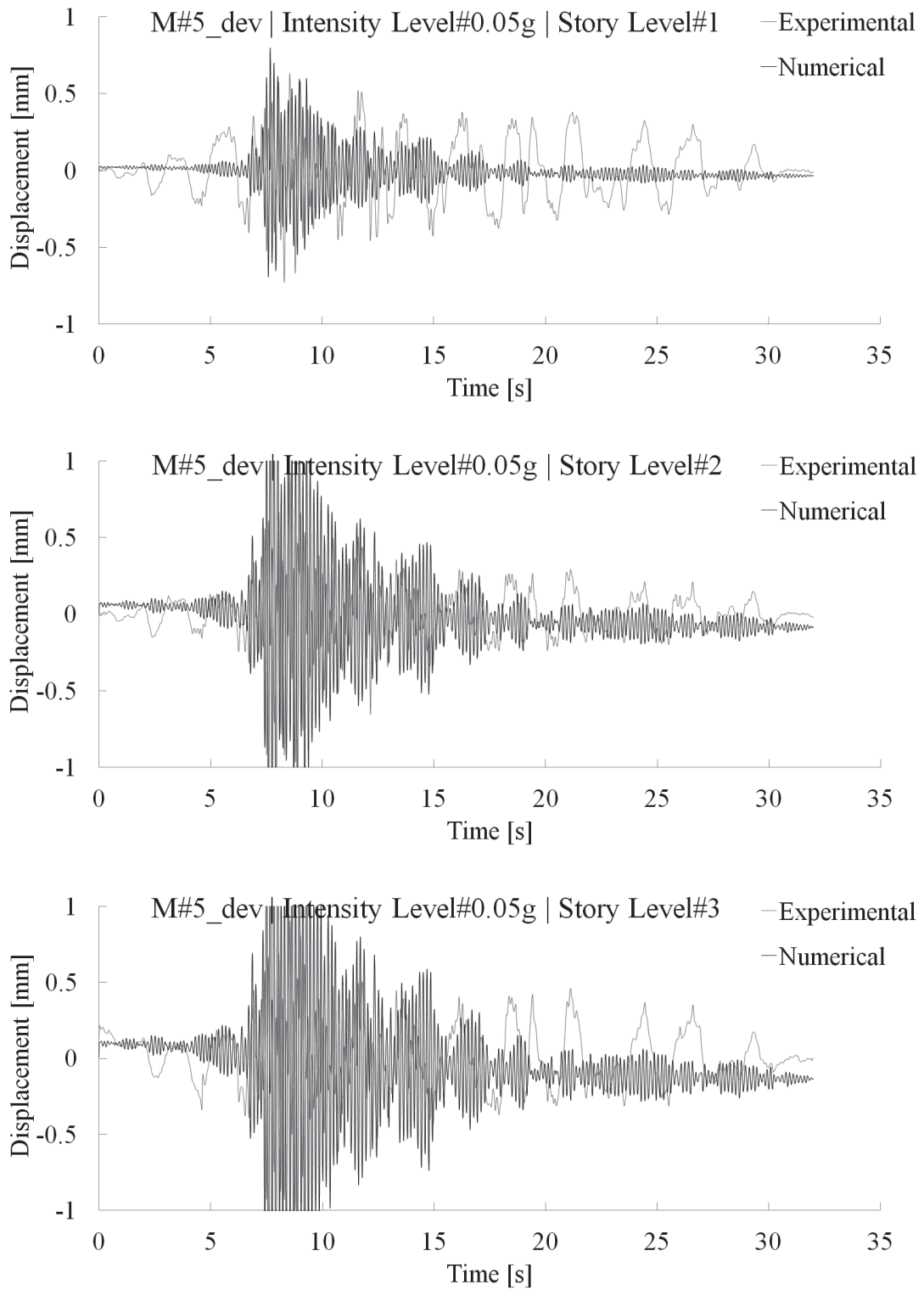


Figure E.40 Experimental/numerical (M#5_dev) time history displacement at different story levels for the structure tested at PGA=0.05g

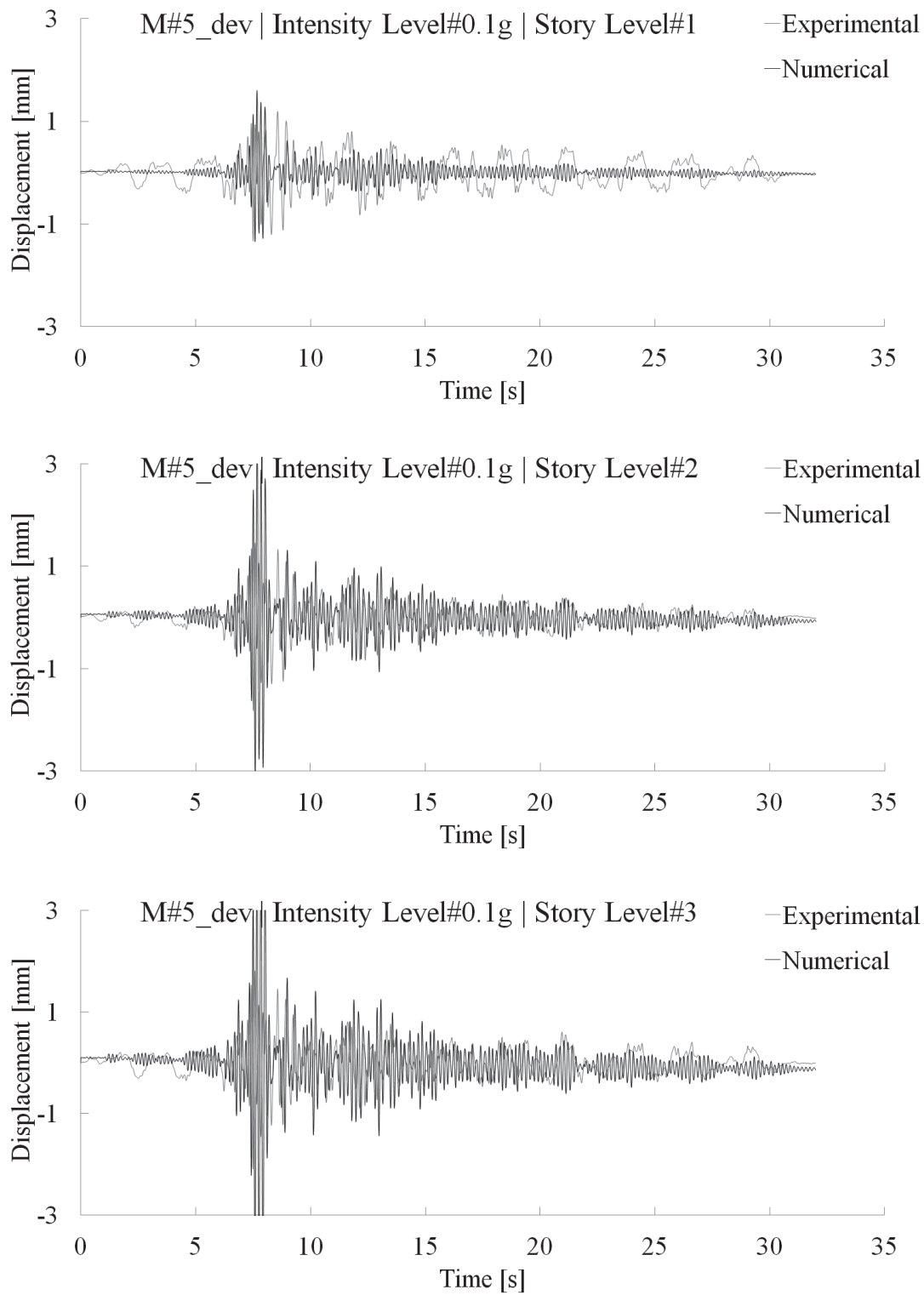


Figure E.41 Experimental/numerical (M#5_dev) time history displacement at different story levels for the structure tested at PGA=0.1g

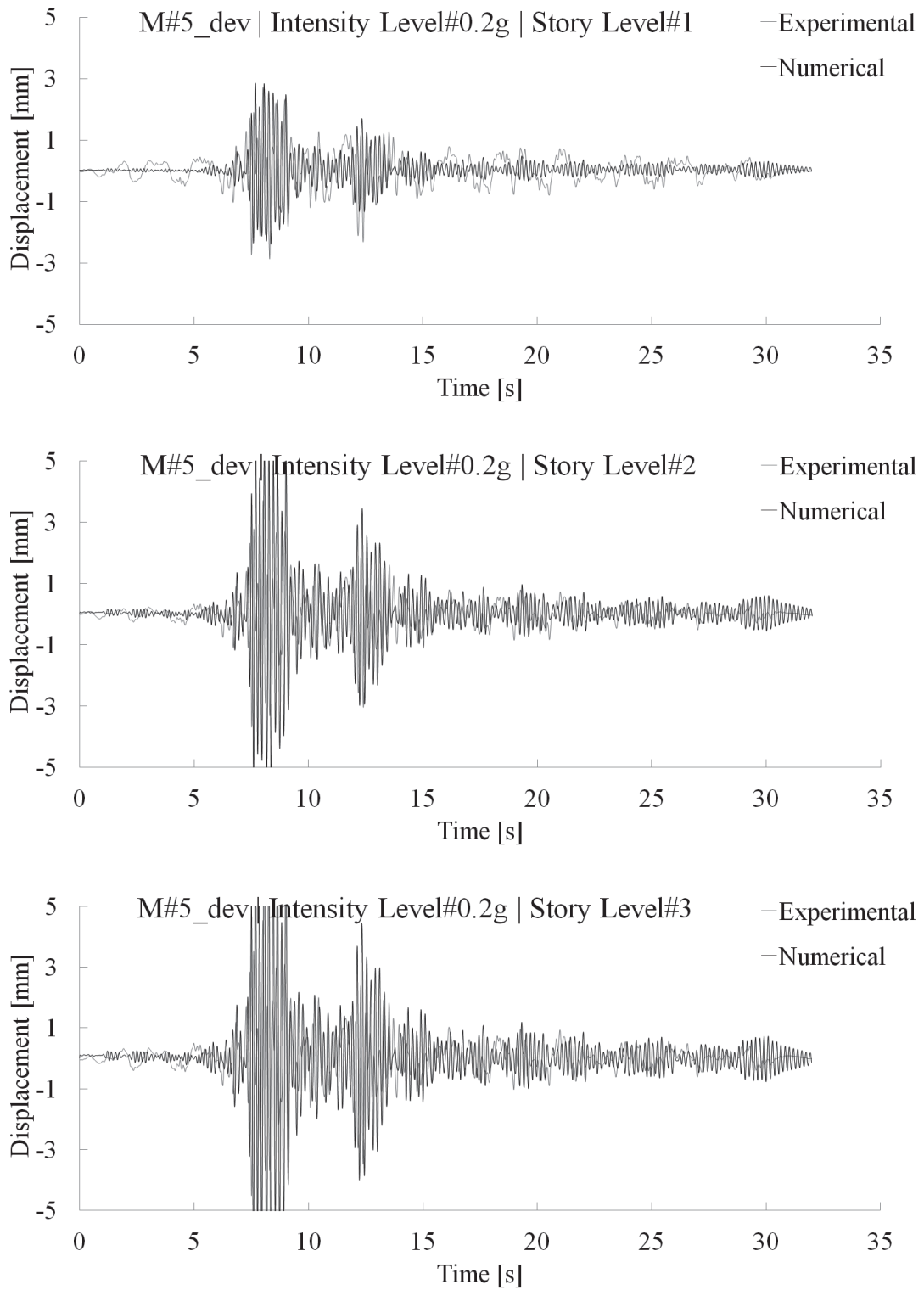


Figure E.42 Experimental/numerical (M#5_dev) time history displacement at different story levels for the structure tested at PGA=0.2g

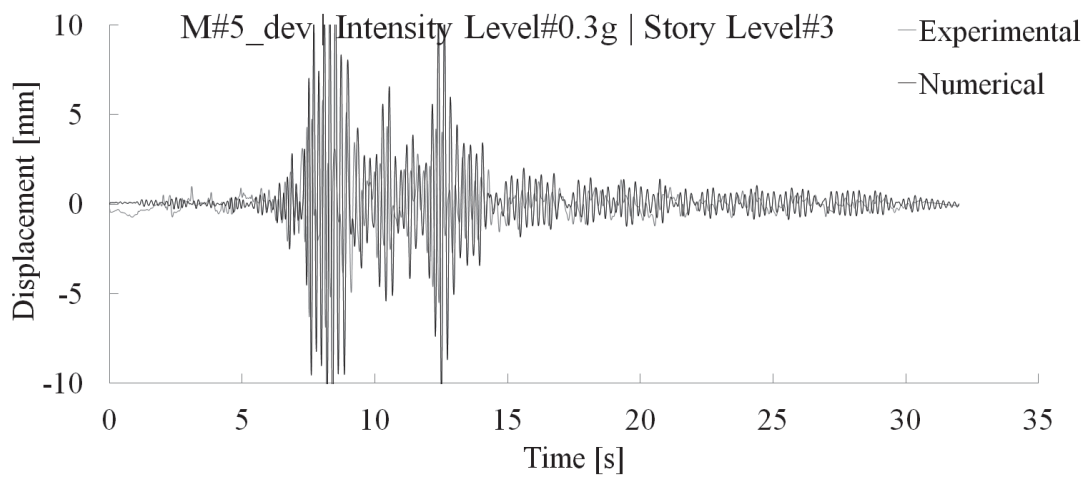
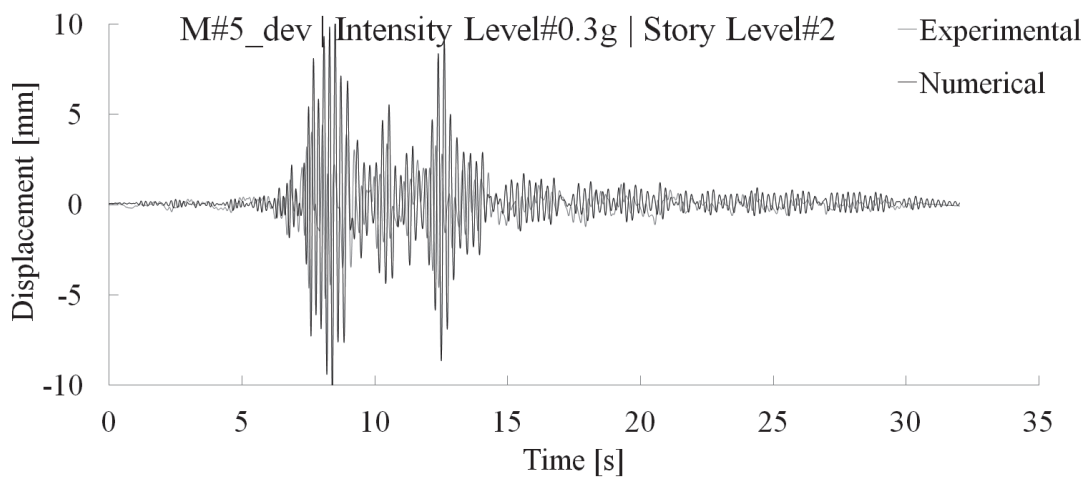
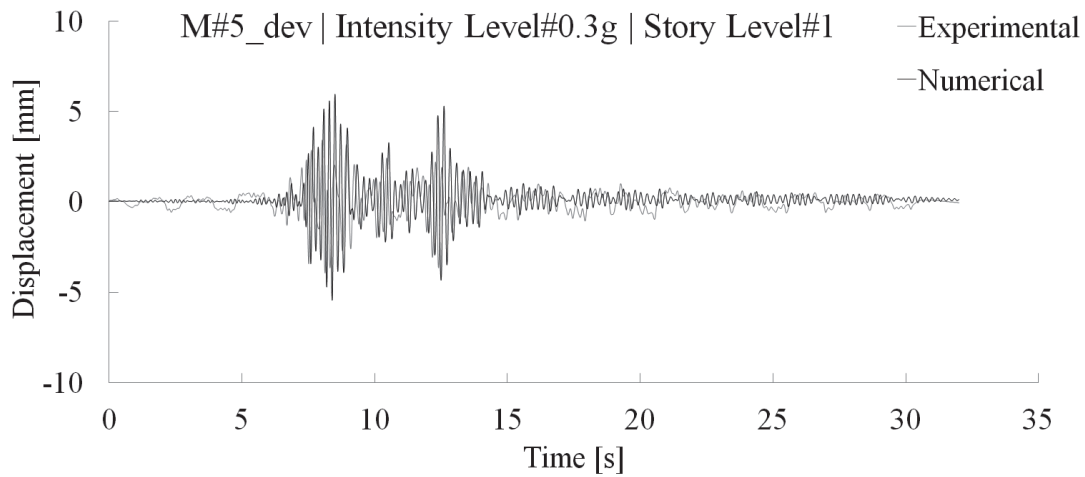


Figure E.43 Experimental/numerical (M#5_dev) time history displacement at different story levels for the structure tested at PGA=0.3g

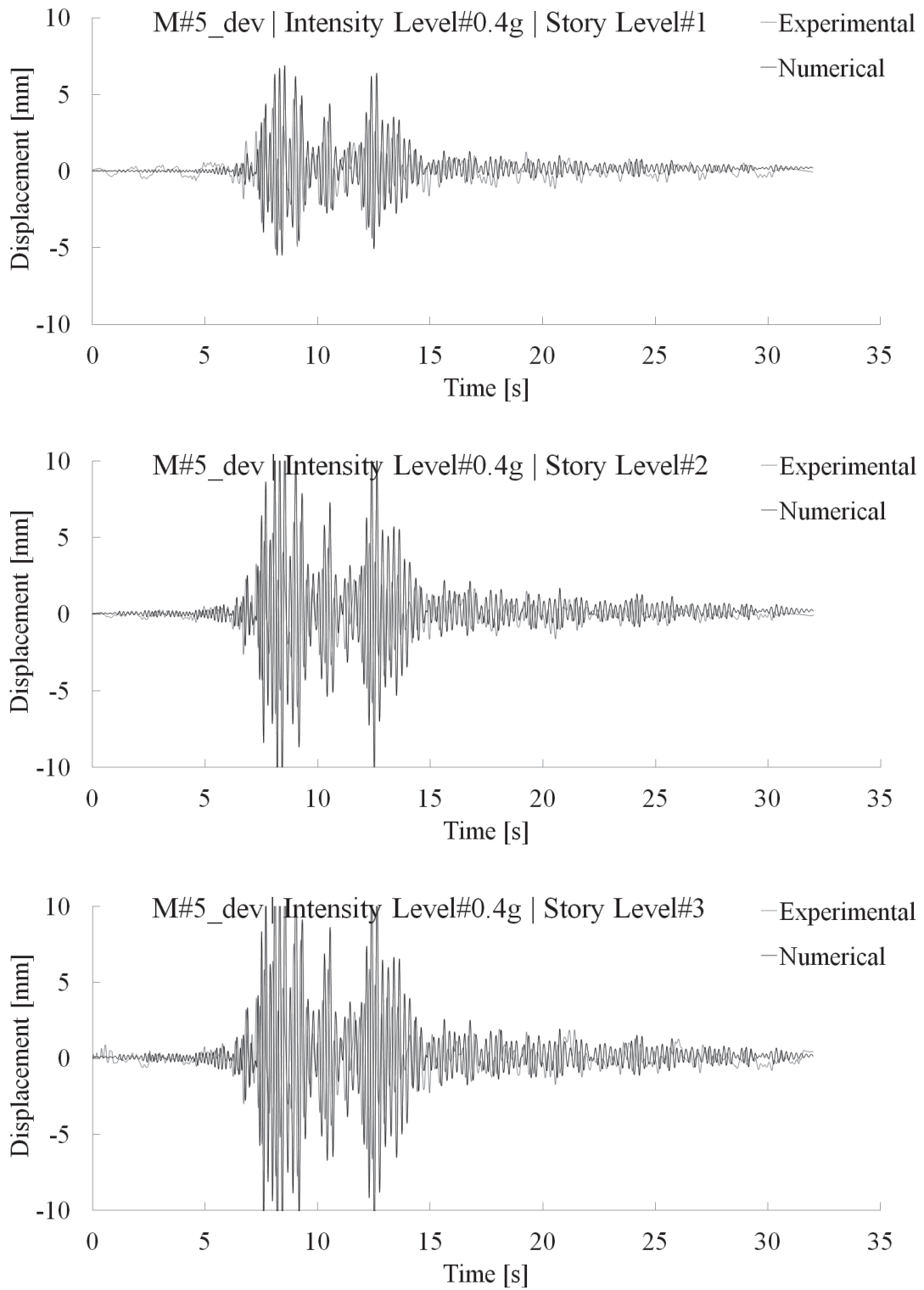


Figure E.44 Experimental/numerical (M#5_dev) time history displacement at different story levels for the structure tested at PGA=0.4g

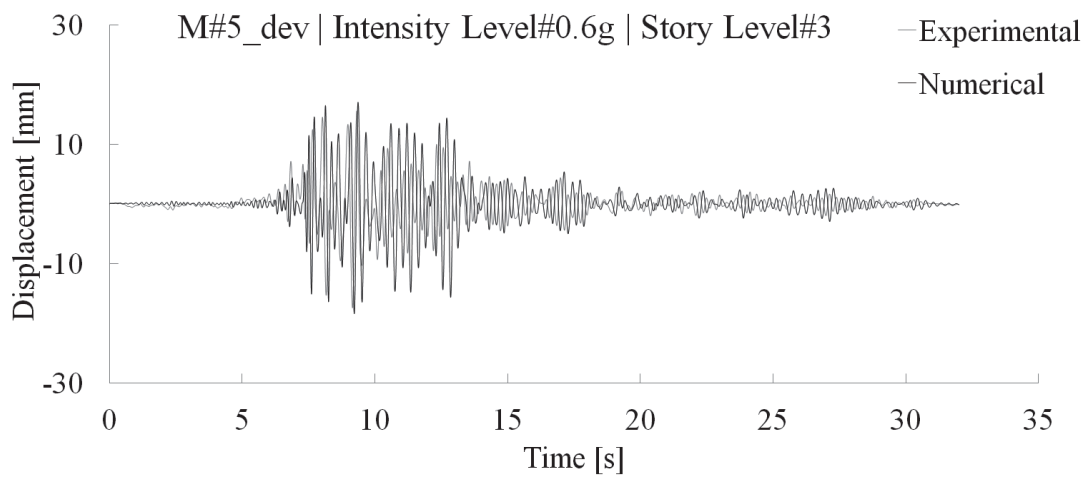
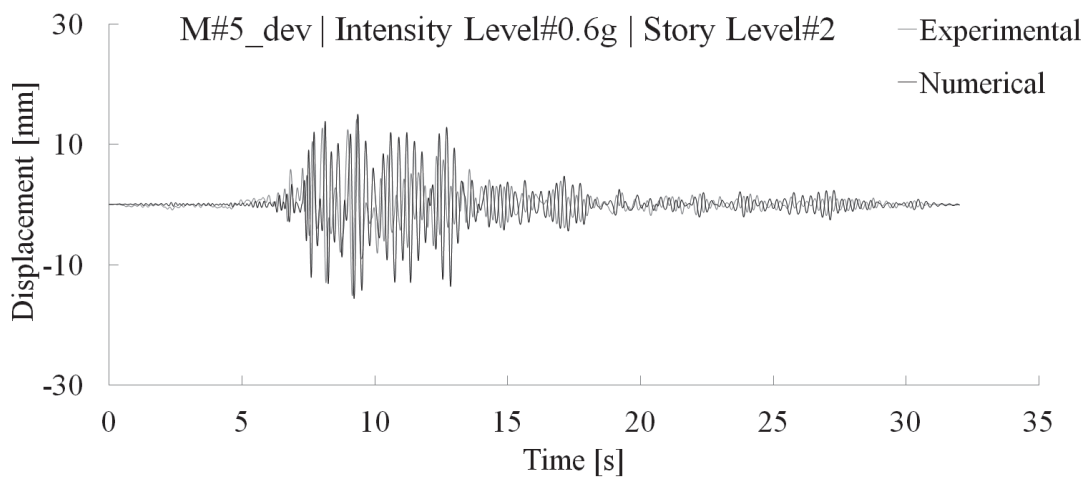
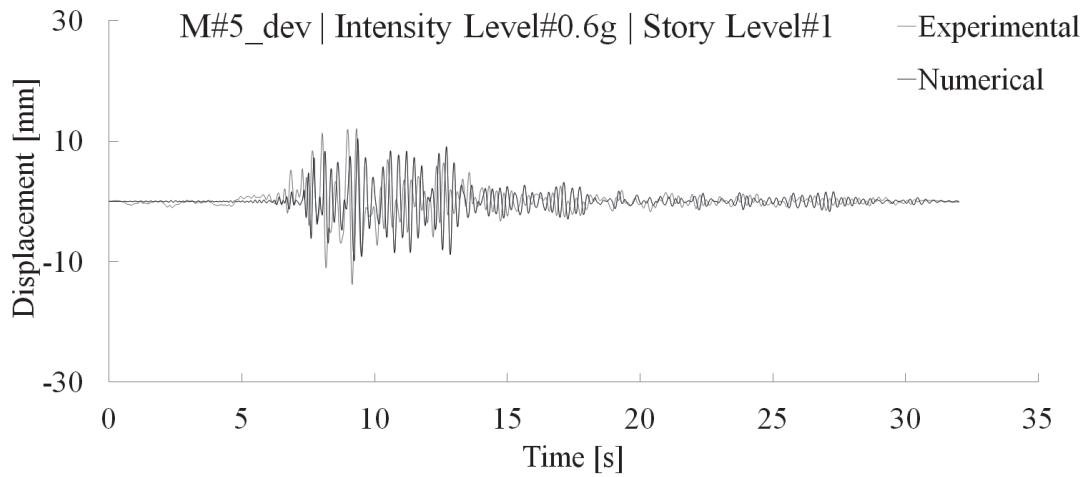


Figure E.45 Experimental/numerical (M#5_dev) time history displacement at different story levels for the structure tested at PGA=0.6g

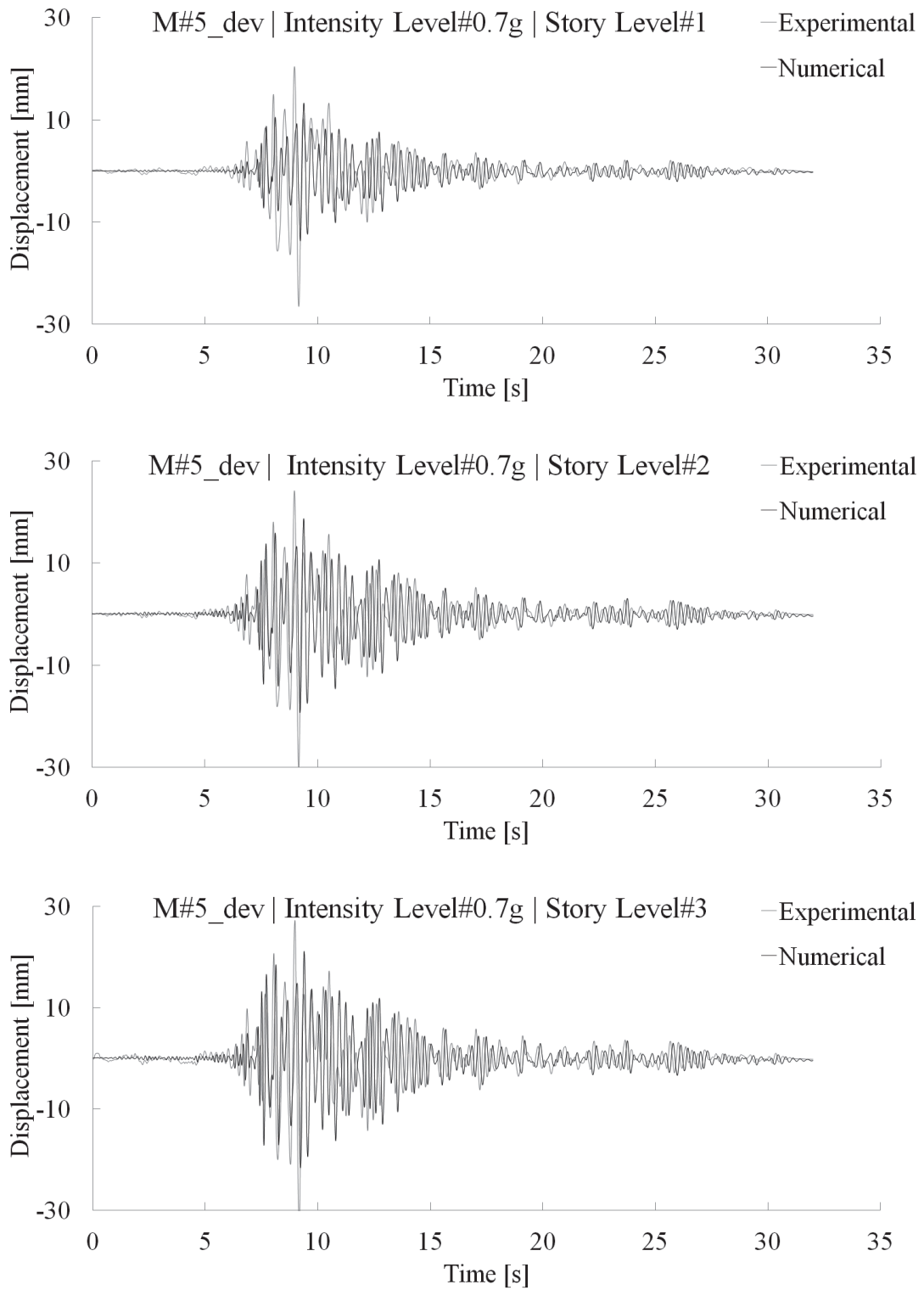


Figure E.46 Experimental/numerical (M#5_dev) time history displacement at different story levels for the structure tested at PGA=0.7g

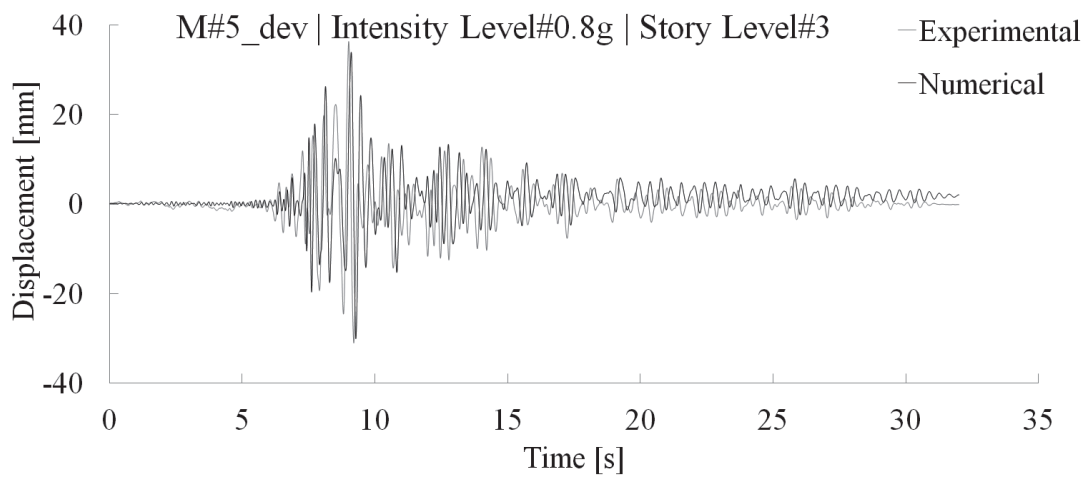
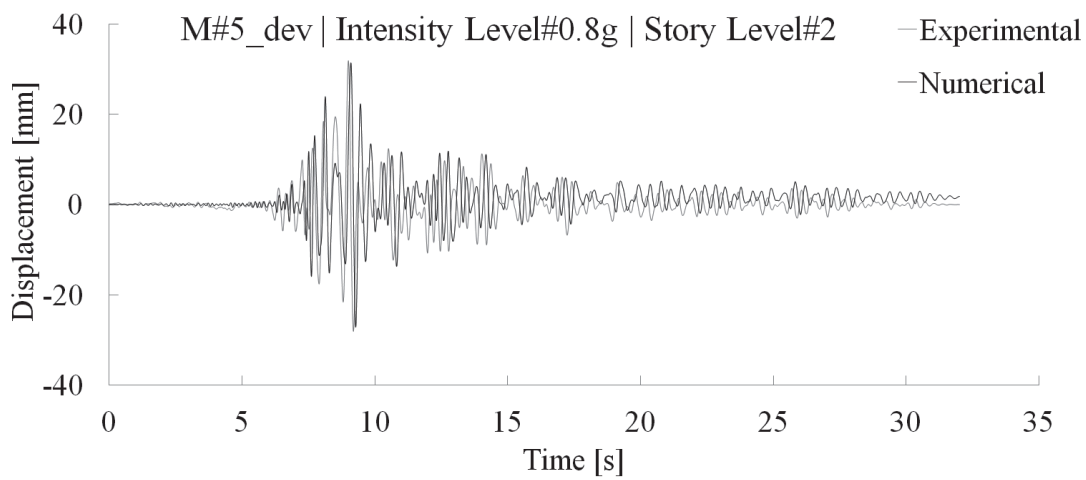
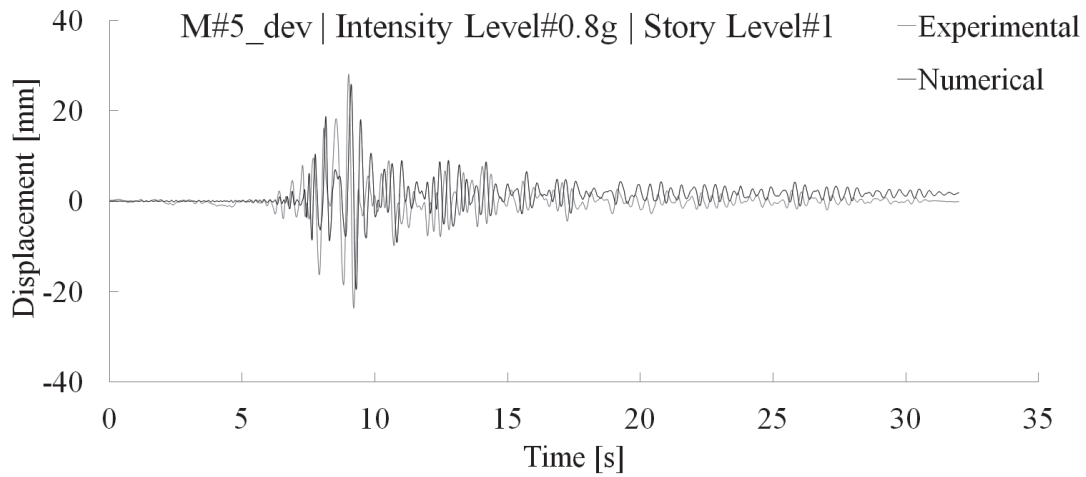


Figure E.47 Experimental/numerical (M#5_dev) time history displacement at different story levels for the structure tested at PGA=0.8g

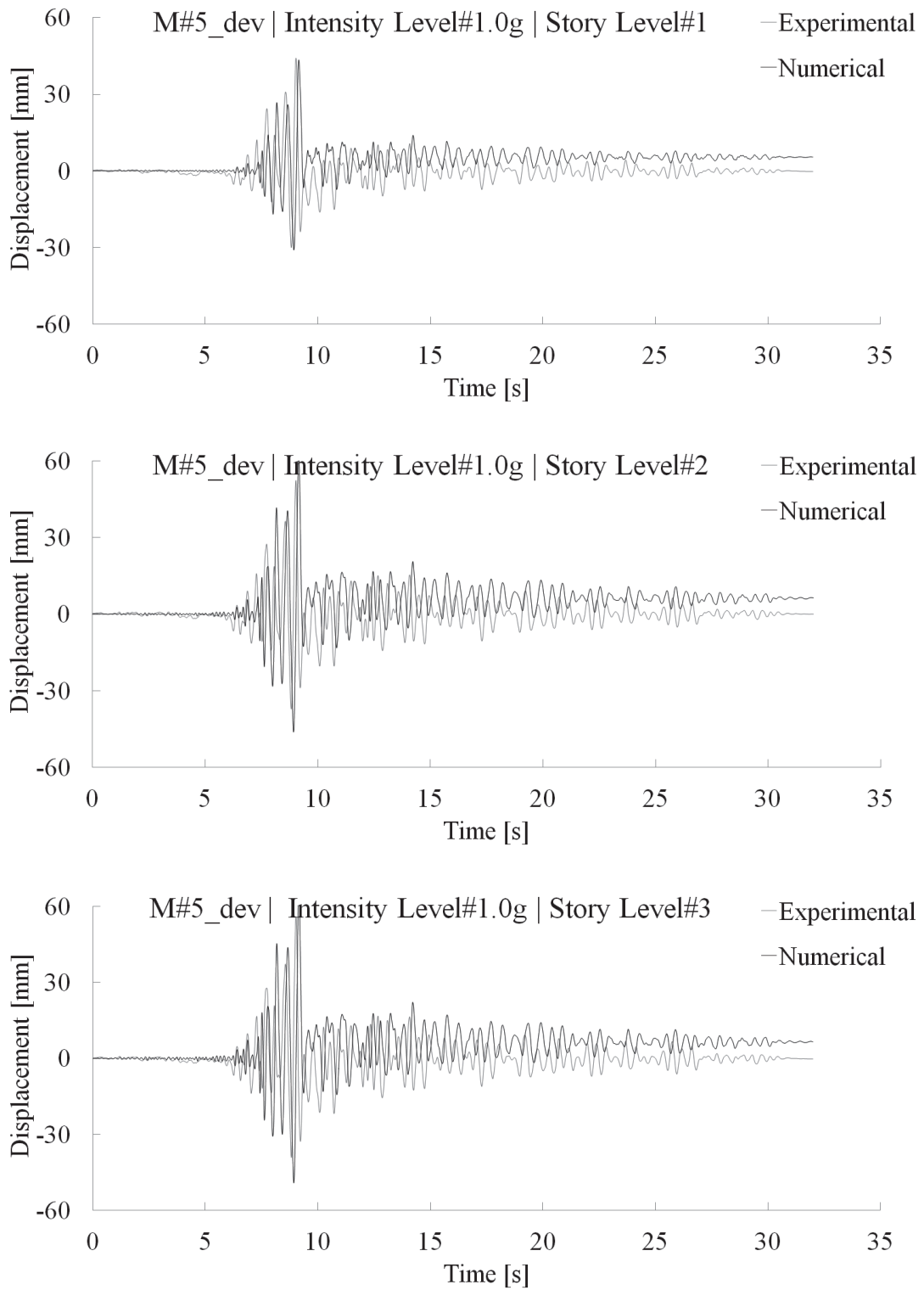


Figure E.48 Experimental/numerical (M#5_dev) time history displacement at different story levels for the structure tested at PGA=1.0g

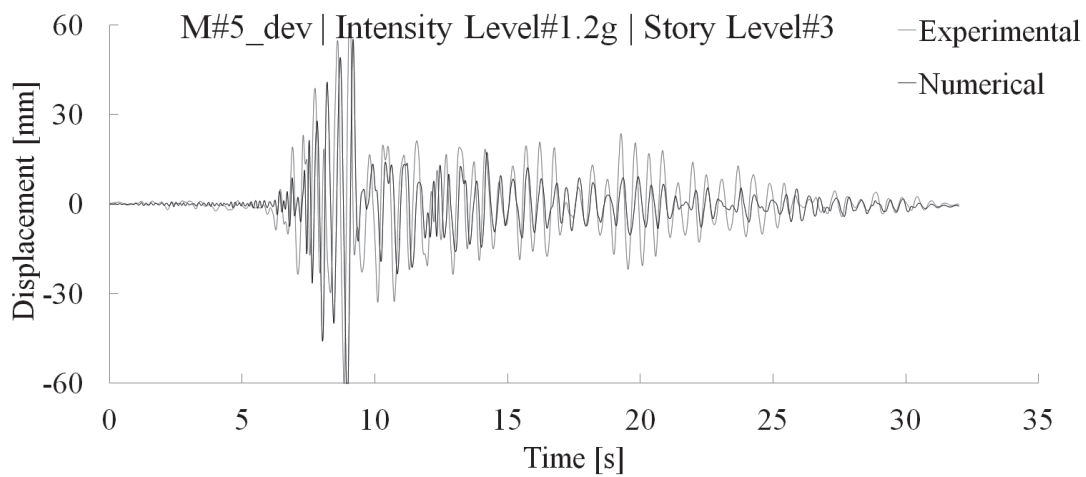
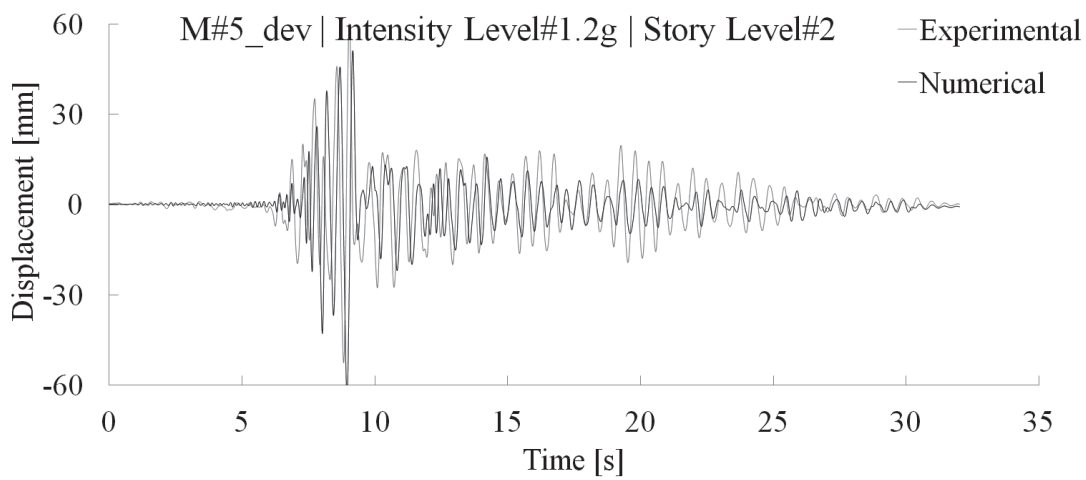
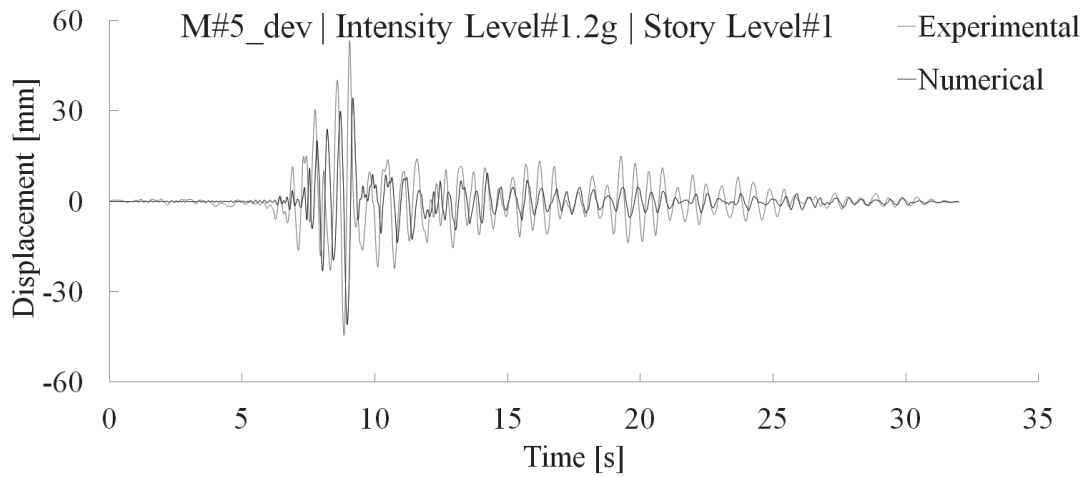
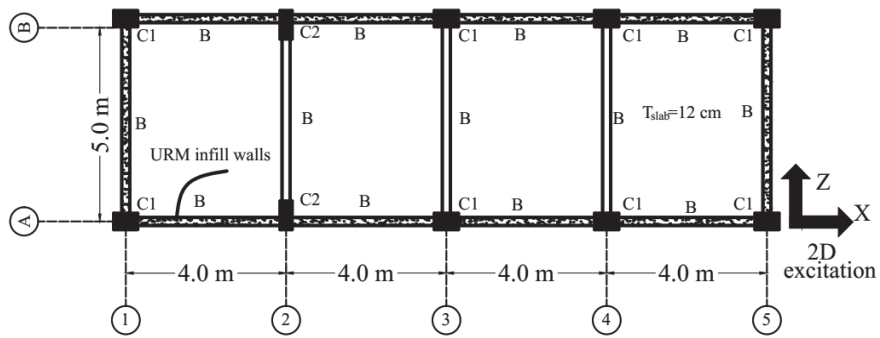


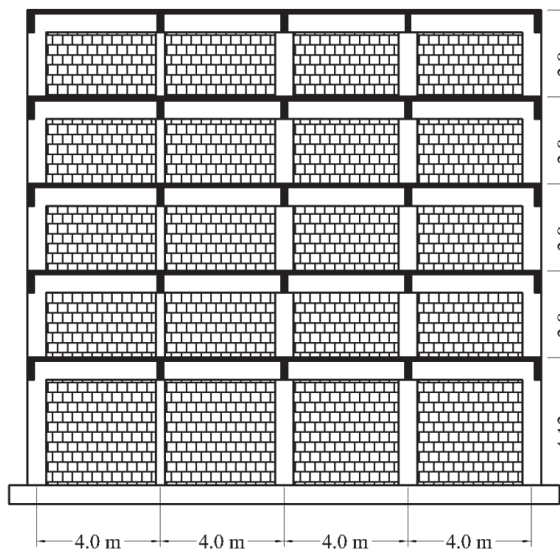
Figure E.49 Experimental/numerical (M#5_dev) time history displacement at different story levels for the structure tested at PGA=1.2g

Appendix F: Application to 3D Multi-Story Structures

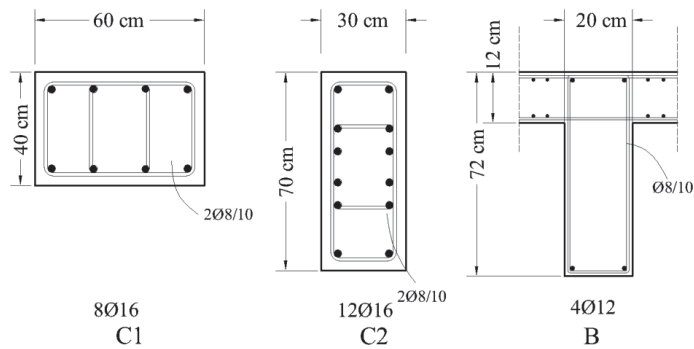
F.1 Structural Layouts (Case Study 1)



a)



b)



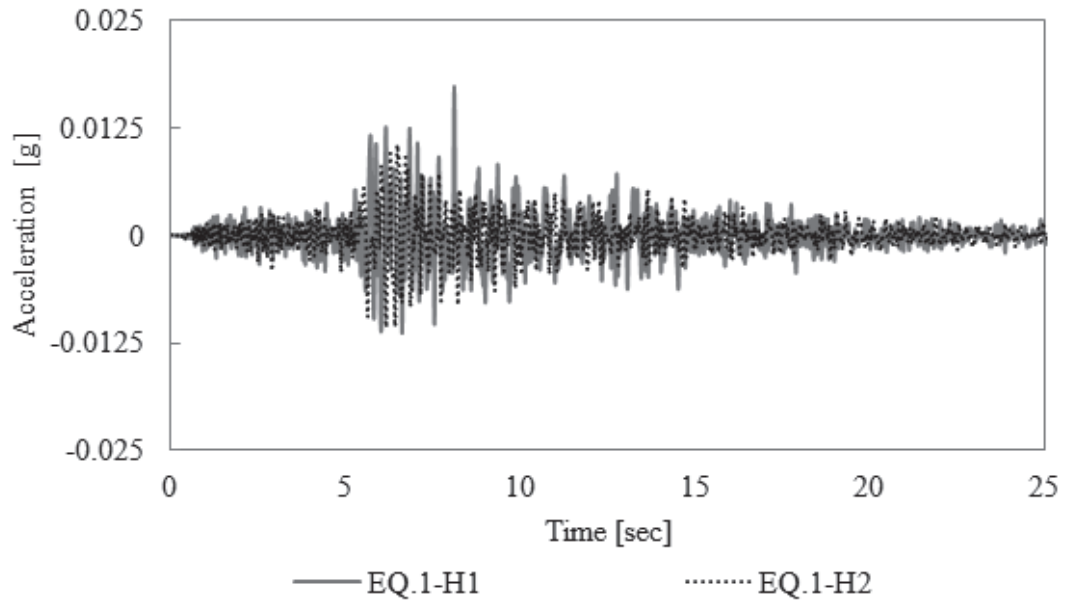
c)

Figure F.1 Case study 1 structure: a) plane layout, b) elevation view, c) cross sections

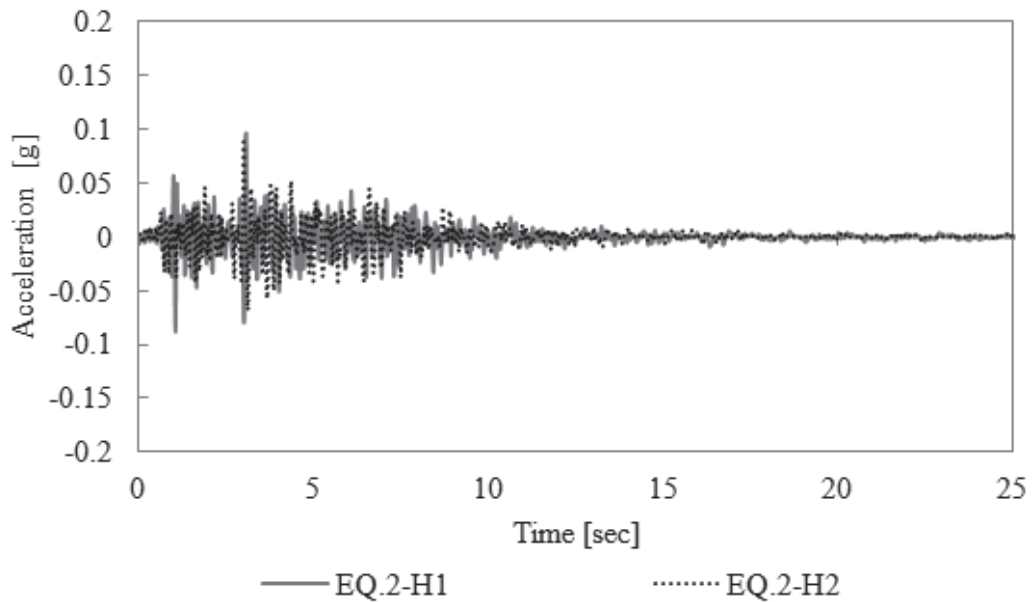
F.2 Seismic Action Based on German Code

Table F.1 Selected ground motions for case study 1 (*Schwarz et al., 2017, 2018*)

Record No.	Soil Type	Earthquake Name	Date	Time	Station	Component	M	R [km]	PGA [g]
1	A-R	Big Bear City	22.02.2003	12:19	White Water Canyon Troutfarm (110)	H1 H2	5.2	40	0.0173 0.0107
2	B-R	Morgan Hill	24.04.1984	21:15	Gilroy Gavilan College (5)	H1 H2	6.1	17	0.0968 0.0876
3	C-R	Yorba Linda	03.09.2002	07:08	Riverside Van Buren (76)	H1 H2	4.8	31	0.011 0.014
4	B-T	San Simeon	22.12.2003	19:16	San Luis Obispo CRC (196)	H1 H2	6.5	29	0.165 0.116
5	C-T	Greater LA	16.06.2005	20:53	Riverside I215 (73)	H1 H2	4.9	32	0.044 0.050
6	B-S	Coyote Lake	06.08.1979	17:05	Gilroy Array Station 3 (42)	H1 H2	5.9	1	0.25 0.26
7	C-S	San Juan Bautista	12.08.1998	14:10	Hollister City Hall Annex (43)	H1 H2	5.2	12	0.034 0.063

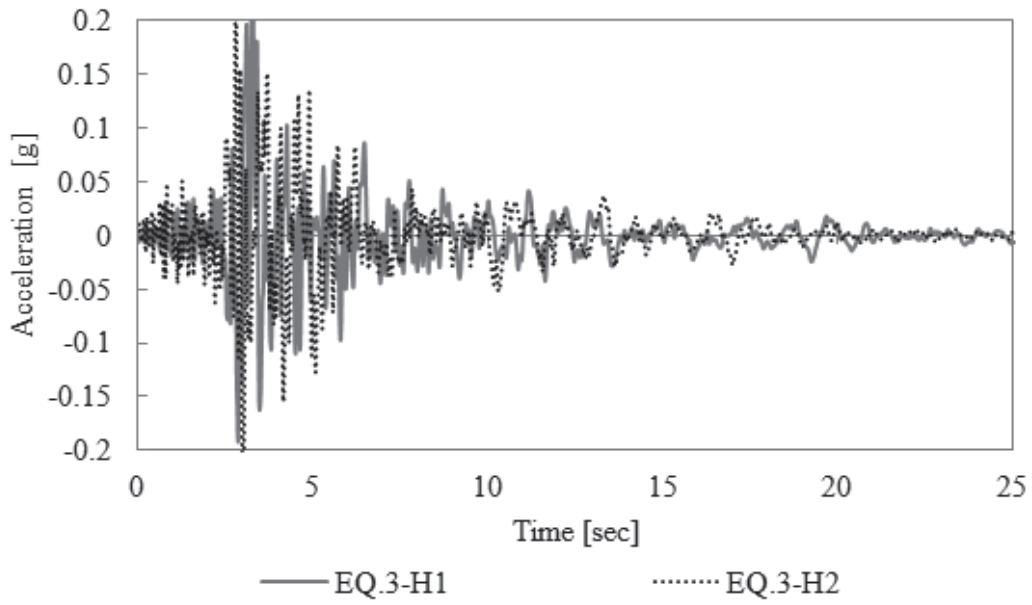


a) H1 & H2 components of EQ.1 recorded on soil type (A-R)

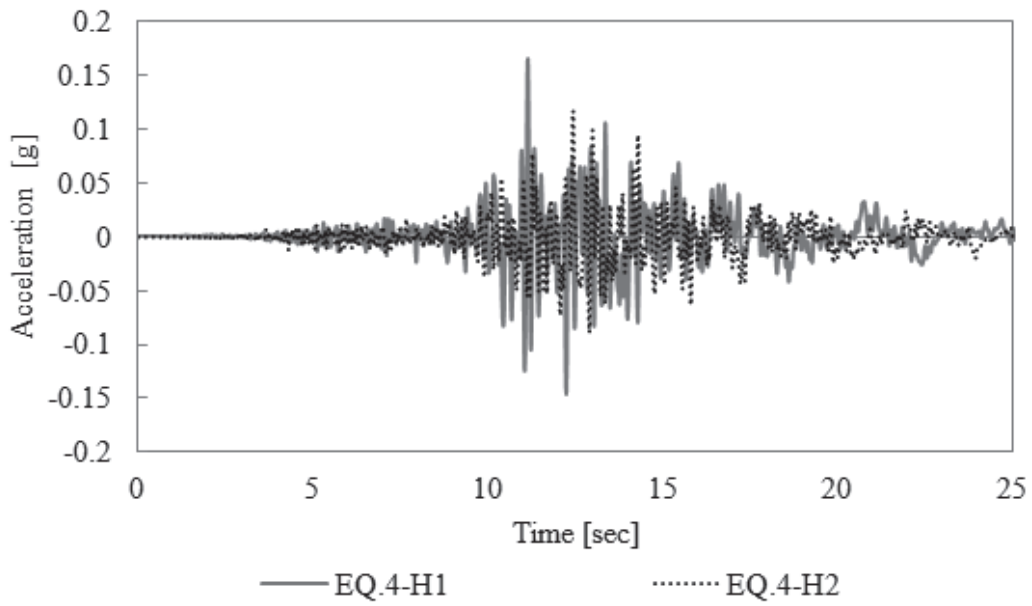


b) H1 & H2 components of EQ.2 recorded on soil type (B-R)

Figure F.2 Respective time history records of the considered seismic action (case study 1)

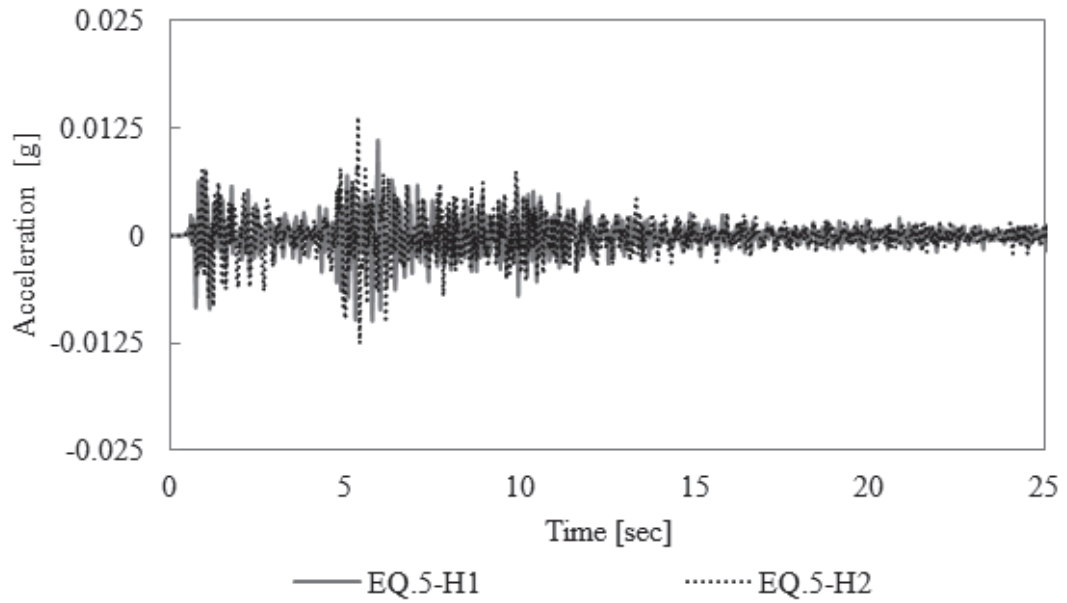


c) H1 & H2 components of EQ.3 recorded on soil type (B-S)

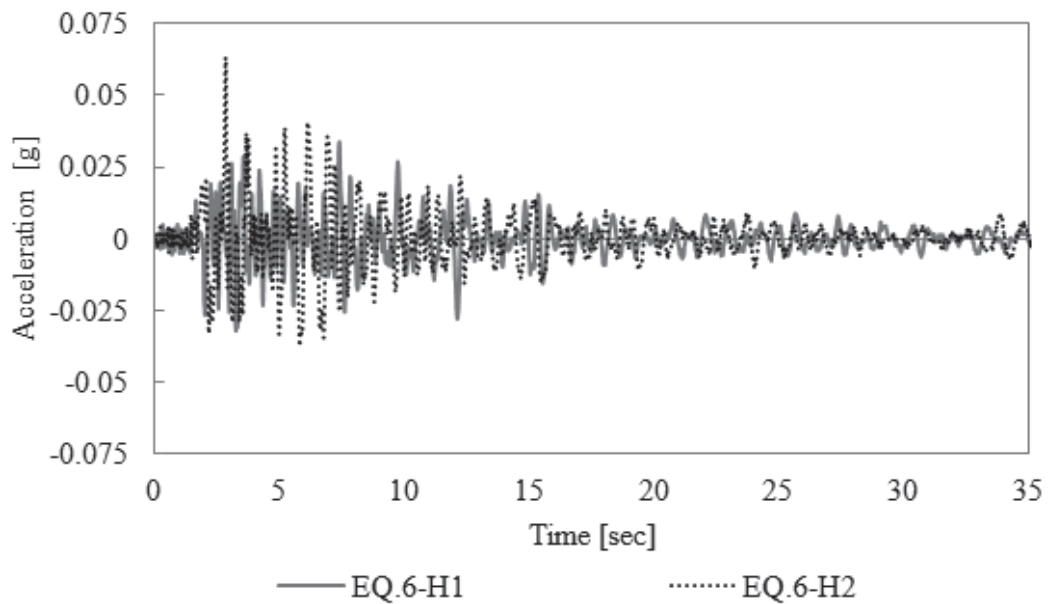


d) H1 & H2 components of EQ.4 recorded on soil type (B-T)

Figure F.2 Respective time history records of the considered seismic action (case study 1) (continued)

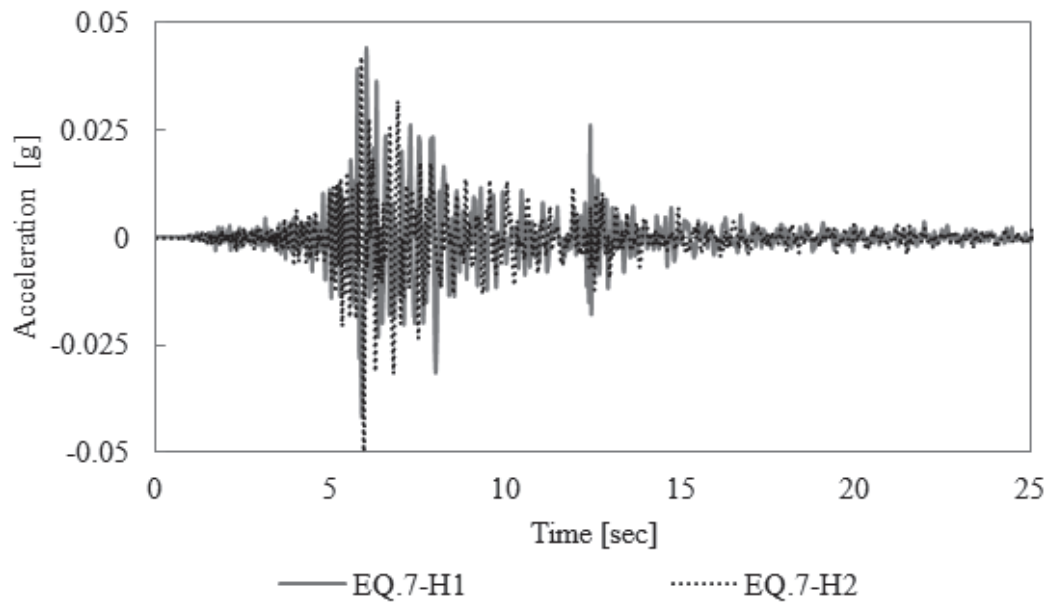


e) H1 & H2 components of EQ.5 recorded on soil type (C-R)



f) H1 & H2 components of EQ.6 recorded on soil type (C-S)

Figure F.2 Respective time history records of the considered seismic action (case study 1) (continued)



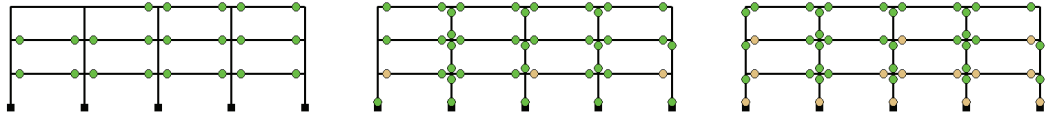
g) H1 & H2 components of EQ.7 recorded on soil type (C-T)

Figure F.2 Respective time history records of the considered seismic action (case study 1) (continued)

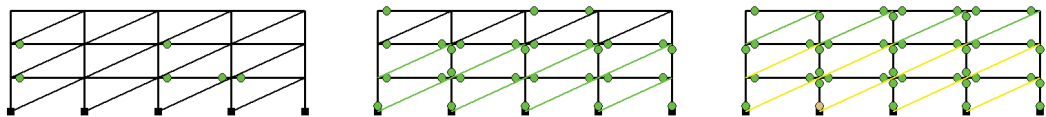
Table F.2 Predicted damage and interstory drift

EQ.1		Soil type (A-R)	
0.1g	0.3g	0.5g	

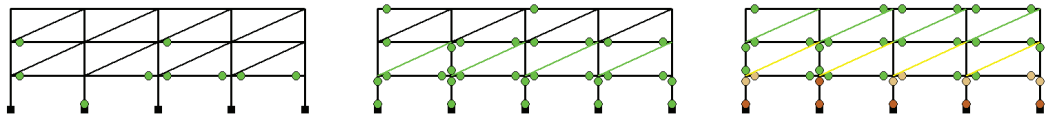
3 Story Model Frame



Model BR



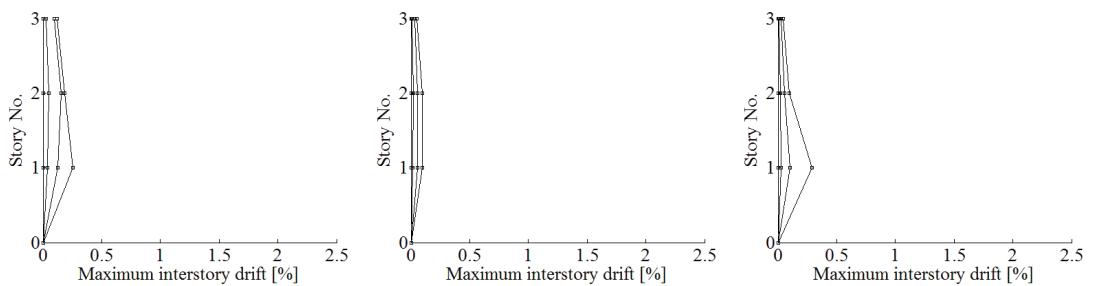
Model FI



Model SS



Interstory drift according to EQ.1



Model BR

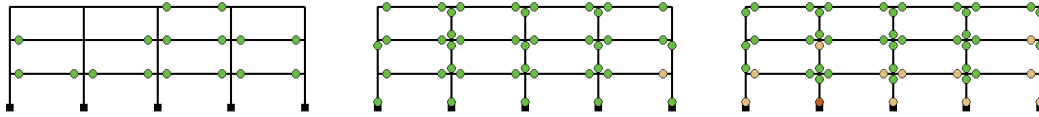
Model FI

Model SS

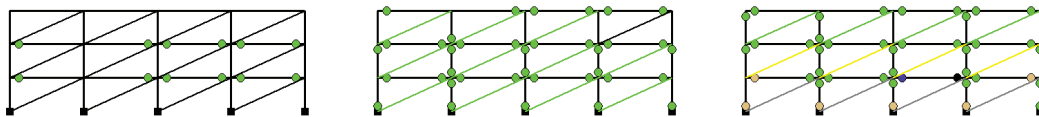
Table F.2 Predicted damage and interstory drift (continued)

EQ.2		Soil type (B-R)	
0.1g	0.3g	0.5g	

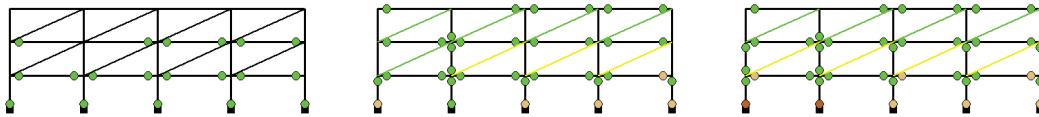
3 Story Model Frame



Model BR



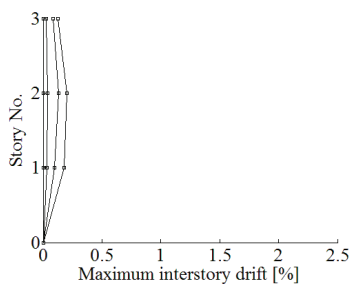
Model FI



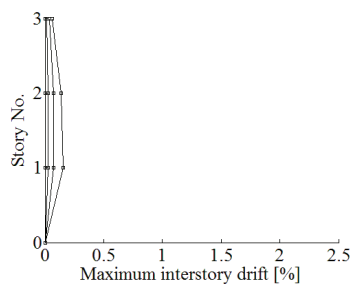
Model SS



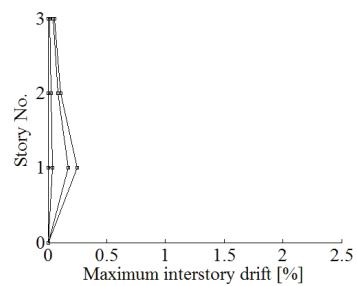
Interstory drift according to EQ.2



Model BR



Model FI



Model S

Table F.2 Predicted damage and interstory drift (continued)

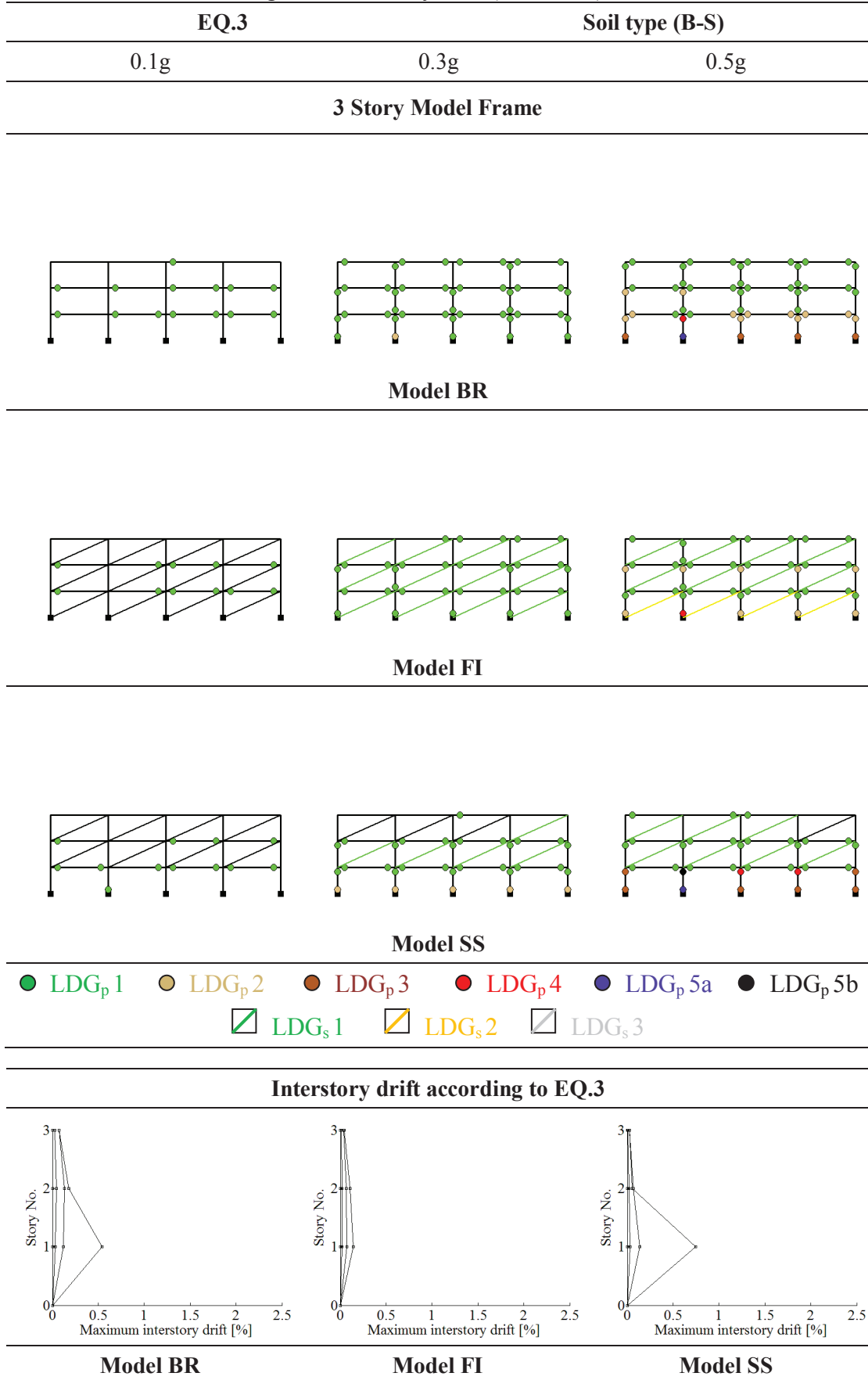
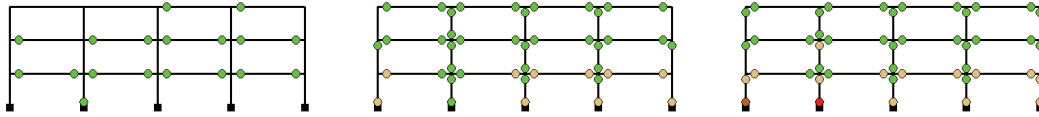


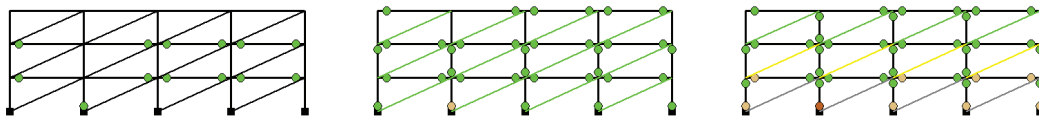
Table F.2 Predicted damage and interstory drift (continued)

EQ.4		Soil type (B-T)	
0.1g	0.3g	0.5g	

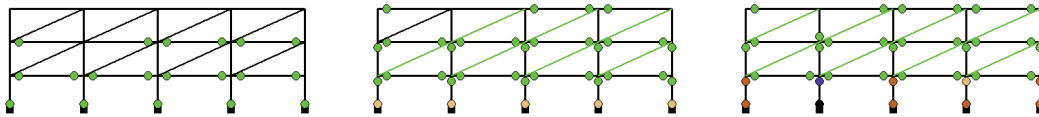
3 Story Model Frame



Model BR



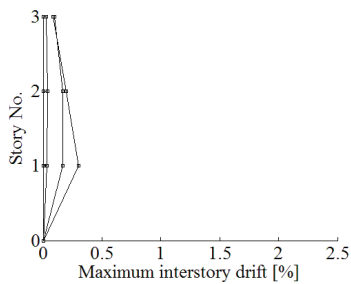
Model FI



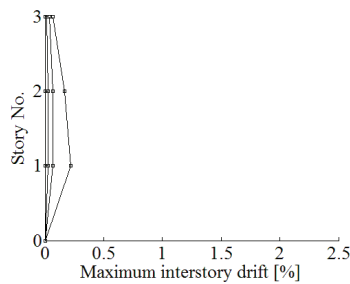
Model SS



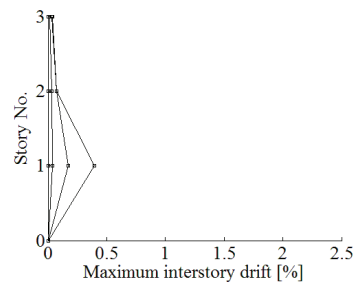
Interstory drift according to EQ.4



Model BR



Model FI



Model SS

Table F.2 Predicted damage and interstory drift (continued)

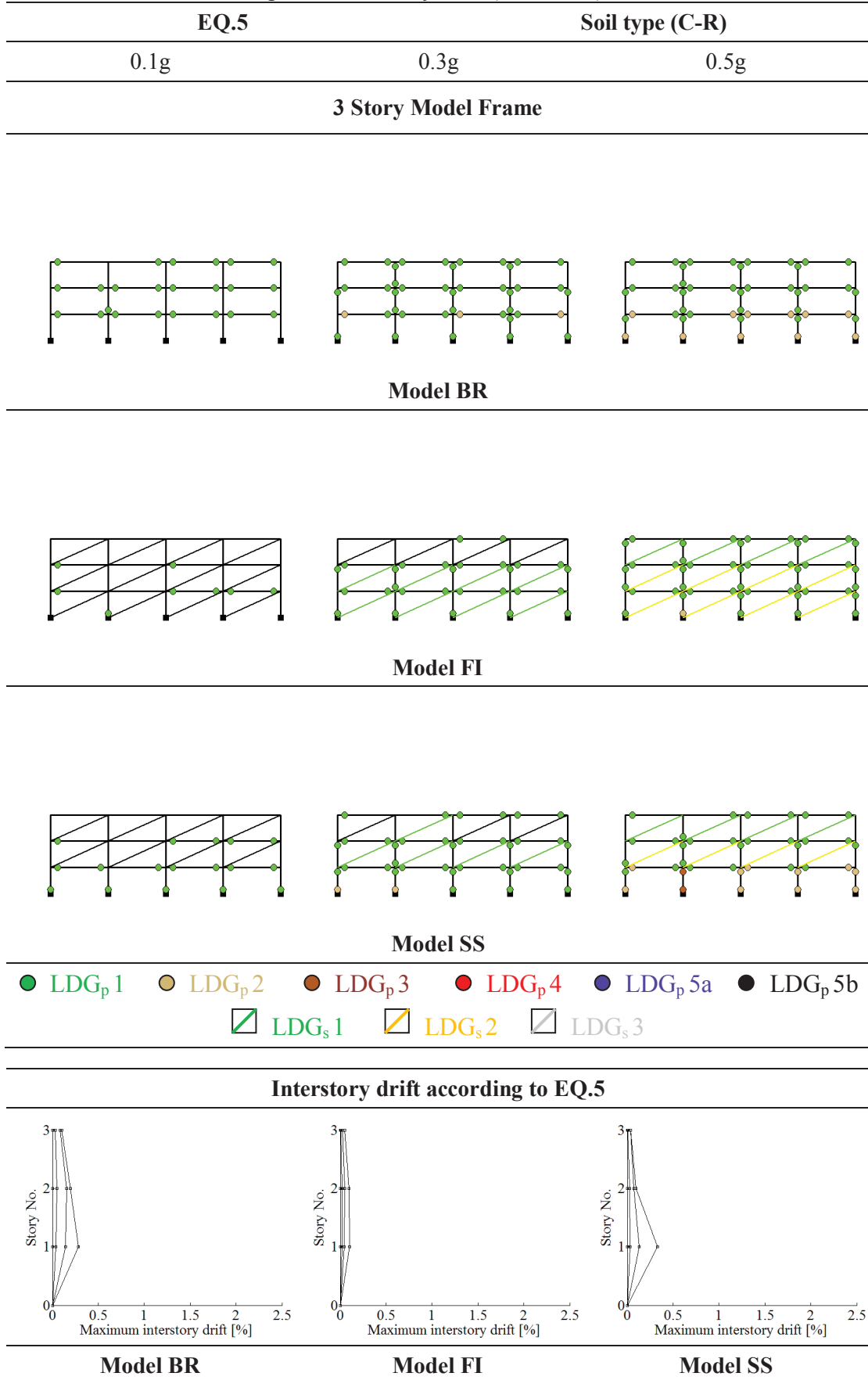
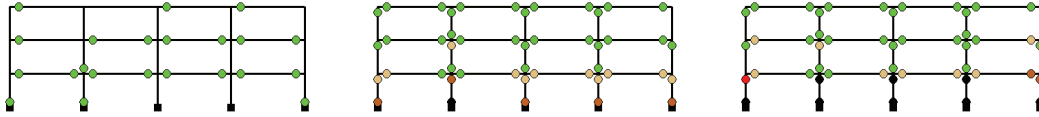


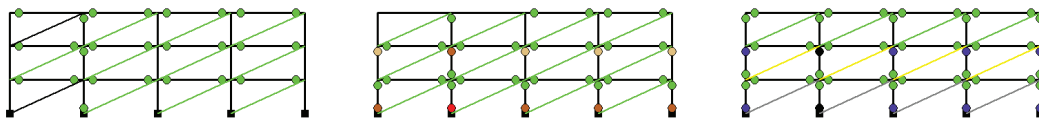
Table F.2 Predicted damage and interstory drift (continued)

EQ.6		Soil type (C-S)	
0.1g	0.3g	0.5g	

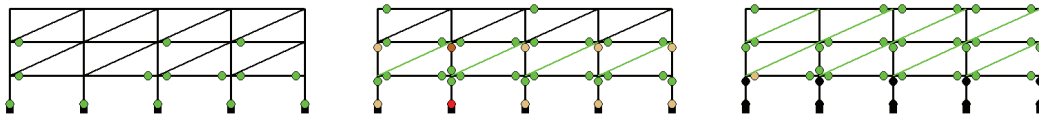
3 Story Model Frame



Model BR



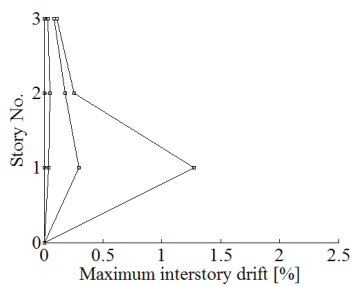
Model FI



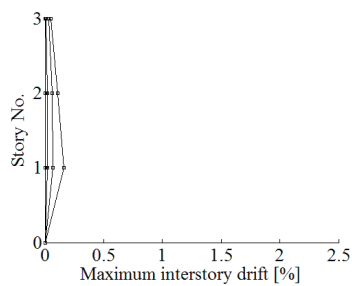
Model SS



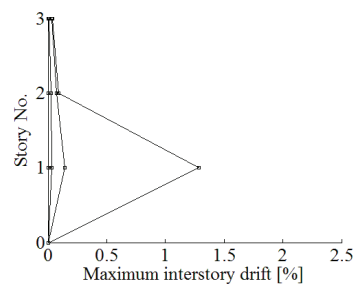
Interstory drift according to EQ.6



Model BR



Model FI



Model SS

Table F.2 Predicted damage and interstory drift (continued)

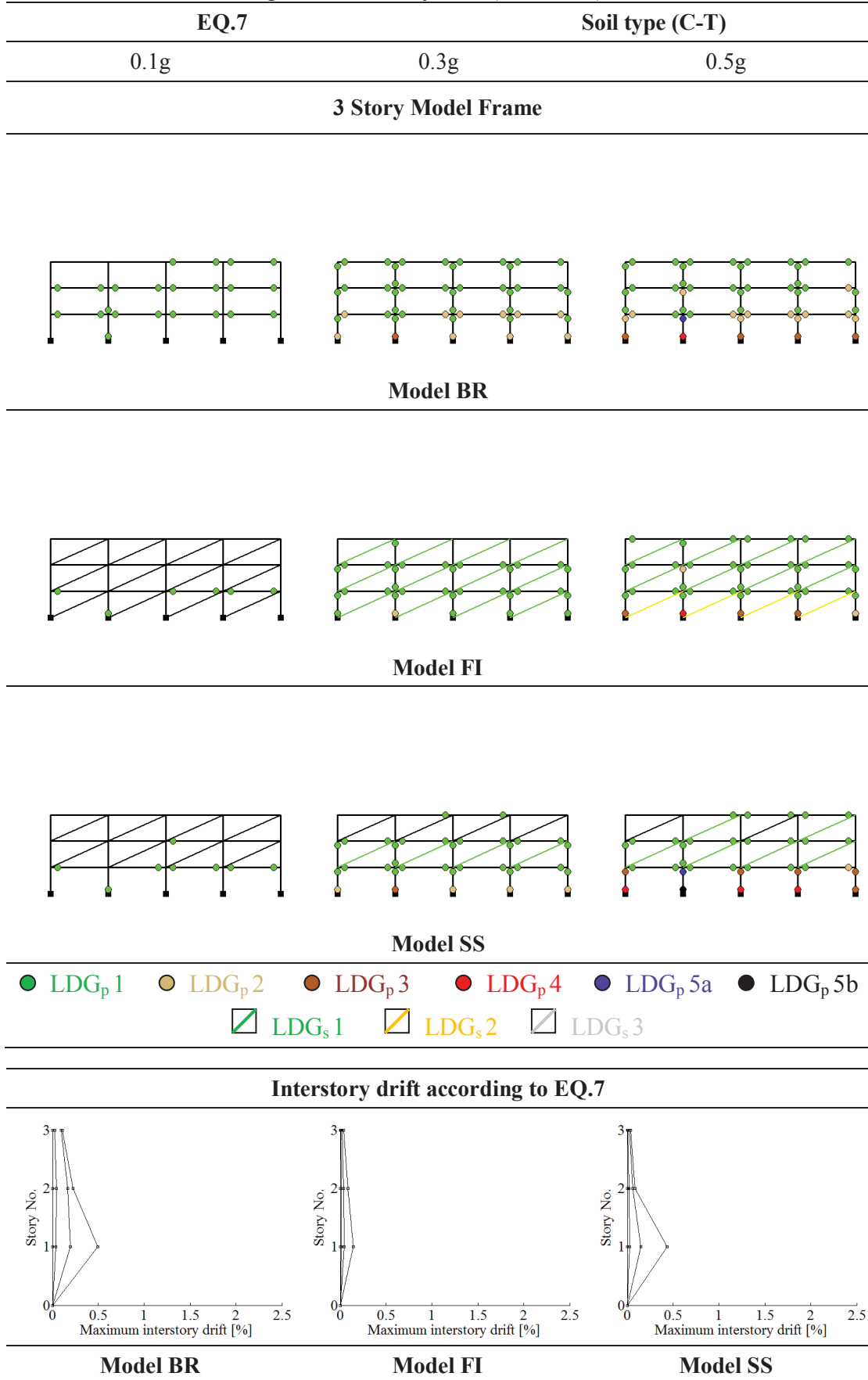
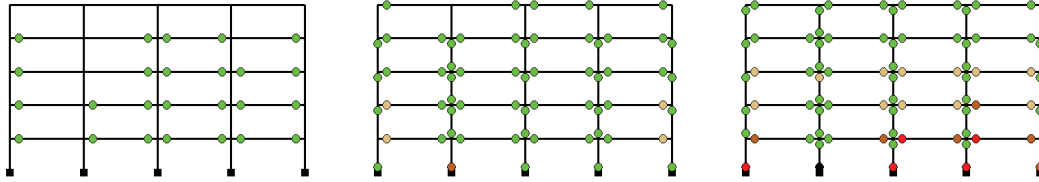


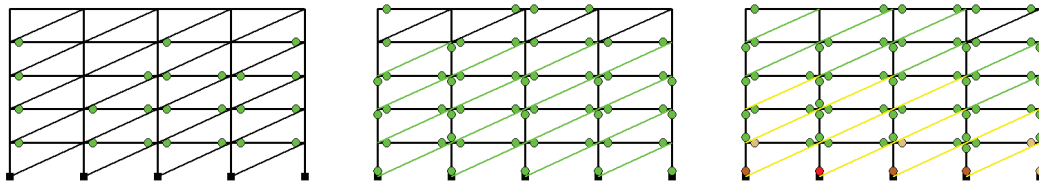
Table F.2 Predicted damage and interstory drift (continued)

EQ.1		Soil type (A-R)	
0.1g	0.3g	0.5g	

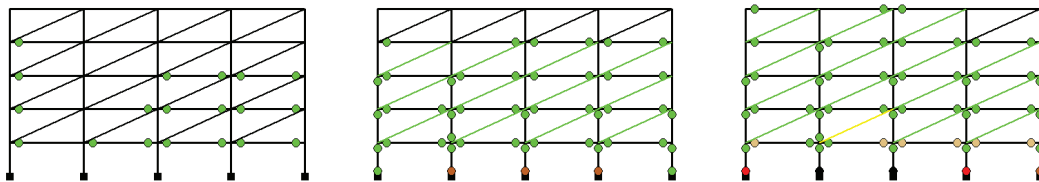
5 Story Model Frame



Model BR



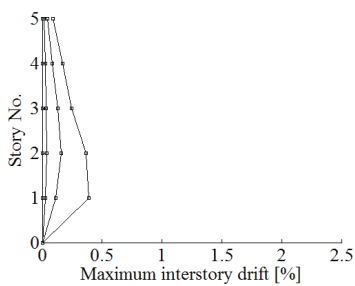
Model FI



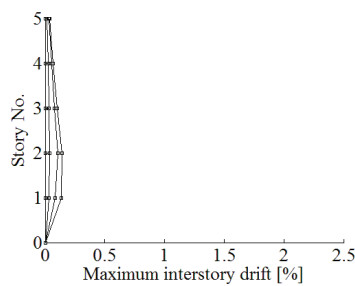
Model SS



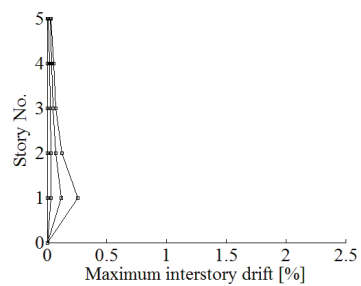
Interstory drift according to EQ.1



Model BR



Model FI

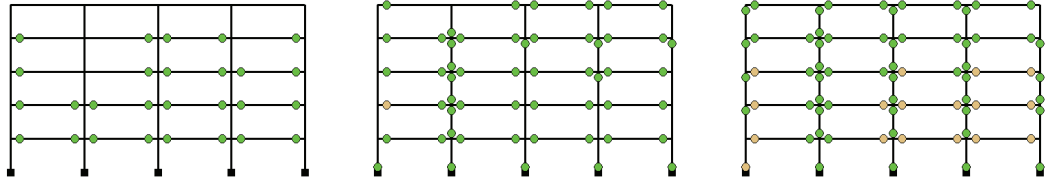


Model SS

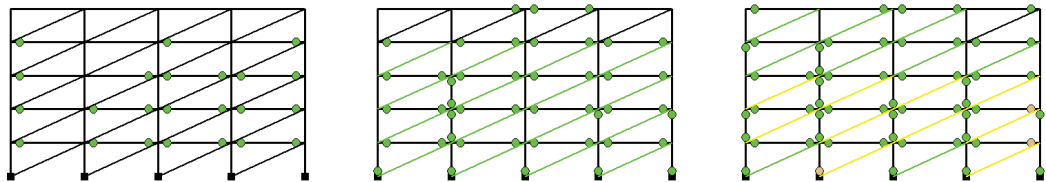
Table F.2 Predicted damage and interstory drift (continued)

EQ.2		Soil type (B-R)	
0.1g	0.3g	0.5g	

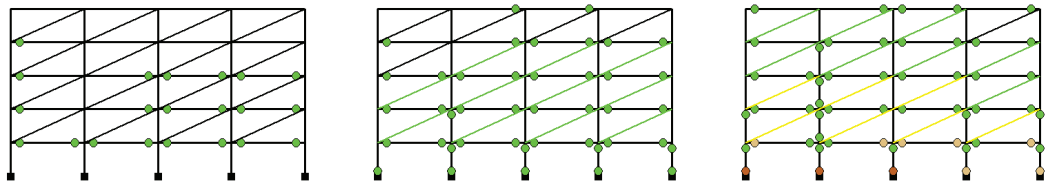
5 Story Model Frame



Model BR



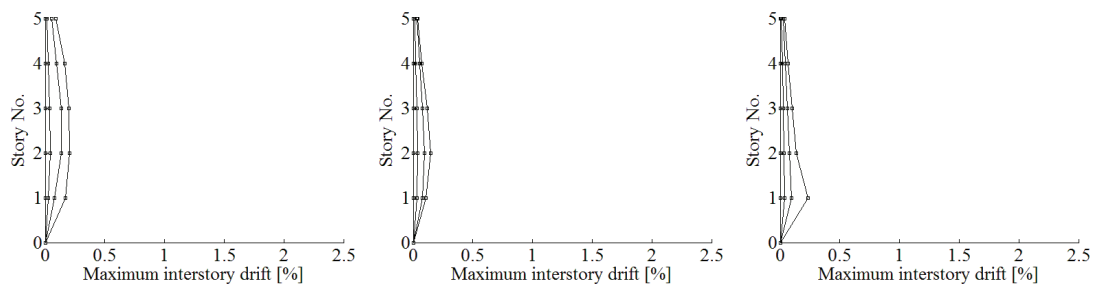
Model FI



Model SS



Interstory drift according to EQ.2



Model BR

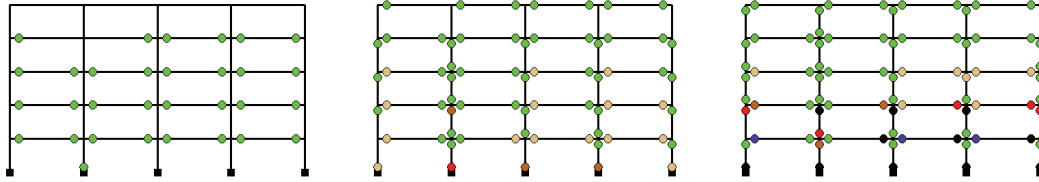
Model FI

Model SS

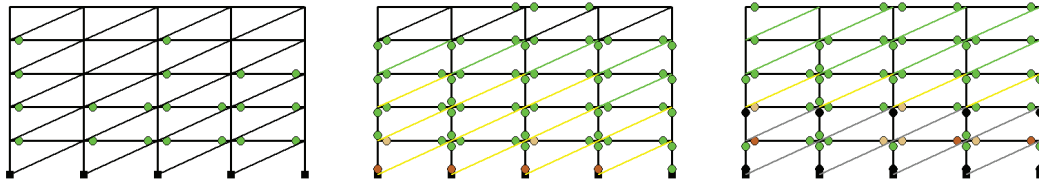
Table F.2 Predicted damage and interstory drift (continued)

EQ.3		Soil type (B-S)	
0.1g	0.3g	0.5g	

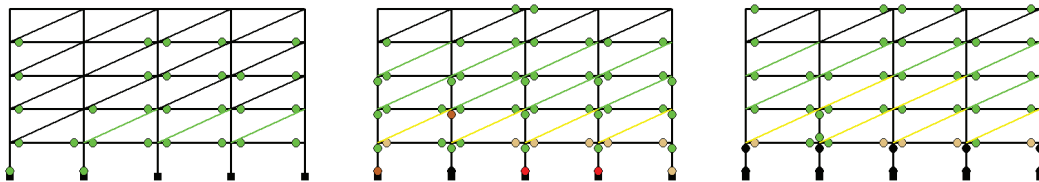
5 Story Model Frame



Model BR



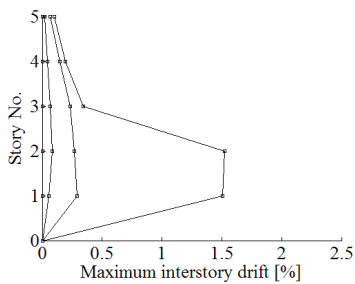
Model FI



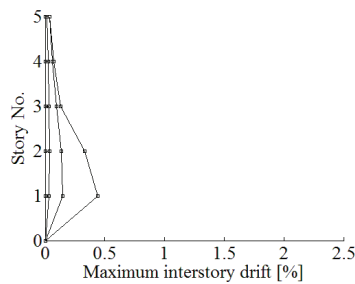
Model SS



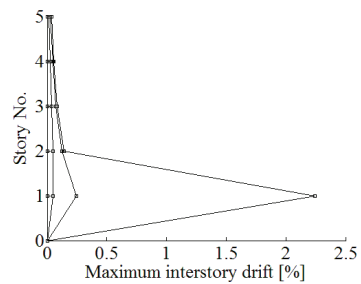
Interstory drift according to EQ.3



Model BR



Model FI

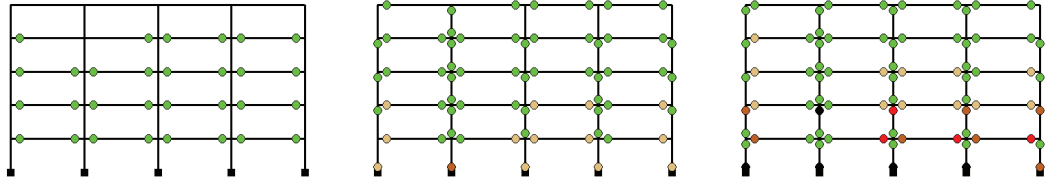


Model SS

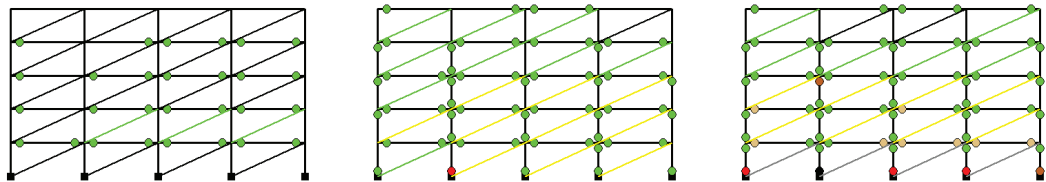
Table F.2 Predicted damage and interstory drift (continued)

EQ.4		Soil type (B-T)	
0.1g	0.3g	0.5g	

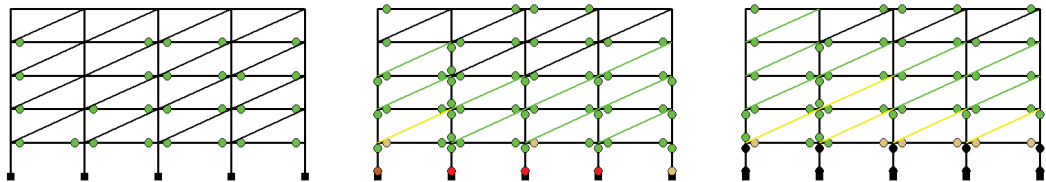
5 Story Model Frame



Model BR



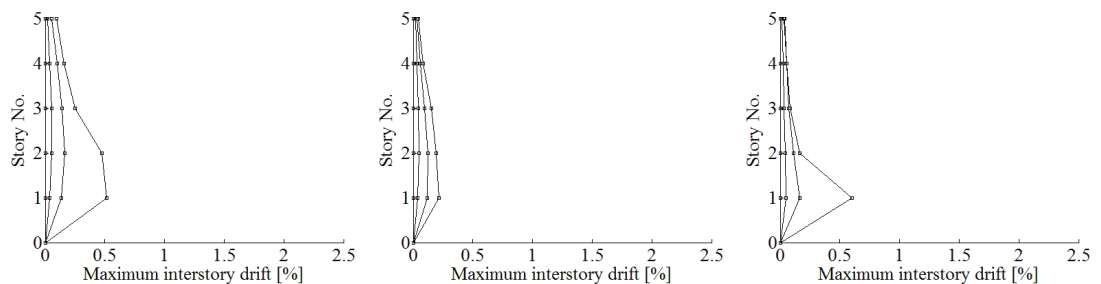
Model FI



Model SS



Interstory drift according to EQ.4



Model BR

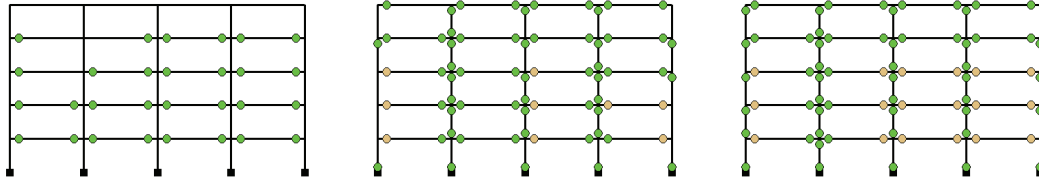
Model FI

Model SS

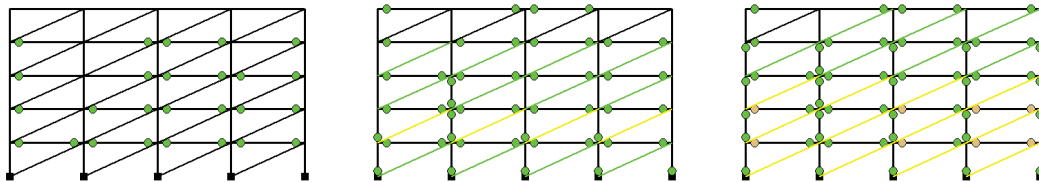
Table F.2 Predicted damage and interstory drift (continued)

EQ.5		Soil type (C-R)	
0.1g	0.3g	0.5g	

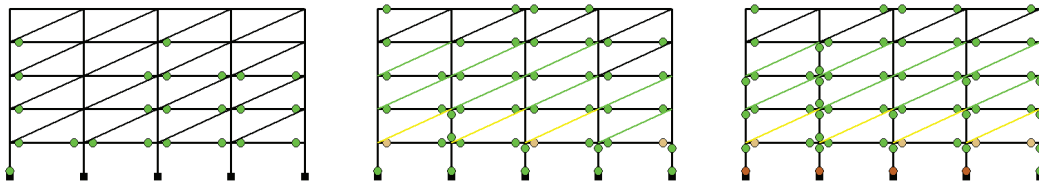
5 Story Model Frame



Model BR



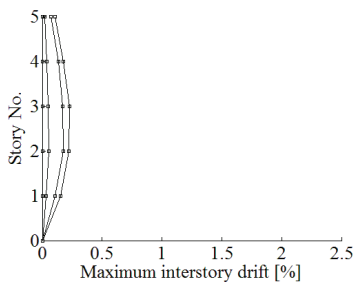
Model FI



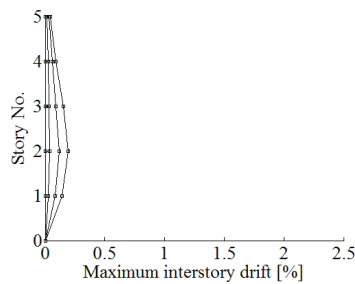
Model SS



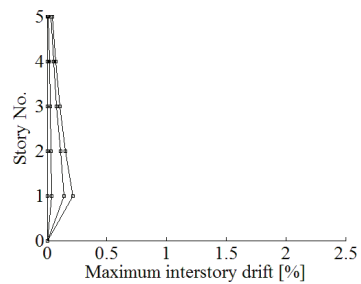
Interstory drift according to EQ.5



Model BR



Model FI



Model SS

Table F.2 Predicted damage and interstory drift (continued)

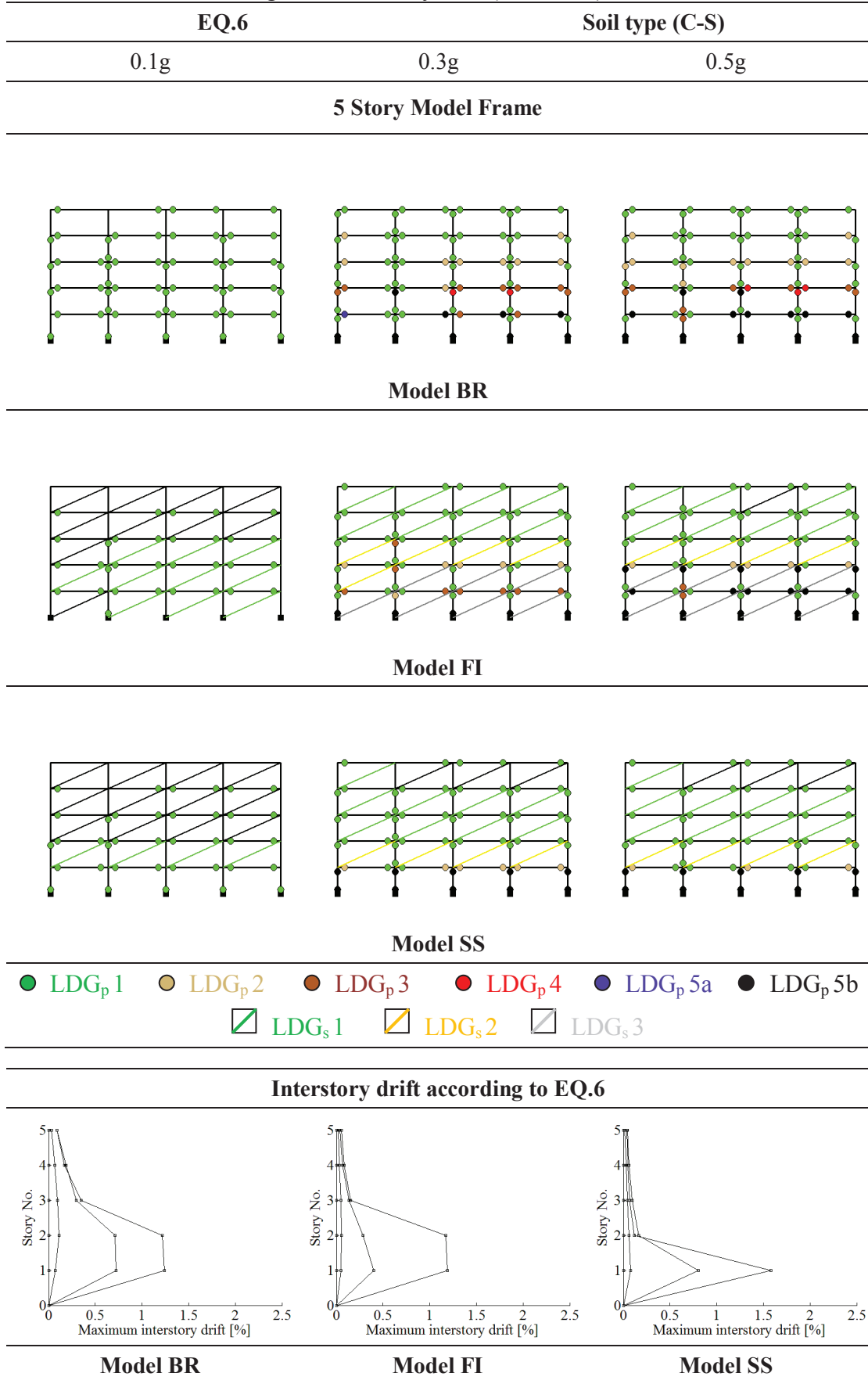
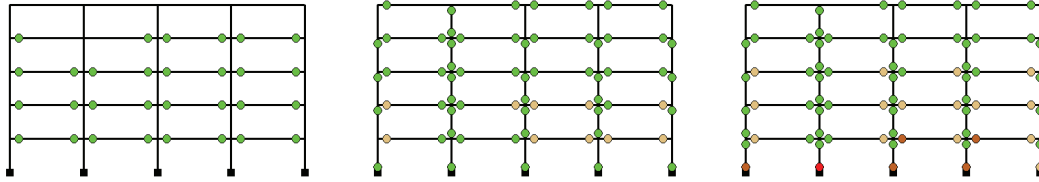


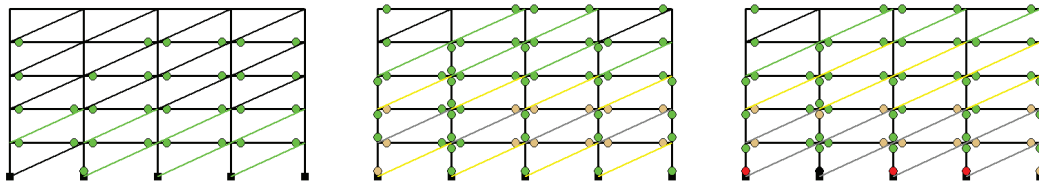
Table F.2 Predicted damage and interstory drift (continued)

EQ.7		Soil type (C-T)	
0.1g	0.3g	0.5g	

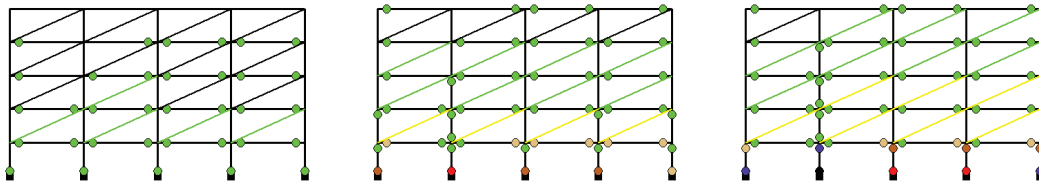
5 Story Model Frame



Model BR



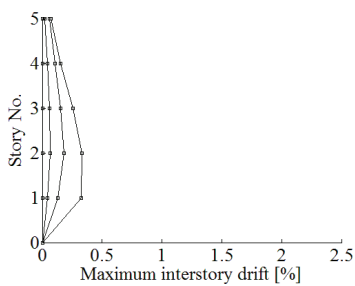
Model FI



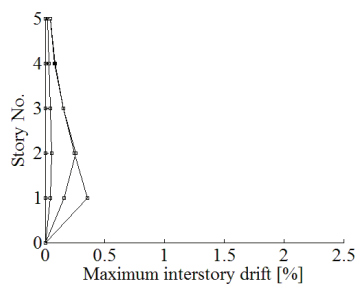
Model SS



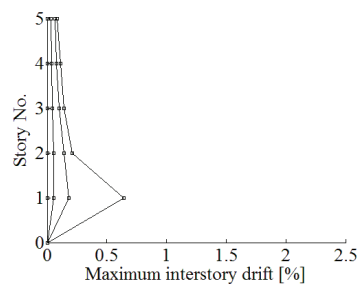
Interstory drift according to EQ.7



Model BR



Model FI



Model SS

Table F.2 Predicted damage and interstory drift (continued)

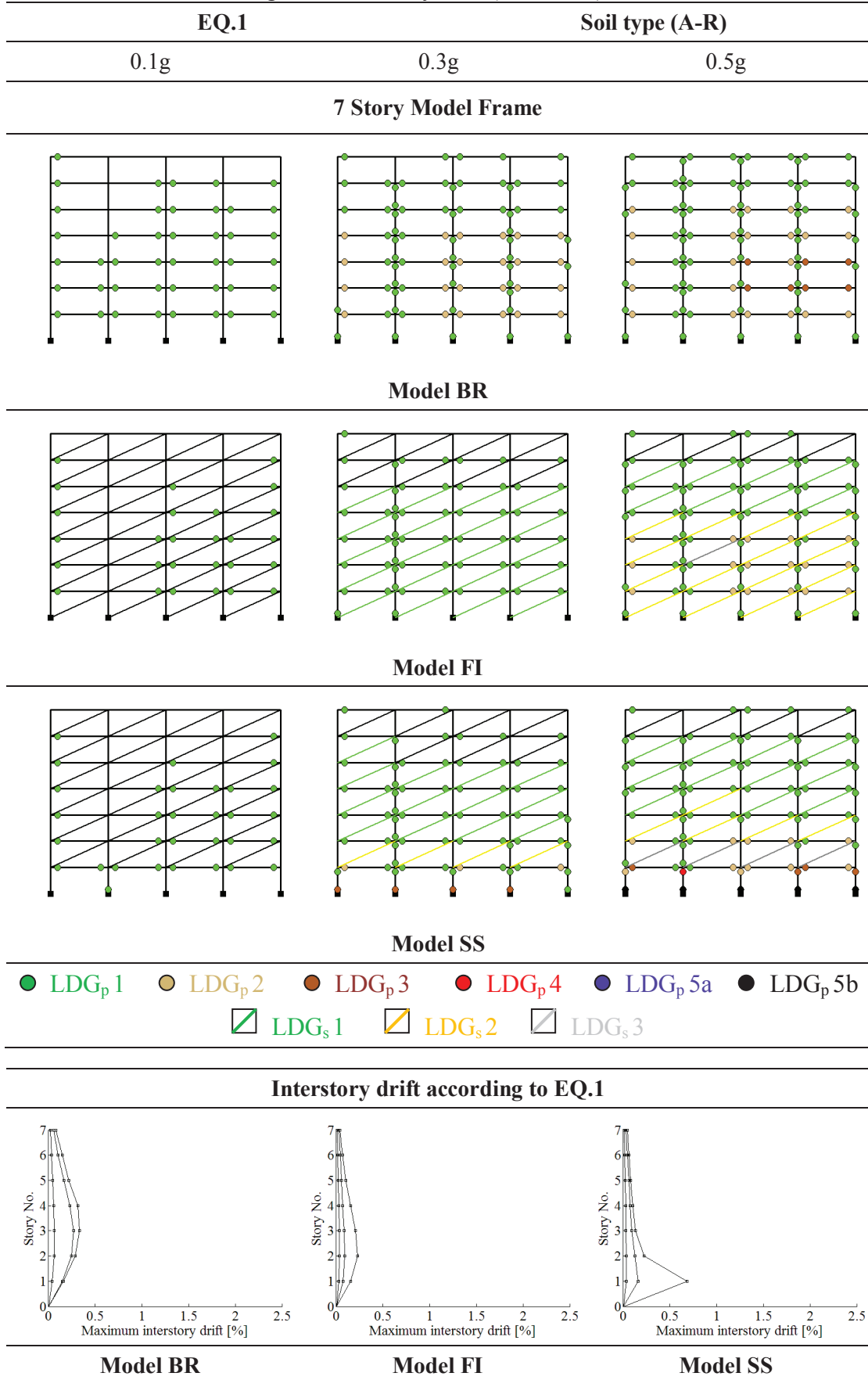
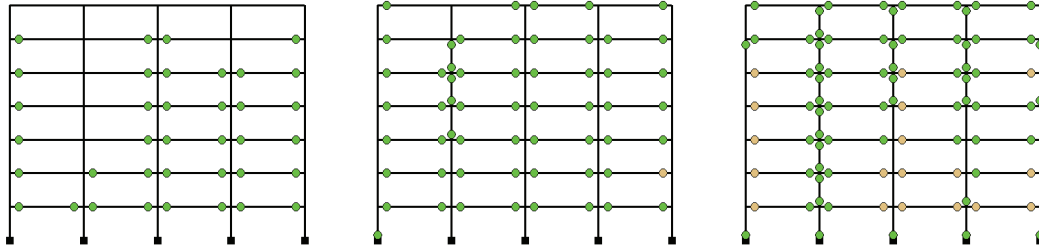


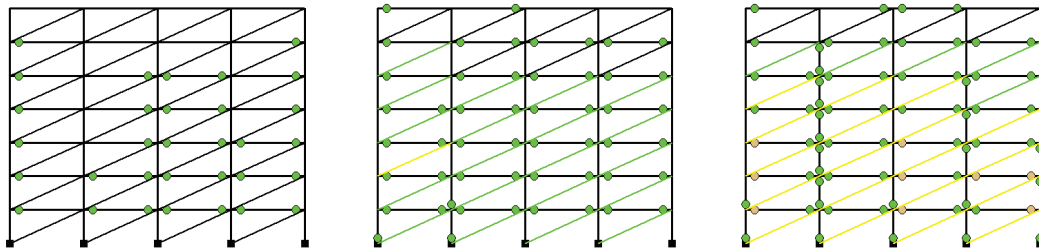
Table F.2 Predicted damage and interstory drift (continued)

EQ.2		Soil type (B-R)	
0.1g	0.3g	0.5g	

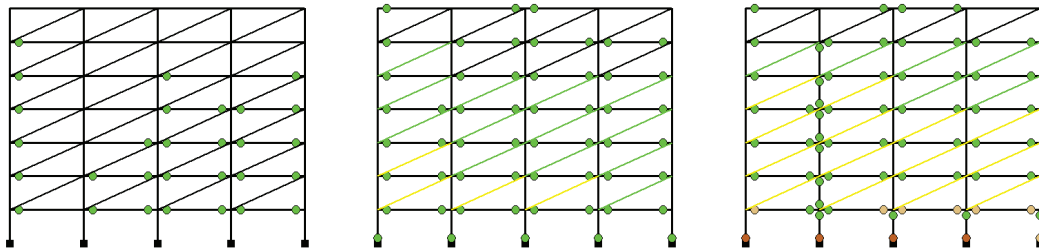
7 Story Model Frame



Model BR



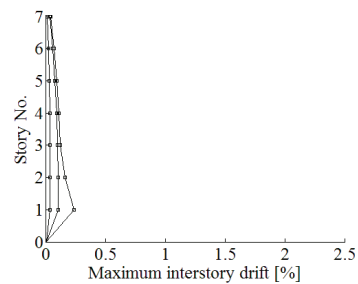
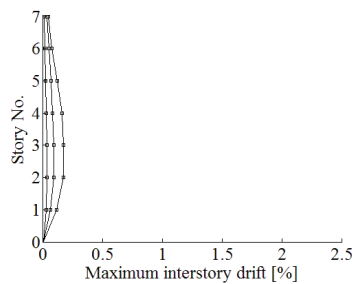
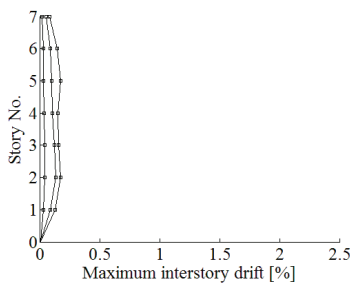
Model FI



Model SS



Interstory drift according to EQ.2



Model BR

Model FI

Model SS

Table F.2 Predicted damage and interstory drift (continued)

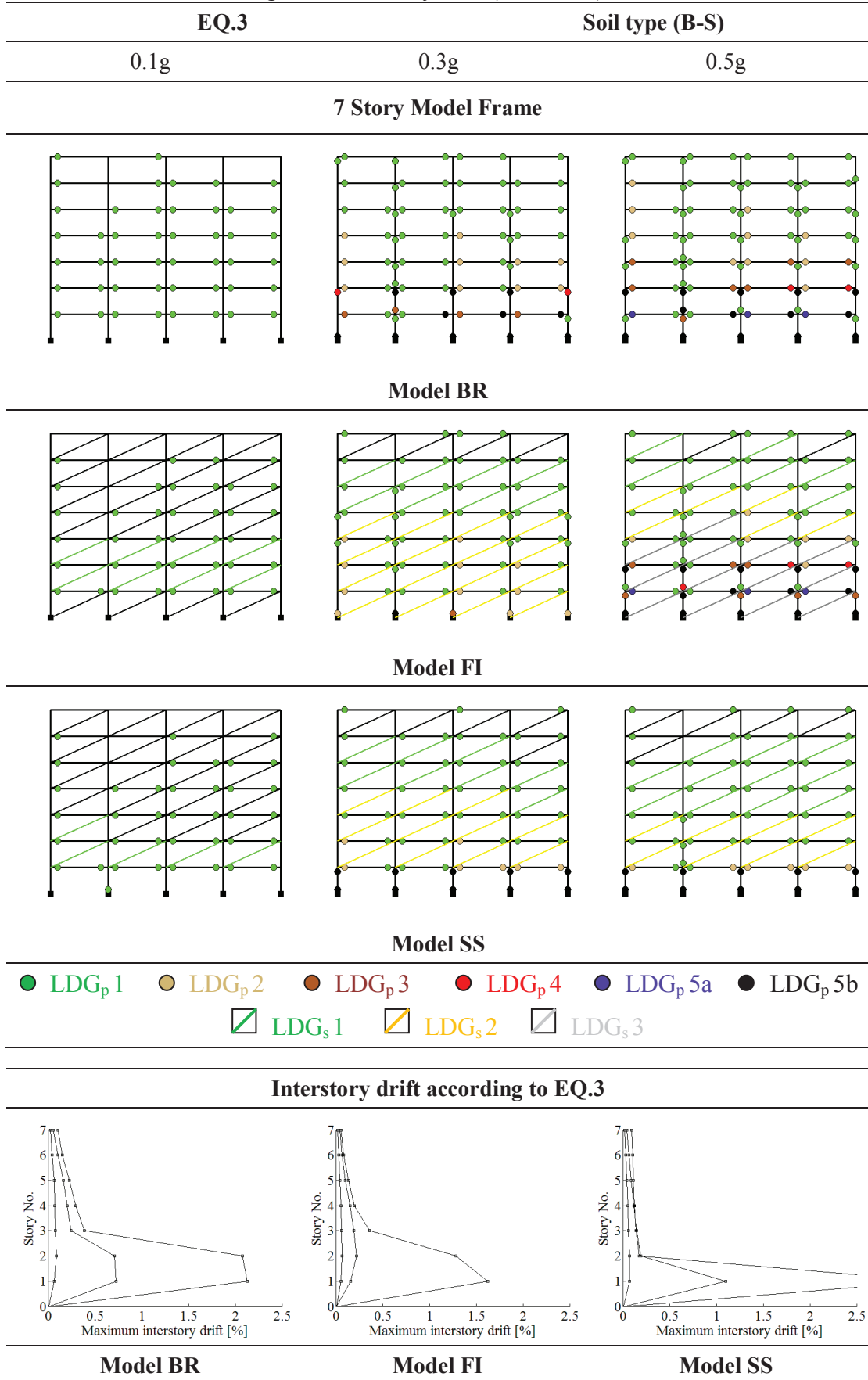
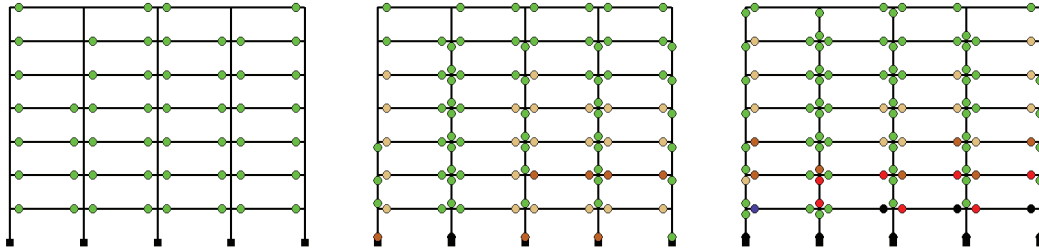


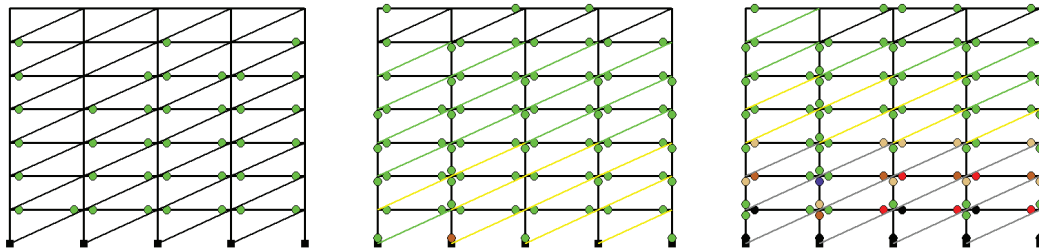
Table F.2 Predicted damage and interstory drift (continued)

EQ.4		Soil type (B-T)	
0.1g	0.3g	0.5g	

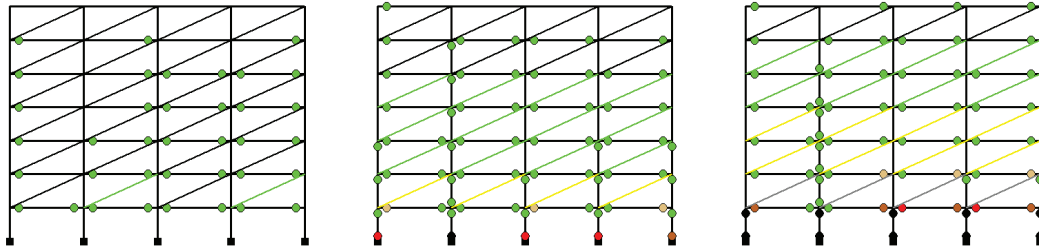
7 Story Model Frame



Model BR



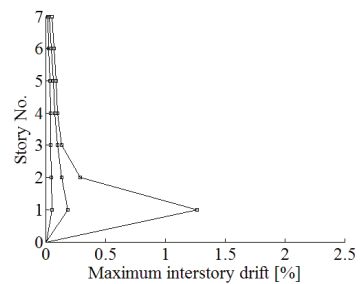
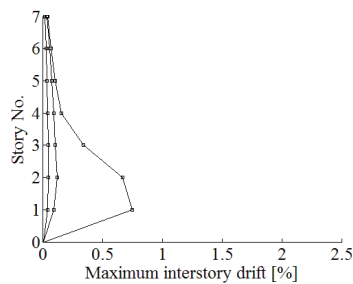
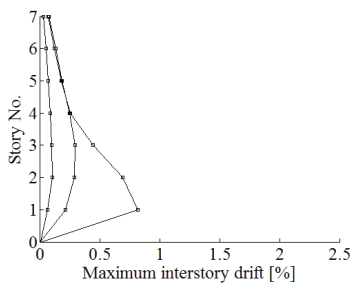
Model FI



Model SS



Interstory drift according to EQ.4



Model BR

Model FI

Model SS

Table F.2 Predicted damage and interstory drift (continued)

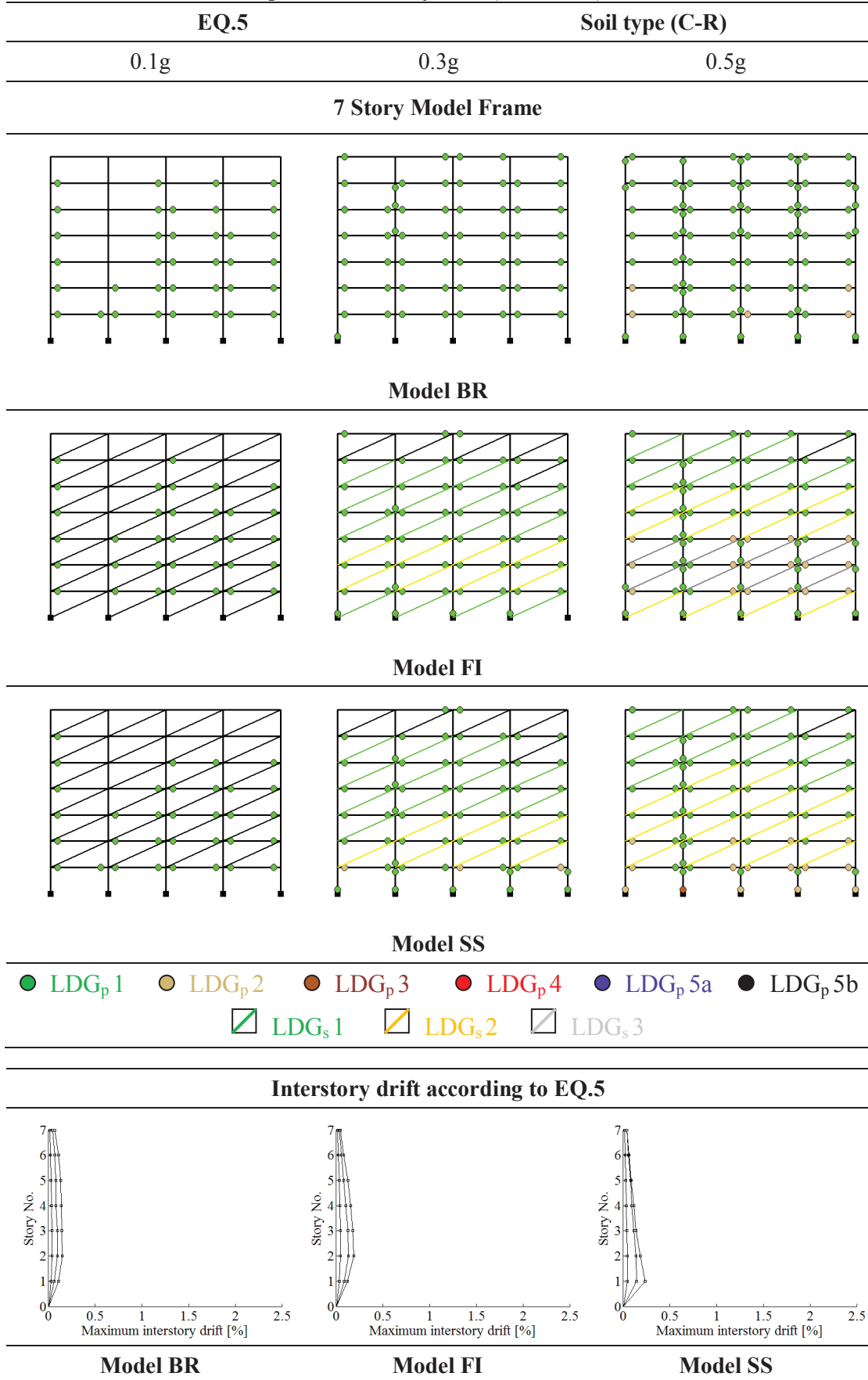
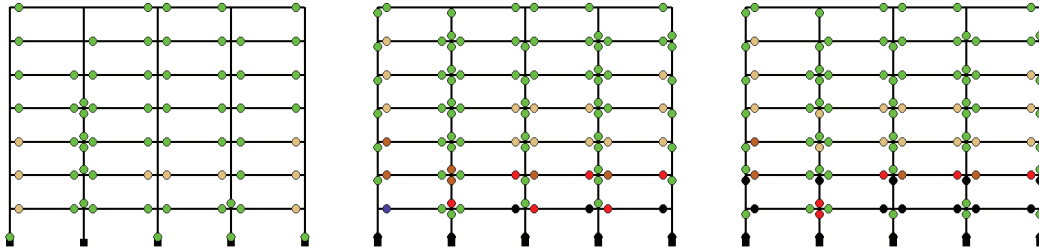


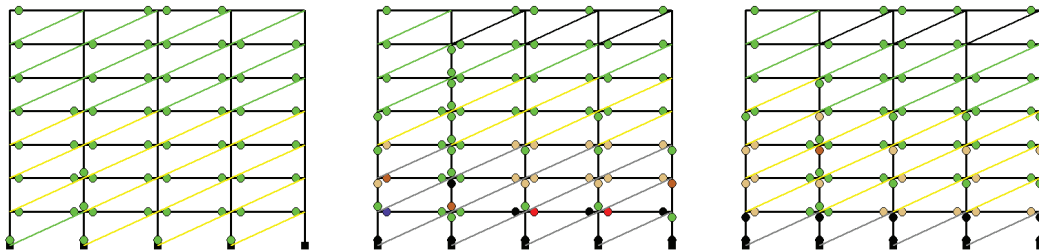
Table F.2 Predicted damage and interstory drift (continued)

EQ.6		Soil type (C-S)	
0.1g	0.3g	0.5g	

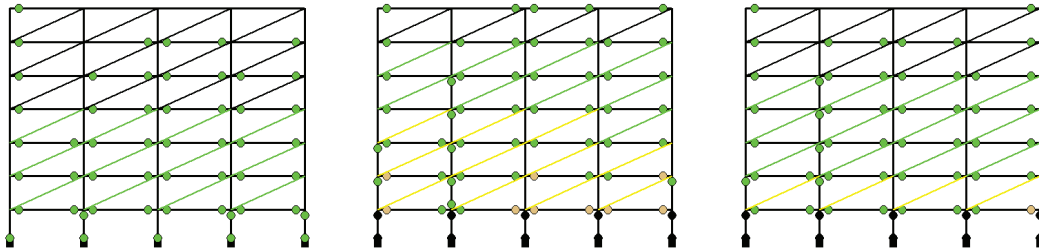
7 Story Model Frame



Model BR



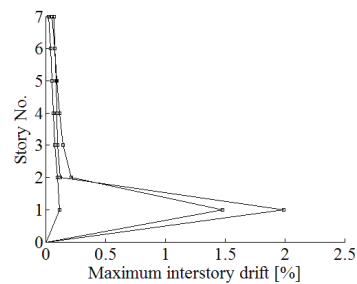
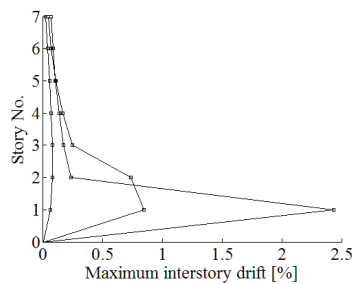
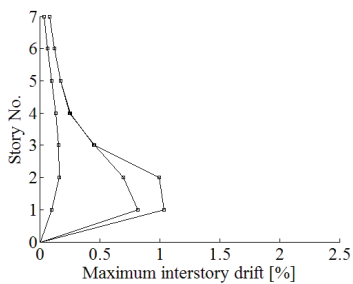
Model FI



Model SS



Interstory drift according to EQ.6

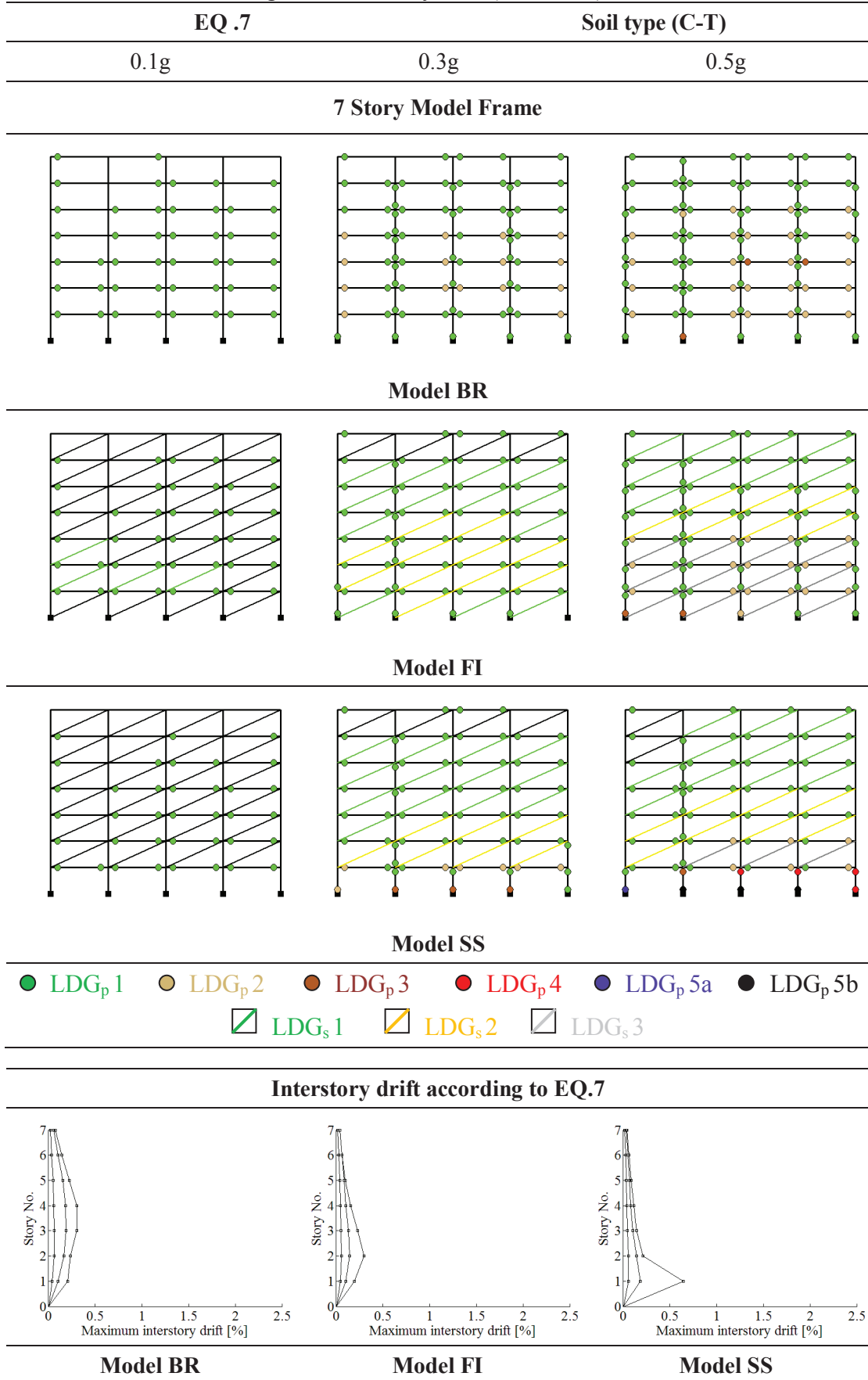


Model BR

Model FI

Model SS

Table F.2 Predicted damage and interstory drift (continued)



F.3 Structural Layout (Case Study 2)

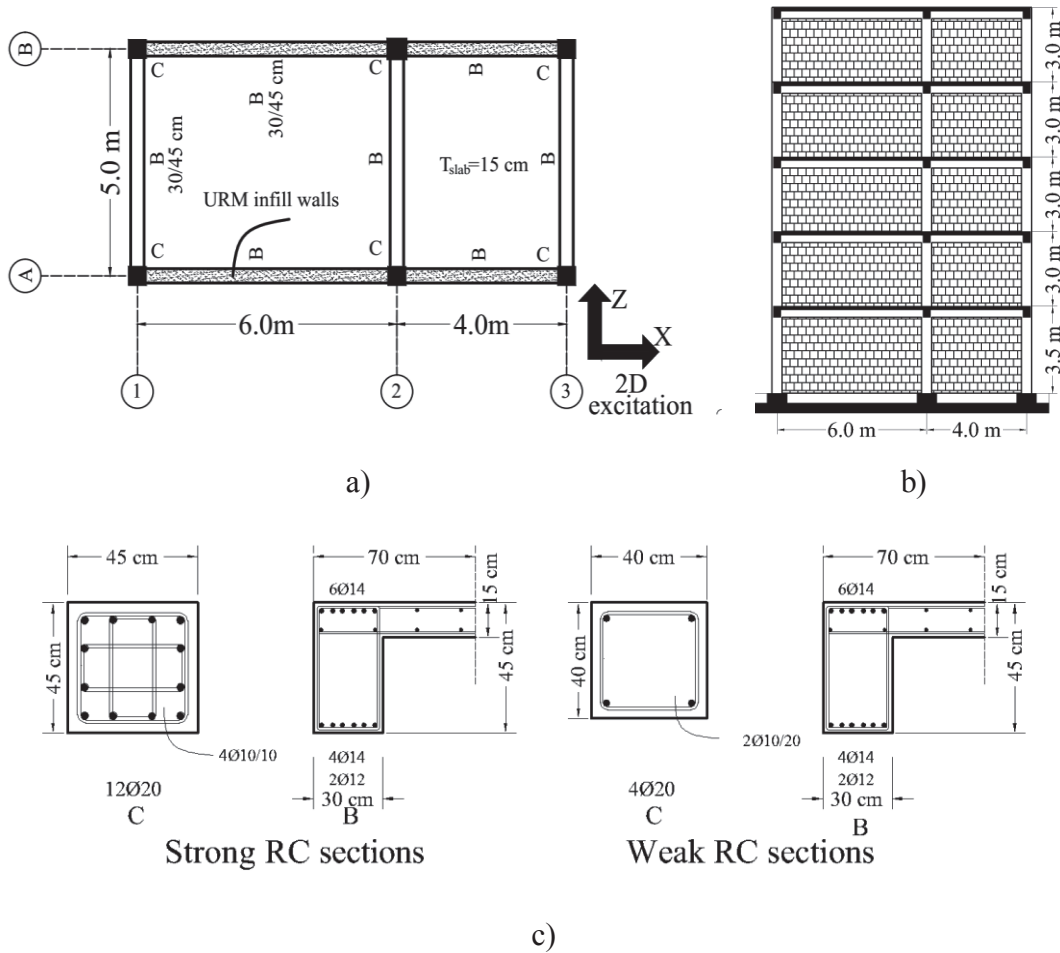


Figure F.3 Case study 2 structure: a) plane layout, b) elevation view and c) cross sections

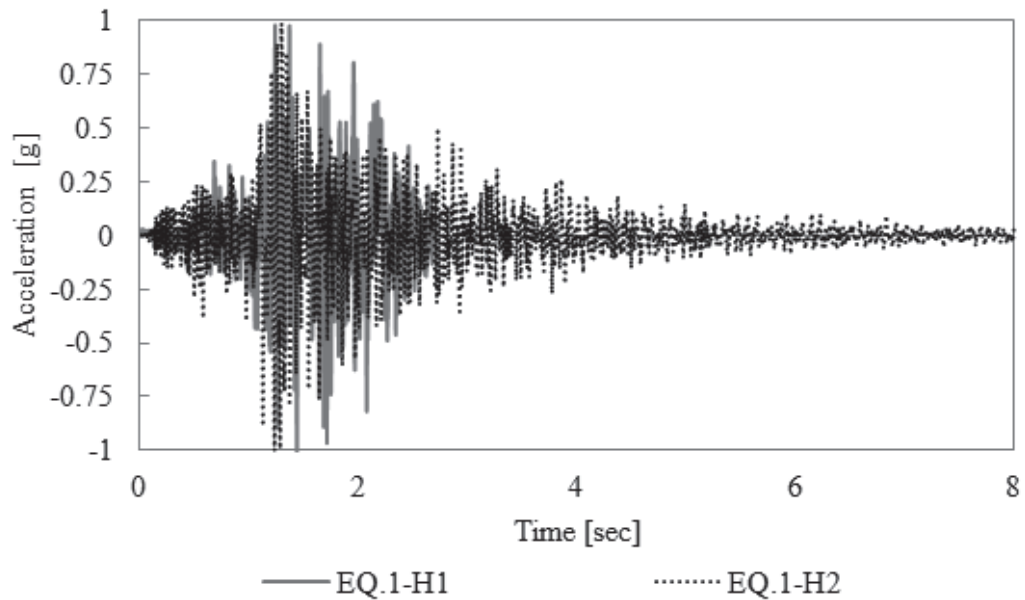
Table F.3 Considered models

Primary system type	Secondary system type	Model	
		Strong RC	Weak RC
Strong RC	Weak URM	Model (SB)	Model (WB)
	Medium URM	Model (SS)	Model (WS)
Weak RC	Strong URM	Model (SM)	Model (WM)
		Model (SW)	Model (WW)

F.4 Seismic Action Based on European Database

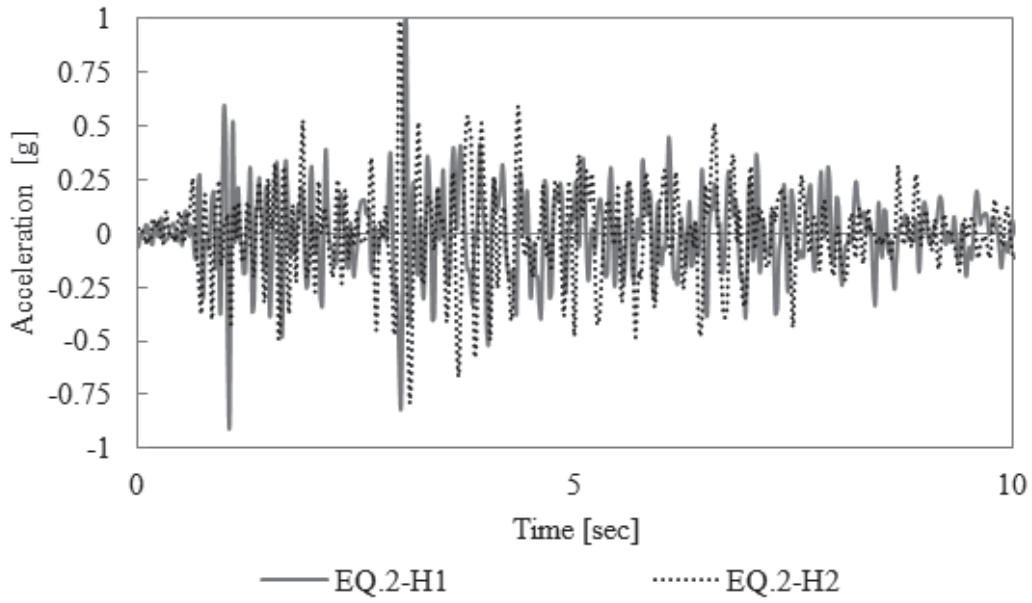
Table F.4 Selected ground motions for case study 2 (*Iervolino et al., 2010*)

Record		Site Class	Earthquake name	Year	Station name	Magnitude	Epicentral Distance [km]
No.	Index						
1	74	D	Gazli	1976	ST27	6.70	5
2	535	B	Erzincan	1992	ST205	6.60	13
3	133	C	Friuli	1976	ST33	6.00	9
4	230	B	Montenegro	1979	ST73	6.20	8
5	600	C	Umbria Marche	1997	ST223	6.00	22
6	197	B	197	1979	ST63	6.90	24
7	329	C	Faial	1998	ST87	6.10	11

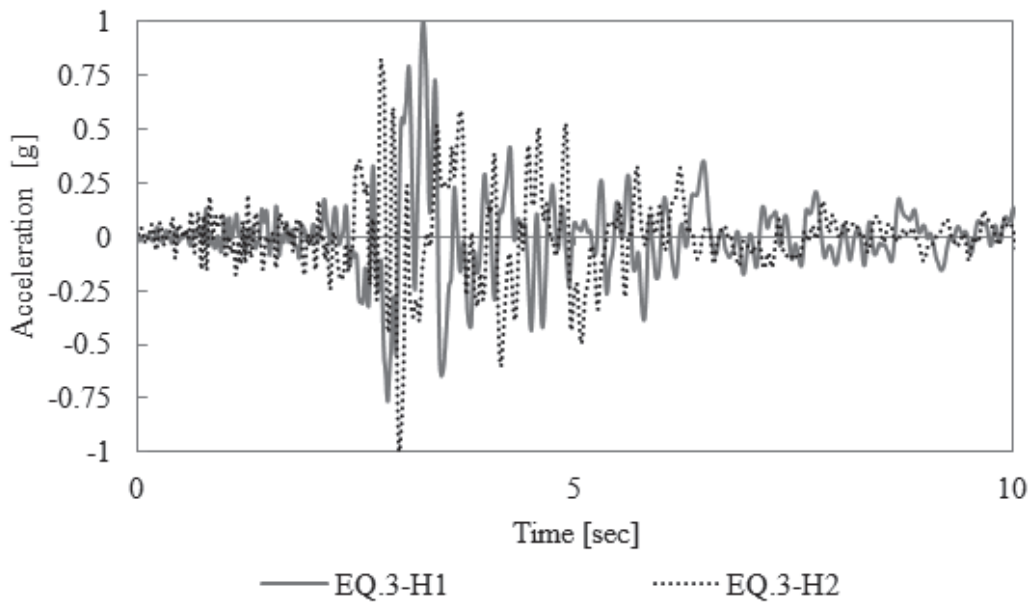


a) H1 & H2 components of EQ.1 recorded on site class (D)

Figure F.4 Respective time history records of the considered seismic action (case study 2)

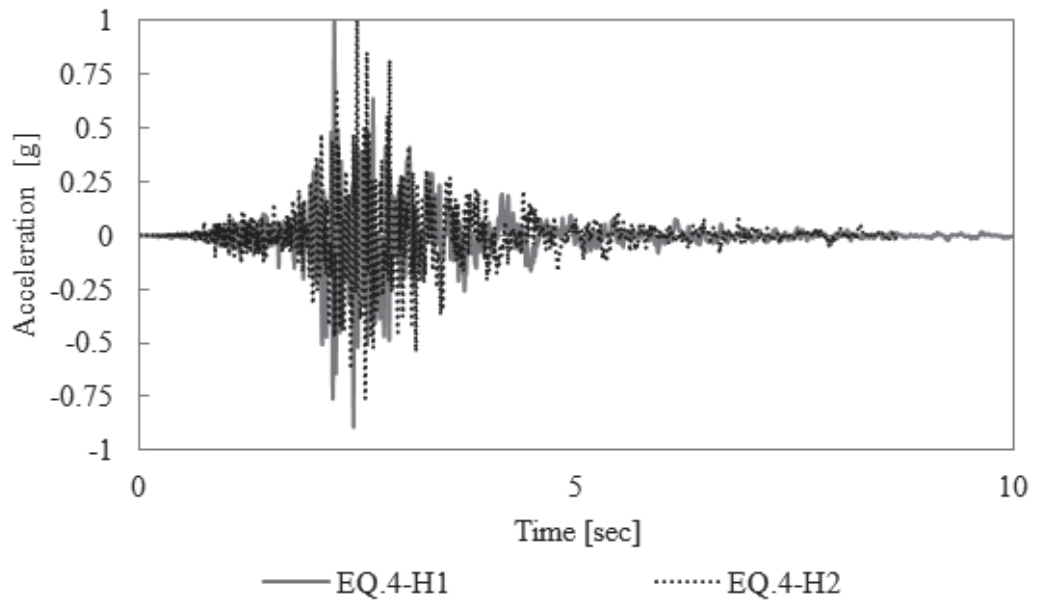


b) H1 & H2 components of EQ.2 recorded on site class (B)

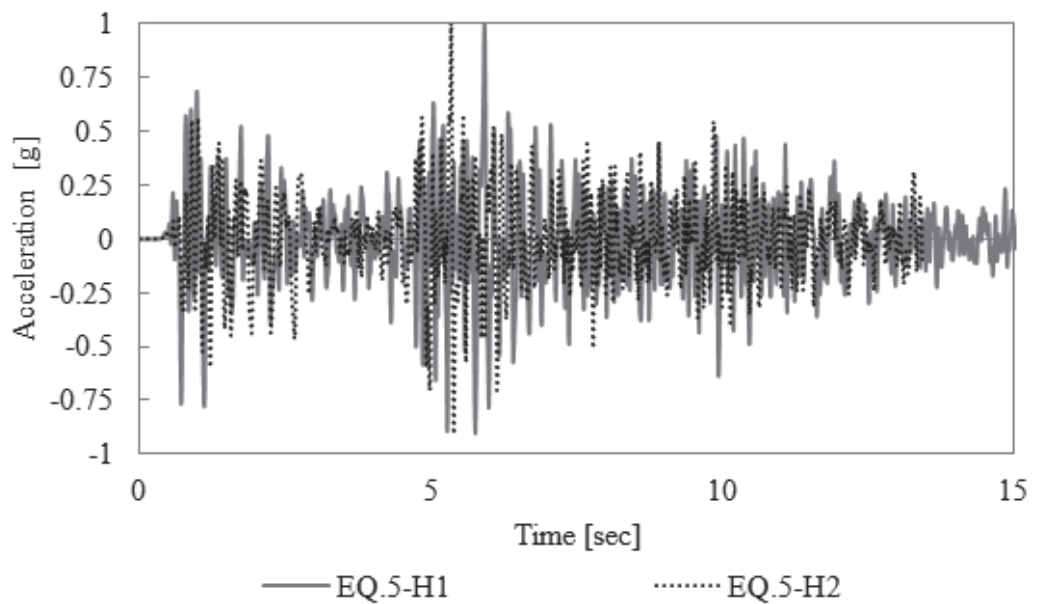


c) H1 & H2 components of EQ.3 recorded on site class (C)

Figure F.4 Respective time history records of the considered seismic action (case study 2) (continued)

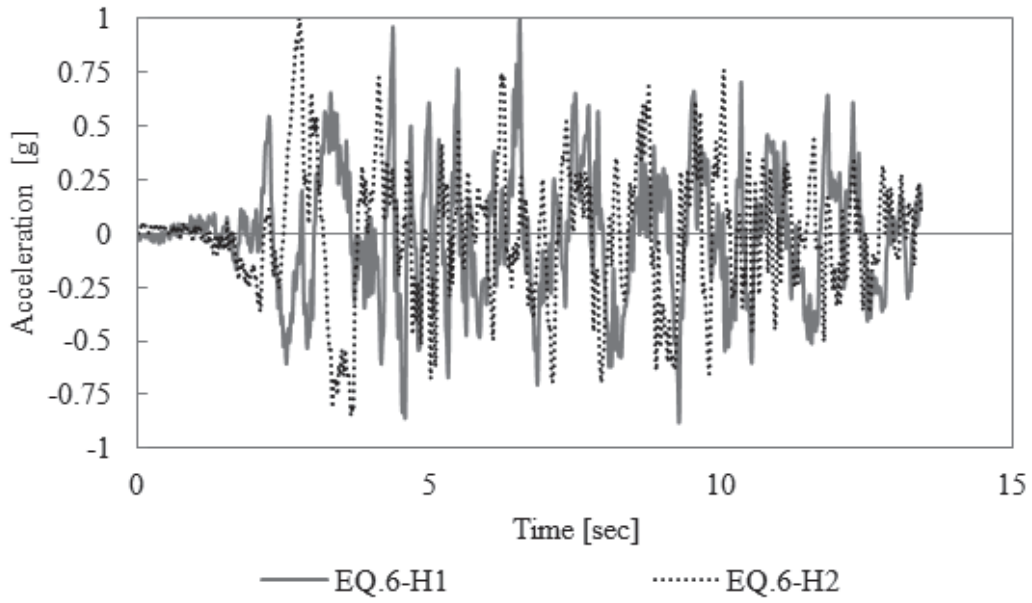


d) H1 & H2 components of the EQ.4 on site class (B)

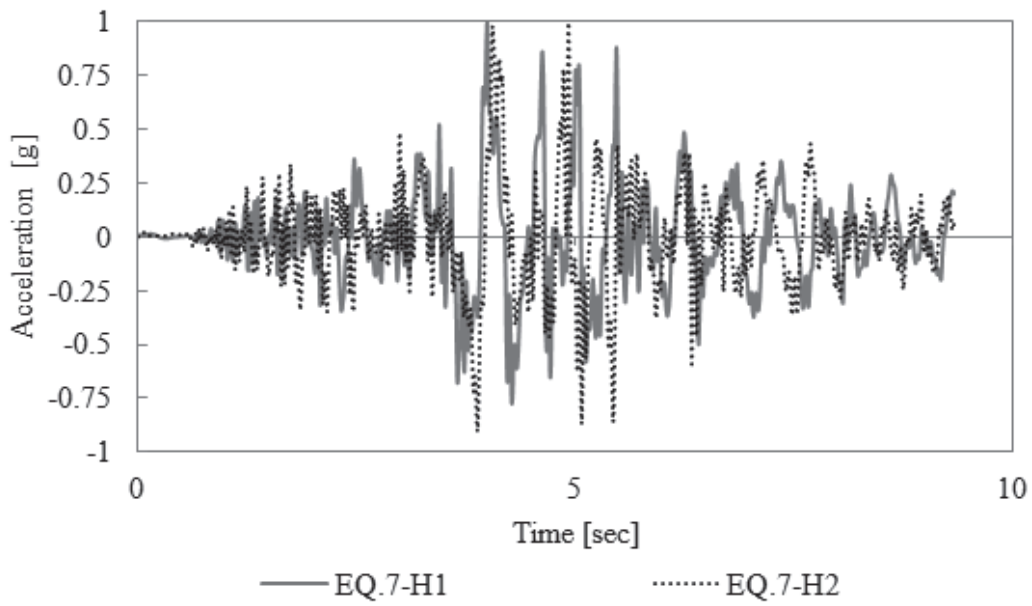


e) H1 & H2 components of EQ.5 recorded site class (C)

Figure F.4 Respective time history records of the considered seismic action (case study 2) (continued)



f) H1 & H2 components of the EQ.6 on site class (B)



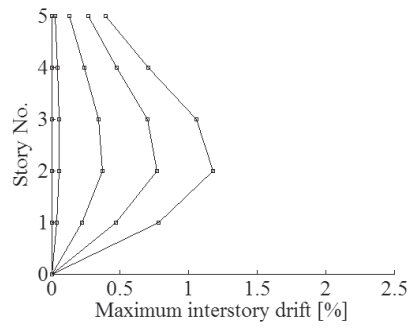
g) H1 & H2 components of EQ.7 recorded on site class (C)

Figure F.4 Respective time history records of the considered seismic action (case study 2) (continued)

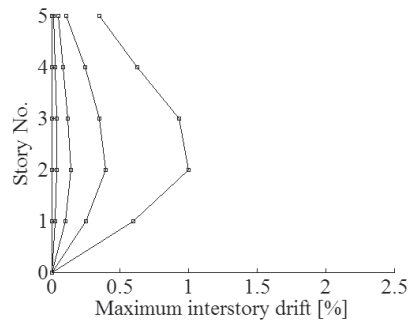
Table F.5 Predicted damage and interstory drift

EQ.1		Site class (D)	
0.2g	0.35g	0.5g	
5 Story Model Frame			
Model SB			
Model SW			
Model SM			
Model SS			
● LDG _p 1	● LDG _p 2	● LDG _p 3	● LDG _p 4
			● LDG _p 5a
			● LDG _p 5b
▧ LDG _s 1	▧ LDG _s 2	▧ LDG _s 3	

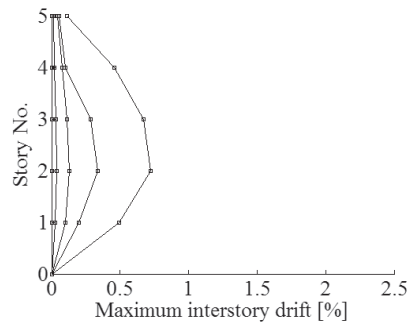
Interstory drift according to EQ.1



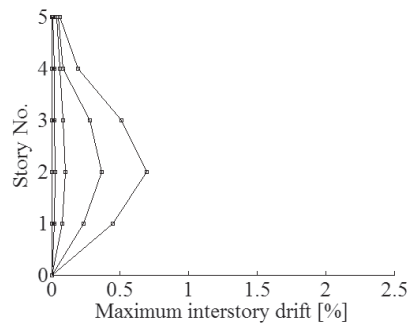
Model SB



Model SW



Model SM

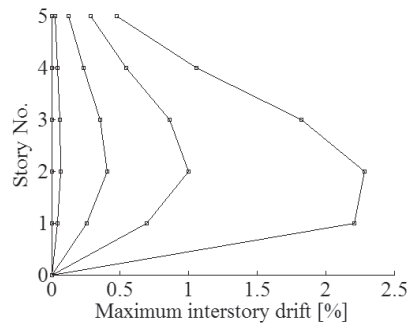


Model SS

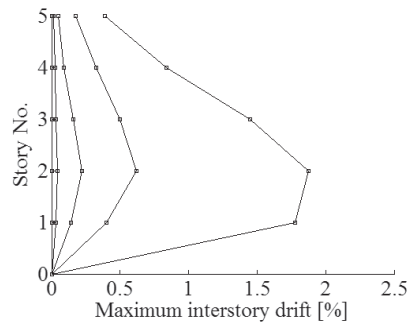
Table F.5 Predicted damage and interstory drift (continued)

EQ.2		Site class (B)	
0.2g	0.35g	0.5g	
5 Story Model Frame			
Model SB			
Model SW			
Model SM			
Model SS			
● LDG _p 1	● LDG _p 2	● LDG _p 3	● LDG _p 4
			● LDG _p 5a
			● LDG _p 5b
▧ LDG _s 1	▧ LDG _s 2	▧ LDG _s 3	

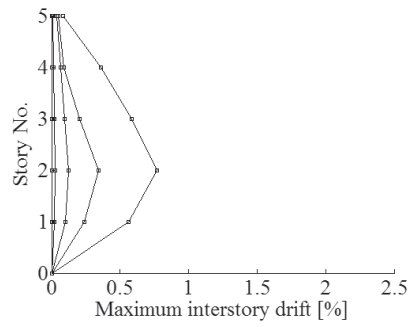
Interstory drift according to EQ.2



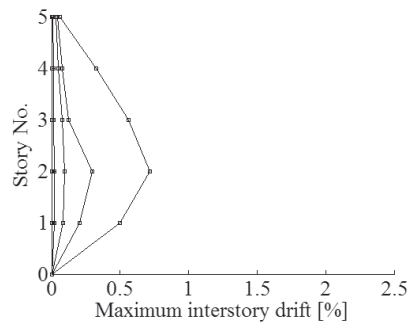
Model SB



Model SW



Model SM

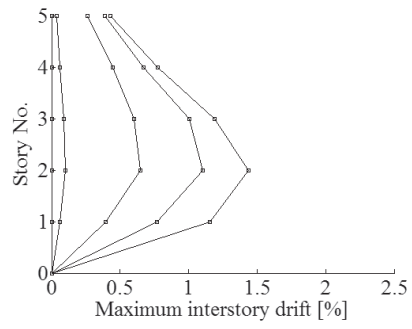


Model SS

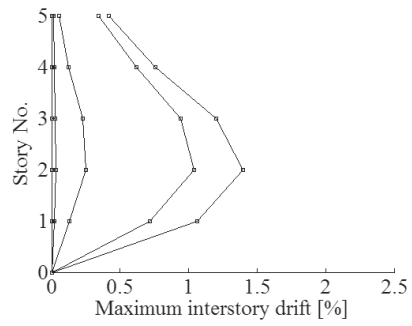
Table F.5 Predicted damage and interstory drift (continued)

EQ.3		Site class (C)	
0.2g	0.35g	0.5g	
5 Story Model Frame			
Model SB			
Model SW			
Model SM			
Model SS			
● LDG _p 1	● LDG _p 2	● LDG _p 3	● LDG _p 4
			● LDG _p 5a
			● LDG _p 5b
▧ LDG _s 1	▧ LDG _s 2	▧ LDG _s 3	

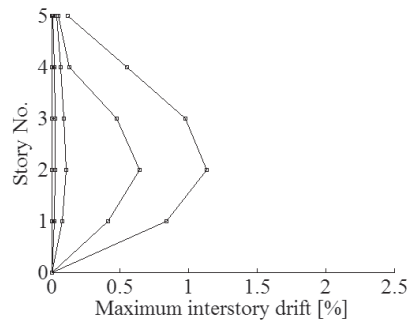
Interstory drift according to EQ.3



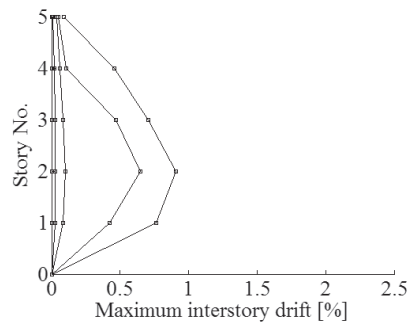
Model SB



Model SW



Model SM

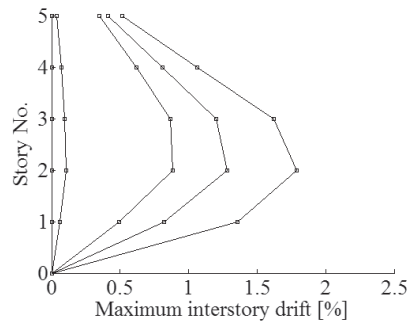


Model SS

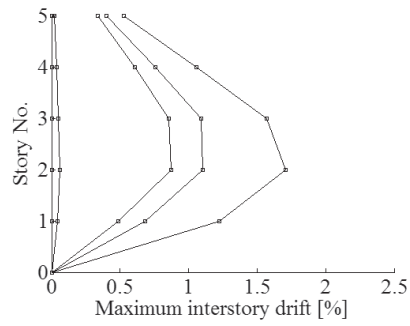
Table F.5 Predicted damage and interstory drift (continued)

EQ.4		Site class (B)	
0.2g	0.35g	0.5g	
5 Story Model Frame			
Model SB			
Model SW			
Model SM			
Model SS			
● LDG _p 1	● LDG _p 2	● LDG _p 3	● LDG _p 4
● LDG _p 5a	● LDG _p 5b	▧ LDG _s 1	▧ LDG _s 2
		▧ LDG _s 3	

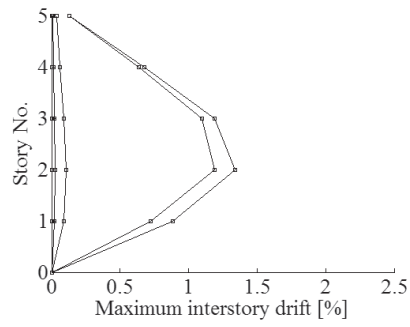
Interstory drift according to EQ.4



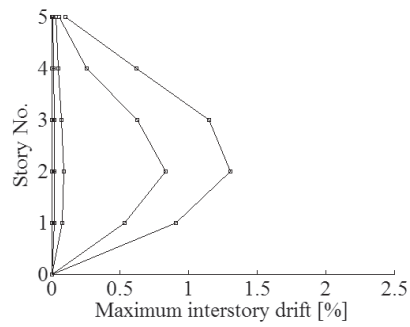
Model SB



Model SW



Model SM

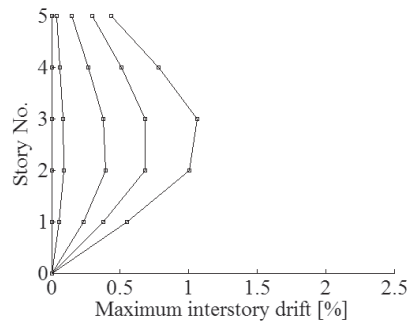


Model SS

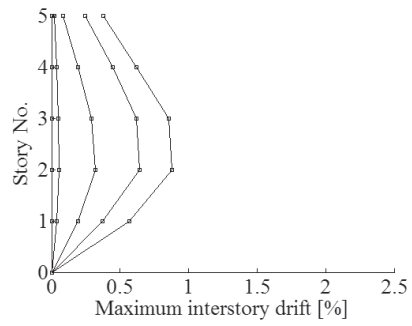
Table F.5 Predicted damage and interstory drift (continued)

EQ.5		Site class (C)	
0.2g	0.35g	0.5g	
5 Story Model Frame			
Model SB			
Model SW			
Model SM			
Model SS			
● LDG _p 1	● LDG _p 2	● LDG _p 3	● LDG _p 4
● LDG _p 5a	● LDG _p 5b	▧ LDG _s 1	▧ LDG _s 2
		▧ LDG _s 3	

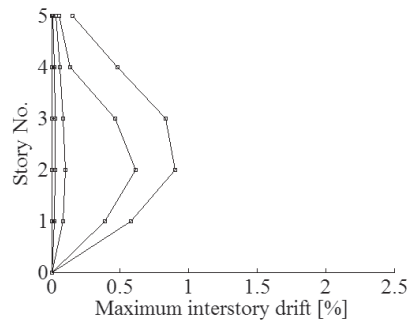
Interstory drift according EQ.5



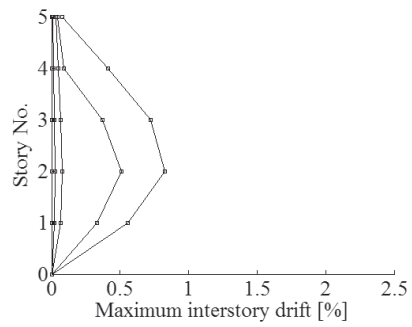
Model SB



Model SW



Model SM

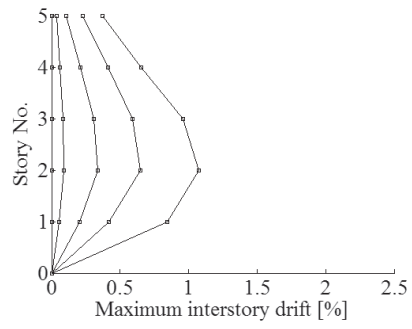


Model SS

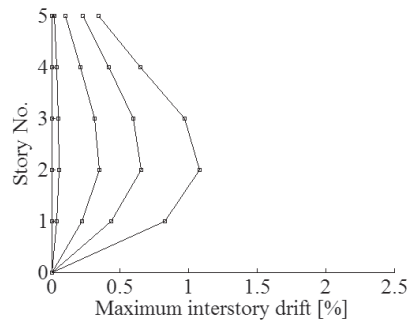
Table F.5 Predicted damage and interstory drift (continued)

EQ.6		Site class (B)	
0.2g	0.35g	0.5g	
5 Story Model Frame			
Model SB			
Model SW			
Model SM			
Model SS			
<div style="display: flex; justify-content: space-around; align-items: center;"> <div style="display: flex; gap: 10px;"> ● LDG_p1 ● LDG_p2 ● LDG_p3 ● LDG_p4 ● LDG_p5a ● LDG_p5b </div> <div style="display: flex; gap: 10px;"> ▧ LDG_s1 ▨ LDG_s2 ▩ LDG_s3 </div> </div>			

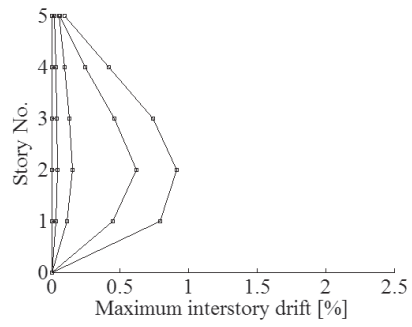
Interstory drift according to EQ.6



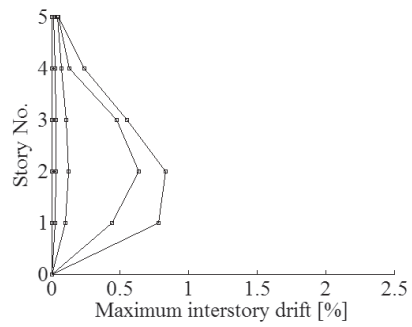
Model SB



Model SW



Model SM

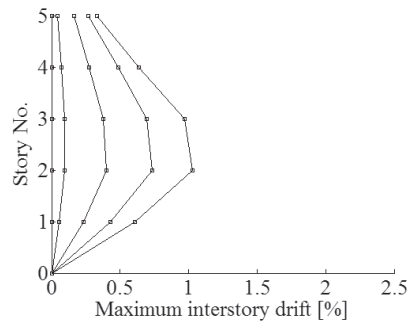


Model SS

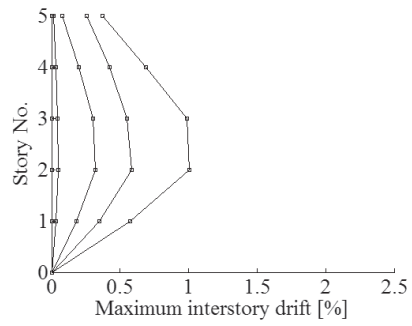
Table F.5 Predicted damage and interstory drift (continued)

EQ.7		Site class (C)	
0.2g	0.35g	0.5g	
5 Story Model Frame			
Model SB			
Model SW			
Model SM			
Model SS			
● LDG _p 1	● LDG _p 2	● LDG _p 3	● LDG _p 4
	● LDG _p 5a	● LDG _p 5b	
▧ LDG _s 1	▧ LDG _s 2	▧ LDG _s 3	

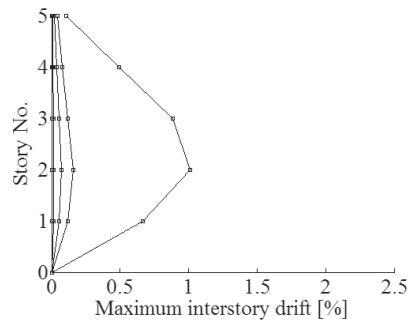
Interstory drift according to EQ.7



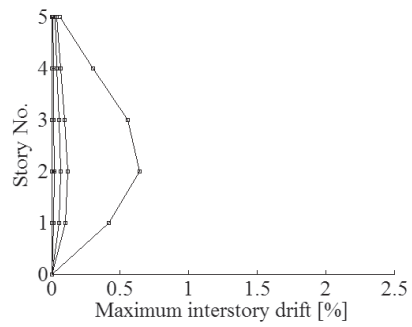
Model SB



Model SW

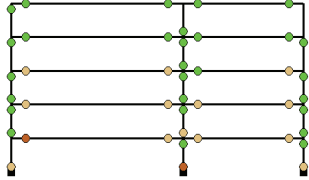
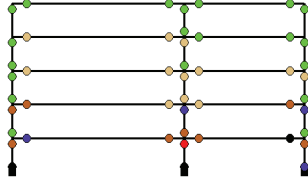
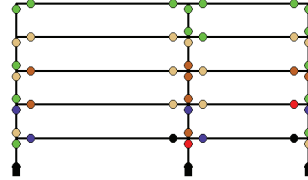
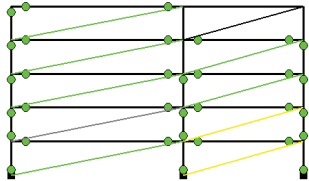
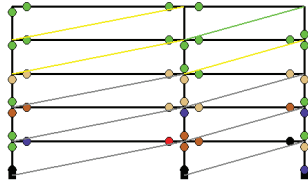
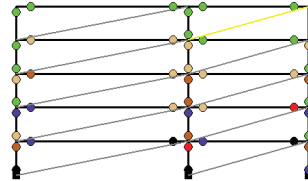
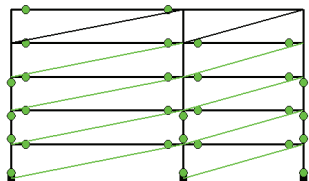
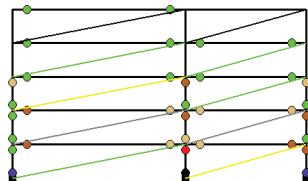
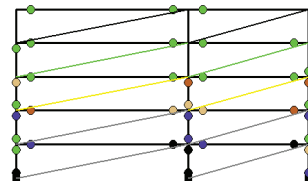
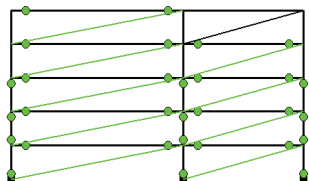
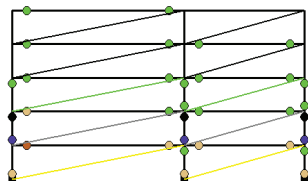
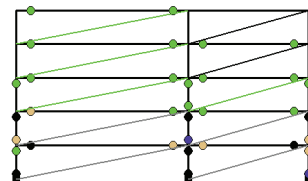


Model SM

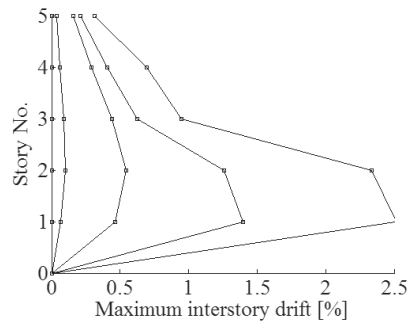


Model SS

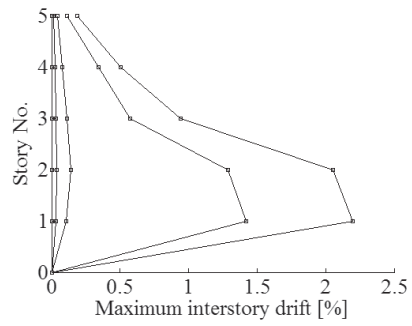
Table F.5 Predicted damage and interstory drift (continued)

EQ.1		Site class (D)			
0.2g	0.35g	0.5g			
5 Story Model Frame					
Model WB					
					
Model WW					
					
Model WM					
					
Model WS					
					
● LDG _p 1	● LDG _p 2	● LDG _p 3	● LDG _p 4	● LDG _p 5a	● LDG _p 5b
▧ LDG _s 1	▧ LDG _s 2	▧ LDG _s 3			

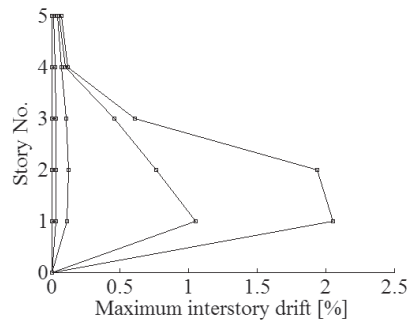
Interstory drift according o EQ.1



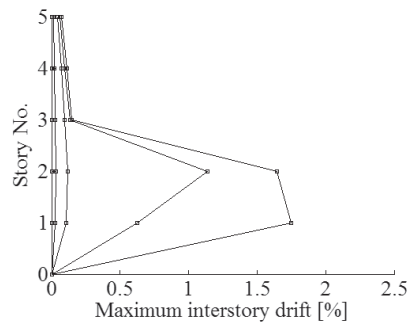
Model WB



Model WW



Model WM

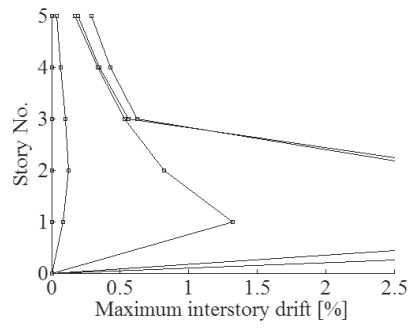


Model WS

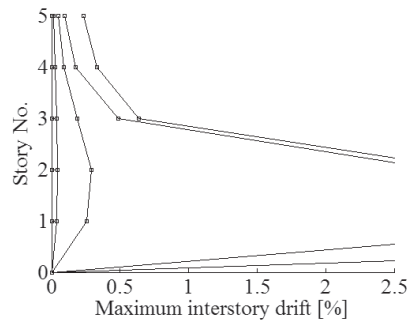
Table F.5 Predicted damage and interstory drift (continued)

EQ.2		Site class (B)	
0.2g	0.35g	0.5g	
5 Story Model Frame			
Model WB			
Model WW			
Model WM			
Model WS			
<div style="display: flex; justify-content: space-around; align-items: center;"> <div style="display: flex; gap: 10px;"> ● LDG_p1 ● LDG_p2 ● LDG_p3 ● LDG_p4 ● LDG_p5a ● LDG_p5b </div> <div style="display: flex; gap: 10px;"> ▨ LDG_s1 ▨ LDG_s2 ▨ LDG_s3 </div> </div>			

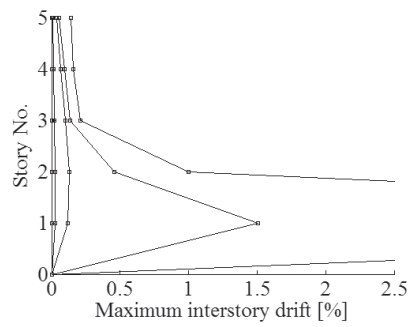
Interstory drift according to EQ.2



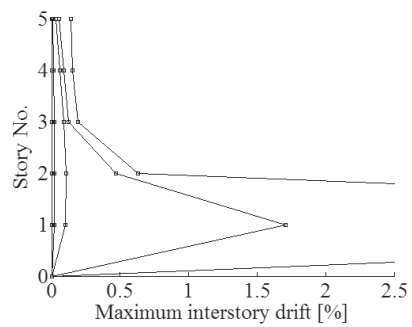
Model WB



Model WW



Model WM

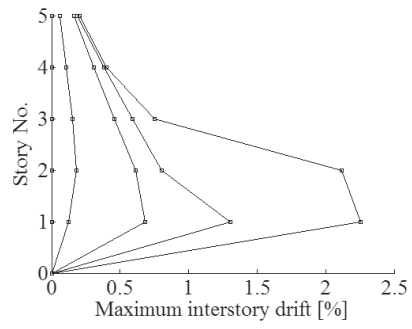


Model SS

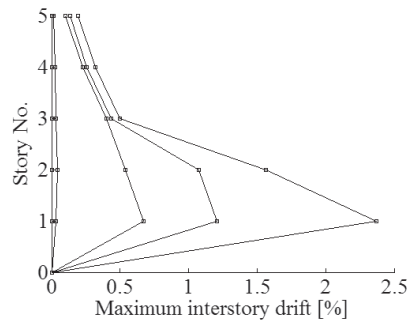
Table F.5 Predicted damage and interstory drift (continued)

EQ.3		Site class (C)	
0.2g	0.35g	0.5g	
5 Story Model Frame			
Model WB			
Model WW			
Model WM			
Model WS			
<div style="display: flex; justify-content: space-around; align-items: center;"> <div style="display: flex; gap: 10px;"> ● LDG_p1 ● LDG_p2 ● LDG_p3 ● LDG_p4 ● LDG_p5a ● LDG_p5b </div> <div style="display: flex; gap: 10px;"> ▧ LDG_s1 ▨ LDG_s2 ▩ LDG_s3 </div> </div>			

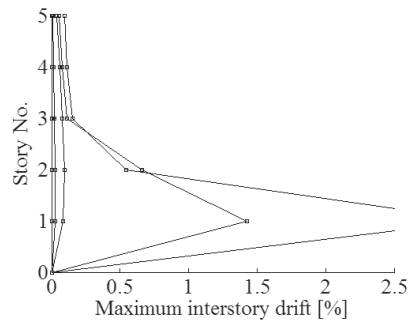
Interstory drift according to EQ.3



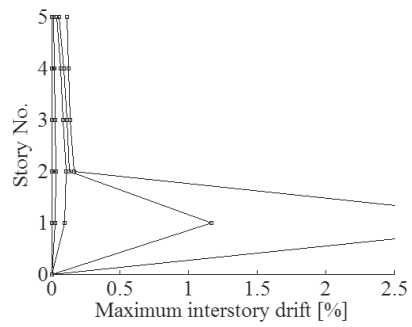
Model WB



Model WW



Model WM

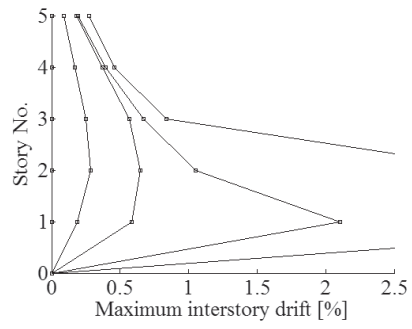


Model WS

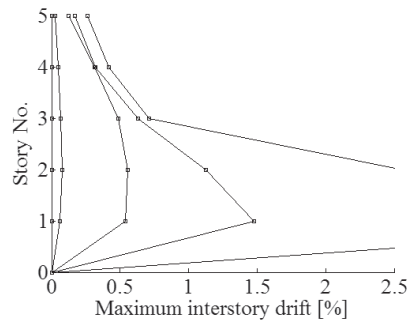
Table F.5 Predicted damage and interstory drift (continued)

EQ.4		Site class (B)	
0.2g	0.35g	0.5g	
5 Story Model Frame			
Model WB			
Model WW			
Model WM			
Model WS			
● LDG _p 1	● LDG _p 2	● LDG _p 3	● LDG _p 4
● LDG _p 5a	● LDG _p 5b	▧ LDG _s 1	▧ LDG _s 2
		▧ LDG _s 3	

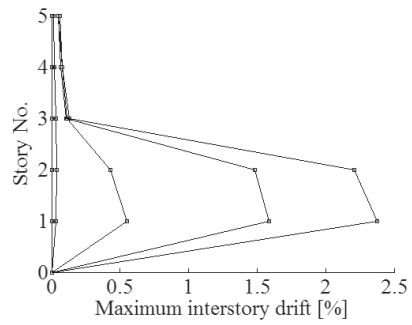
Interstory drift according to EQ.4



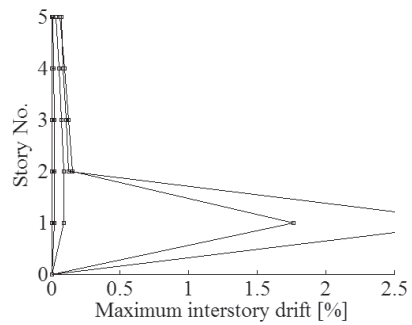
Model WB



Model WW



Model WM

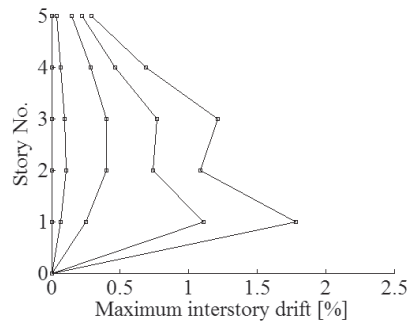


Model WS

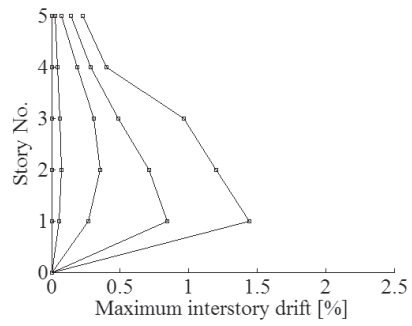
Table F.5 Predicted damage and interstory drift (continued)

EQ.5		Site class (C)	
0.2g	0.35g	0.5g	
5 Story Model Frame			
Model WB			
Model WW			
Model WM			
Model WS			
<div style="display: flex; justify-content: space-around; align-items: center;"> <div style="display: flex; gap: 10px;"> ● LDG_p1 ● LDG_p2 ● LDG_p3 ● LDG_p4 ● LDG_p5a ● LDG_p5b </div> <div style="display: flex; gap: 10px;"> ▧ LDG_s1 ▨ LDG_s2 ▩ LDG_s3 </div> </div>			

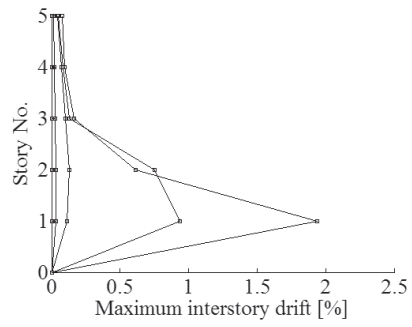
Interstory drift according to EQ.5



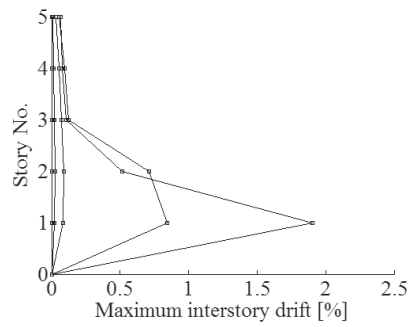
Model WB



Model WW



Model WM

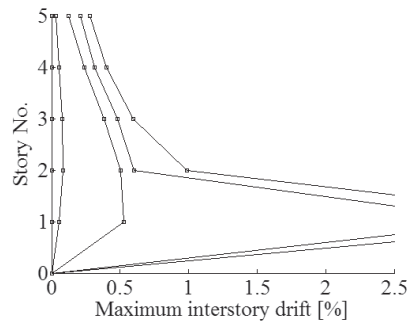


Model WS

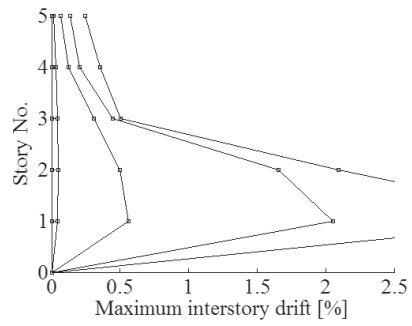
Table F.5 Predicted damage and interstory drift (continued)

EQ.6		Site class (B)	
0.2g	0.35g	0.5g	
5 Story Model Frame			
Model WB			
Model WW			
Model WM			
Model WS			
<div style="display: flex; justify-content: space-around; align-items: center;"> <div style="display: flex; gap: 10px;"> ● LDG_p1 ● LDG_p2 ● LDG_p3 ● LDG_p4 ● LDG_p5a ● LDG_p5b </div> <div style="display: flex; gap: 10px;"> ▧ LDG_s1 ▨ LDG_s2 ▩ LDG_s3 </div> </div>			

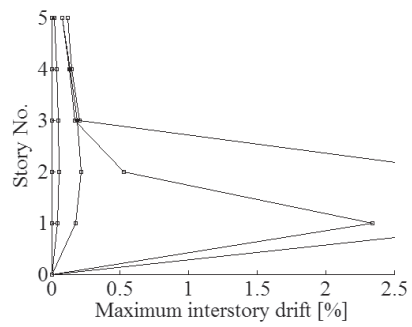
Interstory drift according to EQ.6



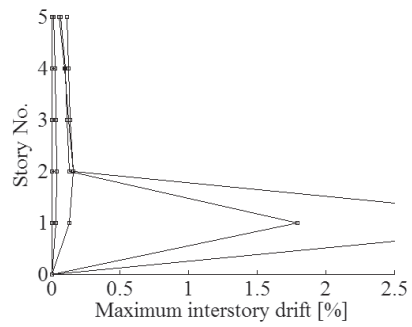
Model WB



Model WW



Model WM

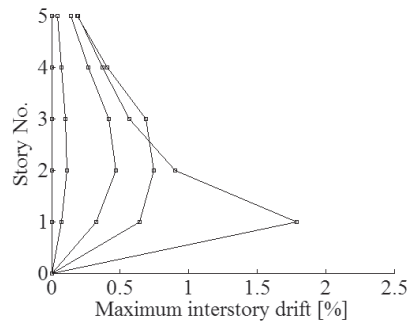


Model WS

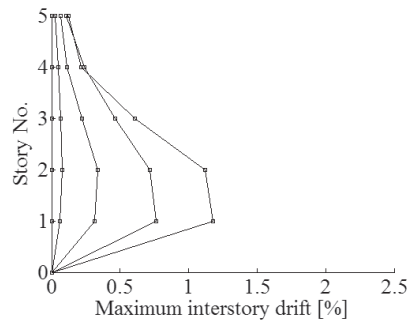
Table F.5 Predicted damage and interstory drift (continued)

EQ.7		Site class (C)	
0.2g	0.35g	0.5g	
5 Story Model Frame			
Model WB			
Model WW			
Model WM			
Model WS			
<div style="display: flex; justify-content: space-around; align-items: center;"> <div style="display: flex; gap: 10px;"> ● LDG_p1 ● LDG_p2 ● LDG_p3 ● LDG_p4 ● LDG_p5a ● LDG_p5b </div> <div style="display: flex; gap: 10px;"> ▧ LDG_s1 ▨ LDG_s2 ▩ LDG_s3 </div> </div>			

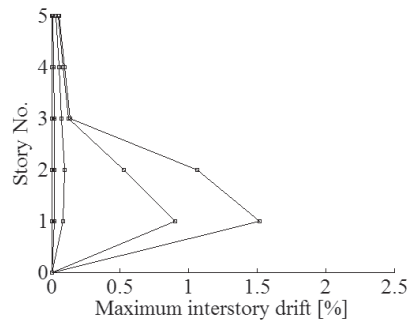
Interstory drift according to EQ.7



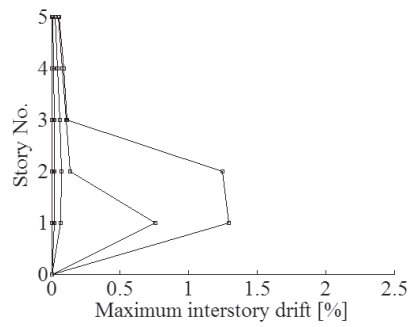
Model WB



Model WW



Model WM



Model WS
